R. Balluffi (p. 1219) is Research Metallurgist for Sylvania Electric Products Inc., Bayside, L. I., and was formerly with the Naval Research Lab in Washington, D. C. He studied at MIT, received his B.S. and Sc. D. degrees, and is a Student Associate of AIME.

R. Balluffi

Earl C. Roberts (p. 1210) is associated with MIT as Research Assistant, having formerly held the same position at Armour Research Foundation. A graduate of Montana School of Mines and MIT, he holds B.S. and M.S. degrees. Fishing, camping, and mountain climbing occupy the spare time of this Junior Member of AIME.

C. S. Roberts (p. 1211) is Research Assistant and a graduate student at MIT. He received his B. Met. E. from RPI, and his M.S. from MIT. A Student Associate of AIME, he likes photography and music.

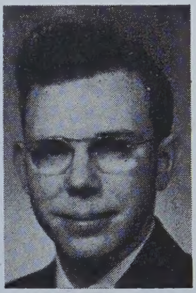
C. S. Roberts

Hsun Hu (p. 1214), Graduate Student in Metallurgy at the Univ. of Notre Dame, was born in China, and was formerly Assistant Engineer for the National Resources Commission of China. He studied at Chiao-Tung Univ. in China, and Lehigh University, receiving B.S. and M.S. degrees. A Student Associate of AIME, he has previously contributed to Transactions.

F. D. Rosi (p. 1217). See Journal of Metals, September, 1950.

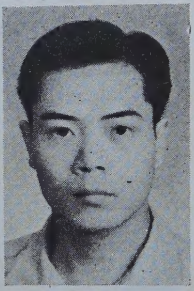
Hsun Hu

Edmund N. Mazza (p. 1218) is Metallurgist for Ekstrand & Tholand, Inc. He studied at Fordham Univ. and Stevens Institute of Technology, and received his B.S. and M.S. degrees.

J. B. Newkirk (p. 1249) is continuing research under a Fulbright Award at Cambridge University, England. He received his B. Met. E. degree from RPI, and his M.S. and D. Sc. degrees from Carnegie Institute of Technology. A Student Associate of AIME, he likes skiing, canoeing, and musical activities.

R. M. Treco (p. 1274) is at MIT, and has been Metallurgist for E. I. du Pont de Nemours, General Electric Co., and Remington Arms Co. An AIME member, he attended Lehigh Univ. for his B.S. degree. His hobbies are photography, wood and metal working, and electronics.

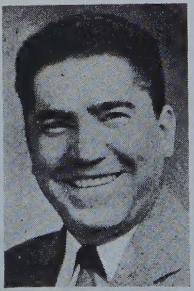
E. N. Mazza

P. A. Beck (p. 1214). See Journal of Metals, September, 1949.

W. R. Opie (p. 1237) is Research Metallurgist for Titanium Div., National Lead Co., having previously held a similar position for American Smelting and Refining Co. Born in Butte, Montana, he received his B.S. from Montana School of Mines, and his Sc. D. degree from MIT. An AIME member, he likes golf and fishing.

N. J. Grant (p. 1237) is Associate Professor of Metallurgy at MIT. He has also been Open Hearth Metallurgist for Bethlehem Steel Co., and Research Associate at MIT. Carnegie Tech and MIT awarded him B.S. and Sc. D. degrees. A member of AIME, he has presented several papers mostly on steelmaking.

J. B. Newkirk

C. A. Wert (p. 1242) is Research Associate Professor of Mining and Metallurgy at Univ. of Illinois. Until this fall term, he was Instructor at the Institute for the Study of Metals, and had previously been asso-

Journal of METALS

VOL. 188, NO. 10

OCTOBER, 195

Published to provide a continuing, authoritative, and up-to-date record of technologic, engineering, and economic progress in all branches of the metals industry by the

Metals Branch
American Institute of Mining and
Metallurgical Engineers, Inc.
29 West 39th Street, New York 18

o o o

THOMAS E. LLOYD
Manager of Publications
Editor, Journal of Metals

o o o

JAMES A. STANGARONE
Advertising Manager

o o o

HAROLD N. UNDERHILL, ALVIN S. COHAN, DOROTHY G. GARRETT, MARGARET BAGG, *Assistant Editors:* GRACE PUGSLEY, *Production Manager;* WALTER J. SEWING, *Assistant.*

o o o

OFFICERS, AIME

D. H. McLaughlin	*President*
A. B. Kinzel	*Vice President*
Philip Kraft	*Vice President*
R. W. Thomas	*Vice President*
C. H. Benedict	*Vice President*
C. V. Millikan	*Vice President*
Andrew Fletcher	*VP & Treasurer*

o o o

AIME STAFF

E. H. Robie	*Secretary*
H. A. Maloney	*Asst. Treasurer*
E. J. Kennedy, Jr.	*Asst. Secretary*
Ernest Kirkendall	*Asst. Secretary*
H. Newell Appleton	*Asst. to Secretary*

o o o

Technical Publications Committee

F. B. Foley	*Chairman*
E. J. Kennedy, Jr.	*Secretary*

o o o

Auxiliary Publications Committee

O. B. J. Fraser	*Chairman, IMD*
Michael Tenenbaum	*Chairman, ISD*
Philip T. Stroup	*Chairman, EMD*

o o o

The AIME Publishes:
Mining Engineering
Journal of Metals
Journal of Petroleum Technology

COVER

To strengthen its national position, Chile through private and governmental investments, recently completed construction of its first fully integrated steel plant. Production capacities will total 280,000 tons of pig iron and 260,000 tons of steel ingot, annually. Finished products will include bars, sheets, pipe, and light sections. Official opening of the plant will be in late November, 1950.

FEATURES AND NEWS

Journal of Metals REPORTER 1203
"Drift of Things" 1204
Engineering Employment Service 1198
Authors in This Issue 1194
New Products and Literature 1200
Personals and Obituaries 128
Coming Meetings 128
Metal Congress Program (AIME) 120
New Conveyor Principle 120
Republic and Armco Buy Mining Co. 120

RESEARCH IN PROGRESS

Precementitic Carbides in Tempered Martensite *E. C. Roberts* 121
Source of Abnormality in Hypereutectoid Steels *Arthur Dube* 121
Yielding in Plain Carbon Steels *C. S. Roberts, B. L. Averbach* 121
On the $\{259\}\gamma$ Habit of Martensite *E. S. Machlin* 121
On the Temperature Dependence of Self-Diffusion in Alpha Iron *I. D. Bakala* 121
Effect of Uniaxial Compressive Stresses on Self-Diffusion in Alpha Iron *F. S. Buffington* 121
Rolling Texture in Aluminum *Hsun Hu, P. A. Beck* 121
Annealing Texture in Rolled Aluminum Strip *P. A. Beck, Hsun Hu* 121
Order-Disorder Phase Change in Cu_3Au Alloys *F. N. Rhines* 121
Measurements on the Rate of Secondary Recrystallization in High Purity Silver *F. D. Rosi, B. H. Alexander* 121
Plastic Behavior of Silver Single Crystals at Various Temperatures *F. D. Rosi* 121
Studies on Control of Growth or Shrinkage of Iron-Copper Compacts During Sintering *J. F. Kuzmick, E. N. Mazza* 121
Experiments on Mechanism of Sintering *B. H. Alexander, R. Balluffi* 121
Interfaces in Diffusion in Solid Solutions *L. C. C. daSilva, R. F. Mehl* 121
The Application of Radioactive Tracers to the Study of Metal-Solution Reactions *M. T. Sinnad* 122

TRANSACTIONS

The Development of the Lead Blast Furnace at Port Pirie *L. A. White* 122
The Isothermal Transformation of a Eutectoid Beryllium Bronze *R. H. Fillnow, D. J. Mack* 122
Hydrogen Solubility in Al and Some Al Alloys *V. R. Opie, N. J. Grant* 123
Solid Solubility of Cementite in Alpha Iron *C. A. Wert* 124
Relative Energies of Grain Boundaries in Silicon Iron *C. G. Dunn, F. W. Daniels, M. J. Bolton* 124
Ordering Reaction in Cobalt-Platinum Alloys *J. B. Newkirk, A. H. Geisler, D. L. Martin, R. Smoluchowski* 124
Alloys of Ti with C, O_2, and N_2 *R. I. Jaffee, H. R. Ogden, D. J. Maykuth* 126
Dendritic Crystallization of Alloys *B. H. Alexander, F. N. Rhines* 126
Thermal Expansion Characteristics of Beryllium *R. M. Treco* 127
Aging Characteristics of Mg-Li Base Alloys *P. D. Frost, J. G. Kura, L. W. Eastwood* 127
Activity of Liquid Silver-Silicon Alloys *H. M. Schadel, Jr., G. Derge, C. E. Birchenall* 128
Crystallography of the Sigma Phase *P. Pietrokowsky, P. Duwez* 128

Published the first day of each month by the American Institute of Mining and Metallurgical Engineers, Inc., 29 West 39th Street, New York 18, N. Y. Telephone: PEnnsylvania 6-9220. Subscription $8 per year for non-AIME members in United States and North, South and Central America; $9, foreign; $6 for AIME members, or $4 in combination with a subscription to *Mining Engineering* or the *Journal of Petroleum Technology*. Single copies, 75 cents; special issues, $1.50 . . . The AIME is not responsible for any statement made or opinion expressed in its publications. . . . Copyright 1950 by the American Institute of Mining and Metallurgical Engineers, Inc. . . . Registered cable address, AIME New York . . . Indexed in Engineering Index, Industrial Arts Index and Chemical Abstracts . . . Reentered as second-class matter Sept. 21, 1949, at the post office at New York, N. Y., under the Act of March 3, 1879.

R. Balluffi (p. 1219) is Research Metallurgist for Sylvania Electric Products Inc., Bayside, L. I., and was formerly with the Naval Research Lab in Washington, D. C. He studied at MIT, received his B.S. and Sc. D. degrees, and is a Student Associate of AIME.

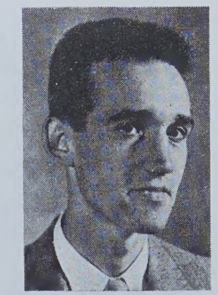
R. Balluffi

Earl C. Roberts (p. 1210) is associated with MIT as Research Assistant, having formerly held the same position at Armour Research Foundation. A graduate of Montana School of Mines and MIT, he holds B.S. and M.S. degrees. Fishing, camping, and mountain climbing occupy the spare time of this Junior Member of AIME.

C. S. Roberts (p. 1211) is Research Assistant and a graduate student at MIT. He received his B. Met. E. from RPI, and his M.S. from MIT. A Student Associate of AIME, he likes photography and music.

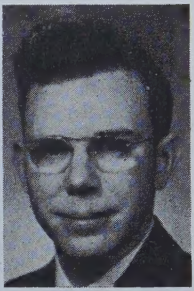
C. S. Roberts

Hsun Hu (p. 1214), Graduate Student in Metallurgy at the Univ. of Notre Dame, was born in China, and was formerly Assistant Engineer for the National Resources Commission of China. He studied at Chiao-Tung Univ. in China, and Lehigh University, receiving B.S. and M.S. degrees. A Student Associate of AIME, he has previously contributed to Transactions.

F. D. Rosi (p. 1217). See Journal of Metals, September, 1950.

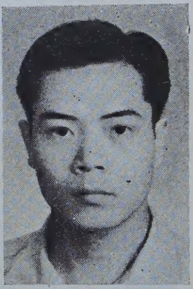
Hsun Hu

Edmund N. Mazza (p. 1218) is Metallurgist for Ekstrand & Tholand, Inc. He studied at Fordham Univ. and Stevens Institute of Technology, and received his B.S. and M.S. degrees.

J. B. Newkirk (p. 1249) is continuing research under a Fulbright Award at Cambridge University, England. He received his B. Met. E. degree from RPI, and his M.S. and D. Sc. degrees from Carnegie Institute of Technology. A Student Associate of AIME, he likes skiing, canoeing, and musical activities.

R. M. Treco (p. 1274) is at MIT, and has been Metallurgist for E. I. du Pont de Nemours, General Electric Co., and Remington Arms Co. An AIME member, he attended Lehigh Univ. for his B.S. degree. His hobbies are photography, wood and metal working, and electronics.

E. N. Mazza

P. A. Beck (p. 1214). See Journal of Metals, September, 1949.

W. R. Opie (p. 1237) is Research Metallurgist for Titanium Div., National Lead Co., having previously held a similar position for American Smelting and Refining Co. Born in Butte, Montana, he received his B.S. from Montana School of Mines, and his Sc. D. degree from MIT. An AIME member, he likes golf and fishing.

N. J. Grant (p. 1237) is Associate Professor of Metallurgy at MIT. He has also been Open Hearth Metallurgist for Bethlehem Steel Co., and Research Associate at MIT. Carnegie Tech and MIT awarded him B.S. and Sc. D. degrees. A member of AIME, he has presented several papers mostly on steelmaking.

J. B. Newkirk

C. A. Wert (p. 1242) is Research Associate Professor of Mining and Metallurgy at Univ. of Illinois. Until this fall term, he was Instructor at the Institute for the Study of Metals, and had previously been asso-

N. J. Grant

F. W. Daniels

C. G. Dunn

H. R. Ogden

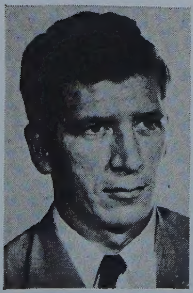

B. H. Alexander

ciated with the MIT Radiation Lab. He holds a B.A. from Morningside College, and M.S. and Ph.D. degrees from Iowa State. His hobbies are hiking, fishing, gardening, and photography.

F. W. Daniels (p. 1245) is Metallurgist at General Electric in Pittsfield, Mass. He was formerly with the U.S. Air Force, and had been Welding Research Fellow at Rensselaer Polytechnic Inst. where he received his B. Met. E. degree. He enjoys bowling, golf, and photography.

C. G. Dunn (p. 1245) is Research Physicist, General Electric Co., in Pittsfield. He obtained his B.A. at Montana State, and his Ph.D. at Univ. of Illinois, where he was also Graduate Assistant in Physics. An AIME member, he has previously contributed several papers. Bird Watching is his hobby.

M. J. Bolton (p. 1245), Group Leader in Nonferrous Metallurgy, for General Electric Co. in Pittsfield, was born in England. After earning his B.S. degree at University of Alabama, he was Research Assistant on the Manhattan Project. His hobbies are golf, bowling, and building ship models.

A. H. Geisler (p. 1249) is Research Associate at General Electric Lab in Schenectady, N. Y., and was formerly Research Metallurgist for Aluminum Research Lab. He studied at Carnegie Institute of Technology for his B.S. and D. Sc. degrees. An AIME member, he has presented several papers before the Institute, and in 1944 was co-recipient of the IMD award.

D. L. Martin (p. 1249) is Research Associate for General Electric Co. at Schenectady, N. Y. He studied at Penn State and Yale, receiving B.S. and D. Eng. degrees. He is a member of AIME.

D. J. Maykuth (p. 1261) is Research Engineer at Battelle Memorial Institute, after serving in the Army as a Corporal in Biological Warfare. He was born in Detroit, and received his B.S. in Met. E. degree at Michigan College of Mining & Technology. An AIME member, he plays golf.

H. R. Ogden (p. 1261) is associated with Battelle Memorial Institute as Research Metallurgist. He was formerly a Captain in Army Ordnance. Michigan College of Mining & Technology awarded him a B.S. in Met. E. degree. A Junior Member of AIME, he likes golf and gardening.

R. I. Jaffee (p. 1261). See JOURNAL OF METALS, September, 1949.

B. H. Alexander (p. 1267) is associated with Sylvania Electric Products Co. at Bayside, L. I. He studied for his B.S. at Montana School of Mines, and his M.S. and D.Sc. degrees at Carnegie Institute of Technology, where he became Assistant Professor of Metallurgy. He is an AIME member.

F. N. Rhines (p. 1267) is Professor of Metallurgy and Member of Staff of the Metals Research Lab, Carnegie Institute of Technology. A long time member of AIME, he has contributed numerous articles to the Institute.

New Products, Services and Information....

Products and services recently announced are described here. Also, new publications offered free by producers servicing the metalworking industry are listed.

For further information on any product or for your copies of the free publications, fill in the coupon below and send it to the *Journal of Metals.*

1—PORTABLE INDUCTION UNIT: To heat a 1-in. length of steel rod to 1500°F in approximately 3 sec, a new high frequency induction heating unit has been designed by the *Lepel High Frequency Laboratories, Inc.* It will braze carbide tips to cutting tools up to 1½ in. square; melt 4 oz of steel or brass in 4 min. Price, $780.

2—NEW METHOD OF INSPECTING METALS: Without the use of electricity, lights or other special equipment, a new process for inspecting metal surfaces and detecting any openings such as cracks, laps, cold-shuts or porosity has been developed. Dy Chek Penetrant is left on the surface for 5 or 6 min, then removed with Dy Chek cleaner. The developer is then applied. The red penetrant will remain in any crevice until it is drawn to the surface by the action of the white developer, providing a white background for red indications. The penetrant costs $9.50 per qt, developer, $4.75 per qt, and cleaner, $3.00 per gal. *Dy Chek Co., Div. of Northrop Aircraft, Inc.*

3—HYDRAULIC-PRESSURE ELECTRIC SWITCH: Designed for precise control of electric circuits by means of hydraulic pressure, the new Pantex hydraulic pressure electric switch of the *Pantex Mfg. Corp.* will cut in and cut out electric circuits with as little as 12 to 18 pct pressure differential. The unit withstands a wide temperature differential ranging from —65°F to +160°F without loss of accuracy or other desirable operational characteristics. It operates immediately with every start of the pump and requires no pressure buildup.

4—PHOTOELECTRIC COLORIMETER: Newly developed by the *Photovolt Corp.* is the Lumetron Photoelectric Colorimeter Model 401. It is designed for measurements on liquids and solutions in analytical laboratories, and production control work. Equipped with a single photocell, it furnishes the readings directly by the indication of the needle on the meter scale. For measuring transparent color of clear liquids it is furnished with 6 color filters to isolate the wavebands in which the liquids have maximum absorption. The Colorimeter is designed to be operated with three sizes of tubes, the standard size of 18 mm OD and the two additional sizes of 22 and 14 mm OD. The standard 18 mm tubes are suitable for most colorimetric applications. Price, $158.

Journal of Metals
29 West 39th St.
New York 18, N. Y.

October

Please send me

More Information ☐
Free Literature ☐
Price Data ☐

on items indicated.

1	2	3	4	5	6	7	8	9	10
11	12	13	14	15	16	17	18	19	20
21	22	23	24	25	26	27	28	29	30
31	32	33	34	35	36	37	38	39	40

Name .... Title.................
Company ....
Street ....
City and Zone .... State................

5—MICROSCOPE LENS: Available for extending the magnification range in electron microscopy is a removable intermediate lens. It is the RCA Model EMU-2C, an accessory for all EMU-Type RCA electron microscopes. Without breaking vacuum any of ten values—between 900 and 21,000 diam—may be changed by merely turning a knob on the control panel. In addition to extending the magnification range from a ratio of 4:1 to one of 25:1, the new lens provides a full field of view at all magnifications. The unit is 2⅜ in. in height and 3¼ in. in diam, permitting it to fit easily through the opening in the intermediate chamber shielding. The lens is supplied with cable, resistor, and installation instructions. *Radio Corporation of America, RCA Victor Div.*

6—ANEROID BAROMETER: Using the first new principle in aneroid construction in over 100 years, the *American Paulin System* has developed a supersensitive aneroid barometer—accurate to 1/1000 in. of mercury. It permits reliable indication of minute changes in air pressure. With etched graduations reading to 1/1000 in. Hg and accurate to one graduation, the micro barometer gives instantaneous readings without corrections for temperature and latitude. Model PMB-1 has a range extending from 24.80 in. to 31.00 in. Hg. Other ranges are available on request.

7—RUST PREVENTATIVE: For spraying metal parts and fabrications in storage and production, guns, firearms, tools, implements, etc. a rust preventative oil and lubricant called 'Gun Guard,' and packaged in an Aerasol container, is being introduced to the market by the *Mitchell-Bradford Chemical Co.* Its use for corrosion resistance is supplemented by use as a nitro powder solvent to facilitate the removal of burnt powder and lead in gun barrels. Because of the water displacing characteristics it is ideal for fishing reels.

8—THERMOMETER TESTER: *Weston Electrical Instrument Corp.,* presents from their Tagliabue Instruments Div., an ASTM certified thermometer testing set, composed of nine matched thermometers with overlapping ranges from —36 to 760°F., and from —38 to 405°C. Calibrations are in 1/10, 1/5 and ½°C and 1/5, ½ and 1°F., with each thermometer accurate to within one scale division. Each thermometer is furnished with a TAG test room certificate of accuracy, listing compensations for individual scale characteristics. Certificates are obtained by calibration against National Bureau of Standards thermometers.

9—RADIOACTIVE WASH: While it does not neutralize radioactivity or the physiological effects of radiation, a new solution for cleaning surfaces contaminated by radioactivity, called Radiacwash, prepared by the *Atomlab,* assists in lifting-up contamination prior to penetration. The liquid acts as a combination detergent, emulsifer, solvent, ion-extractor, surface wetter, and carrier.

10—ARC WELDING PROCESS: Employing welding current densities on 5/64 in. electrodes which melt the electrode at speeds comparable to using 10,000 amp on a standard 5/16 in. diam coated hand electrode, a new process has been devised by the *Lincoln Electric Co.* It uses either a 3/32 or a 5/64 in. diam electrode wire. Welding currents up to 600 amps are used with these wires which, on the small cross sectional area of the wire, produce extremely high current densities. A manual Lincolnweld ML-2 unit for using the Hidensity process is connected to any standard Lincoln SAE 600 or 900 amp welding generator, providing all the features of an automatic head. It can be operated any practical distance from the generator and used on all types of flat and near flat work.

11—FURNACE LINING: At 50 pct of the usual price and able to meet or surpass specifications for any refractory, a super refractory for lining high-temperature furnaces has been developed by the *Babcock & Wilcox Co.* It is called Allmul and will not melt until heated to more than 3300°F, a point nearly one-third higher than the melting point of steel. Manufactured principally in the form of firebrick it will also be available in the form of grain and ramming mixes.

12—CHECK VALVES: Circle Seal check valves are now available from ⅛ to 1 in. NPT. Two models are designed for standard and very low pressure systems; both are poppet type using an "O" ring seal. Absolute sealing, minimum flow resistance, and leakproof dependability for pneumatic and hydraulic systems are features of the new line. They are manufactured by *James-Pond-Clark.* An added feature of the design is quick opening and positive closing at extremely low pressures. The valves have positive action, long life, minimum maintenance, negligible flow resistance, and leakproof performance.

13—PROVING RINGS: For calibrating loads of various types of testing machines Steel City Proving Rings of the direct reading type, whereby deflection of the ring under load is accurately measured by a dial indicator, come from the *Steel City Testing Machines, Inc.* Graduations on the indicator are in 0.0001 in. and the resultant readings are translated into pounds. No skilled operator is necessary to get accurate results. They are made in two styles, oval shaped having a capacity up to 20,000 lb, and round shaped for rings up to 110,000 lb capacity. All rings conform to ASTM standard E4.

14—PLASTIC DESIGN MODELS: "Internal vision" for design engineers is provided by a new plastic that can be made into scale models of machine parts and tools. Three dimensional scale models cut from the plastic enable engineers to get a portrait in color of the strains encountered in tools, machine parts and other objects. *Westinghouse Electric Corp.*

15—STRAIN AMPLIFIER: *Baldwin Locomotive Works* announced a portable strain amplifier for use with any standard cathode ray oscilloscope to measure almost any mechanical reaction detected by SR-4 bonded resistance wire strain gages. It may be used for load measurements, stress analysis and function analysis during operation of equipment to show amplitude, frequency and wave form of sharp transients, steady state oscillations, static loads or their combinations. The amplifier reproduces all frequencies between flat 5 to 20,000 cps.

16—TESTING MACHINE: Newly marketed is a simplified table model universal testing machine for tension, compression, flexure, shear, and transverse tests, in two capacities, 30,000 and 15,000 lb. It is 42 in. high, 64 in. wide, and weighs 1200 lb. *Testing Machine Div., National Forge and Ordnance Co.*

* A new process for producing electrolytic chromium will be put into operation by the Electro Metallurgical Div., Union Carbide and Carbon Corp., in a proposed plant at Sault Ste. Marie, Mich. The process combines steps developed by the Bureau of Mines and by the company. The metal produced is said to be a higher purity than any chromium metal now available commercially.

* Dutch Parliament approved Dutch participation in extending the Ymuiden blast furnace and steelworks, and forming a company to erect and work a wide strip rolling mill and tinplate factory. ECA is indicating availability of $23 million for purchase of U.S. industrial equipment.

* An aluminum shell with a plastic liner, providing a lighter and tougher helmet for the Army, is undergoing field tests and may replace the present heavy steel helmet.

* A single magnesium casting of the outer half of an aircraft wing will be made by Northrup Aircraft, Inc. under a U. S. Air Force Contract. The new wing will be compared with an identical part made by conventional fabrication methods.

* Bi-metallic gas turbine stator blades, having aluminum alloy roots for easy machining, are under study in England by Wellworth Pistons, Ltd., holder of the British license for the molecular bonding of aluminum to steel by the Al-Fin process. Primary object of the study is to develop a rapid, economical method of manufacturing compressor stator assemblies.

* To spend some of the sterling received in payment for oil products by agreement with the British Gov't. Standard Oil Co. (N.J.) will purchase new tankers from British shipbuilders. The new tankers will be modifications of the more recent types built here, and will have a deadweight tonnage of 26,650 tons.

* A seamless aluminum sheathing for telephone and electric power cables, thinner, stronger, and lighter in weight than lead sheathing, now can be applied by a new method involving swaging, developed by Alcoa.

* Manganese, one of the most critical of strategic metals, will be produced in this country through money granted by the House Appropriations Committee for development of manganese resources.

* Economy and efficiency are keynotes in Defense Dept. contracts, according to a policy announced by the Munitions Board on contracting, pricing and profit. Adequate profit margins will be allowed, but contingency allowances will be curtailed. Prevention of excess profits, rather than subsequent renegotiation, is one aim, as well as conservation of manpower, materials and facilities.

* Another prospective producer is setting up for a capacity of 2000 lb. of titanium alloy ingot per day. Sponge will be obtained from an outside source.

* Higher-than-going rates have been authorized by the Munitions Board for its stockpile program, in cases where domestic production of scarce materials is low or uneconomical. Payment in excess of 25 pct over the foreign price is now permitted.

The
Drift of Things . . . . as followed by Edward H. Robie

At Salt Lake City

This is a warm Sunday morning in Salt Lake City at the end of a hectic convention week. Some 4500 mining men have stormed "The Crossroads of the West," a new record by far. Today the Sunday quiet is welcome, even though we had to eat breakfast alone. We have just returned from the Temple grounds where, from 8:30 to 9, we heard the 1098th Sunday broadcast of the Tabernacle choir and organ. Thousands of others were there too. Having heard it in their homes they were curious. They were not let down, for the setting is most impressive. After the formal program we listened to a 20-min rehearsal of a future program. Also, we introduced ourselves to Richard Evans, he of "the spoken word." Mr. Evans is a bespectacled, slender, black-haired, earnest, pleasant man of about 40. He was formerly a radio announcer on station KSL. He himself writes the little 3-min sermons that he delivers so well.

When in Salt Lake one of the interesting things to do is to participate in one of the guided tours through the Temple grounds. This morning the groups were large. To what extent they were convinced of the authenticity of the story of the founding of the Mormon Church through the revelation bestowed on teen-age Joseph Smith at Palmyra, N. Y. more than a hundred years ago we do not know. The guide admitted the episodes sounded fantastic. No more so, however, than the early history of other religions. Though unconvinced, one would indeed be rash to say that miracles cannot happen.

Salt Lake is one of our favorite cities. It is clean and well kept. Its streets, some 90 ft wide, were laid out with surprising vision. Water continuously flows down the gutters of Main St. The busses are unobtrusive and quiet. The water has a good taste, with no suggestion of chlorine. The people look like good Americans. The only place, so far as we see, where liquor is sold is in a comparatively obscure store, not listed in the telephone book, run by the Utah Liquor Control Commission. We accompanied one of our renegade friends who knew his way there. One must have a permit, and purchase of more than a bottle or two is viewed with some suspicion.

The Hotel Utah, owned by the Mormon Church, is one of America's fine hotels, reasonably priced, well kept, staffed and provisioned. The young ladies who greet you at the desk, run the elevators, and wait on the tables are attractive and well groomed. Practically not a red fingernail in the lot, and is that a relief. The Starlite Gardens on the 10th floor is equally as attractive as the Starlite Roof of the Waldorf-Astoria in New York, and the absence of cocktails lends it a unique atmosphere. To be sure, one may be disillusioned if one peeks under the tables, but that isn't fair. In the Coffee Shop—and won't someone please think up a new name for an informal restaurant—one may have the privilege of breakfasting off a Cranshaw melon and a Utah Pioneer griddle cake. The paper money one gets in change is all brand new. Even the half dollars and quarters are polished to mint-brightness, a stunt that we believe the St. Francis Hotel in San Francisco practices. The Treasury Dept., as we recall, got after them for presumably illegally recovering the silver from the operation, but the hotel proved that it all went down the drain. If they wasted it, it was all right.

All of which is introductory to saying that the AIME has a new field office in Salt Lake. Roy E. O'Brien, an Anaconda man, has been appropriately embued with enthusiasm for the AIME, has passed the elementary examination on what makes it tick and why one should belong, and has set up an office in the Newhouse Bldg., 10 Exchange Place, as Western Secretary of the Mining Branch. He will be glad to see his many friends there and to do what he can for AIME members west of the Mississippi. Even metallurgists and oil men will be welcomed if they don't stay too long. Much of Roy's time, though, will be spent in the field, helping members in the more remote places who may have problems, assisting in building up Local Sections, promoting interchange of technical information, and interesting new people in the Institute. Any members wishing him to call on them when in their neighborhood should drop him a line. The success of Bill Strang and Joe Alford in establishing the Dallas office of the Petroleum Branch presages an equally bright future for the Salt Lake office.

We have already mentioned the reason why we are here—the 1950 Metal Mining Convention and Exposition of the Western Division of the American Mining Congress. Julian Conover and his staff did a marvelous job. Of the record attendance of some 5588, 4525 were operating men, suppliers, and 1063 ladies. The exhibits were worthy of attendance, the 125-odd exhibitors having their newest models on display in profusion. The AIME had a booth for the first time in recent years. The Institute's meetings do not feature machinery and equipment, except on a small scale by the Petroleum Branch, so the Mining Congress offers a unique opportunity for sales engineers and operating men to get together. Problems of economics, taxation, and legislation loomed large in the group meetings. We did not attend too many sessions, nor stay too long, the temperature being what it was. But we gathered that the small mine still has its ups and downs—mostly the latter so far this year; that the Government isn't doing what it should; and that there is a difference of opinion as to just what action we should take.

Utah's Governor, J. Bracken Lee, made a wonderful impression on everyone at the Welcoming Luncheon. He talks like the kind of man we need at Washington. As to whether his actions are in accord with his words, the comment of Utahns (we don't like that term much either) is favorable, but we are just naturally suspicious after the experience of the last two decades. How about Eisenhower and Lee in 1952?

Bingham Canyon was the destination on the first night. An al fresco spaghetti and bean supper was served on long tables on the new parking lot overlooking the pit. The "Galena Days" celebration was on, which means the natives had grown beards, the store windows were full of old-time signs, and gambling games were unrestricted. Bingham is the greatest man-made sight we have ever seen—maybe the greatest in the world.

Thursday night's annual banquet was at the Rainbow Randevu, "the World's Largest Ballroom," where 1700 were comfortably seated. Here we got our biggest scare in some time. A short circuit in a power cable in the street put all lights out for half an hour. Matches were lighted here and there, and candles appeared. Not a sign of a red exit light in the entire place. When the lights came on, only two green exit lights could be noted. We hope God continues to watch over Salt Lake City.

Our own AIME Minerals Beneficiation Division and our Board of Directors had meetings, too, and well attended and most successful ones. But we must thank the Mining Congress for bringing the crowd.

New Conveyor Principle

Self-Centers Load

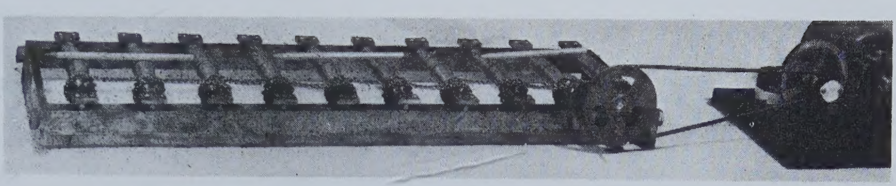

Pencils line up after passing over a series of self-centering rolls.

A new self-centering roll promises to revolutionize conveying methods for an almost unlimited list of materials. The principle of *planar action* was built into working models by E. T. Lorig, chief of the senior engineering staff of Carnegie-Illinois Steel Corp., largest subsidiary of United States Steel, and is now being used in various steel handling applications in corporation operations.

Fundamentally the Lorig self-centering roll is a slightly crowned roll cut transversely at the center. The two halves are fixed to rotate as a unit. The working surfaces of the two parts are approximately horizontal, while the axes are at an angle. In this way, the planes, or lines of force in both halves twist evenly toward the center in the direction of movement, conferring a self-centering action on any materials passing over the rolls.

The rolls have been tested for various types of applications including runout tables, feed and guide rolls for electrolytic tinning, galvanizing and pickling lines, gravity conveyors, belt pulleys and conveyors and similar applications in the steel industry.

In its practical applications in the steel industry, the self-centering roll will eliminate the need for table guides and side rails on runout tables and in many other conveyor applications, thus eliminating edge and corner damage to sheets, strip and plates. Width of conveyor tables and runout tables can be reduced; and gravity conveyors, whether straight or curved, can be built to operate efficiently with no guide rails. Belt drives are practical and safe, even with an overhung takeoff. Operating on self-centering rolls, stainless steel conveyor belts are now practical and safe under low operating tensions.

Self-centering rolls are now being manufactured at Carnegie-Illinois Steel Corp.'s Johnstown Works, and experiments are underway at the Isabella Furnaces to develop a stainless steel conveyor belt operating on self-centering rolls to handle hot sintered ferromanganese flue dust. A pickling line equipped with self-centering rolls is in operation at the McDonald Works at Youngstown, Ohio, and another installation is operating on a galvanizing line at the Tennessee Coal, Iron & Railroad Co. plant at Fairfield, Alabama.

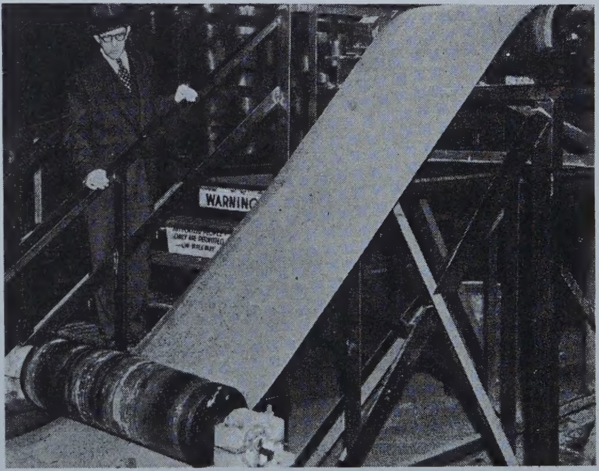

The Lorig roll eliminates the need for guides on this pickling line installation.

Republic and Armco Acquire Reserve Mining Co. Stock, To Build Pellet Plant

Republic Steel Corp. and Armco Steel Corp. have joined in a $160,000,000 project for the production of iron ore from Taconite in the Lake Superior mining region. The two companies announced acquisition in equal shares of 100 pct ownership of the stock of Reserve Mining Co., which controls a vast deposit of magnetic Taconite iron ore on the eastern end of the Mesabi range in Minnesota.

Through Reserve Mining the two companies will build a plant for manufacturing high grade ore from Taconite near Beaver Bay on the north shore of Lake Superior. The first announcement calls for about a $60,000,000 plant which will be built as soon as plans are completed and will have an annual capacity of about 2,500,000 tons of iron ore pellets.

Longer range development plans call for future expansion of the plant to provide an annual capacity of 10,000,000 tons. This will amount to an additional investment of $100,000,000, the company said. Financing and actual production plans were not disclosed. An organization meeting of Reserve Mining under the new ownership is planned for next month, when financing and other operating details will be worked out.

Armco had held one third interest in Reserve Mining with Wheeling Steel Corp. holding one third and the remainder being held by Cleveland-Cliffs Iron Co. and Montreal Mining Co. Republic Steel has now acquired the former holdings of Cleveland-Cliffs and Montreal Mining and half the interest of Wheeling. Armco has acquired the other one half of Wheeling Steel holdings—thus, each of the companies holds a half interest in the new Reserve Mining Co. structure. Oglebay, Norton & Co., Cleveland, who has managed Reserve Mining properties, will continue in that capacity.

Research in Progress

Research, the foundation of American industrial growth, is a major feature of the AIME, Institute of Metals Div., Technical Sessions at the Metal Congress and Exposition, Oct. 23 to 25, 1950, Chicago. Reports at the Research in Progress sessions have been abstracted and are included in this section of JOURNAL OF METALS. These reports, many of which are incompleted projects, bring to light new work and new techniques.

AIME, through its Institute of Metals Div., will participate as in former years in the Metal Congress and Exposition through the media of a series of technical sessions. These sessions, scheduled for the first three days of the Metal Show, will be held at the Hotel Sheraton. One of the features of the AIME sessions will be its ***Research in Progress*** sessions, designed to bring to light incompleted research projects. These discussions may help in the completion of the work, as well as help others working on similar projects.

This year registration for the Fall Meeting of the Institute of Metals Div., AIME, will start on Sunday, Oct. 22, the day before the meeting opens. Members are urged to register on Sunday at the Sheraton Hotel. On the following three days registration will be near the session rooms. The registration fee for members is $2 and for non-members, $4, and includes reprints of most of the papers, as long as the supply lasts. There will be no registration fee for Student Associates of AIME, or for those attending the dinner only.

The Annual Fall Dinner will be held in the Boulevard Room of the Sheraton Hotel on Tuesday, Oct. 24 at 7 pm. At 6 pm preceding the dinner, there will be a cocktail party in the Tropical Room for dinner guests, given with the compliments of the Chicago members of AIME and their friends. Tickets for the dinner will admit the holders to the cocktail party. Ladies are cordially invited to the cocktail party and dinner. Business suits will be appropriate. The principle speaker will be Dr. Louis L. Thurstone, Charles F. Grey Distinguished Service Professor of Psychology, University of Chicago. Dr. M. Gensamer, Chairman of the IMD will be the toastmaster.

There will be no formal seating plan, although the local committee has made arrangements to reserve complete tables of ten. Dinner tickets will cost $5 each and tables can be reserved for $50 per table through J. H. Reese, Revere Copper and Brass, Inc., 2200 North Natchez Ave., Chicago 35, Ill. Individual tickets will be on sale at the registration desk during the meeting.

The Program Committee has planned two new types of sessions at this Fall Meeting in addition to the usual technical sessions of preprinted papers. A session on ***Research in Progress*** reports has been arranged by Morris Cohen. Abstracts of the reports appear on pages 1210 to 1220 in this issue. A few of these reports will be scheduled as part of the regular technical sessions. A few technical notes also are being presented this year, as well as some papers approved for publication too late to permit prepublishing.

A second innovation at the Fall Meeting will be the informal technical session on Monday evening. This session, also arranged by Morris Cohen, will provide a discussion on Precipitation Hardening. Following the discussion limited to panel members, the audience will be encouraged to participate. Finally, the large group will be broken up into informal groups with a member of the panel assigned to each group. Light refreshments will be available, for which there will be a small charge.

The Program Committee is anxious that ample time be provided for discussion of each paper. Those who plan to discuss a paper are urged to advise the secretary of the session on which the paper is scheduled. The secretary should be advised, preferably well in advance of the meeting, of how much time is required (maximum 5 minutes) so that he may plan a tentative time schedule.

☆ INSTITUTE OF METALS DIV.

HOTEL SHERATON

Sunday 7:30 p.m.—Oct. 22 Rooms 809-810

Institute of Metals Division Program Committee Meeting

Monday 9 a.m. to 12 m.—Oct. 23 Boulevard Room

Plastic Deformation

B. Averbach, Chairman
P. Kosting, Secretary

An Experimental Survey of Deformational and Annealing Processes in Zinc. D. C. Jillson, The New Jersey Zinc Co. JOURNAL OF METALS, August.

Quantitative Stress-Strain Studies on Zinc Single Crystals in Tension. D. C. Jillson. JOURNAL OF METALS, September.

A Study of the Plastic Behavior of High-Purity Aluminum Single Crystals at Various Temperatures. F. D. Rosi, Sylvania Research Laboratories, and C. H. Mathewson, Yale University. JOURNAL OF METALS, September.

A Study of Strain Markings in Aluminum. B. R. Banerjee, Standard Oil Co. (Ind.). JOURNAL OF METALS, September.

Rolling Texture in Aluminum. H. Hu and P. A. Beck, University of Notre Dame. Research in Progress, JOURNAL OF METALS, October.

Monday 4 p.m.—Oct. 23 Rooms 809-810

Institute of Metals Division Membership Committee Meeting

Monday 2 p.m. to 5 p.m.—Oct. 23 Boulevard Room

Recrystallization and Annealing Textures

R. Maddin, Chairman
C. Dunn, Secretary

Activation Energy for Recrystallization in Rolled Copper. B. F. Decker and D. Harker, General Electric Co. JOURNAL OF METALS, June.

Recrystallization Reaction Kinetics and Texture Studies of a 50 Iron 50 Nickel Alloy. W. E. Seymour, Rensselaer Polytechnic Inst., and D. Harker, General Electric Co. JOURNAL OF METALS, August.

Annealing Texture in Rolled Aluminum Strip. P. A. Beck and H. Hu, University of Notre Dame. Research in Progress, JOURNAL OF METALS, October.

The Textures of Cold-Rolled and Annealed Titanium. H. T. Clark, Jr., Remington Arms Co., Inc. JOURNAL OF METALS, September.

Relative Energies of Grain Boundaries in Silicon Iron. C. G. Dunn, F. W. Daniels and M. J. Bolton, General Electric Co. JOURNAL OF METALS, October.

Production and Examination of Zinc Single Crystals. D. C. Jillson, The New Jersey Zinc Co. JOURNAL OF METALS, August.

Monday 2 p.m. to 5 p.m.—Oct. 23 Tropical Room

Structure of Alloys

B. D. Cullity, Chairman
Earl Parker, Secretary

Solid Solubility of Cementite in Alpha Iron. C. A. Wert, University of Illinois. JOURNAL OF METALS, October.

The Structure of Intermediate Phases in Alloys of Titanium with Iron, Cobalt, and Nickel. P. Duwez and J. L. Taylor, California Inst. of Technology. JOURNAL OF METALS, September.

The Alloys of Titanium with Carbon, Oxygen and Nitrogen. R. I. Jaffee, H. R. Ogden, and D. J. Maykuth, Battelle Memorial Institute. JOURNAL OF METALS, October.

Correlation Between Electrical and Thermal Conductivity in Ni and Ni Alloys. M. E. Fine, Bell Telephone Laboratories. JOURNAL OF METALS, July.

Monday 7:30 p.m.—Oct. 23 Tropical Room

Informal Evening Session—Panel Discussion on Precipitation Hardening

Morris Cohen, Moderator

Panel members: B. L. Averbach, MIT; C. S. Barrett, Univ. of Chicago; W. L. Fink, Aluminum Co. of America; A. H. Geisler, General Electric Co.; A. Guinier, Conservatorie Nat'l. des Arts et Metiers, Paris; J. H. Hollomon, General Electric Co.; R. F. Mehl, Carnegie Institute of Technology; Cyril Stanley Smith and Clarence Zener, University of Chicago.

Tuesday 9 a.m. to 12 m.—Oct. 24 Tropical Room

Transformations

A. R. Troiano, Chairman
J. B. Hess, Secretary

On the Martensitic Transformation at Temperatures Approaching Absolute Zero. S. A. Kulin and M. Cohen, Massachusetts Inst. of Technology. JOURNAL OF METALS, September.

Austenite Formation During Tempering and its Effects on Mechanical Properties. E. F. Bailey and W. J. Harris, Jr., Naval Research Laboratory. JOURNAL OF METALS, August.

The Isothermal Transformation of a Eutectoid Beryllium Bronze. R. H. Fillnow, Westinghouse Electric Corp., and D. J. Mack, University of Wisconsin. JOURNAL OF METALS, October.

The Ordering Reaction in Cobalt-Platinum Alloys. J. B. Newkirk and R. Smoluchowski, Carnegie Institute of Technology, A. H. Geisler and D. L. Martin, General Electric Co. JOURNAL OF METALS, October.

Tuesday 9 a.m. to 12 m.—Oct. 24 Boulevard Room

Properties of Alloys

R. M. Parke, Chairman
V. Pulsifer, Secretary

The Effect of Alloying Elements on the Plastic Properties of Aluminum Alloys. J. E. Dorn, P. Pietrokowsky and T. E. Tietz, University of California. JOURNAL OF METALS, July.

The Properties of Some Mg-Li Alloys Containing Al and Zn. R. S. Busk, D. L. Leman, and J. J. Casey, Dow Chemical Co. JOURNAL OF METALS, July.

The Effect of Sodium Contamination on Magnesium-Lithium Base Alloys. P. D. Frost, J. H. Jackson, C. H. Lorig, Battelle Memorial Institute, and A. C. Loonam, Deutsch and Loonam. JOURNAL OF METALS, September.

Young's Modulus and its Temperature Dependence *in 36 to 52 Pct Nickel-Iron Alloys.* M. E. Fine and W. C. Ellis, Bell Telephone Laboratories. Journal of Metals, September.

Hydrogen Embrittlement of SAE 1020 Steel. J. B. Seabrook, N. J. Grant and Dennis Carney, Massachusetts Institute of Technology. Not prepublished.

Aging Characteristics of Magnesium-Lithium Base Alloys. P. D. Frost, J. G. Kura and L. W. Eastwood, Battelle Memorial Institute. Journal of Metals, October.

Tuesday 12:15 p.m.—Oct. 24 Room 815

Institute of Metals Division Executive Committee Luncheon Meeting

Tuesday 2 p.m. to 5 p.m.—Oct. 24 Boulevard Room

Metal—Gas Reactions

M. Bever, Chairman
T. Leontis, Secretary

The Vapor Pressure of Silver. H. M. Schadel, Jr. and C. E. Birchenall, Carnegie Institute of Technology. Journal of Metals, September.

Hydrogen Solubility in Aluminum and Some Aluminum Alloys. W. R. Opie, National Lead Co., and N. J. Grant, Massachusetts Institute of Technology. Journal of Metals, October.

Composition of Atmospheres Inert to Heated Carbon Steel. R. W. Gurry, United States Steel Corp. Journal of Metals, April.

Equilibrium in the Reaction of Carbon Dioxide with Liquid Copper from 1090° C to 1300° C. D. J. Girardi, Timken Roller Bearing Co., and C. A. Siebert, University of Michigan. Journal of Metals, September.

The Intermittent Oxidation of Some Nickel-Chromium Base Alloys. B. Lustman, Westinghouse Electric Corp. Journal of Metals, August.

Hydrogen Elimination by Aging. C. E. Sims, Battelle Memorial Institute. Not prepublished.

Tuesday 2 p.m. to 5 p.m.—Oct. 24 Tropical Room

Solidification, Thermal Expansion & Ductility

R. S. Busk, Chairman
A. J. Smith, Secretary

Dendritic Crystallization of Alloys. B. H. Alexander, Sylvania Electric Products Co., and F. N. Rhines, Carnegie Institute of Technology. Journal of Metals, October.

The Supercooling of Aggregates of Small Metal Particles. D. Turnbull, General Electric Co. Journal of Metals, September.

The Thermal Expansion Characteristics of Beryllium. R. M. Treco, Massachusetts Institute of Technology. Journal of Metals, October.

The Ductility of Cast Molybdenum. R. B. Fischer and J. H. Jackson, Battelle Memorial Institute. Journal of Metals, September.

Effect of Rate of Freezing on Degree of Segregation in Alloys. W. T. Olsen, Jr. and R. Hultgren, University of California. Not prepublished.

Wednesday 12:15 p.m.—Oct. 25 Rooms 809-810

Institute of Metals Division Powder Metallurgy Committee Luncheon Meeting

Wednesday 2 p.m. to 5 p.m.—Oct. 25 Tropical Room

Technical Session on Research in Progress

M. Cohen, Co-chairman
R. F. Mehl, Co-chairman

On the Temperature Dependence of Self-Diffusion in Alpha Iron. I. D. Bakalar, Massachusetts Institute of Technology. Research in Progress, Journal of Metals, October.

Effect of Uniaxial Compressive Stresses on Self-Diffusion in Alpha Iron. F. S. Buffington, Massachusetts Institute of Technology. Research in Progress, Journal of Metals, October.

Interfaces in Diffusion in Solid Solutions. L. C. C. da Silva and R. F. Mehl, Carnegie Institute of Technology. Research in Progress, Journal of Metals, October.

Order-disorder Phase Change in Cu_3Au Alloys. F. N. Rhines, Carnegie Institute of Technology. Research in Progress, Journal of Metals, October.

Application of Radioactive Tracers to the Study of Metal-Solution Reactions. M. T. Simnad, Carnegie Institute of Technology. Research in Progress, Journal of Metals, October.

Measurements on the Rate of Secondary Recrystallization in High Purity Silver. F. D. Rosi and B. H. Alexander, Sylvania Electric Products, Inc. Research in Progress, Journal of Metals, October.

The Plastic Behavior of Silver Single Crystals at Various Temperatures. F. D. Rosi, Sylvania Electric Products, Inc. Research in Progress, Journal of Metals, October.

Yielding in Plain Carbon Steels. C. S. Roberts and B. L. Averbach, Massachusetts Institute of Technology. Research in Progress, Journal of Metals, October.

On the $\{259\}_\gamma$ Habit of Martensite. E. S. Machlin, Massachusetts Institute of Technology. Research in Progress, Journal of Metals, October.

Precementitic Carbides in Tempered Martensite. E. C. Roberts, Massachusetts Institute of Technology. Research in Progress, Journal of Metals, October.

Source of Abnormality in Hypereutectoid Steels. Arthur Dube, Sylvania Electric Products, Inc. Research in Progress, Journal of Metals, October.

Wednesday 2 p.m. to 5 p.m.—Oct. 24 Boulevard Room

Powder Metallurgy

F. V. Lenel, Chairman
J. C. Redmond, Secretary

A Process for Hot Pressing Beryllium Powder. A. U. Seybolt, R. M. Linsmayer and J. P. Frandsen, General Electric Co. Steel, March 27.

The Densification of Pre-reduced Copper Powder Compacts in Vacuum and in Hydrogen. C. B. Jordan and P. Duwez, California Institute of Technology. Journal of Metals, July.

Experiments on the Mechanism of Sintering. B. H. Alexander and R. Balluffi, Sylvania Electric Products, Inc. Research in Progress, Journal of Metals, October.

Studies on Control of Growth or Shrinkage of Iron-Copper Compacts During Sintering. J. F. Kuzmick, Welded Carbide Tool Co., and E. N. Mazza, Ekstrand & Tholand, Inc. Research in Progress, Journal of Metals, October.

Precementitic Carbides in Tempered Martensite

by Earl C. Roberts

THE third stage of tempering quenched steel is the development of cementite from an initial product which makes its appearance during the first stage. While studies of cementite have shown it to be relatively amenable to investigation, studies of the first stage product have been limited, for the most part, to evaluation of the physical changes it causes in the martensite in which it forms. Thus X-ray[1], magnetic, dilatometric, specific volume and hardness[2] determinations have all contributed to the evidence for its presence but because of its transitory nature the actual composition and structure of the carbon-bearing phase which precedes cementite formation have proved quite difficult.

As a result of the physical determinations which were made on steel tempered to the first stage condition, the postulation has been that the changes which occur are typical of a transition phase or one which exists in a temporary or transient status. This picture has been somewhat altered, however, by the isolation of the carbide phases which occur in tempered steel. It now appears quite definite that the initial carbon-rich structure is not a transition precipitate, in the usual sense, but a distinct entity in itself with no coherency existing between the carbide and matrix. Its individuality also indicates that it forms in quenched martensite with greater rapidity than cementite, and its growth to larger particle size than early cementite[3] must mean that the cementite particles form as a result of a competitive process. In such a process the initial carbide is visualized as gradually redissolving in the matrix and thus giving way to cementite precipitation.

Carbides showing a structure other than that of cementite were isolated previously in the hydrochloric acid cell used by Crafts and Lamont[4]. Investigations made with a martensitic anode in a complex electrolytic cell have shown that it is possible to extract similar carbide structures in an apparently more perfect condition. Martensitic steel tempered to different states with respect to time and temperature has shown that a phase (or phases) other than cementite exists over a wider range of tempering conditions than was previously realized. More specifically, cementite is not the only carbide present after tempering a 1.06 C Steel up to 16 hr at 700°F (371°C) and up to 128 hr at 500°F (260°C).

The carbides obtained from each condition of the steel were identified by X-ray diffraction—reference being made to X-ray data obtained (a) from synthetically prepared carbides of the composition $Fe_{20}C_9$[5, 6, 7] and Fe_2C[5, 7] and (b) from cementite extracted from a plain carbon steel[8]. Even though special techniques were used in handling the extracted residues, the diffraction patterns were somewhat vague. Attempts to overcome this defect by compensating for fluorescence were fruitless. Chemical analyses have not been run because a special method has yet to be devised to prevent the dried residues from burning on exposure to air. Until analysis is possible, the only definite statement that can be made is that $Fe_{20}C_9$ (and possibly the Fe_2C), structures are present prior to the formation of cementite. It must be emphasized that, while the structure of the initial precipitate corresponds to that of $Fe_{20}C_9$ (or possibly Fe_2C), these formulas may not be indicative of the composition of the precipitate. Chemical analysis will be necessary before the composition of the various carbide residues is definitely known.

The fact remains, however, that the initial precipitate is not a transition form of cementite inasmuch as it maintains its identity even after removal of the supporting matrix by electrolytic isolation. Therefore, the initial carbide should be regarded, not as a stepping stone to cementite precipitation but rather as a distinct phase in its own right, having a greater rate of nucleation and growth than cementite.

References

[1] M. Arbusov and G. Kurdjumov: The Condition of Carbon in Tempered Steel, *Journal of Physics USSR* 5 (1941) 101.

[2] D. P. Antia, S. G. Fletcher and M. Cohen: Structural Changes During the Tempering of High Carbon Steels, *Trans. ASM* **32** (1944) 290.

[3] J. Trotter and D. McLean: Electron Microscope Studies of Quenched and Tempered Steel, *Journal Iron & Steel Inst.*, September 1949, 9.

[4] W. Crafts and J. L. Lamont: Secondary Hardening of Tempered Martensitic Alloy Steel, T.P. 2439, *Metals Technology*, September 1948.

[5] K. H. Jack: A Study of Interstitial Alloys of the Fe-C-N System, *British Iron and Steel Research Assn.*, Project MG/C/26.

[6] G. Hägg: *Z. Physik, Chem.* B8, 1930, 455.

[7] L. E. Hofer, E. M. Cohn and W. C. Peebles: Modification of the Carbide Fe_2C; Their Properties and Identification, *Journal Amer. Chem. Soc.* **71** (1949) 189.

[8] H. J. Goldschmidt: Interplanar Spacings of Carbides in Steels, *Metallurgia*, **40**, No. 236, June 1949.

Earl C. Roberts is Research Assistant at Massachusetts Institute of Technology, Cambridge, Mass.

Source of Abnormality in Hypereutectoid Steels

by Arthur Dube

IN hypereutectoid steels the normal mode of formation of ferritecarbide aggregates from austenite leads to a microstructure consisting of proeutectoid cementite and pearlite. However microstructures have been observed which exhibit a partial or complete disappearance of pearlite. These structures thus show a cementite network enveloping the core of the former austenite grains which now consists of a mixture of ferrite and pearlite.

This type of abnormal structure has already been the subject of many investigations. However no general agreement has yet been reached as to what factors will lead to its occurrence. According to the present viewpoint, the abnormal structure results from a synchronous deposition of the ferrite and carbide phase at temperatures just slightly below Ae_1. The continued growth of the primary cementite network after the ferrite phase is formed is possible by the diffusion of carbon through the α phase.

The cessation of this synchronous deposition can occur only through the precipitation of new cementite nuclei at the ferrite-austenite interface. Such precipitation always leads to the formation of pearlite. This formation of pearlite is a comparatively faster process than the growth of the ferrite envelope and, when initiated, effectively stops the further growth of the latter.

It is clear from the above mechanism that in order to develop an abnormal structure a steel must be reacted completely at temperatures near Ae_1. Such a condition is obtained by very slow cooling or by isothermal transformation in this temperature range. Lowering of the temperature will cause the cessation of the development of abnormal structure through precipitation of new cementite nuclei.

A second essential condition to the development of abnormal structures is a sufficiently fine austenite grain. In view of the fact that the thickness x of the ferrite envelope varies with time t according to $x = k\sqrt{D^c_\alpha t}$ when k is a constant and D^c_α is the coefficient of carbon in α iron, it is clear that with steels of larger austenite grains the precipitation of new cementite grains after ferrite has been found is much more readily formed.

Finally the carbon content of the steel is also important in the sense that it is easier to completely envelop the austenite grains with cementite when the carbon content of the steel is higher.

Preliminary experiments performed at the Metals Research Laboratory at the Carnegie Institute of Technology have substantiated the validity of the ideas presented herein.

Arthur Dube is associated with Sylvania Electric Products, Inc., Bayside, L. I.

Yielding in Plain Carbon Steels

by C. S. Roberts
and
B. L. Averbach

THE elastic limits and yield points of a series of plain carbon steels and pure irons in different states of microstructure and residual stress have been determined by a sensitive method. The elastic limit is defined as that stress above which the first plastic deformation is observed. The yield point, a parameter present only with special microstructures, is defined as that relatively constant stress at which the plastic strain shows large discontinuous increases.

The specimens used were threaded 4 in. test bars with a strained region 2½ in. long and 0.252 in. diam. The ends were spherically ground to a 4 in. diameter. The length of each bar was determined to ± 2 microinches per inch by the precision comparator method of Averbach, Cohen and Fletcher. It was then loaded in a hydraulic testing machine to a given stress, unloaded and then measured again. If no increase in length was observed after the conclusion of any relaxation effects, the strain was still purely elastic, and the specimen was reloaded to a slightly higher stress. By this procedure, the first plastic strain, within a sensitivity of $\pm 2 \times 10^{-6}$ could be detected. The initial stages of plastic deformation have been studied in detail and stress-plastic strain curves have been plotted. Relaxation effects with time, whenever existent, have been readily observed.

C. S. Roberts is Research Assistant, and B. L. Averbach is Assistant Professor at Massachusetts Institute of Technology, Cambridge, Mass.

An attempt has been made to correlate the yield points and elastic limits with microstructure. The relationship suggested by Gensammer and coworkers between flow stress, tensile strength or hardness of steels and the mean ferrite path prompted an initial investigation of this microstructure parameter. Mean ferrite paths have been determined for the series of steels and pure irons by a lineal analysis method employing a traveling microscope stage and a Hurlbut counter.

The results obtained to date show that:

1. Residual stress lowers the elastic limit, rounds off the yield point phenomenon, and raises the yield point stress considerably.

2. No plastic relaxation effects are observed until a plastic strain of at least 5000 × 10^{-6} has been applied and the magnitude of the relaxation is then of the order 25 to 50 × 10^{-6}.

3. A step-like behavior is obtained in the initial plastic strain curves of materials which contain no free ferrite.

4. For stress-relieved materials the yield point is a linear function of the logarithm of the mean ferrite path. This relation holds over the range of the logarithm equal to 3.8 to 5.5, where ferrite paths are in angstrom units. Grain boundaries, carbide particles, pearlite patches and inclusions are considered terminations of the ferrite paths.

5. A similar relation has been found for the elastic limit of stress-relieved materials but the linearity does not appear to hold well in the end of the range corresponding to higher strength and shorter mean ferrite path.

On the $\{259\}_\gamma$ Habit of Martensite

by Eugene S. Machlin

MEASUREMENTS were made of the non-diagonal components of the martensite transformation strain matrix using single crystals of a 70 pct Fe, 30 pct Ni alloy. The habit planes associated with each strain matrix were determined simultaneously, and were found to belong closely to the $\{259\}_\gamma$ family. A matrix method of analysis yielded the following conclusions:

1. The habit plane is the only plane of no distortion and no rotation associated with the measurable strain of the martensite plate.

2. To each measured strain matrix there corresponds one and only one permutation of ± $\{259\}_\gamma$ and vice versa.

3. There are 24 measurably different strain matrices. These matrices can be arranged in two groups (12 in each group). These groups have the property that any strain matrix belonging to one group is crystallographically equivalent to every other strain matrix belonging to that group. One group is related to the other by the property that any strain matrix belonging to one group has a crystallographic mirror symmetry with every strain matrix belonging to the other group.

4. The reaction path (motion of the atoms during the transformation) is the same crystallographically for every martensite plate formed.

5. There are at least two homogeneous strains required to form the martensitic structure. The first comprises the measurable strain. The second is homogeneous only over a small region and is not measurable. The elements of these strains are:

	1st Strain	2nd Strain*
Plane of zero distortion and zero rotation	$(259)_\gamma$	Between $(112)_M$ and $(011)_M$ and 6½° from $(112)_M$.
Direction of motion of plane of zero distortion and zero rotation	Between $[0\bar{1}1]_\gamma$ and $[\bar{1}\bar{1}2]_\gamma$ and ∞ 10° from $[0\bar{1}1]_\gamma$	∞ 2½° from $[11\bar{1}]_M$, coincident with $[1\bar{1}0]_\gamma$.

* This strain is based on the assumption of a Greninger-Troiano orientation relation between the parent austenite and the martensite.

6. There are four martensite habit planes having directions of motion of the bounding austenite within 10° of any $<110>_\gamma$. This fact is used to account for the burst effect in $\{259\}_\gamma$ systems.

7. The difference between the elements of motion yielding $\{225\}_\gamma$ habits and those yielding $\{259\}_\gamma$ habits is the presence of shear components yielding rotations of directions about $[111]_\gamma$ in the latter system. A correlation is suggested as follows: $(225)_\gamma$ Kurdjumow-Sachs orientation
$(259)_\gamma$ Greninger-Trolano orientation

8. The angles between martensite plates in the $\{225\}_\gamma$ and $\{259\}_\gamma$ systems are dependent upon the bounding plates having the same direction of austenite motion.

9. Finally, the sequence of events determining the choice of habit plane is believed to be as follows: During the martensite transformation the atoms move with respect to each other along a unique reaction path of minimum potential energy. During the first homogeneous strain, each atom moves along a straight line path. At any point along this reaction path, the strain matrix has only one plane of no distortion and no rotation associated with it. It is the same plane at any point along the reaction path. Because the surface and coherency energy associated with this plane as an interface between austenite and martensite is the least of all possible planes, the strain spreads along this plane into the austenite to form the martensite plate. This plane of zero distortion and zero rotation is then the interface plane and also the habit plane.

E. S. Machlin is associated with Massachusetts Institute of Technology, Cambridge, Mass.

On the Temperature Dependence of Self-Diffusion in Alpha Iron

by I. D. Bakalar

A SELF-DIFFUSION study in iron has been underway at M.I.T. for several years. Part of the results reported at the Sylvania Conference on "The Physics of Sintering"[1] gave the diffusion equation $D\alpha \doteq 5.8e^{\frac{-59.700}{RT}}$ (1) as holding between 809°C and 905°C. This equation has turned out to be in serious conflict with the $D\alpha \doteq 2.3 \times 10^{3}e^{\frac{-73,200}{RT}}$ (2) later reported by Birchenall and Mehl.[2] It was felt that a check could best be made upon the reported equations by carrying out some diffusion runs in the δ region where the diffusion values predicted by (1) and (2) differ by more than 600 pct. Such runs have verified that equation (1) holds in the α and δ regions for temperatures greater than 800°C.

The low temperature work of Birchenall and Mehl has also indicated that the log D vs. $\frac{1}{T}$ plot for the α iron curves downwards somewhere below 800°C. It was impossible to check this possible curvature with the standard surface-decrease specimens (2×10^{-3} cm plate thickness) because of low sensitivity. Attempts were therefore made to use a thinner radioactive plate such as adopted by Birchenall and Mehl. Results were obtained which indicated curvature but had to be considered unreliable because of large anomalous scatter. It was felt that this scatter might be due to surface diffusion. A new "surface increase" specimen was therefore devised to overcome this possibility. At the present time further runs are underway and results will be available for the October Meeting.

I. D. Bakalar is with the Metallurgy Dept., Massachusetts Institute of Technology, Cambridge, Mass.

---

[1] Bayside, Long Island, August 24-26, 1949.

[2] JOURNAL OF METALS, January, 1950, p. 144.

Effect of Uniaxial Compressive Stresses on Self-Diffusion in Alpha Iron

by F. S. Buffington

THE effects of uniaxial compressive stresses on self-diffusion rates in pure iron are being studied at temperatures high in the alpha range. The diffusion specimen is of the surface-decrease type, formed by plating radioactive iron on one face of a disc of inert iron. A quartz disc is placed directly against the electroplated layer and a load applied on the quartz to stress the specimen in simple compression.

This method has several advantages over other possible ones in that:

(1) The sensitive surface-decrease method permits short diffusion runs with little distortion and little change in cross-sectional area of the specimen.

(2) Any distortion which does occur is uniform within the diffusion zone, so that boundary conditions are maintained.

(3) The quartz disc in intimate contact with the plated face minimizes the loss of radioactive iron in the vapor phase, again maintaining boundary conditions.

(4) The stress system within the specimen is simple, so that no complications occur in determining the existing true stress.

(5) Analysis of results is rapid, requiring only a few hours.

A possible disadvantage of the method is that the interdiffusion between quartz and iron and loss of radioactive iron as vapor may give erroneously high D values. However, it was found that this method gives a D value less than 50 pct higher than the correct value at 885°C for unstressed specimens. It is possible to correct for this error, since it is a systematic discrepancy.

F. S. Buffington is associated with Massachusetts Institute of Technology, Cambridge, Mass.

Rolling Texture in Aluminum

by Hsun Hu
and
Paul A. Beck

MAKING use of recent improvements in X-ray diffraction technique, quantitative pole figures were determined for rolled 2S aluminum. The central portion of the pole figures (up to 40° away from the center) was determined by the Schulz reflection method,[1] the peripherial part of the pole figures (from 40° to 90° away from the center) was determined by the Decker, Asp and Harker transmission method.[2]

The aluminum strip was produced according to the following schedule: Alternate annealing (30 min at 380°C) and rolling (33 pct reduction) to a thickness of 0.500 in. Penultimate anneal at 380°C for 30 min and final rolling reduction of 95 pct to a thickness of 0.024 in. Three and one-half in. diam rolls were used, lubricated with light mineral oil. The reduction per pass was approximately 10 pct. Two rolling procedures were used: A—continued rolling in the same direction, B—strip reversed end to end between passes. X-ray specimens were prepared of both the center of the strip and the surface. The center specimens were obtained by dissolving the strip in acid at both surfaces until the thickness was reduced to 0.004 in. The surface specimens were prepared in the same way, except that one surface was protected from the acid by paint.

The results indicate that the center portion of the strip has very similar texture regardless of whether rolling procedure A or B is used. The outstanding feature of the pole figure (Fig. 1), apparently not previously reported, is the presence of two sharp, high intensity maxima 25° away from the center, toward, respectively away from the rolling direction. These maxima, which represent by far the highest intensities in the whole pole figure, are not accounted for by either one of the "ideal textures" previously reported: a-(110) // Rolling Plane, [112] // Rolling Direction, b-(112) // Rolling Plane, [111] // Rolling Direction, or c-(236) // Rolling Plane, [533] // Rolling Direction. It was found that an "ideal texture", consisting of four symmetrical orientations corresponding approximately to (7, 12, 22) // Rolling Plane, [4, 5, 8] // Rolling Direction fits the data best. These orientations account very well for the strongest maxima near the center, fairly well for the four second highest intensity maxima at the periphery, but only approximately

---

Hsun Hu is a Graduate Student, and Paul A. Beck is Professor in the Dept. of Metallurgy, University of Notre Dame.

Fig. 1—(Left) (111) pole figure for rolled 2S aluminum. Last reduction 95 pct by rolling to 0.024 in. Specimen 0.004 in. thick from center portion of strip. △ indicates "ideal position" of (111) poles for (7, 12, 22) [4, 5, 8] texture. ▲ indicates (110) [112] texture. ◭ indicates (112) [111] texture. Thin contour lines show intensity increments of 100, thick contour lines show intensity increments of 300, in arbitrary units.

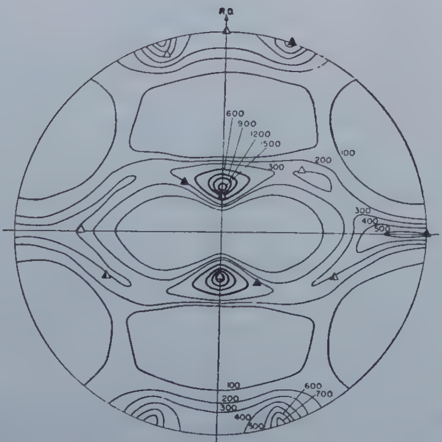

Fig. 1

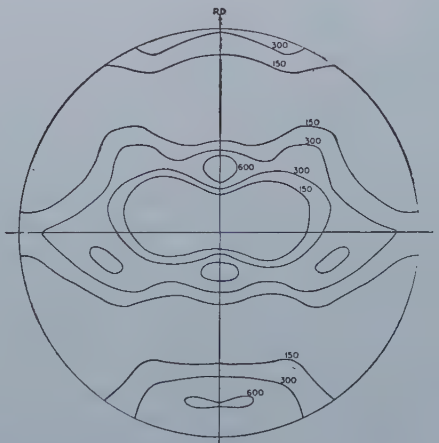

Fig. 2

Fig. 2—(Right) (111) pole figure for surface of rolled 2S aluminum (rolled in one direction). Last reduction 95 pct by rolling without reversing strip end to end between passes. Strip 0.024 in. thick, specimen 0.004 in. thick from surface of strip. Contour lines show intensities successively doubled for each increment, in arbitrary units.

for the other maxima shown in the pole figure.

The surface texture of the strip given a final rolling reduction with each pass in the same direction, procedure A, was somewhat similar to the texture in the center. The deviations can be largely described in terms of a shifting of all poles forward, i.e. toward the direction of rolling. The resulting assymetrical pole figure is shown in Fig. 2. The surface texture of the strip final-rolled with reversals between passes, procedure B, was entirely different. It corresponded closely to an ideal position (100) [011], which was previously reported by Vargha and Wassermann[3]. These authors associated the occurrence of the (100) [011] surface texture with a larger strip thickness (5 mm). They found in thinner strips (1 mm or less) a surface texture similar to the inside texture. The present work shows that both types of surface texture can be obtained at the same strip thickness. The type of surface texture is determined by the rolling procedure.

This work was supported by the Office of Naval Research, U. S. Navy, Contract No. N6ori-165, T.O. 1.

References

[1] L. G. Schulz: A Direct Method of Determining Preferred Orientation of a Flat Reflection Sample using a Geiger Counter X-ray Spectrometer. *Journal of Applied Physics,* **20,** (1949), 1030.

[2] B. F. Decker, E. T. Asp and D. Harker: Preferred Orientation Determination using a Geiger Counter X-ray Diffraction Goniometer. *Journal of Applied Physics,* **19,** (1948), 388. See also *ASTM Tentative Standard E81-49T,* (1949).

[3] G. Vargha and G. Wassermann: Uber die Abbangigheit d. Kristallitanordnung in gewalzten Aluminium blechen von der Blechdicke. *Metallwirtschaft,* **12,** (1933), 511.

Annealing Texture in Rolled Aluminum Strip

by Paul A. Beck
and
Hsun Hu

THE rolling texture of 2S aluminum has been re-determined by quantitative methods and found to consist, essentially, of four symmetrical (7, 12, 22) [4, 5, 8] orientations[1] two of which are shown in Fig. 1. It was found that a salt bath anneal of 5 min at 300°C was just sufficient to completely recover the hardness which had been increased as a result of rolling. The quantitative pole figure determined for the inside of the specimen annealed for 5 min at 300°C is given in Fig. 2. It is seen that, essentially, the four orientations present in the rolling texture are retained and that an additional orientation, namely the "cube orientation", (100) [100], appears. This is borne out by the (200) pole figures determined but not shown here.

Microscopic observations were made by the oxide film-polarized light method of the structure of high purity aluminum as rolled, and of the changes occurring upon annealing. These observations indicate that in the as rolled condition considerable orientation spread exists within each deformed grain, connected with the very general occurrence of kink-bands. By means of color, two predominant orientations can be identified in the deformed material; neighboring kink-bands alternate between these two orientations. Considering that the optical method used cannot discriminate between two orientations related to each other by 180° rotation around the optical axis (the specimen surface normal), the two microscopically observed orientations correspond to the four orientations in the pole figure.

As observed microscopically, during annealing

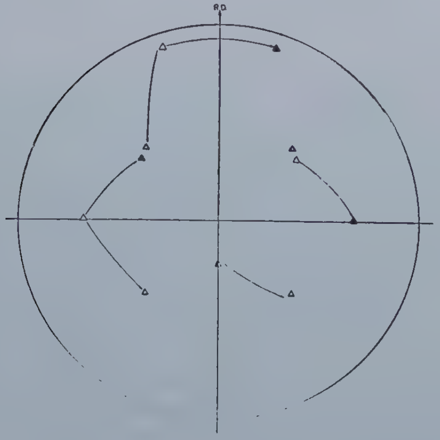

Fig. 1

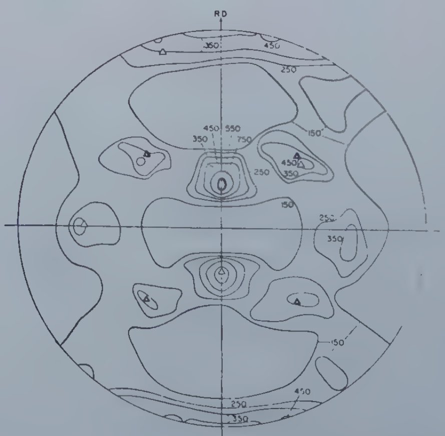

Fig. 2

Fig. 1—(Left) Relationship between two components of the (7, 12, 22) [4, 5, 8] rolling texture. Component a (indicated by △) transforms into component b (indicated by ▲) by a rotation of about 38° around a common [111] direction (Δ). A (111) pole of each component of the rolling texture and a (111) pole of the "cube texture" (indicated by Δ) nearly coincide. The "cube texture" can be approximately derived from any component of the rolling texture by a [111] rotation of 40°.

Fig. 2—(Right) Annealing texture of 2S aluminum. Strip annealed 5 min. at 300°C, after rolling reduction of 95 pct. Specimen 0.004 in. thick from center of 0.024 in. thick strip. "Ideal position" of (7, 12, 22) [4, 5, 8] component of annealing texture shown by △, the "cube" component is shown by Δ. Thin contour lines show intensity increments of 100, thick contour line shows an intensity increment of 200, in arbitrary units.

a considerable portion of the material within each kink-band retains its original orientation. Even though such a region essentially retains its average orientation, it becomes subdivided into a large number of small domains of slightly deviating orientations. This complete recovery without orientation change apparently corresponds to the process designated by Crussard[2] as "recrystallization in situ" and by Orowan[3] as "polygonization"; it now turns out to constitute a major part of the softening process in highly deformed (e.g. 95 pct rolled) high purity aluminum. Microscopic observations indicate, in addition to polygonization, the occurrence upon annealing of two sets of recrystallized grains corresponding to two new orientations, within each region having predominantly a single orientation in the as rolled condition. The orientation of one set of recrystallized grains growing in regions predominantly of the *a* orientation, as rolled, corresponds quite well with a *b* orientation of the deformed material, and vice versa. As seen in the pole figure (Fig. 1) an *a* and a *b* orientation have a common [111] pole; the relationship between these two orientations is equivalent to a [111] rotation of about 38°. The importance of this orientation relationship in recrystallization has been previously demonstrated for slightly deformed single crystals[4] and for highly rolled and compressed single crystals of high purity aluminum[5]. It now appears to govern as well the re-orientation upon recrystallization in polycrystalline 2S aluminum after high deformations. Both the "recrystallization in situ" and the re-orientation of the type described result in the retainment of the deformation texture upon annealing.

The orientation of the second set of recrystallized grains growing upon annealing is very similar everywhere in the rolled specimen, regardless of the local orientation of the region in which the new grains are growing. By means of color, it is possible to identify this orientation as one with a cube face parallel to the specimen surface. This set of new grains then corresponds to the "cube orientation" (100), [100], which is formed during annealing, as seen in the pole figure. It is remarkable that a [111] pole of the recrystallized "cube grains" approximately corresponds to a [111] pole of each of the four matrix orientations; the formation of the cube orientation component of the annealing texture can be also described approximately as a [111] rotation of 40°. As found previously[4], a re-orientation of this type is the result of the orientation dependence of the rate of grain boundary migration.

This work was supported by the Office of Naval Research, U. S. Navy, Contract No. N6ori-165, T.O. 1.

References

[1] Hsun Hu and Paul A. Beck: Rolling Texture in Aluminum. AIME Research in Progress Abstract.

[2] C. Crussard: Etude du Recuit de l'Aluminium. *Revue de Metallurgie* (1944) **41,** 140.

[3] E. Orowan:

[4] Paul A. Beck, Philip R. Sperry and Hsun Hu: The Orientation Dependence of the Rate of Grain Boundary Migration. *Journal of Applied Physics,* **21,** No. 5, (1950) 420.

[5] Paul A. Beck and Hsun Hu: Recrystallization Texture and Coarsening Texture in High Purity Aluminum. *Transactions AIME,* **185,** 627 (1949).

Order-disorder Phase Change in Cu_3Au Alloys

by F. N. Rhines

TRANSFORMATION from the disordered to the ordered state, and the reverse, has been followed by electrical resistivity measurements, in which equilibrium has been established for each increment of temperature change, in Cu-Au alloys, ranging in composition from about 20 to about 32 atomic pct of gold. Equilibrium was attained very quickly at temperatures above the transformation; up to three weeks was required within the transformation interval and a matter of a day or two below the temperature interval of transformation. The temperature-resistivity curves have two sharp inflections corresponding to the limits of the transformation interval, the temperature spread between these inflections being least near 25 atomic pct of gold (Cu_3Au) and greater the more the composition departs from this value.

A nearly exhaustive survey of the literature upon order-disorder transformations has revealed a number of cases in which a sharply defined temperature interval of transformation has been reported for other alloy systems. Moreover, it has been found that the absence of such finding has generally been associated with tests run under conditions that are not expected to ensure the attainment of equilibrium.

It is concluded, upon the basis of this and other evidence, that the order-disorder transformation proceeds as a classical Gibbsian phase change. Ordering is believed to occur by a nucleation and growth process. Except at the ideal composition of Cu_3Au (which has virtually no effective composition range, but exists only at a sharply defined composition), the ordered and disordered phases are capable of coexistence at equilibrium within the transformation interval, i.e. the two-phase region of the phase diagram. It is recommended, therefore, that phase diagrams involving order-disorder transformations be drawn in accordance with the requirements of the Phase Rule.

F. N. Rhines is Professor of Metallurgy and Member of Staff of the Metals Research Lab at Carnegie Institute of Technology, Pittsburgh, Pa.

Measurements on the Rate of Secondary Recrystallization in High Purity Silver

by F. D. Rosi

and B. H. Alexander

THIS investigation is one of a series primarily designed to measure the rate of growth of secondary grains at various temperatures for a number of high-purity metals (Al, Ag and Cu). It is hoped that this will lead to a better understanding of the underlying atomic processes governing this recrystallization reaction.

In this first group of experiments, measurements have been made of the secondary transformation in high purity silver (99.99+) in the form of cold-rolled sheets 0.02 in. thick. Annealing these sheets in the temperature range of 433° to 533°C produced a primary recrystallized structure with a grain size of the order of 0.02 mm. On prolonged heating in this temperature range, secondary crystals appeared at various points ranging in size up to approximately 2 mm diam. Generally speaking, these crystals exhibited a preferential growth in the direction of rolling and showed corrugated boundaries demonstrating visibly that the growth is proceeding preferentially along grain boundaries in accordance with the principles of boundary migration.

The results of the growth velocity measurements showed that the rate of growth, V, is invariant with time similar to the growth rate of primary grains in a uniformly deformed test piece. Furthermore, it was established that the temperature dependence of the average velocity of invisible grain growth (reciprocal of "induction period") as well as the time independent velocity of visible grain growth may be given by the expression ($V = V_0 \, e^{-Q/RT}$).

Thus, the velocity of grain growth in secondary recrystallization corresponds with the growth rate of most processes in solids involving relative movements of atoms.

Activation energies have been calculated describing the temperature dependence of both the visible and invisible growth processes. These values strongly suggest that the underlying atomic process of crystal growth is one of grain boundary self-diffusion. These results further suggest that grain growth is taking place during the so-called induction period by the same processes governing the growth of visible grains, and that this early-stage growth is probably impeded by the small number of contact areas between the growing grain and its surrounding fine-grained structure.

Some studies have been made of the orientation relationships between the deformed and recrystallized structures. It was found that the secondary grains exhibited an orientation similar to the deformation texture. This indicates that the nuclei responsible for secondary recrystallization are formed during the deformation process, and that the orientation dependence of the secondary crystals is responsible for their growth.

Experiments are also being conducted to study the effect of grain size of the primary recrystallized structure on the growth velocity of secondary grains.

F. D. Rosi and B. H. Alexander are Senior Engineers for Sylvania Electric Products, Inc., Bayside, L. I.

The Plastic Behavior of Silver Single Crystals at Various Temperatures

by F. D. Rosi

THE plastic properties of silver single crystals (99.99+) have been investigated at room temperature (295°K) and the temperature of dry ice (205°K) for small amounts of extension (max 2 pct). Determinations of critical resolved shear stress and coefficient of shear hardening were made, and both properties were found to increase with a decrease in temperature. Furthermore, these properties were consistent with the Schmid law of critical shear stress governing the initiation of the slip process. Values of the elastic modulus at 295°K showed a marked dependence on the crystallographic orientation.

At both temperatures the stress-strain diagrams demonstrate a rather sharp advent of plastic flow, and an almost linear rate of strain hardening. In all cases, the hardening rate increases after definite values of shear stress and shear strain which are independent of orientation. An analysis has been made of the dependence of this inflection in the shear stress-shear curve on the temperature of testing.

Short time creep tests (max 3 minutes) were made by interrupting the loading along different portions of the stress-strain curves. These tests have yielded some interesting data correlating the rate of creep with both the rate of strain hardening and the temperature of testing. In addition, an orientation dependence of these curves has been established.

At present this work is being extended to include investigations at 77°K and 373°K. Similar studies are also being made on single crystals of copper and magnesium.

F. D. Rosi is Senior Engineer for Sylvania Electric Products, Inc., Bayside, L. I.

Studies on Control of Growth or Shrinkage of Iron-Copper Compacts During Sintering

by Jerome F. Kuzmick
and
Edmund N. Mazza

COPPER powder is a popular additive to iron powder in the production of iron base porous bearings and molded machine parts produced by powder metallurgy. Sintering is usually done above the melting point of copper, so that it occurs in the presence of a liquid phase. Sufficient diffusion of copper occurs to materially strengthen the iron powder compact.

However, there is more difficulty in controlling dimensions of sintered iron-copper compacts as compared to pure iron. Most iron powders mixed with copper, pressed and sintered, show excessive growth. A few show excessive shrinkage. None remains constant.

The experiments described in this paper were made primarily on Swedish sponge iron powder produced from magnetite. A series of specimens produced with additions in a range of 1 to 10 pct copper showed maximum strength between 7 and 10 pct. However maximum growth also occurred in this range. A series of 93 pct iron—7 pct copper specimens sintered over a range of temperatures showed that maximum growth occurred at about 1150°C. Increasing sintering time decreased growth, indicating that maximum growth occurred early in the sintering cycle.

Many experiments were performed with various additives in an attempt to decrease the excessive growth. Additions of graphite up to 1 pct cut down growth from 2 pct to 0.3 to 0.5 pct, a more reasonable figure. The graphite simultaneously carburized the compact, increasing its hardness and strength. Such iron-copper-graphite mixtures have come into popular use for wear resistant parts which do not have to be sized to close dimensions. Subsequently it was found that the addition of a small amount of cast iron powder to the iron-copper-graphite mixture further cut growth and increased hardness and strength. It was found that the cast iron melted, and, being soluble in the iron, caused a shrinkage effect which partially offset the growth effect of the copper.

Since the carbon additives resulted in parts too hard for sizing, an investigation was made to determine the cause of growth. An iron powder produced from mill scale which showed shrinkage with copper was examined microscopically and found to have a more porous surface than the Swedish powder. A powder produced from decarburized steam atomized cast iron had the least porous surface. Compacts containing 10 pct copper were produced under identical conditions from the three powders and showed 0.5 pct shrinkage, 2 pct growth, and 2.8 pct growth respectively. This indicated that particles with porous surfaces absorbed copper during sintering causing shrinkage. With less porous surface, more of the copper penetrated between the particles by capillarity, causing growth.

To further prove this theory, the iron powder with the most porous surface was annealed at 2000°F until sufficient sintering occurred to cause some sealing of the surfaces. The sinter cake was reground to powder. The annealed powder showed 0.6 pct expansion with copper against 0.5 pct shrinkage annealed. A powder was prepared in the laboratory from Swedish magnetite under conditions which resulted in porous particle surfaces. Shrinkage of about 1 pct occurred against growth of 2 pct for the normal material.

Finally, it was thought that the addition of an organic material to the Swedish iron-copper compacts would solve the problem. If the organic material volatilized at about the melting point of copper, it would promote new pores for copper infiltration. Various additives were tried including resins, carbon black, and pitch. All helped reduce growth, and the best results were obtained with powdered coal tar pitch. 1 pct of

---

J. F. Kuzmick is President of the Welded Carbide Tool Co., Clifton, N. J., and E. N. Mazza is Metallurgist for Ekstrand & Tholand, Inc., Carlstadt, N. J.

the latter cut growth from 2 pct to 0.5 pct; 2 pct pitch eliminated growth, and 3 pct pitch showed about 0.3 pct shrinkage. Weight loss tests showed that most of the pitch volatilized a little above the melting point of copper.

Thus the coal tar pitch additive can be used to control dimensional changes of iron-copper compacts during sintering. It does not excessively harden the parts, so that they can be successfully sized.

Experiments on the Mechanism of Sintering

by B. H. Alexander
and
R. Balluffi

BY a method similar to that of Geech & Jones[1] the change in size and shape of the interstices between 5 mil copper wires has been followed as a function of time at various sintering temperatures. It has been found that the initial rate of decrease in the size of these voids is greater the higher the temperature. Upon sintering, the triangular cusp shaped voids between the wires become circular in cross-section and are connected to each other by grain boundaries. As long as these grain boundaries are present the voids continue to decrease in size. After a length of time, which decreases with increasing temperature, these grain boundaries disappear, and after their disappearance no further decrease in the size of the voids occurs. Because the grain boundaries disappear sooner at higher temperature, the overall decrease in the size of the voids is smaller, even though the initial rate of decrease is greater, at the higher temperatures.

We have concluded from these experiments that grain boundaries are essential for the sintering of powdered metal compacts, and that the finer the grain size, the more rapid sintering will occur. A series of experiments on powdered silver compacts is in progress, and it has been found that any treatment which can affect the initial recrystallization, and hence the grain size, of the pressed compacts will change the rate of sintering markedly. The effects of recovery at room temperature; recrystallization at low temperatures; rate of heating; and atmosphere are being studied in silver compacts, and it has been found that all of these can have a pronounced effect on the rate of sintering. An attempt is being made to explain these effects according to variations in grain size of the specimen.

B. H. Alexander and R. Balluffi are associated with Sylvania Electric Products, Inc., Bayside, L. I.

---

[1] *Research*, Vol. 2, p. 493, 1949

Interfaces in Diffusion in Solid Solutions

by L. C. C. da Silva
and
R. F. Mehl

THIS is an experimental study of the movement of markers during diffusion in solid solutions, the phenomenon discovered by Kirkendall and theoretically studied by Seitz, Darken, Bardeen, and others. Six systems have been investigated, at a series of temperatures: Cu/α brass; Cu/Sn-α solid solution; Cu/Al-α solid solution; Cu/Ni; Ag/Au; Cu/Au diffusion couples have been made by welding. Markers of many types have been used, including W, Mo, Ni, Pt wires; Pt, Ta, W, Fe, Ni, foils; C, Al_2O_3, Fe_2O_3 powders. All markers move, and by the same amount in a given system, the phenomenon is thus not a property of the marker; the movement, with respect to the Matano interface, has been measured for the separate systems. In the Cu/α brass couples, the markers move toward the high Zn side; in the Cu/Al system, toward the high Al side; in the Cu/Sn system, toward the high Sn side; in the Cu/Ni system, toward the Cu; in the Ag/Au system, toward the Ag; in the

L. C. C. da Silva and R. F. Mehl are associated with the Dept. of Metallurgical Engineering at Carnegie Institute of Technology, Pittsburgh, Pa.

Cu/Au system, toward the Au. Measurements agree well with Kirkendall's, showing that the technique of joining is unimportant. The Matano interface agrees with the original interface, showing conservation of lattice sites. The amount of marker shift differs from system to system, for unexplained reasons; the amount of shift is sometimes near the maximum possible; it is large in Cu/Zn and Cu/Ni systems, smaller in others. Dimensional changes seem to be restricted to the direction parallel to diffusion flow. Cu/Zn couples exhibit apparent traces of porosity in the diffusion zone (and anomalously low hardness therein) while no such porosity could be found in other systems. Only the vacancy mechanism of diffusion appears to be useful in explaining these phenomena, though other theoretical points remain to be explored. Inasmuch as the amount of shift is independent of the nature of the external surface of the diffusion couple, and of the dimensions of the couple, it appears that operating vacancies cannot come from external surfaces but must be generated within the diffusion zone itself.

The Application of Radioactive Tracers to the Study of Metal-Solution Reactions

by M. T. Simnad

As part of a general project to study the properties of metal surfaces, experiments are being carried out designed to elucidate the influence of surface treatment and structure upon the reactions taking place when metals are placed in ionic solutions containing radioactive ions. The behavior of metals in solutions may be studied in greater detail with the aid of radioactive tracers than has been possible with the methods previously available. This applies especially to cases where some of the ions in solution are composed of the same element as the metal, and the tracer technique is then the only method that can be used to follow the reaction.

The first part of the work deals with the so-called phenomenon of "exchange" between metals and radioactive ions in solution. This was first demonstrated in 1929 by Hevesy who found that when a specimen of lead was placed in a solution containing thorium B ions it acquired a surface activity corresponding to over 1000 atoms thick of thorium B. No further work appears to have been done on the subject until recent years when Rollin, Coffin and Tingley, and Hensley et al published notes on some experiments confirming this phenomenon with radioactive silver and sodium ions. In our studies, radioactive ions of cobalt, chromium, nickel and iron are being used in solutions into which are immersed numerous metals and alloys with various surface treatments. The effect of the presence and absence of oxygen in the solutions and of oxide films on the metals, the influence of time, temperature and pH are being studied. The distribution of the radioactive ions deposited on the metal surfaces is shown by means of autoradiographs and their quantity measured by counting with a Geiger-Müller counter.

The experiments with radioactive cobalt and chromium indicate that the phenomenon of exchange is actually a local electrolysis resulting from differences in electrode potential on the metal surfaces. The experiments with radioactive chromium, in which active chromate ions were used in the solutions, have served to show that passivity in chromate solutions results from the deposition of chromate ions at anodic points on the metal surface, and the distribution of these points following various passivating treatments is brought out in autoradiographs of the specimens. Further experiments have been designed or are in progress using radioactive chromium to study the nature and composition of oxide films on stainless steels and their behavior in solutions, and to throw further light on the phenomenon of grain-boundary sensitization of stainless steels.

In conjunction with these experiments, work is in progress to study the kinetics and mechanism of electrodeposition in very dilute solutions and in its earliest stages. The influence of the numerous factors which affect the nature of electrodeposits will be studied, especially the influence of surface structure upon the nucleation and growth of the deposits. The use of tracers is a highly sensitive tool for the study of this subject.

M. T. Simnad is associated with the Metals Research Lab at Carnegie Institute of Technology, Pittsburgh, Pa.

The Development of the Lead Blast Furnace At Port Pirie, South Australia

by L. A. White

This paper describes the developments of the lead blast furnace at The Broken Hill Associated Smelters Pty., Ltd., from the original standard furnace to the present wide shaft type, with two superimposed rows of tuyeres. The metallurgical operations of the blast furnace section of the Port Pirie Works are also described.

IN this paper it is proposed to follow the developments in the design of the lead blast furnace at Port Pirie from the time The Broken Hill Associated Smelters Pty. assumed control in 1915 to the present time, with special reference to the development of the system using two superimposed rows of tuyeres as is now in operation.

Lead smelting operations first commenced in 1889, when the British Broken Hill Pty. Ltd. started its first furnace. This was followed by installing two more furnaces during the same year and another the following year. In 1892, Broken Hill Proprietary Co. Ltd. acquired the smelting works and combined operations with those at Broken Hill, New South Wales; by 1897, the whole of the smelting operations had been transferred to Port Pirie and thirteen blast furnaces were built to treat the Broken Hill ore production.

In 1915, The Broken Hill Associated Smelters Pty. Ltd. took over from the Broken Hill Proprietary and have carried out operations since that time.

From its inception, the present company started on a long range program of reconstruction, in which the development of the lead blast furnace has played a prominent part.

A definite trend in plant development has been towards the simplification of plant control by a reduction in the number of operating units. The great advantages of technical control which resulted from the very simplified flowsheet established in the continuous refining process stimulated the desire to extend the principle to the smelting operation.

Thus in the sequence of furnaces described here, it will be noted that the trend has been towards larger and, of course, fewer units. With each such development it is significant that the operating conditions and metallurgical results have shown steady improvement.

Standard Furnace

In 1920 there were seven furnaces operating, five of a type subsequently called the standard furnace and two of the original thirteen smaller furnaces, the latter type being used for the treatment of drosses, etc. produced from the refinery section, while the standard type carried out the main, lead-smelting operations.

The standard furnace (figs. 1 and 2) had the dimensions given in table I.

L. A. WHITE is Smelter Superintendent, The Broken Hill Associated Smelters Pty. Ltd., Port Pirie, South Australia.

AIME New York Meeting, February 1950.

TP 2889 D. Discussion (2 copies) may be sent to Transactions *AIME before Dec. 15, 1950. Manuscript received Jan. 1, 1950.*

This page of Transactions AIME is a continuation from p. 1176. The missing pages appeared in Journal of Metals.

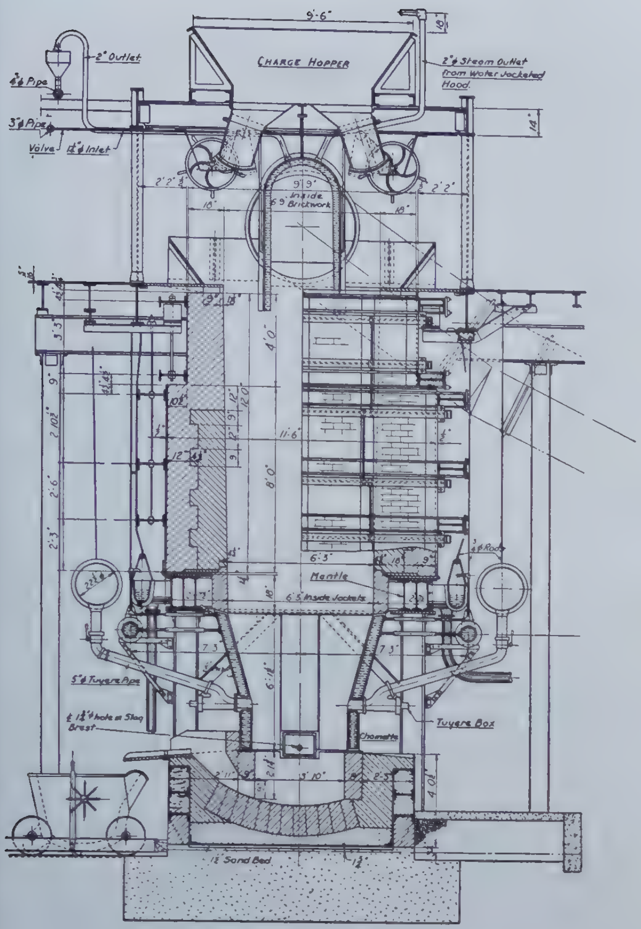

Fig. 1—Standard blast furnace.

This furnace had a single row of mild steel riveted jackets 6 ft high, 22 tuyeres (11 per side) with 5-in. openings. The first 9 ft of the shaft above the jackets was constructed with firebrick, the remainder being built of hard red brick which stood up better than the firebrick to the abrasive action of the charge and the effect of the barring operation for accretion removal.

The furnace was fitted with a thimble type top and the gases were drawn off at both ends by steel offtake flues leading by downcomers to a main brick flue delivering to a baghouse. A system of cable-drawn charge cars with bottom discharge doors ran over the whole line of furnaces.

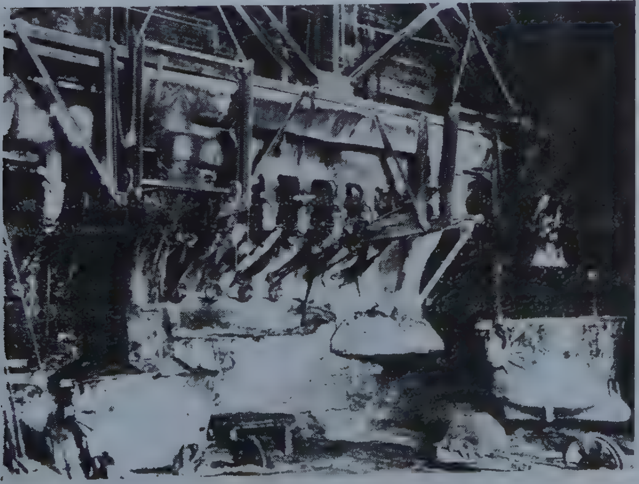

Fig. 2—Standard blast furnace.

This standard type furnace design remained in operation till 1934, minor alterations carried out in the meantime were: (1) Mild steel jackets were replaced with cheaper cast-iron jackets. (2) The vertical distance of the tuyeres from the top of the crucible was increased from 12 to 24 in., as it had been proved that better settling of the lead from the slag could be obtained by being able to hold the slag inside the furnace for a longer period. (3) Installation of water-cooled gas offtake hoods. The offtakes prior to this change were made of mild steel which, in time, became distorted to such a degree through heat that draughting at the top of the furnaces was not satisfactory, which in turn meant loss of fume and was also a health hazard to the operators.

Other major alterations carried out between 1920 and 1929 were: (1) The installation of the overhead telpher handling system for the delivery of charge to the furnaces (fig. 3). (2) The change to slag granulation on the furnaces instead of tapping molten slag into pots, transporting and tipping at the slag storage in this form. (3) Installation of a traveling crane at the tapping floor section for handling bullion in the molten state instead of moulding into bars which it was necessary to manhandle and remelt in the refinery section. With the installation of this crane, the copper drossing operation was transferred to the blast furnace section from the refinery.

In 1934, No. 4 furnace was rebuilt, the dimensions being similar to the standard type, but the effective smelting shaft was reduced by 5 ft, i.e., from 18 to 13 ft, following certain American designs at this time. The object was to determine the effect of a shorter shaft on the furnace production rate and lead content of the slag.

Table I. Standard Furnace Dimensions

Crucible	Length 17 ft 0 in. Width 3 ft 10 in. Depth 2 ft 3 in.
Furnace shaft at bottom of jackets	Length 17 ft 0 in. Width 3 ft 10 in.
At top of jackets	Length 18 ft 6 in. Width 6 ft 0 in.
At feed floor	Length 19 ft 6 in. Width 7 ft 0 in.
Depth from top of crucible to feed floor	20 ft 0 in.
Depth from center of tuyere to feed floor	19 ft 0 in.

The furnace was started in 1935 and operated until 1940. In its early stages the furnace was slower in speed than the standard type furnaces, and the lead content of the slag was higher.

Alterations were made increasing the furnace shaft by 2 ft, and a standard offtake hood was fitted, after which this furnace became the fastest smelting standard type though the lead content of the slag was still the highest.

It was felt that no particular advantages could be claimed for this furnace except that barring operations were easier due to the shorter shaft.

First Modified Furnace

In 1935, research work was carried out with a small experimental blast furnace with multiple rows of tuyeres, three sets in all being used stepped outward from the lower to the higher rows, and from the results obtained the first double row tuyere furnace came into operation in 1936.

After considerable work on the height of the charge column and the width at the tuyeres the following conclusions were reached: (1) There is a plastic condition in the furnace shaft which tends to bridge the gap between shaft accretions and prevent a regular movement of the charge through the furnace. (2) The active penetration of the blast at the tuyere zone is limited to approximately 24 in. (3) The width of the active zone in the wider part of the furnace is only 12 in. greater than that at the tuyere zone.

From these points it was deduced that the useful width of the furnace appeared to be related to the penetration of the blast air at the tuyere zone, and the spread of the blast air on reaching the wider part of the furnace. That is, for a furnace having a single row of tuyeres, the active shaft width appears to be limited to 6 ft. If now an additional row of tuyeres on each side of the furnace is installed above the bosh and assuming a similar degree of penetration to be obtained in this zone as in the case of the lower tuyeres, it should be possible to obtain a shaft width of 12 ft.

From the above observations it was decided to rebuild No. 5 furnace with two rows of tuyeres, but having in mind recent furnace developments in America the width across the lower tuyeres was increased to 5 ft.

The main dimensions were: length, 17 ft; width between lower tuyeres, 5 ft; width between upper tuyeres, 10 ft; maximum width of shaft, 12 ft; vertical distance between upper and lower tuyeres, 3 ft; distance from feed floor to lower tuyeres, 18 ft; height of lower tuyeres above crucible, 24 in.

The furnace comprised two sets of jackets, the bottom row being the unconventional "chair" jacket, the second row retaining a slight bosh. Above the second row of jackets to the feed floor, the shaft was brickwork.

This furnace was blown-in in October 1936 and operated until 1943. It was closed down for several weeks to install short water jackets to replace a row of tiles above the second tier of jackets which tended to burn-out at this location. At the same time, tuyeres were installed in the end jackets at the level of the second row of tuyeres to try to prevent end accretions forming in the shaft.

Table II. Comparison of Furnace Operations, 1939

	Standard Type Furnace (18 ft Shaft)	Standard Type Furnace (13 ft Shaft)	1st Modified Furnace
Charge treated per day, tons	267.2	316.03	439.35
Coke on charge, pct	11.10	10.60	10.63
Fixed carbon on charge, pct	8.85	8.45	8.47
Stoppages, hr per day:			
Barring	1.29	0.44	0.41
Maintenance	0.26	0.18	0.29
Total stoppages	1.55	0.62	0.70
Operating efficiency, pct	93.53	97.42	97.08
Average blast pressure, oz per sq. in.	38	33	40
Average blast volume, cfm	5,800	6,000	7,800
Lead in slag, pct	2.48	2.61	2.22
Lead tenor of furnace charge	37.31	37.31	37.36

Note: All tonnage figures in this paper are expressed in long tons.

During the first month, tapping of the furnace was carried out at both slag ends and lead wells, but it was found that tapping at one end could be carried out quite successfully even with maximum production.

The advantages shown on this furnace when compared to the standard furnace were: (1) Increased capacity, approximately 60 pct; (2) less top blowing; (3) less tendency for the charge to bridge due to the wider shaft; (4) variations in the grade of sinter had less effect on operating conditions; (5) more stable tapping floor conditions; and (6) increased operating efficiency due to less time lost for barring.

Operating details comparing the various furnaces in operation during year ending June 1939, are given in table II.

Second Modified Furnace

From the experience and information obtained from the operation of No. 5 blast furnace, it was decided to rebuild No. 1 furnace on similar lines.

The main design closely followed that of No. 5 with the addition of several new features: (1) The shaft was completely water jacketed except the top section which had cast iron plates 30 in. deep. Three sets of jackets comprised the shaft. (2) Tuyeres were placed in end jackets at the height of the top row of tuyeres. (3) The jackets sloped outwards from the bosh of the second row of jackets resulting in a shaft opening at the top 22x14 ft, shaft width at the top row of tuyeres 17x9 ft, and at the bottom row of tuyeres 17x4 ft. (4) The tuyere opening in the jackets was in the form of a slot, oval in shape, providing three tuyere punching holes per slot, the aim being to have, as nearly as possible, a continuous opening for the admittance of air at the tuyere sections.

This furnace was completed and blown-in in July

Fig. 3—High-lift telpher cranes discharging at blast furnace charge hoppers.

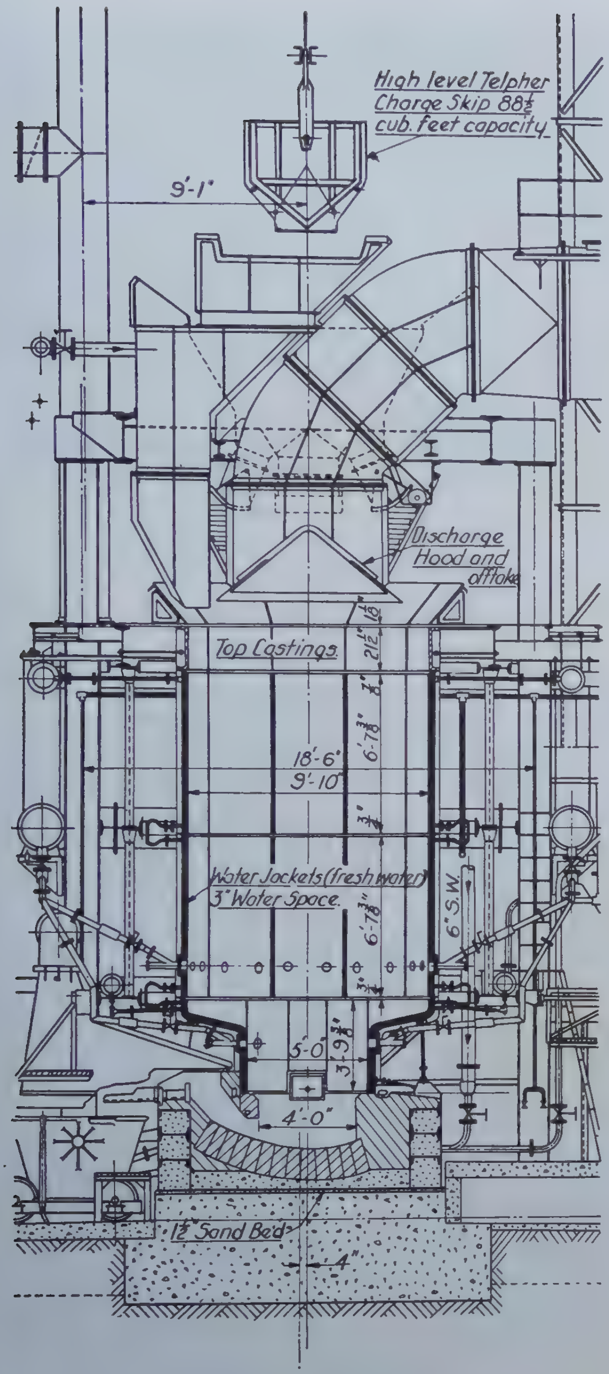
High level Telpher Charge Skip 88½ cub. feet capacity
9'-1"
Discharge Hood and offtake
Top Castings
21½"
18'-6"
9'-10"
6'-7⅞"
3'
Water Jackets (fresh water)
3" Water Space
6'-7⅞"
6" S.W.
5'-0"
3'-9½"
4'-0"
1½" Sand Bed
4"

Fig. 4—Fourth modified furnace.

1938, and is still available for smelting. The performance of this furnace was generally poor, top accretions forming quickly, causing frequent top blowing and increased barring for the removal of these accretions.

Even with the increased tuyere area openings, the speed was slower than its predecessor, No. 5 furnace.

The trouble experienced with the accretion formation was felt to be caused by the shape of the furnace and the completely water-jacketed shaft.

The bottom accretion formed at the bosh of the second row of jackets and, because of the slope of the upper jackets, a ledge was formed causing the accretions to build vertically from this point and extend to the top of the shaft; thus the effective smelting width was reduced to approximately 10 ft and accretion removal was difficult under operating conditions.

The furnace was shut down for several weeks and the top set of jackets made vertical, thus reducing the dimensions at the top of the shaft to 18x10 ft. At the same time, instead of maintaining the three-tuyere slot opening, as this gave no noticeable advantage, a steel plate was inserted between the tuyere and the jacket opening with a 2 in. diam central hole.

The furnace operating conditions were generally improved, but the speed was still slower than No. 5 furnace, the main variation now being the difference in width at the tuyeres: The width at bottom row of tuyeres of No. 1 furnace was 48 in.; of No. 5, 60 in.; and the width at upper tuyeres of No. 1 furnace was 9 ft; of No. 5, 10 ft.

Third Modified Furnace

Due to the success obtained with the furnaces using two rows of tuyeres and with increased production becoming necessary, it was decided to build an even larger furnace. It was felt that the optimum furnace width had been established fairly well and that any increase in size must come by adding to the furnace length.

This larger furnace (referred to as No. 3 furnace) was constructed in 1939 and came into operation in January 1940.

The design was partly on the lines of both Nos. 1 and 5 furnaces, though the length was increased to 35 ft (twice the length of the previous furnaces). Width at the bottom row of tuyeres was 5 ft and at the second row 10 ft, the second and third row jackets rising vertically from the bottom jackets. This alteration was made to try to reduce accretion formation.

The square ends were replaced by semicircular ends thus eliminating corners for the accumulation of accretions.

The covering fume hood conformed to the shape of the shaft with a central offtake, thus allowing for charge feeding around the whole furnace top, and also allowing for removal of top accretions during normal furnace operation.

From its inception this furnace operated satisfactorily with good smelting rate. Operating conditions were good especially at the feed floor.

Due to the increased length (35 ft, double that of a normal furnace), it was necessary to tap slag and bullion using both slag ends and lead wells, and the control here was not always easy. The furnace would get out of balance rather quickly, as it was not unusual to tap two thirds of the production during one shift from one end of the furnace while during the following shift production might swing to the other tapping end. There were occasions when the slag conditions were excellent at one end of the furnace with a good flow, while at the other end the slag would be viscous and small in quantity. This condition would also apply to the lead syphon. There were times when this furnace was tapped at one end without any trouble, for example, during short periods when driving approximately at two thirds normal capacity, though if slag conditions deteriorated there was a tendency for lower tuyeres to fill at the closed end due to the long travel to the tapping end.

On the whole this furnace gave very good results, the major operating difficulty being the replacement of leaking shaft jackets which at times partly flooded the furnace. In these cases it would be some days before the furnace was operating on full production again.

Due to the increased bullion flow, the capacity of the bullion handling ladles was increased from 5 to 10 tons, which is now standard on all furnaces.

A weak point was the capacity of the slag settler pot, which was approximately one ton. Very close attention was necessary to the lead syphon, because if any hold up occurred here the settler pot would fill and overflow lead into the slag granulating launder, with explosive result. Because of its low capacity, the slag settler also gave relatively inefficient separation of any entrained lead from the slag.

Operating efficiency was increased further as less barring down was required, and, in the latter life of this furnace, barring was not carried out at all, as it was found that accretions grew to a limiting distance of about 18 in. and did not increase, providing smelting rate and tuyere conditions were good.

This furnace had a normal production rate treble that of the standard furnaces and about twice that of either Nos. 1 or 5 furnaces. Due to the necessity of operating both tapping ends and the high flow of bullion through the lead syphon, it was necessary to shut the furnace down after three years' operations and reline the crucible at the lead well sections. At the same time the bottom row of jackets was renewed and extensive repairs carried out to super hoppers at the feed floor.

It should be stated here that one of the most serious troubles encountered in the water jackets on the furnaces results from a marine growth forming in the water space, thereby lowering the rate of heat transfer. This was more frequent in the "chair" type jacket on the modified furnaces, and as failures began to occur after two years' service, it was also necessary to renew these shaft jackets. It must be understood that all cooling water used was sea water pumped from the local sea-port channel.

The furnace operated until 1946, when it was decided to demolish it and proceed with the building of a new type, incorporating jackets cooled by fresh water.

Table III gives the operating details, comparing the first, second, and third modified furnaces when working together during year ended June 1940.

Fourth Modified Furnace

The next step in blast furnace design was to construct a furnace aiming at the maximum capacity that could be obtained using only one tapping end, increasing the holding capacity of the slag settlers, trying to eliminate leaking shaft jackets, and installing an improved type of refractory block at the lead syphon section in the crucible in order to increase the duration of a furnace campaign. With these points in mind the present No. 4 furnace was designed and constructed (figs. 4 and 5), coming into operation in January 1947.

Furnace design was identical with the previous No. 3 furnace with regard to shaft width, height of shaft, tuyeres, etc., but approximately two thirds the length, thus giving a corresponding smelting capacity while being able to operate on one end of the furnace and handle the production with reasonable ease.

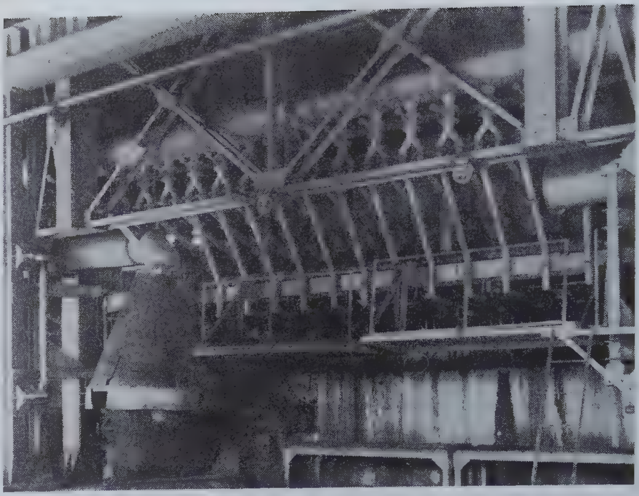

Fig. 5—Fourth modified furnace.

Slag settlers were increased to 5-ton capacity and sillimanite crucible blocks installed at the lead syphon of the crucible lining.

Fresh water circulation was used through the shaft jackets, the supply being pumped through a closed circuit. The water was cooled by passing it countercurrent to a flow of sea water through a heat exchanger, the salt water then being used for slag granulation.

The volume of fresh water pumped through the jackets was 700 gpm, while the volume of sea water used through the heat exchanger for cooling was 1000 gpm.

The average rise in water temperature after passing through the jackets was 6°C, and the sea water rise on the heat exchanger was 4.5°C. The average working temperature of the jacket water was 40° to 50°C.

As stated above, this furnace came into production on January 1947, and has operated with very good conditions both at the feed floor and tapping section; stoppages for accretion removal have been further reduced and it can be stated that the main reasons for stoppages have been for maintenance and other causes not due to furnace operation.

Shaft-jacket failures through leakages have totaled four in nearly three years and in each case a small hole has been burnt through on the flat of the "chair" jacket, indicating that the cause was prob-

Table III. Comparison of Furnace Operations, 1940

	1st Modified Furnace	2nd Modified Furnace	3rd Modified Furnace
Charge treated per day, tons	471	409	954
Coke on charge, pct	10.34	10.42	10.21
Fixed carbon on charge, pct	8.17	8.23	8.07
Stoppages, hr per day:			
Barring	0.30	0.31	
Maintenance, etc.	0.26	0.82	0.016
Total stoppages	0.56	1.13	0.016
Lead contents of slag, pct	2.21	2.20	2.40
Operating efficiency, pct	97.67	96.58	99.43
Blast pressure, oz per sq in.	39	39	34
Blast volume, cfm	7,700	8,000	13,900
Lead tenor of charge, pct	40.37	40.37	40.37

Note: In the above tabulation 3rd modified furnace was placed in operation January 1940, and had not been barred at the time the summary was prepared.

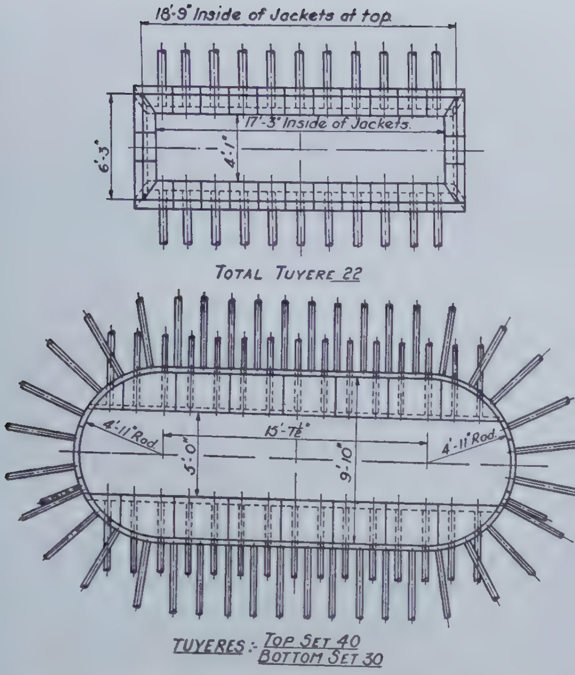

Fig. 6—Tuyere arrangement of the standard and fourth modified blast furnaces.

ably a piece of speiss or pig iron lodging here and burning through the steel plate.

Due to reduced ore supplies this furnace was closed down in December 1948 after two years' operation. There were indications that the crucible lining at the lead well section was failing, but after examination it was found to be in perfect condition.

On account of the successful results achieved by this furnace, a second furnace was constructed of the same design and dimensions and came into operation in June 1948. Its operation has been equally satisfactory.

Table IV shows operating details of the furnaces for year ending June 1948.

The present battery of blast furnaces and the equivalent refined lead production per day is as follows: furnace No. 1, 180 tons; No. 2, 120 tons; No. 3, 250 tons; No. 4, 250 tons; total, 800 tons.

Fig. 6 is a diagrammatic plan of the tuyere arrangement of the standard blast furnace and the fourth modified furnace.

Metallurgical Operations

Although furnace design has greatly improved operating conditions and efficiency, continued developments and improvements in the blast sintering section also have had their effects.

With the introduction of the present sintering plant in 1940, the product has been of a very uniform quality, as the roasting operations are carried out on two 10 ft wide sintering machines with careful attention to charge preparation, charge mixing, and prevention of segregation.

Table IV. Comparison of Furnace Operations, 1948

	Standard Furnace	4th Modified Furnace
Charge treated per day, tons	291	586
Coke on charge, pct	10.66	10.83
Fixed carbon on charge, pct	7.40	7.52
Stoppages, hr per day:		
Barring	0.61	0.07
Maintenance	0.25	0.13
Total	0.86	0.20
Operating efficiency, pct	96.42	98.98
Blast pressure, oz per sq in.	35	35
Blast volume, cfm	5,400	8,000
Lead tenor of charge, pct	45.15	45.15
Lead in slag, pct	1.39	1.40

All fluxes needed for final slag composition are incorporated in the Dwight-Lloyd charge; the only materials not added here are refinery drosses and broken slag settler skulls which are added directly to the furnaces.

Screening of all sinter is carried out over a ⅝ in. screen, the undersize being retreated through the sintering plant.

Each sinter charge produced is weighed automatically, as is the coke per charge, thus the weight control is kept within very close limits.

All coke used passes through a coke breaker, set to reduce the larger pieces down to a maximum size of 4 in. After breaking, the whole of the coke is screened over a ¾-in. screen, the fines being stored for use on the Dwight-Lloyd sintering machine when necessary.

These limiting sizes were chosen having in mind the experience with the experimental blast furnace previously mentioned.

The following general conclusions were drawn from the operation of this experimental furnace: (1) Small coke improves reduction, but through the tendency to burn out in the upper parts of the shaft, it leads to hot furnace top and poor conditions at the tuyere zone. (2) Large coke gives excellent tuyere conditions, but results in poor reduction, and likewise tends to cause hot furnace top and sticky conditions near the charge surface.

Scrap iron is added directly to the blast furnaces in varying proportions, the average being 1.5 pct of the charge weight.

Charge Preparation and Handling

The handling of all charge materials for the furnaces is carried out by an overhead telpher handling system comprising high lift cranes, secondary telphers, and storage bin system. The total capacity of the high lift cranes is 5 tons, and the secondary cranes, 2 tons.

The overhead tracks, which are 58 ft above ground level, span a section from the coke unloading area at the wharf front, and extend over the bin storage system, sinter loading floor to the charging section of the blast furnaces.

The charge handling operation consists in transferring the weighed Dwight-Lloyd sinter in a skip to a position under the secondary telpher from which the weighed amount of coke, etc. is added, after which the skip is moved under command of the high lift crane. The skip is lifted and conveyed to the charge hoppers over the blast furnaces, which feed continuously into the furnaces.

A storage system under command of both types of telpher cranes contains bins for the storage of the charge materials, having the following capacities: coke, 170 tons; lead dross, 300 tons; returned slag, 300 tons; Dwight-Lloyd sinter, 1600 tons.

Lead dross is returned from the refinery section and comprises kettle skimmings and the slag produced from the final refining furnace, which is treated to recover the metal values.

Returned slag consists of broken slag skulls from settler pots from the blast furnaces which are usually contaminated with lead.

During periods when the Dwight-Lloyd plant is closed down, the stored sinter is conveyed to skips by the secondary telpher, then handled in the usual way to the furnace charge hoppers.

The high lift crane takes approximately 5 min to make a complete cycle per charge which is equivalent to 100 charges delivered to the furnaces per 8-hr shift.

Table V. Composition of Charge Material

	D.L. Sinter	Returned Slag Skulls	Lead Dross, Pct
Pb	42.5 pct	Pb 5.0 pct	Pb 70
Ag	12.0 oz per ton	Ag 2.2 oz	
SiO_2	8.9 pct		Zn 9.0
FeO	12.4 pct		
MnO	2.7 pct		
CaO	8.8 pct		
Zn	10.2 pct		
S	1.9 pct		
S as SO_4	1.0 pct		

The coke used (table VI) is mainly mixed coke produced by various companies from coal from the South Coast of New South Wales, the largest supplier being Illawarra Coke Co.

Slag Handling

Slag is tapped from one end of each operating furnace into a cast steel settler pot of 5-ton capacity from whence it overflows into a cast iron granulating launder where it meets a jet of salt water and is broken into granules, the largest size being ⅛ in. diam.

A wide mouthed chute is used at the delivery into the granulating launder thus spreading the stream of slag before it comes into contact with the water jet.

In practice the water is supplied from the heat exchanger system of the fresh water-cooled furnaces; prior to the construction of these furnaces the overflow jacket water was used, supplemented by water from salt water tank storage when necessary. Approximately 1000 gpm of water per furnace is used for slag granulation.

After granulation the slag passes down a curved cast iron launder to an elevator boot from which it is lifted by a bucket elevator into a storage bin of 150-ton capacity and transported by 10-ton motor transport units to the slag storage.

Slag is sampled from the settler overflow at hourly intervals and assayed at 8-hr intervals for plant control.

An average slag analysis is as follows: Pb, 1.37 pct; SiO_2, 21.1 pct; FeO, 28.3 pct; MnO, 4.5 pct; CaO, 13.2 pct; Al_2O_3, 6.3 pct; Zn, 17.55 pct; S, 2.0 pct; Ag, 0.10 oz per ton; new slag fall, 0.67; slag fall arising from circulating slag, 0.56; total slag fall, 1.23; and lead lost in slag per 100 tons lead produced, 0.92 tons.

Bullion Handling

Lead bullion is tapped continuously from the lead syphon into brick-lined cast steel ladles of 10-ton capacity. These ladles rest on a low, four-wheeled carriage mounted on rails which lead under the bullion overflow spout. Two sets of rails, carriages, and ladles are available at each bullion overflow, thus the only time the bullion flow is stopped is when changing ladles. This operation occupies only 2 to 3 min and the normal time for filling a ladle on the present large furnaces is approximately 45 min.

The molten bullion is conveyed by means of an overhead crane to the copper drossing section. The crane runway is parallel to the blast furnaces and covers the copper drossing section as well as the battery of furnaces, also a section north of the furnaces where spare kettle units are stored and the breaking of slag settler skulls is carried out.

There are two cranes, the main hoist of each being capable of lifting 20 tons, while the auxiliary can lift 5 tons; the traveling speed is 300 fpm. Normal operations are usually carried out using one crane.

Copper Drossing

The copper drossing section comprises five 100-ton cast iron kettles each weighing approximately 11 tons. The kettles are oval in shape, set on reinforced concrete foundations lined with firebrick and arranged for oil under-firing. Nos. 1, 2, and 4 are used as drossing kettles, No. 3 as sulphur treatment kettle, and No. 5 as reheating kettle.

The time cycle of operations which can be carried out is as follows: for drossing kettles—filling kettle, 3 hr; removing heavy dross, 1 hr; cooling to 340°C, 3½ hr; pumping to sulphur treatment kettle, ½ hr; total, 8 hr; and for sulphur treatment kettles—filling from drossing kettle, ½ hr; sulphur treatment, 1 hr; pumping to reheating kettle, ½ hr; total, 2 hr.

After filling, each dross kettle is skimmed with the bullion at a temperature of 450° to 500°C, approximately 10 to 15 tons of copper dross being removed and charged into the copper dross treatment furnace.

The charge is now allowed to cool back to 340°C during which time further copper is thrown out of solution, but this dross is not removed. When the temperature has fallen to 340°C, a motor driven pump delivers the liquid metal into the sulphurizing kettle where it is treated with sulphur at the rate of 2 lb per ton of bullion for final copper removal. The sulphur is stirred in over a period of 20 min holding the temperature of the bullion as near to the freezing point as possible. The dross formed is skimmed off and returned to the drossing kettle for treatment in the next filling cycle.

After sulphur treatment the bullion is pumped to the reheating kettle (No. 5) where it is heated to 450°C and then transported molten in a 15-ton brick-lined ladle to the refinery section for final refining.

Table VI. Analysis of Coke

Analysis of Coke, Pct			Analysis of Coke Ash, Pct		
	Type A	Type B		Type A	Type B
VHC	1.6	2.9	SiO_2	46.5	58.5
Fixed Carbon	79.1	68.1	Fe_2O_3	5.57	8.6
Ash	19.3	29.0	MnO	0.45	0.4
Sulphur	0.41	1.6	CaO	5.43	1.2
Porosity	48.7	40.0	MgO	1.8	0.4
			Al_2O_3	33.5	30.2

Typical Blast Furnace Charge	
Dwight-Lloyd sinter	6,600 lb
Refinery lead dross	200 - 300 lb
Returned slag	Nil - 300 lb
Scrap iron	100 lb
Coke	740 - 800 lb

Table VII. Copper Removal

	Furnace Bullion	Bullion after Hot Drossing	Bullion after Cooling to 340°C	Bullion after Sulphur Treatment
Cu	1.1	0.21	0.04	0.004 pct
As	0.25	0.20	0.14	0.14 pct
Sb	0.93	0.90	0.90	0.90 pct
Ag	46.0 oz per ton	46.0	46.0	46.0 oz per ton
Au	0.04 oz per ton	0.04	0.04	0.04 oz per ton
Fe	0.2			
Bi	0.002 pct			0.002 pct
S	0.12 pct			

Table VII shows the copper removal through this section.

Copper Dross Treatment

The copper dross skimmed from the kettles is charged directly into a reverberatory furnace together with pig iron and a small quantity of silica sand.

The top of the dross furnace is on the same level as the skimming floor of the copper drossing section, the dross is wheeled in small pots (1/3-ton capacity) and enters the furnace through one of two water-cooled charging ports set in the arch of the furnace.

Bullion is drawn off through a syphon tap (similar in design to the lead blast furnace) into a bullion ladle with 10-ton capacity under command of the bullion crane, then delivered to the drossing kettles for retreatment.

A double hole tapping breast is set in the furnace side, the center of the top hole being 3 in. higher than the bottom hole.

Slag is tapped from the top hole, also matte, while copper speiss is tapped from the bottom hole. The whole of these products in turn is delivered to an endless chain casting machine, cooled by water spray, and discharged into skips under command of the bullion crane.

The slag is returned to the blast furnace charge for recovery of the metal values, and the copper matte and copper speiss are stored and shipped to Port Kembla, New South Wales, for copper recovery by the Electrolytic Refining and Smelting Co. of Australia.

The furnace is fired with a 5 in. Major Oil Burner using 35 to 45 gph of oil (Imp. gal).

The normal furnace charge is: copper dross, 2240 lb; silica sand, 25 to 40 lb; iron, 50 to 150 lb.

Table VIII gives the composition of copper dross treated and products from the furnace.

A furnace is now being constructed to treat the copper dross using soda ash as is practiced by some American smelters and will be ready for operation in a short time.

Fume Recovery and Handling

Blast furnace gases from the downtake flues enter the top of a main brick flue which is parallel with the furnaces and connects with the main smoke stack. This flue is 520 ft long, 15 ft wide, 16 ft high, constructed of brick. The main stack is 205 ft high.

The fume laden gas is delivered to a baghouse, constructed of brick, through a 9-ft diam steel flue 180 ft long, being forced into the baghouse by means of Sirocco fan running at 442 rpm driven by a 250 hp Metropolitan Vickers Synchronous motor. The filtered gases are drawn out by a similar type fan and motor and delivered to the flue at the base of the main stack. The baghouse is divided into eight sections, each section being 57 ft long, 14 ft 9 in. wide, and 49 ft 6 in. high, equipped with 156 woolen bags, 20 in. in diam, 29 ft 6 in. long, the material having 22 threads per inch in both warp and weft. The bags are in rows of 26, six rows per chamber. The total filtering surface is 190,000 sq ft.

Beneath the thimble floors are mild steel collecting troughs and screw conveyors, two to each chamber, thus three rows of bags discharge into each screw conveyor.

After mechanical shaking of the bags, the collected fume is dislodged and falls into hoppers from which it is removed by means of the screw conveyors. On discharge from the conveyors it is conveyed by a stream of water down sloping launders to a central sump where it is agitated by means of a wooden paddle stirrer. This solution is circulated by means of a centrifugal pump until the pulp is built up to a density of 30 pct solids.

The pulped material is then dewatered by American filters in the sintering plant where the filter cake again enters the lead treatment system after the first sintering machine.

The filtrate, which contains water soluble cadmium, is passed through precipitating tanks, six in all, each tank containing a cylindrical moving trommel, containing zinc slabs, which precipitates the cadmium as a fine metallic sponge which settles out in the tanks.

Table VIII. Composition of Copper Dross Treated and Furnace Products

	Copper Dross	Bullion Produced	Copper Matte Produced	Copper Speiss Produced	Slag Produced
Pb, pct	71.0		14.2	15.4	4.5
Cu, pct	12.0	1.96	40.8	40.8	6.0
As, pct	2.2	0.35	3.0	8.5	
Sb, pct	0.5	0.90	0.5	1.1	
Fe, pct	1.9		16.0	15.4	
S, pct	2.7		14.4	9.5	
Ag, oz per ton			15.5	20.0	

This sponge contains impurities, the main one being lead. It is melted under caustic soda and cast into 7-lb pellets, these pellets in turn are refined by distillation in retorts, the refined cadmium then being remelted and cast into rods 5/16 in. in diam, 12 in. long, weighing about 5 oz each. The rods are then packed into 1 cwt. boxes for shipment.

The average analysis of blast furnace baghouse fume is as follows: Pb, 48.6 pct; Zn, 17.7 pct; Cd, 4.07 pct; Cd (water sol), 1.87 pct; Ag, 0.96 oz per ton; S, 7.3 pct; Cl, 6.9 pct; As, 0.59 pct; Sb, 0.12 pct; volume of gas handled, 120,000 cfm; fume recovered, pct of charge, 2.1 pct; lead loss (tons per week), 1.36; lead loss, pct of new input lead, 0.04 pct; and filtering efficiency 98.2 pct.

The average composition of crude and refined cadmium is shown in table IX.

Table IX. Cadmium Composition

	Crude Cadmium	Refined Cadmium	
Pb	1.0 pct	Pb	0.018 pct
Ag	5.0 oz per ton	Zn	0.003 pct
Cd	98.9 pct	Cu	0.001 pct
		Fe	0.001 pct
		Cd not less than	99.97 pct

Acknowledgment

The writer is indebted to the management of The Broken Hill Associated Smelters Proprietary Limited, for permission to publish this paper.

The Isothermal Transformation
Of a Eutectoid Beryllium Bronze

by

Ronald H. Fillnow

and

David J. Mack

Above the nose of the T-T-T curve the first product is fine lamellar pearlite, which subsequently transforms to a coarse pearlite, also by nucleation and growth. At lower temperatures this coarse pearlite forms directly from beta. Numerous metastable structures are formed before the pearlite reactions begin. The transformation is followed by metallographic microhardness and X-ray methods.

IT has been demonstrated that alloys in systems structurally analogous to steel undergo reactions during heat treatment similar to those of steel, and yet very little work has been done on such systems, particularly from the standpoint of isothermal transformation. The literature shows that most of the isothermal work has been done on copper-aluminum alloys.[1-3] One paper has been reported on a eutectoid copper-silicon alloy,[4] and one on iron-nitrogen alloys.[8]

There are no published reports of previous investigations on the isothermal transformation of a eutectoid beryllium bronze. At least two papers have been reported on isothermal age-hardening phenomena in beryllium-copper alloys of lower beryllium content.[5, 6] No information on eutectoid transformations in this alloy is given in Rimbach's book, "Beryllium."[7]

This paper reports the results of an investigation on the isothermal transformation characteristics of a eutectoid beryllium bronze.

Materials Used and Procedure

The eutectoid beryllium bronze used in this investigation was centrifugally cast at the Ampco Metal Co., Inc., Milwaukee, Wis. A master beryllium-copper alloy, purchased from the Brush Beryllium Co., was used to make the beryllium addition to the copper. The alloy was melted under a protective carbon cover and centrifugally cast into a graphite mold preheated to 920°F. Some trouble with segregation of beryllium in the melt was encountered but was eliminated by violent stirring during melting and pouring.

Since very thin specimens were used for the various heat treatments, only one casting of the four prepared was necessary for the complete isothermal study, thus eliminating any discrepancies caused by a change in composition. The analysis of this casting was 94.035 pct copper and 5.965 pct beryllium. A slight trace of iron was found.

The castings were sawed into specimens approximately 3/32 in. in thickness. The specimens were first given an "austenitizing" heat treatment at 788°C, well within the single phase beta region, in a vertical tube furnace. The specimens were then quenched individually into an adjacent molten salt bath and held there for a definite time, after which they were quenched into water at room temperature. Temperature was held to ± 2°C in the salt bath. No homogenizing treatment was given the specimens other than the soak at 788°C. Despite the fact that this was a cast alloy, no evidence of segregation or coring was found in the microstructure of any specimen, either as cast or as heat-treated.

Upon completion of the heat treatment, the specimens were subjected to metallographic examination

---

RONALD H. FILLNOW is associated with Westinghouse Electric Corp., Pittsburgh, Pa., and DAVID J. MACK, Member AIME, is Assistant Professor of Metallurgical Engineering, University of Wisconsin, Madison, Wis.

AIME Chicago Meeting, October 1950.

TP 2926 E. Discussion (2 copies) may be sent to Transactions *AIME before Dec. 15, 1950. Manuscript received April 5, 1950; revision received July 17, 1950.*

This paper is extracted from a thesis submitted by Ronald H. Fillnow to the Graduate faculty at the University of Wisconsin in partial fulfillment of the requirements for the degree of Master of Science (Metallurgical Engineering).

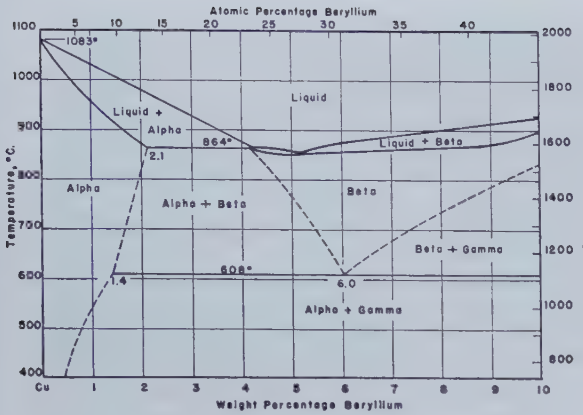

Fig. 1—Equilibrium diagram.

and microhardness tests. An electrolytic etch with 1 pct chromic acid was used for the micrographs presented herein unless otherwise stated. The fine pearlite structures obtained isothermally at temperatures below 450°C were irresolvable with the light microscope, so a number of Formvar replicas, shadow cast with uranium, were made of the surface for examination with the electron microscope. X-ray diffraction methods were used as a third means of identification of phases, in addition to metallographic examination and microhardness tests.

The Eutectoid Temperature

The modified phase diagram for the copper-rich end of the copper-beryllium system is shown in fig. 1, which was taken from the Metals Handbook. It became apparent early in this work that the accepted eutectoid temperature of 575°C was too low. Determination of the eutectoid temperature by means of heating and cooling curves (the rate in both cases being less than 1°C per min) gave values of 614° and 598°C, respectively. Isothermal transformation of the high temperature beta gave a value of 608°C, no decomposition of the beta occurring at 610°C in 90 hr. The value of 608°C was chosen as the eutectoid temperature in fig. 1. Since no determination of the maximum solubility of beryllium in copper was made, the values shown are those from the accepted diagram from which fig. 1 was taken.

As will be shown, the beta transforms at 592° to lamellar pearlite, but when it transforms at the eutectoid temperature, 608°, the first product formed is alpha, followed by gamma from the beryllium-rich beta immediately adjacent to the alpha, then more alpha and so on; i.e., alternate precipitation. Ultimately, the remaining beta also begins to transform simultaneously to pearlite. These structures are shown in fig. 2. A similar type of reaction has just been reported by Bose and Hawkes[8] in a eutectoid iron-nitrogen alloy.

Results: Isothermal Transformation at 592°C

The initial transformation product is a fine pearlite consisting of alternate lamellae of alpha and gamma phases. The early growth of the fine pearlite is along the grain boundaries, but, at this high temperature, nucleation and growth within the grain are almost simultaneous with the grain boundary reaction, fig. 3.

It is necessary in most instances to go to high magnifications to resolve the fine pearlite lamellae completely, fig. 4. In nodules where the growth has been very rapid, the lamellae of one colony may extend unbroken completely across the full width of the nodule.

Before the fine pearlite reaction has gone to completion, a coarse pearlite* begins to grow within the areas of fine pearlite. The coarse pearlite is nucleated within the areas of fine pearlite and grows in nodular form in much the same manner as the fine pearlite, fig. 5. The wide, well-defined areas of

---

* The authors are aware that an objection can be raised to calling this structure pearlite, in view of its possible origin. However, since it is essentially a lamellar structure the use of the term "coarse pearlite" seemed permissible.

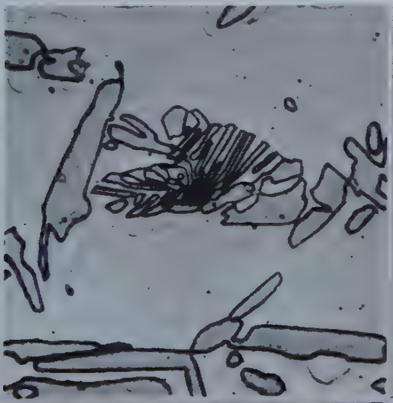

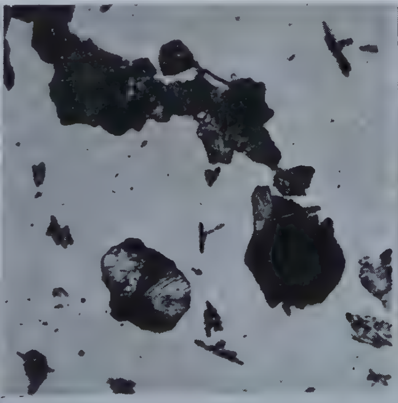

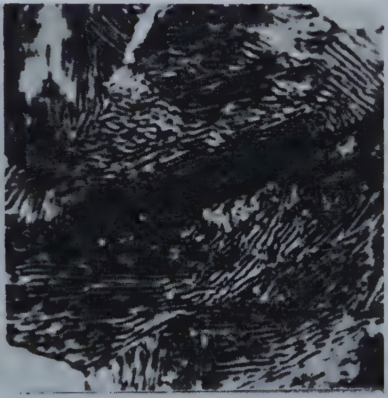

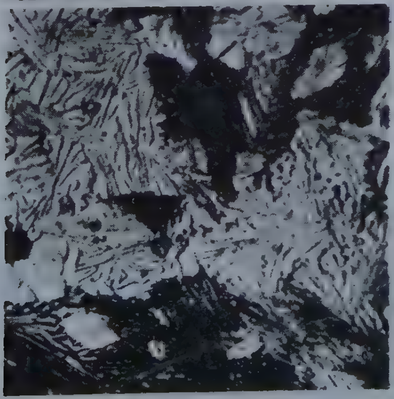

Fig. 2 (upper left)—15 hr and 20 min at 608°C.
The dark etching areas are alpha surrounded by faint gamma. Pearlite is also forming. X500.

Fig. 3 (center)—90 sec at 592°C.
Fine pearlite in retained beta. X750.

Fig. 4 (right)—105 sec at 592°C.
Fine pearlite in retained beta. X2000.

Fig. 5 (lower left)—17 hr at 592°C.
Fine pearlite is dark, the coarse pearlite is light. Lighting was slightly oblique. X750.

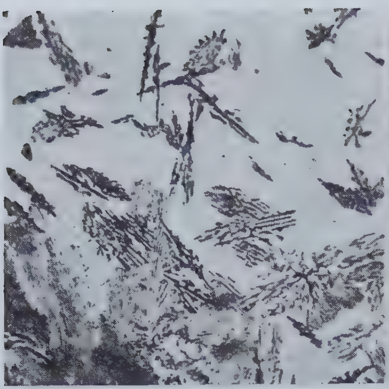

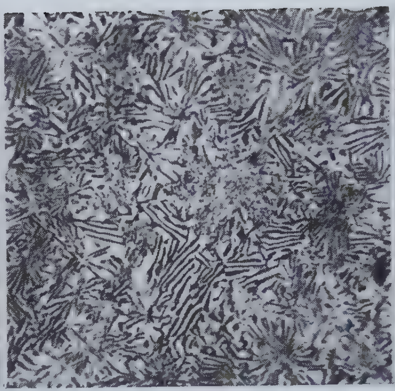

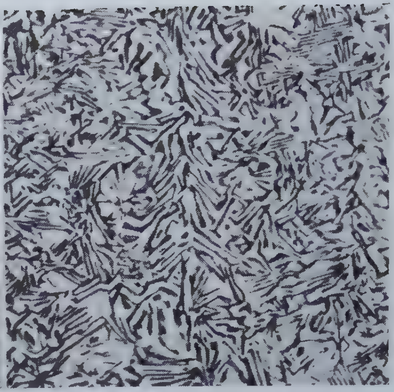

Fig. 6 (left)—5 min at 592°C.

Fine pearlite in retained beta. Structure of the needle-like phase is unknown. X750.

Fig. 7 (center)—4 hr and 21 min at 550°C.

Coarse pearlite with some fine pearlite. X750.

Fig. 8 (right)—92 hr and 42 min at 550°C.

All coarse pearlite. X750.

alternate alpha and gamma are easily distinguished from the feathery, gray, etching areas of fine pearlite.

The two pearlite structures are the result of two separate, distinct reactions. With the nucleation of the coarse pearlite nodule, a definite dissimilarity is seen between it and the surrounding fine pearlite. The conclusion is drawn, therefore, that no gradual coarsening reaction is taking place. The fine pearlite with its narrow, straight lamellae in fig. 4 should be compared with the broad irregular shaped lamellae of the coarse pearlite in fig. 5, better shown in fig. 8. Additional evidence for the existence of two separate pearlite reactions is the growth of the coarse pearlite across the lamellae of the fine pearlite as shown by faint pseudomorphs of the fine pearlite which are occasionally visible, although the writers were unsuccessful in photographing them.

An unusual microstructure suggesting an additional precipitate is shown in fig. 6. The fine pearlite reaction is about 60 pct complete. The needle-like precipitate seems to indicate a third reaction. These coarse needles, however, soon disappear with the subsequent growth of the fine pearlite, although a few of them are still apparent 10 min later.

The changes in microhardness during isothermal transformation at 592°C are shown in fig. 9. It is seen that they correlate well with microstructural changes.

Isothermal Transformation at 550°C

The fine pearlite reaction is completely finished at a holding time of 40 sec. The coarse pearlite reaction begins at 5 min, but the growth is slower than at higher temperatures. With a lowering of the isothermal temperature from 592° to 550°C, the lamellae in both the coarse pearlite and the fine pearlite are considerably finer.

The method of growth of the coarse pearlite is difficult to establish. Generally the growth is in a nodular form, but very often the growth is irregular and disorganized. This makes it very difficult at times to distinguish between the two pearlites as shown in fig. 7. The transformation of fine pearlite to coarse pearlite is approximately 60 pct complete in the specimen shown in fig. 7. This is supported by hardness data given in fig. 10. The fine pearlite is more readily resolvable at the longer holding time. The appearance of the coarse pearlite after a long holding time is shown in fig. 8. It is rather remarkable that little, if any, spheroidization has occurred in this 92-hr period.

Isothermal Transformation at 502°C

The nucleation and growth of the fine pearlite is extremely rapid at this temperature. The fine pearlite appears only as a dark etching material completely irresolvable with the light microscope, fig. 11.

The beta phase retained from this temperature has a somewhat mottled appearance in comparison with the clear, almost structureless beta retained in the quench from higher isothermal temperatures.

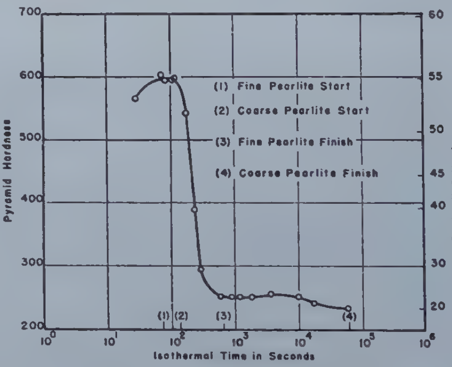

Fig. 9—Changes in microhardness at 592°C.

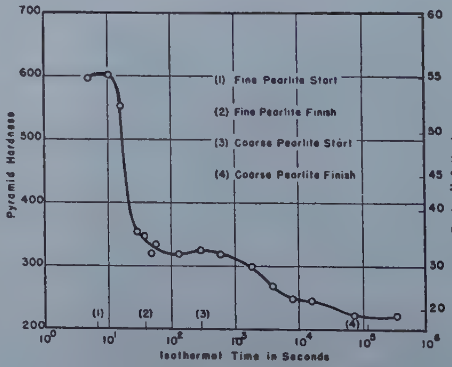

Fig. 10—Changes in microhardness at 550°C.

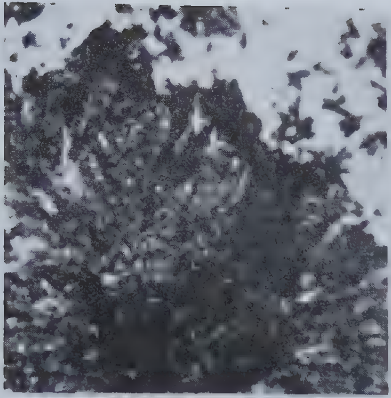

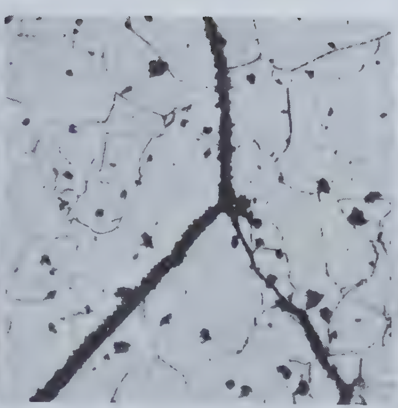

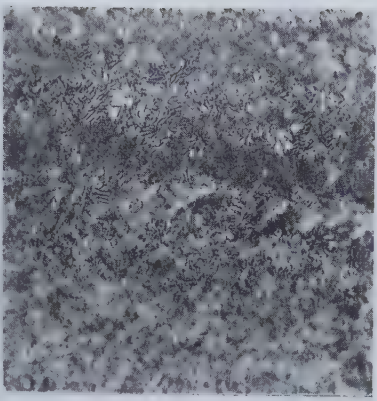

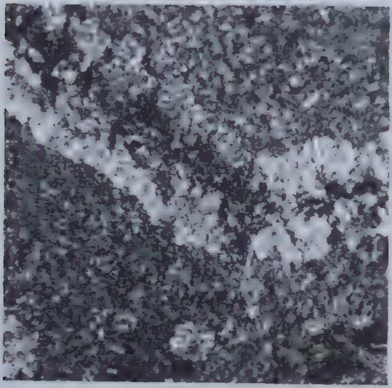

Fig. 11 (top left)—10 sec at 502°C.
Fine pearlite in retained beta. X2000.

Fig. 12 (center)—6 sec at 502°C.
Fine pearlite along the old beta boundaries and as nodules in retained beta. The pseudo-grain boundary network is formed by the precipitation of an unknown phase. X750.

Fig. 13 (right)—30 min at 502°C.
Fine pearlite with some coarse pearlite along the old beta grain boundary. X750.

Fig. 14 (bottom left)—4 hr at 452°C.
Fine pearlite (dark etching) along the old beta grain boundary surrounded by coarse pearlite (light etching) in dark retained beta. X500.

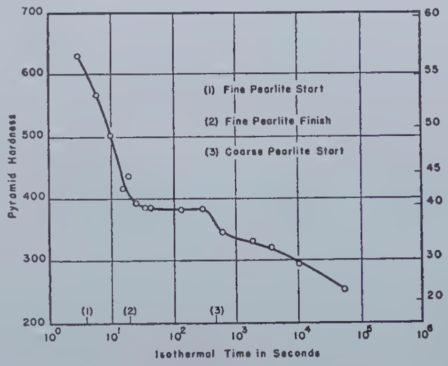

Fig. 15—Changes in microhardness at 502°C.

In several grains, the "particles" responsible for the mottled effect tend to align themselves into a fine pseudo-grain boundary network, fig. 12. This is not a recrystallization phenomenon, since the particles later disappear completely with subsequent growth of the fine pearlite. A micrograph taken at a slightly longer holding time, fig. 13, shows no evidence of these particles or the pseudo-grain boundary network.

Fig. 14 is one of several micrographs showing a change in the etching characteristics of the retained beta at this temperature and below as contrasted with the clear etching beta retained from higher isothermal temperatures. The etching reagents used, 1 pct chromic acid or 5 pct ferric nitrate, give a simulated lamellar appearance to the dark etching beta matrix when viewed with oblique light. This etching phenomenon appears at longer holding times after the pseudo-grain boundaries of fig. 12 disappear. That this is only an etching effect was confirmed by electron micrographs of this structure. The coarse pearlite lamellae decrease in size as the transformation temperature is lowered, fig. 13.

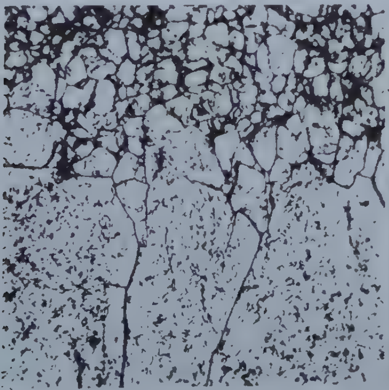

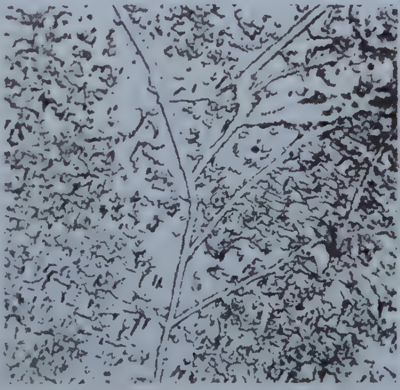

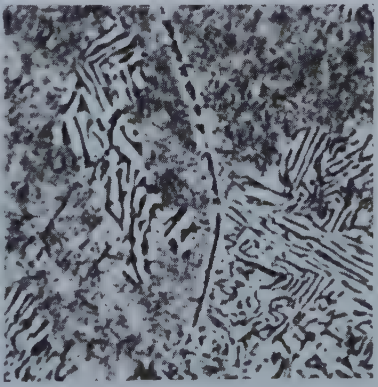

Fig. 16 (left)—4 sec at 452°C.
An unknown metastable phase dispersed in retained beta. X250.

Fig. 17 (center)—6 sec at 452°C.
Unknown metastable phase in retained beta. This is termed a "rippled" structure. No fine pearlite is visible in this field. X750.

Fig. 18 (right)—17 hr at 452°C.
Coarse pearlite in a matrix of mottled retained beta. Some fine pearlite exists in the upper right corner. X2000.

Microhardness data, fig. 15, again validate the fine pearlite start and finish and the coarse pearlite start.

Isothermal Transformation at 452°C

This transformation temperature lies well within the range of age hardening for copper-beryllium alloys of lower beryllium content. The formation of fine pearlite begins at the grain boundaries at 6 sec, but the growth is very slow. Nucleation and growth of the nodules within the grains does not become evident until holding times of approximately 30 min have been reached. The fine pearlite lamellae become resolvable only after a considerable holding time.

Some form of a metastable precipitate also forms rapidly at this temperature, only to disappear a few seconds later. The particles precipitate as tiny rods which align themselves to form a pseudo-grain boundary network very similar to that formed at 502°. Some particles also precipitate within the beta grains, fig. 16.

With an additional holding time of 2 sec, this pseudo-grain boundary network has disappeared to form the "rippled" structure of fig. 17. This "rippled" structure in turn is replaced by a "mottled" structure as shown in fig. 22, for a specimen transformed at lower temperature. The rippling of the beta is presumably caused by a metastable phase which remains only momentarily. On the other hand, the mottled appearance of the retained beta is very stable, especially at lower temperatures. It should be emphasized that all of these changes occur before any appreciable amount of pearlite has formed and that the hardness remains approximately constant during these microstructural changes, fig. 19.

Guy, Barrett, and Mehl[5] proposed that the similar rippling, or striping, as they describe it, of the beta in their lower beryllium alloys was caused by a decomposition of the beta grains. If this were true, it should be accompanied by a corresponding change in hardness, which was not observed, fig. 19.

With the appearance of the grain boundary reaction, this rippled precipitate disappears completely to form the mottled dark etching matrix previously shown in fig. 14.

The grain boundary reaction exhibits age-hardening characteristics as demonstrated by a slight rise in hardness, fig. 19. For lower beryllium-copper alloys, Bumm[6] found this grain boundary reaction to grow to only a limited extent at temperatures below 500°C. Aging at temperatures of 500°C or higher, he found the reaction to cover the entire grain. This is in complete agreement with the results of this investigation. He interpreted the halting of the grain boundary reaction as indicative of the presence of a submicroscopic reaction in the center of the grain.

The structure formed initially at the grain boundaries at 425°C is irresolvable, but the similarity of this grain boundary reaction at 452°C to the reaction at 502°C, which results in a completely pearlitic structure, is such that the writers believe the fine pearlite to be formed at the lower temperature as well.

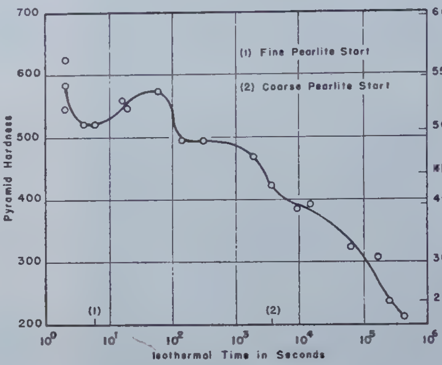

Fig. 19—Changes in microhardness at 452°C.

The nucleation and growth of the coarse pearlite at this temperature is not confined to areas of fine pearlite, as was the case at higher temperatures. The coarsening transformation products grow in completely untransformed beta areas as well as in the fine pearlite areas. A submicroscopic reaction, as suggested by Bumm, may halt the growth of the fine pearlite but may offer no resistance to the growth of the coarse pearlite. The progress of both reactions is shown in fig. 18, which also indicates the growth of the coarse pearlite directly into the beta matrix.

Microhardness readings taken on specimens which have been held at this temperature for 15 hr, or more, show a definite softening of the retained beta. This may indicate the presence of

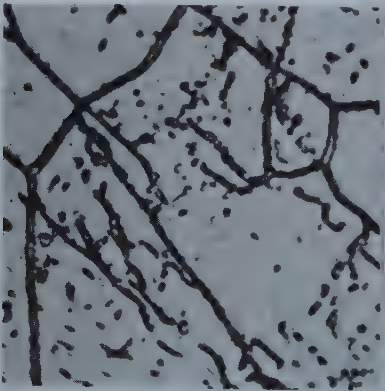

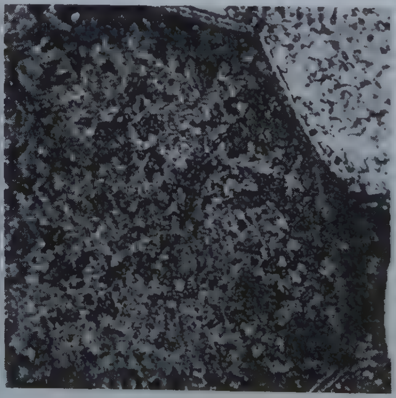

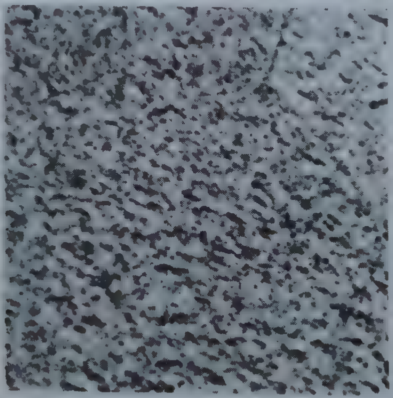

Fig. 20 (left)—4 sec at 402°C.

An unknown metastable phase forming a pseudo-grain boundary network in retained beta. X2000.

Fig. 21 (center)—6 sec at 402°C.

Retained beta showing the rippling effect with fine pearlite at the grain boundaries. Ferric nitrate etch. X1000.

Fig. 22 (right)—12 sec at 352°C.

Mottled retained beta. Ferric nitrate etch. X2000.

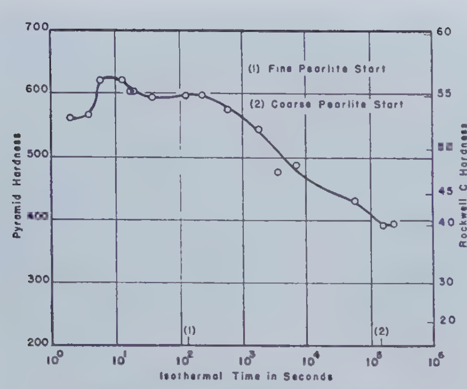

Fig. 23—Changes in microhardness at 402°C.

some reaction within the areas of retained beta. The writers believe that the softening of the retained beta is due to the formation of very small areas of fine pearlite, too small to be resolved microscopically, but visible under highly oblique polarized light.

Isothermal Transformation at 402°C

The sequence of reactions is the same at this temperature as at 452°C. The pseudo-grain boundary network is shown in fig. 20, and the subsequent appearance of the rippled structure of the beta is shown in fig. 21. The hardness data at this temperature, fig. 23, indicate a slight early rise in hardness, associated with the formation of the rippled structure in the beta, fig. 21.

The coarse pearlite reaction is approximately 3 pct complete at a transformation time of 63 hr. Examination of the specimen under polarized light showed many minute areas, within the grain, exhibiting the same structural characteristics as the coarse pearlite. These small areas apparently are nucleating centers for subsequent growth of the coarse pearlite nodules.

Isothermal Transformation at 352°C

The pseudo-grain boundary network disappears so rapidly that at a holding time of 12 sec, no evidence remains of its former existence, fig. 22. This mottled retained beta remains practically unchanged in structure except for a very slight grain boundary reaction. Hardness values remain constant until the start of the grain boundary reaction, fig. 24.

Isothermal Transformation at 305°C

The microstructure, from a holding time of less than 1 sec to holding times of 12 hr, remains unchanged and is the mottled beta previously described. Some of the small rodlike particles are formed, but they do not align themselves into a network as occurred at higher transformation temperatures. The grain boundary reaction, presumably fine pearlite, beginning at 12 hr, has the same appearance as the age-hardening precipitate formed at temperatures of approximately 300°C in the investigation by Guy, Barrett, and Mehl.[5] The initial stage of the grain boundary reaction is shown in fig. 26. The lamellar nature of the precipitate is not distinguishable even at a holding time of 116 hr. Hardness data for this temperature are shown in fig. 25.

Isothermal Transformation at 254°C

A very fine pseudo-grain boundary network is formed at this temperature but disappears almost immediately. The individual particles are too small to be resolved with a light microscope. A slight trace of the network still remains at longer holding times, fig. 27.

With an isothermal time of 30 sec, a rod shaped precipitate is formed in a pattern resembling a Widmanstätten structure, fig. 28. A slight trace of the pseudo-grain boundary network is still visible in this micrograph. At an isothermal time of 60 sec this Widmanstätten precipitate has completely disappeared, leaving a mottled appearing structure with an evenly distributed, finely divided precipitate similar to that shown in fig. 29. Hardness data for this temperature are shown in fig. 30.

Isothermal Transformation at 204°C

The microstructure formed at this temperature remains practically unchanged from an isothermal transformation time of less than 1 sec to a time of 19 hr. The temperature is too low for any transformation of the retained beta to take place, as is confirmed by hardness data, fig. 31.

X-ray Diffraction Studies

No extensive analysis of the structures produced by isothermal transformation was attempted, the diffraction studies being limited to an identification of suspected beta and the fine and coarse pearlites. It should be mentioned, however, that in no case were lines observed which could not be ascribed to either the alpha, beta, or gamma phases.

Fig. 32 shows comparative diffraction pictures of the fine and coarse pearlites, as produced by isothermal transformation at 518° and 520°C, respectively. Also included is a picture of the pearlitic structure produced by allowing the alloy to cool slowly in the furnace to room temperature. It is obvious that all three pictures have identical lines indicating that the same phases, alpha and gamma,

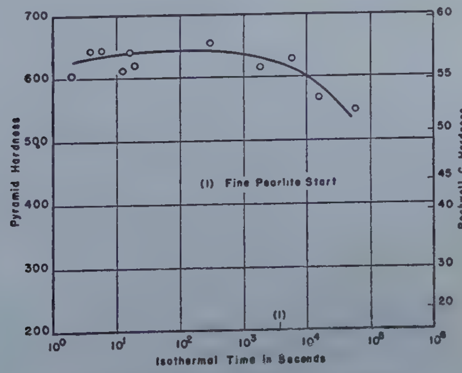

Fig. 24—Changes in microhardness at 352°C.

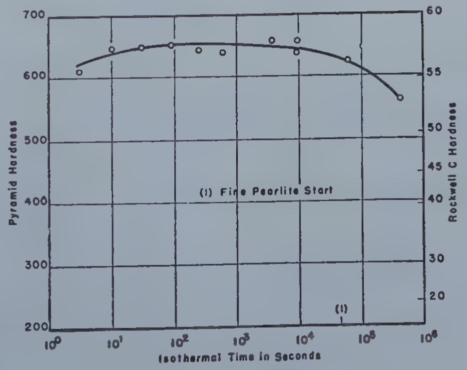

Fig. 25—Changes in microhardness at 305°C.

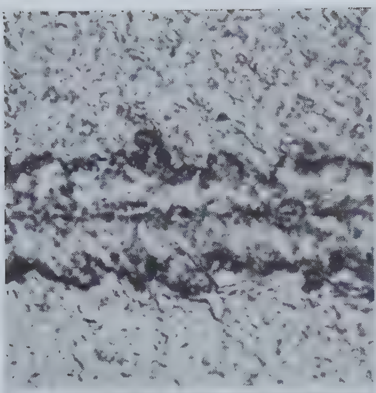

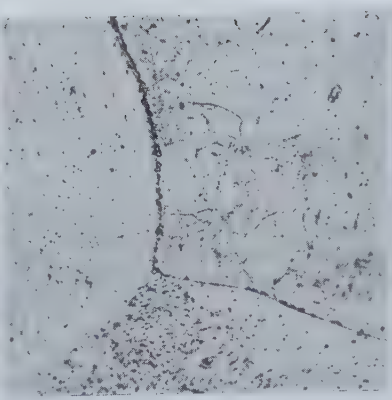

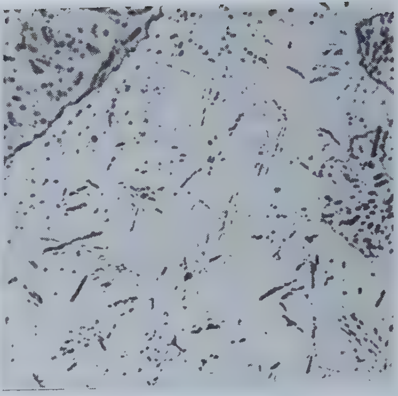

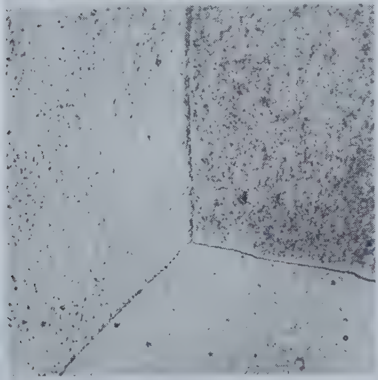

Fig. 26 (top left)—17 hr at 302°C.
Fine pearlite along the grain boundary in retained beta (mottled). X2000.

Fig. 27 (center)—10 sec at 254°C.
Unknown precipitate in retained beta. X750.

Fig. 28 (right)—30 sec at 254°C.
Unknown precipitate in retained beta. X500.

Fig. 29 (bottom left)—18 hr and 41 min at 204°C.
Retained beta with a finely divided precipitate. Ferric nitrate etch. X750.

are present in all three specimens. As might be expected because of the relatively large size of the alpha and gamma platelets in the coarse pearlite and the small size of the sliver specimen employed, the coarse pearlite pattern shows considerable spottiness. Measurement of the patterns shows that the alpha lattice parameter is somewhat smaller in the coarse pearlite than in the fine pearlite.

It is interesting to note that all of the lines due to the gamma phase can be accounted for by a simple cubic lattice, which is, at first glance, anomalous. However, the gamma phase corresponds to the compound, CuBe, which is body-centered cubic with the CsCl type of ordering. Hence the beryllium atoms contribute very little to the diffraction pattern, the observed "simple-cubic" lines coming exclusively from the copper atoms.

Discussion of Results

The results of these studies are shown on the usual isothermal transformation diagram in fig. 33. The shape of the curves is similar to those published for other binary alloys. There is no positive microstructural evidence of a bainite reaction, although some of the structural changes in the retained beta before the fine pearlite reaction begins may be associated with a bainite reaction of the type described by Klier and Grymko[3] for aluminum bronze.

The stresses developed in a quench from the single phase beta region to room temperature were often sufficient in magnitude to shatter the specimen. The fracture was very coarse and granular. Upon quenching directly to a temperature of —76°C (obtained with dry ice and acetone), the specimen was quite tough when fractured. The fracture was smooth, indicative of a ductile material. Subsequent fracture at room temperature, however, again revealed a coarse granular structure. This suggests the presence of a reversible martensite reaction with an M_s below room temperature. This possible reaction was not investigated further.

X-ray diffraction studies of the isothermal structures proved conclusively the retention of the beta phase at room temperature. The diffraction pictures also showed that the two pearlites were composed of the same phases—alpha and gamma, thus simplifying the T-T-T diagram, fig. 33, considerably.

It is possible to have two successive pearlite-type reactions only if the second product is of a coarser

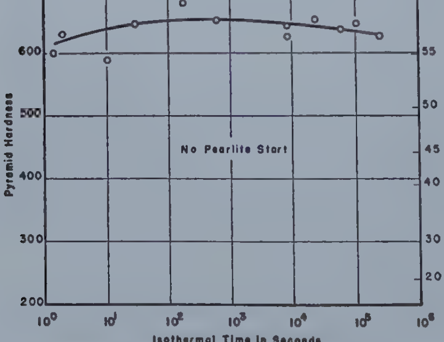

Fig. 30—Changes in microhardness at 254°C.

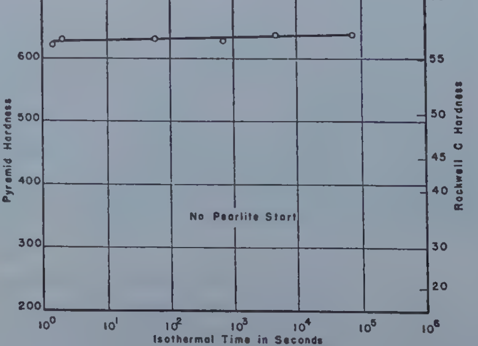

Fig. 31—Changes in microhardness at 204°C.

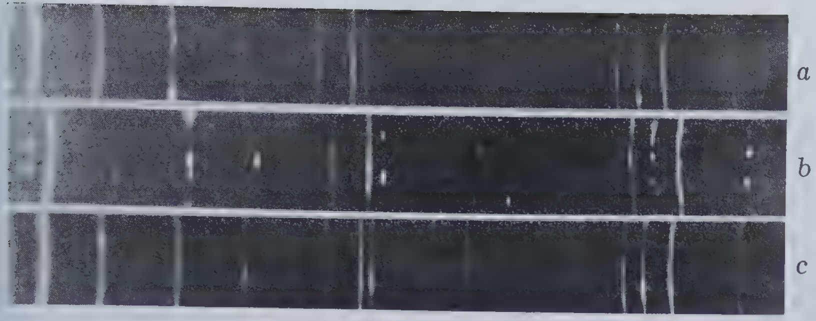

Fig. 32—X-ray diffraction pictures of the pearlites. Filtered copper radiation.

a. Fine pearlite produced by isothermal transformation, 4 min at 518°C. *b.* Coarse pearlite produced by isothermal transformation, 50 hr at 520°C. *c.* Pearlite produced by slow cooling in the furnace. All pictures show the same lines, indicating only the alpha and gamma phases.

nature than the first and has a correspondingly lower hardness than the preceding pearlite structure. Each reaction is accompanied by a release of energy and approaches more closely the final equilibrium end product.

When the eutectoid is first formed, the alpha therein is supersaturated with respect to beryllium, but with longer isothermal times, it rejects beryllium atoms which migrate to the adjacent gamma which is considerably richer in beryllium. As this rejection continues, the alpha becomes softer, slowly approaching its equilibrium state. The rejection of the excess beryllium from the supersaturated alpha is substantiated by the decrease in lattice parameter and results in better delineation of the pearlite lamellae.

The formation of the second, or coarse, pearlite is undoubtedly associated with the recrystallization of the alpha phase in the primary, or fine, pearlite. The general features of this recrystallization reaction in age-hardening alloys have been described by Geisler,[9] and such a reaction has been shown[5] to exist for lower beryllium alloys whose composition lies in the usual age-hardening range. That it could occur when the matrix structure is as *relatively* coarse as the fine pearlite was totally unexpected.

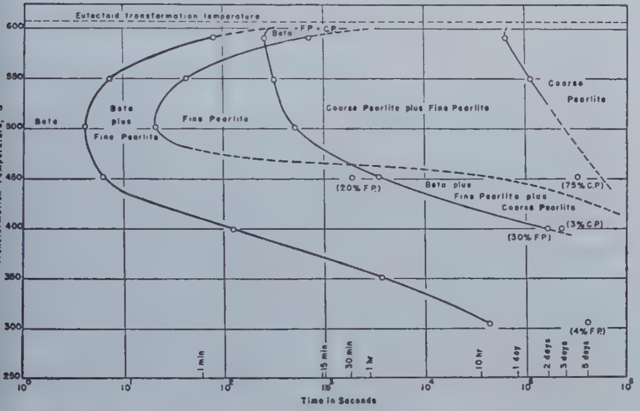

Fig. 33—T-T-T diagram for a eutectoid beryllium bronze.

Summary

The isothermal transformation characteristics of a eutectoid copper-beryllium alloy have been determined. The following significant observations have been made.

1. The eutectoid temperature has been relocated at 608°C instead of the accepted temperature of 575°C.
2. The transformation generally occurs as in eutectoid steel, although no microstructural evidence of a bainite reaction was found. As the transformation temperature decreases, the inter-lamellar spacing of the pearlite decreases.
3. Two separate and distinct pearlite reactions have been described. The first pearlite formed from the high-temperature beta phase is fine and uniformly lamellar. The second pearlite, which forms by nucleation and growth from the first pearlite at high temperatures but also directly from the beta at lower temperatures, is much coarser and less regular. It is suggested that the coarse pearlite forms from the fine pearlite as a consequence of recrystallization of the alpha matrix in the eutectoid.
4. The possibility of a reversible martensite reaction at sub-zero temperatures has been shown to exist.
5. It is readily possible to retain the high-temperature beta to room temperature provided the cooling rate is sufficiently rapid. Even though the cooling of the specimen is interrupted by an isothermal holding at an intermediate temperature, the remaining beta can also be retained at room temperature by the subsequent quench.
6. The three identified products, fine pearlite, coarse pearlite and beta, have characteristic microhardness.
7. Microhardness data correlates well with observed microstructures.
8. At temperatures below the nose of the T-T-T diagram (500°C) the beta phase undergoes a series of microstructural changes involving unknown effects before transforming to pearlite. The microhardness is not affected by these changes.

Acknowledgment

The authors wish to express their appreciation for the cooperation and aid of J. F. Klement, of Ampco Metal, Inc.; K. F. Wendt, of the Engineering Experiment Station; John Hanson, senior student; and Ray C. Wiggen in the construction of the experimental equipment for this investigation.

References

[1] C. S. Smith and W. E. Lindlief: *Trans.* AIME (1933) **104**, 69-115.

[2] D. J. Mack: *Trans.* AIME (1948) **175**, 240-261; *Met. Tech.* (Sept. 1947) TP 2242 E.

[3] E. P. Klier and S. M. Grymko: *Trans.* AIME, **185**, 611-620; *Jnl. Met.* (Sept. 1949) TP 2573 E.

[4] W. R. Hibbard, Jr., G. H. Eichelman, Jr., and W. P. Saunders: *Trans.* AIME (1949) **180**, 92-100; *Met. Tech.* (Sept. 1948) TP 2441 E.

[5] A. G. Guy, C. S. Barrett, and R. F. Mehl: *Trans.* AIME (1948) **175**, 216-239; *Met. Tech.* (Feb. 1948) TP 2341 E.

[6] H. Bumm: *Ztsch. Metallkunde.* (1937) **29**, 30-32.

[7] R. Rimbach and A. J. Michel: Beryllium. (1932). New York. Chem. Catalogue Co., Inc.

[8] B. N. Bose and M. F. Hawkes: *Trans.* AIME, **188**, 307-316; *Jnl. Met.* (Feb. 1950) TP 2790 E.

[9] A. H. Geisler: *Trans.* AIME (1949) **180**, 230-254; *Met. Tech.* (Aug. 1948) TP 2436 E.

Hydrogen Solubility In Aluminum and Some Aluminum Alloys

by W. R. Opie and N. J. Grant

HYDROGEN in molten aluminum and aluminum alloys, which precipitates during cooling and solidification, is the principal cause of pin hole porosity in ingots and castings. Much attention has been given to determining the effect of temperature and pressure on the solubility of hydrogen in pure aluminum, but little data are available on hydrogen solubility in aluminum alloys. This investigation was undertaken to check results reported for pure aluminum and to show the effect of silicon and copper additions on the amount of hydrogen contained by molten alloys.

W. R. OPIE, Junior Member AIME, is Research Metallurgist, Titanium Division, National Lead Co., Sayreville, N. J., and N. J. GRANT, Member AIME, is Associate Professor of Metallurgy, Massachusetts Institute of Technology, Cambridge, Mass.

AIME Chicago Meeting, October 1950.

TP 2928 E. Discussion (2 copies) may be sent to Transactions *AIME before Dec. 15, 1950. Manuscript received April 17, 1950; revision received July 17, 1950.*

Previous determinations of the solubility of hydrogen in molten pure aluminum are plotted in fig. 1. The most reliable data appear to be those of Ransley and Neufeld[1] and of Baukloh and Oesterlen.[2] The latter authors also report some results on the effect of copper and silicon additions. Up to 6 pct these elements decrease the solubility of hydrogen quite rapidly, with a definite minimum noted at 6 wt pct for both copper and for silicon, although no reason is apparent for these minima.

Experimental Procedure

The solubility of dry hydrogen in pure aluminum, aluminum-silicon, and aluminum-copper alloys was determined by the method of Sieverts.[3] This consists of determining the volume of the gas system above the molten metal at a given temperature and pressure by using an insoluble gas. This volume is referred to as the "hot volume." The system is then evacuated and the soluble gas is introduced at the same temperature and until the same pressure is reached. It is necessary to introduce enough of the soluble gas to fill the space above the metal plus the soluble amount. The difference in the volume of soluble gas and the "hot volume" is the solubility. The accuracy of solubility measurements by the Sieverts' method is primarily depend-

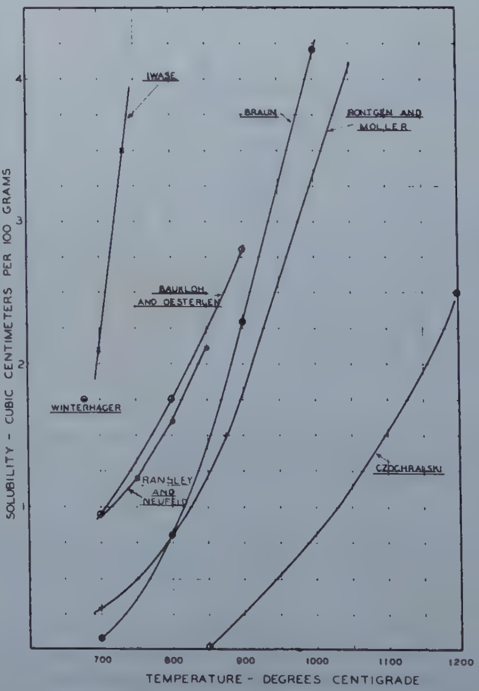

Fig. 1—The solubility of hydrogen in liquid aluminum as reported by various investigators.

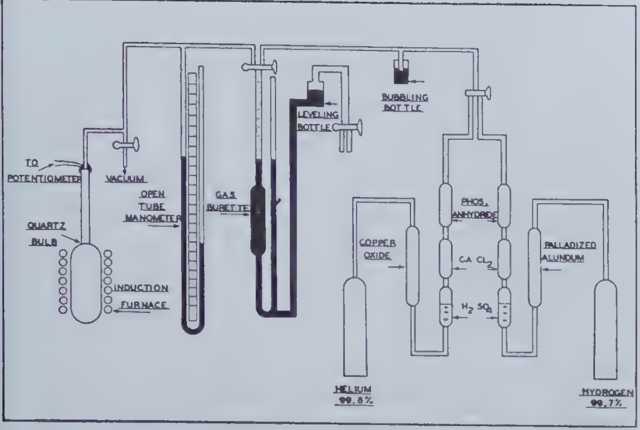

Fig. 2—Sketch of the apparatus for determining the solubility of hydrogen in aluminum alloys.

ent upon the accuracy of measurement of the gas volumes and upon the weight of the metal samples. To attain greater accuracy than had previously been possible, large samples were used and a burette was specially prepared which could be read to 0.01 cc. Each time a burette reading was made, the room temperature was read to 0.1°C and the barometric pressure read to 0.01 mm of mercury. Correction of all test values was made to standard conditions of temperature and pressure.

Fig. 2 is a sketch of the apparatus and gas purification system. Laboratory grade helium, which was thoroughly purified, as indicated, was used to determine the "hot volume."

High purity aluminum (99.996 pct) was furnished by the Aluminum Co. of America. Silicon of 99.8 pct purity was obtained from the Electrometallurgical Corp. Spectroscopically pure copper and copper of 99.9+ pct purity were furnished by the American Smelting and Refining Co.

The metal samples, which weighed from 105 to 158 g, were melted by induction in Norton RA84 alundum crucibles sealed into the quartz bulb as shown in fig. 2. To prevent cracking of the crucibles, the metal slugs were carefully machined to permit free expansion on heating.

The stirring action of induction heating aided not only in the degassing of the metal but also in attaining rapid equilibrium in the solubility measurements. Approximately 10 min was usually required to attain equilibrium. This is much faster than is possible by resistance heating. Measurements were made by approaching equilibrium from both high and low temperatures and high and low pressures. The samples were prepared by melting under a hydrogen atmosphere, flushing with hydrogen five times at 1050°C, and degassing under a vacuum of 10^{-3} mm of mercury. Solubility measurements were made at temperatures of 700° to 1000°C and at pressures of 50 to 800 mm of mercury. The temperature of the metal was read by means of a chromel-alumel thermocouple.

Discussion of Results

The effects of copper and silicon additions on hydrogen solubility are shown in figs. 3 and 4. The pressure measurements for the aluminum-copper and aluminum-silicon alloys were made only at 1000°C, whereas the same measurements for pure aluminum were made at 700°, 800°, 900° and 1000°F. The results obtained during the constant-temperature, varying-pressure tests are plotted against the square root of the pressure; a straight line relationship exists for pure aluminum, aluminum-copper, and aluminum-silicon alloys (figs. 5 to 7).

Figs. 8 and 9 are plots of hydrogen solubility vs. copper content and silicon content at 1000°C as a function of the hydrogen pressure above the metal. It will be observed that there are no minima in any of the curves over the composition ranges in-

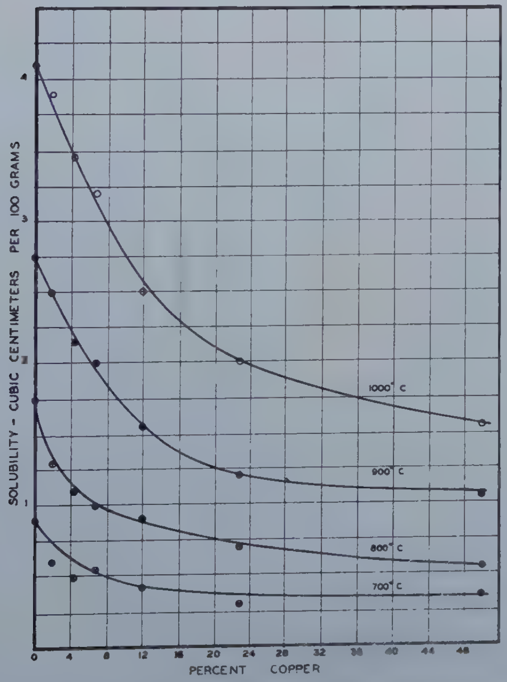

Fig. 3—Effect of copper additions upon the solubility of hydrogen in liquid aluminum at 760 mm pressure and various temperatures.

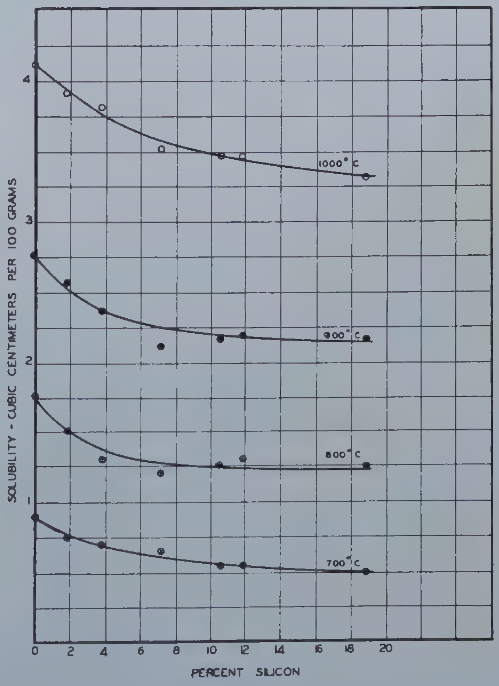

Fig. 4—Effect of silicon additions upon the solubility of hydrogen in liquid aluminum at 760 mm pressure and various temperatures.

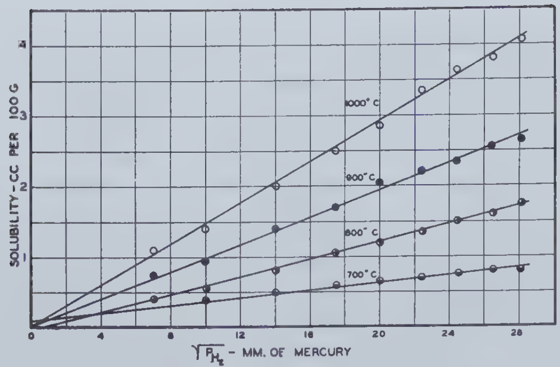

Fig. 5—Relationship between the solubility of hydrogen in liquid aluminum and the square root of the pressure of hydrogen above the melt.

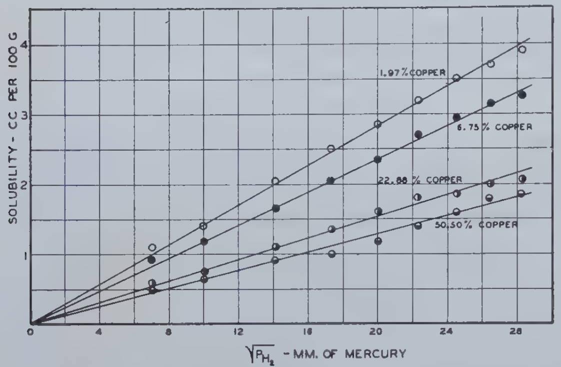

Fig. 6—Relationship between the solubility of hydrogen in liquid aluminum-copper alloys and the square root of the hydrogen pressure above the melt at 1000°C.

vestigated. This is contrary to evidence presented previously by Baukloh and Oesterlen.[2]

Both silicon and copper decrease the hydrogen solubility, the effect of copper being considerably

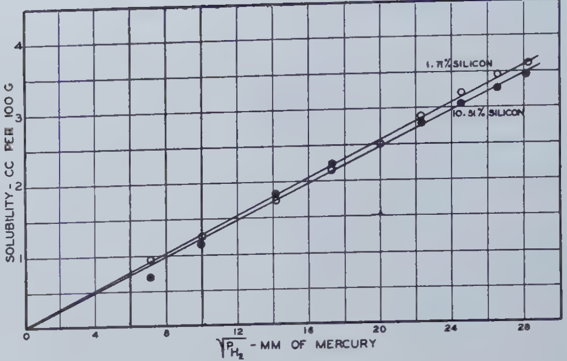

Fig. 7—Relationship between the solubility of hydrogen in liquid aluminum-silicon alloys and the square root of the hydrogen pressure above the melt at 1000°C.

greater than that of silicon. Copper additions cause the solubility to decrease up to the composition of the intermetallic compound $CuAl_2$, which occurs in the composition range 52.3 to 54.7 pct copper.[4]

The hydrogen solubility results determined at various pressures in pure aluminum and its copper and silicon alloys show that Sieverts' law is obeyed.

Sieverts' law relating pressure and solubility may be restated by saying that the solubility of hydrogen in aluminum alloys at constant temperature varies directly as the pressure of monatomic hydrogen above the metal. The partial pressure of monatomic hydrogen when 1 mol of diatomic hydrogen dissociates to form 2 mols of monatomic hydrogen can be calculated[5] from the equation

$$H_2(g) \rightleftarrows 2H\ (g)$$

$$\Delta F_T = 97{,}000 - 3.5\,T\ln T + 0.00045T^2 + 1.17T$$

Sieverts' relationship can then be shown to exist by plotting the solubility data, determined at various temperatures with the pressure held constant at 1 atm, against the partial pressure of monatomic

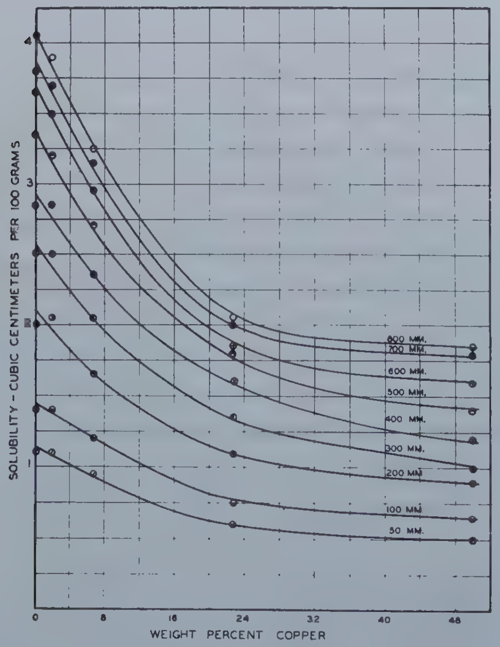

Fig. 8—Effect of the addition of copper to aluminum upon the amount of hydrogen that will dissolve at 1000°C and various pressures.

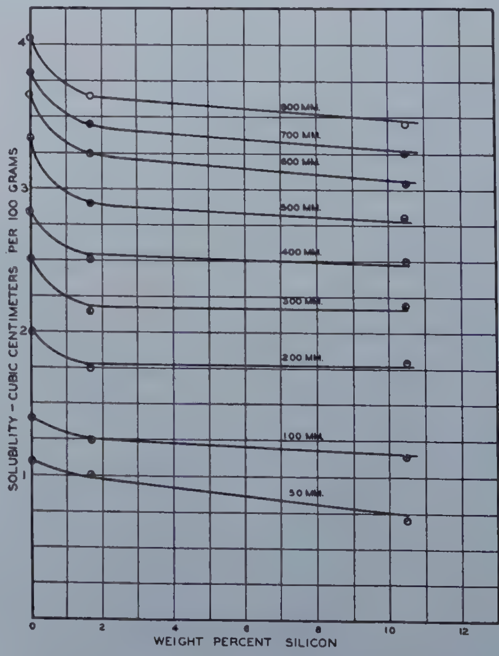

Fig. 9—Effect of the addition of silicon to aluminum upon the amount of hydrogen that will dissolve at 1000°C and various pressures.

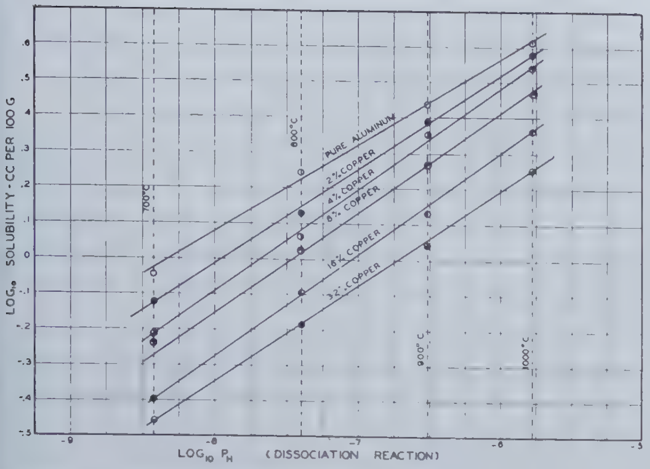

Fig. 10—Relationship between the solubility of hydrogen in aluminum-copper alloys and the partial pressure of monatomic hydrogen above the melt.

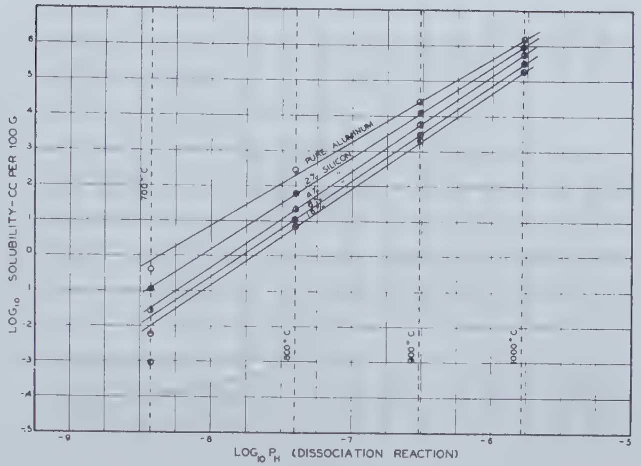

Fig. 11—Relationship between the solubility of hydrogen in aluminum-silicon alloys and the partial pressure of monatomic hydrogen above the melt.

hydrogen resulting from diatomic hydrogen dissociation at the corresponding temperatures. Figs. 10 and 11 show that straight lines can be drawn through the data when log plots are used. From plots such as these the solubility of hydrogen in aluminum alloys can be determined, if the partial pressure of monatomic hydrogen above the melt is known. Accordingly, any change in the atmosphere above the metal that will increase the partial pressure of monatomic hydrogen will increase the amount of hydrogen that will go into solution in the metal. This happens if water vapor present in the atmosphere reacts with the metal producing the metal oxide and hydrogen.

In order to derive equations relating solubility and temperature, values of $\log_{10}$ of the solubility were plotted against the reciprocal of the absolute temperature (figs. 12 and 13). The best straight line was drawn through the points for each alloy. It was necessary to favor the values determined at temperatures higher than 700°C for some of the alloys in selecting the curve. From these plots, it can be seen that the 700°C values tend to deviate most from the straight lines drawn through the other three points, indicating, usually, that 700°C values may be low. A higher percentage of error in the low temperature determinations, plus the possibility that complete solution may not have been obtained can account for this deviation. The equations of the straight lines for the various alloys have been determined and are listed in table I, col. 2.

Table I Equations relating solubility and temperature.

Alloy	Solubility Equation	Total Heat of Solution (cal per mol)*	Heat of Solution of Monatomic Hydrogen (cal per mol)
Pure aluminum	$\log_{10}S = -\frac{2550}{T} + 2.62$	23,300	—77,000
2 pct Cu	$\log_{10}S = -\frac{2950}{T} + 2.90$	27,000	—73,300
4 pct Cu	$\log_{10}S = -\frac{3050}{T} + 2.94$	27,900	—72,400
8 pct Cu	$\log_{10}S = -\frac{3150}{T} + 2.94$	28,800	—71,500
16 pct Cu	$\log_{10}S = -\frac{3150}{T} + 2.83$	28,800	—71,500
32 pct Cu	$\log_{10}S = -\frac{2950}{T} + 2.57$	27,000	—73,300
2 pct Si	$\log_{10}S = -\frac{2800}{T} + 2.79$	25,600	—74,700
4 pct Si	$\log_{10}S = -\frac{2950}{T} + 2.91$	27,000	—73,300
8 pct Si	$\log_{10}S = -\frac{3050}{T} + 2.95$	27,900	—72,400
16 pct Si	$\log_{10}S = -\frac{3150}{T} + 3.00$	28,800	—71,500

* Heats of reaction are given in calories per mol of diatomic hydrogen.
Average heat of dissociation, 100,300 cal per mol.

When values of the equilibrium constant ($\log_{10}$), determined by expressing the solubility as the mol fraction, are plotted against the reciprocal of the absolute temperature, the total heat of solution for

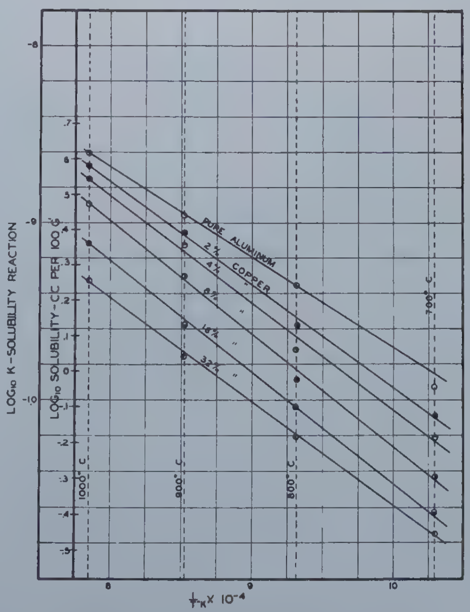

Fig. 12—Van't Hoff plot for aluminum-copper alloys.

the hydrogen dissociation reaction and the solution of monatomic hydrogen can be calculated from the slope of the line using the van't Hoff equation

$$\log_{10}K = \frac{-\Delta H}{4.575\ T} + C$$

The ordinates in figs. 12 and 13 are marked in units of $\log_{10}$ of the solubility constant as well as $\log_{10}$ of the solubility for convenience in calculating the heats of solution.

The heat of solution for the total reaction,

$$H_2 = 2\underline{H}$$

where, $\underline{H}$ signifies hydrogen dissolved in the metal, is made up of the heat of dissociation for the reaction

$$H_2 \rightleftarrows 2H$$

and the heat of solution of monatomic hydrogen as it goes into solution in the metal

$$2H \rightleftarrows 2\underline{H}.$$

In order to use the straight line relationship, it is necessary to assume that the total heat of solution is a constant in the temperature range investigated. This is a good assumption because, from 700° to 1000°C, the heat of dissociation, which contributes the greater percentage of the total heat exchange, varies only between 99,980 and 100,620 cal per mol of diatomic hydrogen dissociated.[5]

The total heats of solution, the average heat of dissociation, and the heats of solution of monatomic hydrogen in the various alloys have been determined from the van't Hoff plots and are listed in table I, cols. 3, 4, and 5.

Ransley and Neufeld[1] derived the equation

$$\log_{10} S = \frac{2760}{T} + 2.796$$

for the solubility of hydrogen ($H_2 \rightleftarrows 2\underline{H}$) in pure aluminum and calculated the total heat of solution to be 25,000 cal per g mol of diatomic hydrogen. These compare well with the results of this investigation (23,300 cal).

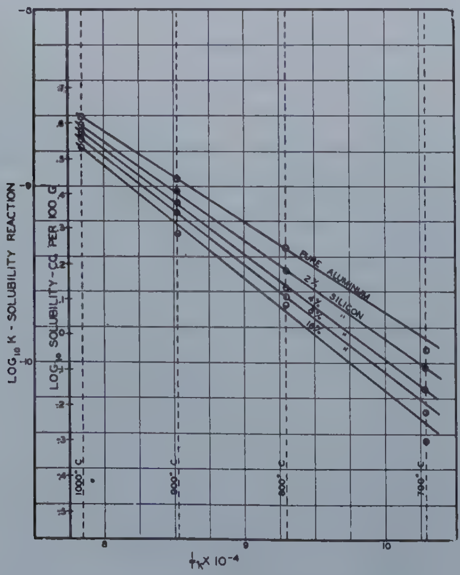

Fig. 13—Van't Hoff plot for aluminum-silicon alloys.

The equations derived by Dardel[6, 7] relating free energy and the equilibrium constant to temperature are based on solubility results that are low at temperatures near the melting point.

When argon is used to measure the hot volume, considerable error, due to the difference in heat conductivity of hydrogen and argon, is introduced that will give low solubility values. This probably accounts for the low results, especially at temperatures near the melting point, which many investigators have obtained, previously.

A few measurements were made to determine the solubility of hydrogen in solid 2S aluminum. Just below the melting point the metal was found to absorb 0.04 cc per 100 g of metal. Ransley and Neufeld[1] report that the solubility at 600°C is 0.036 cc per 100 g. It was not possible to measure accurately the very small hydrogen solubility in the solid aluminum using apparatus similar to that shown in fig. 2, even when very large aluminum samples were used.

Conclusions

1. The solubility of hydrogen in aluminum, aluminum-copper, and aluminum-silicon alloys follows an equation of the general form

$$\log_{10} S = -\frac{A}{T} + B$$

where S is the solubility in cubic centimeters of hydrogen at standard conditions per 100 g of metal. The constants have been evaluated.

2. Copper and silicon both decrease the solubility of hydrogen in aluminum; copper is more effective than silicon. No minima are noted when hydrogen solubility is plotted against copper content (up to 50 pct) or silicon content (up to 18 pct).

3. Sieverts' law is obeyed for aluminum and aluminum-copper alloys from 0. to 50.5 pct copper, and aluminum-silicon alloys from 0 to 18 pct silicon. The temperature range investigated was from 700° to 1000°C and the pressure range was from 50 to 800 mm of mercury.

Acknowledgment

The authors wish to express their thanks for the very able and extensive assistance of Miss Edith Weiser and to the Bureau of Aeronautics who sponsored this research program. Thanks are also expressed to C. F. Floe and M. B. Bever for their advice and assistance.

References

[1] Ransley and Neufeld: *Jnl.* Inst. Metals. (Aug. 1948) **74**, 599.

[2] Baukloh and Oesterlen: *Ztsch. Metallkunde.* (1936) **30**, 386.

[3] A. Sieverts: *Ztsch. Metallkunde.* (1929) **21**, 37.

[4] L. F. Mondolfo: Metallography of Aluminum Alloys. 1943. New York. John Wiley and Sons.

[5] International Critical Tables. **7**, 231.

[6] Y. Dardel: *Trans.* AIME (1948) **175**, 497; *Met. Tech.* (Sept. 1947) TP 2247 E.

[7] Y. Dardel: *Trans.* AIME (1949) **180**, 273; *Met. Tech.* (Dec. 1948) TP 2484 E.

[8] W. R. Opie: DSc Thesis. (1948).

Solid Solubility of Cementite In Alpha Iron

by Charles A. Wert

By the use of the internal friction of carbon in α-iron the solubility of cementite in α-iron has been measured down to a temperature of 150°C. The yield strength of ingot iron containing small amounts of cementite has also been determined as a function of carbon concentration.

THE solid solubility of cementite in α-iron has been investigated a number of times and there is now general agreement on the solubility of about 0.018 wt pct at the eutectoid temperature, 720°C. With decreasing temperature, the solubility falls off so rapidly and to such a low value that no data obtained by standard metallurgical methods are available below 500°C. Using a new technique, however, Dijkstra[1] has obtained apparently accurate solubilities down to 400°C; which data agree well with previously measured solubilities in the 600° to 700°C temperature range.[2] The present paper has in part the purpose of extending his work to still lower temperatures.

Earlier work of Low and Gensamer[3] on iron has established that the presence of a relatively small amount of carbon can play a tremendous role in affecting the mechanical properties. In particular they found that the yield point remained high as they reduced the amount of carbon in the iron; the yield point dropped only after the carbon content had fallen to something less than 0.003 wt pct, the point where their carbon analysis failed. It seemed desirable to the present author to see if some means could not be found to extend this part of their work. This investigation has then the additional purpose to determine the range of carbon concentration in which the major change occurs.

Solubility

The method used in the present work to measure small percentages of carbon in α-iron utilizes internal friction. Since this method may not be familiar to the reader, the following explanation will be given (a part of this procedure is from unpublished results of Dijkstra): It is known that the internal friction associated with the diffusion of

---

CHARLES A. WERT is associated with the Institute for the Study of Metals, University of Chicago, Chicago, Ill.

AIME Chicago Meeting, October 1950.

TP 2949 E. Discussion (2 copies) may be sent to Transactions *AIME before Dec. 15, 1950. Manuscript received Feb. 27, 1950; revision received July 31, 1950.*

carbon in α-iron is linearly dependent on the amount of carbon present in solid solution; i.e., wt 0/0 C $= K\ Q^{-1}$. In this expression Q^{-1} is the internal friction and K is a constant. To measure amounts of carbon, one needs only to determine the magnitude of the internal friction appropriately; if one knows the proportionality constant K, one can compute the carbon concentration. Dijkstra measured K by the following method: He first measured the increase in weight and the increase in electrical resistivity at room temperature caused by adding carbon to a bar of iron.[4] Hence he was able to find an equation wt 0/0 C $= A_1\ \Delta R/R$, where A_1 is determined empirically. Then on an iron wire he measured Q^{-1} and $\Delta R/R$ for various carbon concentrations, obtaining an equation $\Delta R/R = A_2 Q^{-1}$ where A_2 is also determined empirically. Hence, he could say that wt 0/0 C $= A_1 A_2 Q^{-1}$ where $A_1 A_2 = K$. He found that if internal friction was expressed in units Q^{-1}, then (by chance) the constant K was about unity for polycrystalline iron, so that

$$\text{wt } 0/0 \text{ C} = Q^{-1} \qquad [1]$$

To measure solid solubilities the specimens were in the form of wires 0.03 in. in diam and 1 ft long. The specimens were swaged and drawn from a ⅜ in. bar of Puron iron with appropriate intermediate vacuum anneals. They were then freed from carbon and nitrogen by a 4-hr treatment in wet hydrogen at 750°C. These wires were carburized to about 0.02 wt pct C, and, after they were quenched, they were tempered at the desired temperatures for varying periods of time. During this time the internal friction decreased for a time as the carbon precipitated into Fe_3C, but it finally reached a stable value. The background damping (i.e., the damping due to air, etc.) was then measured. The difference between these two values represented the damping due to carbon in equilibrium with Fe_3C at that temperature. Use of eq 1 then gave the equilibrium concentration of carbon.

The solubilities obtained in this way are shown in fig. 1. Here is also given the work of Stanley[3] and Dijkstra,[1] showing the relatively good agreement between the two methods at the higher temperatures. This good agreement provides an independent check on the accuracy of calibration of the present method. The present work has extended the measurements down to 150°C where the equilibrium value is of the order of 4×10^{-5} wt pct. The most striking fact to be noted about this plot is the extremely low value that it indicates for the solid solubility at room temperature. If the straight line of log C vs. $1/T$ is extrapolated to 20°C, the solubility there is of the order of 10^{-7} wt pct. This estimate is orders of magnitude lower than previous estimates. It means that without extreme care, one may never have a piece of iron at room temperature which is not supersaturated with carbon.

The Puron iron used in this investigation contains oxygen as the major impurity, which is present to the extent of about 0.04 pct, according to the Westinghouse Corp. The solubility of oxygen in iron in the range 200° to 500°C is not known, but most of the oxygen present is assumed to be in the form of oxides. No large amount of metallic impurities is believed to be present, spectrographic analysis failed to disclose any significant impurities after treatment. It is possible that the oxide present, as well as some lattice imperfections, may bind some of the carbon to particular regions of the lattice. The present method of internal friction does not measure these particular carbon atoms but rather measures those which are situated in the normal regions of the lattice. Those carbon atoms which are bound to particular sites, however, are not in solid solution in the same sense as those which are free to move about in the normal lattice. In this paper, it is these latter atoms which are referred to when the solubility limit is stated.

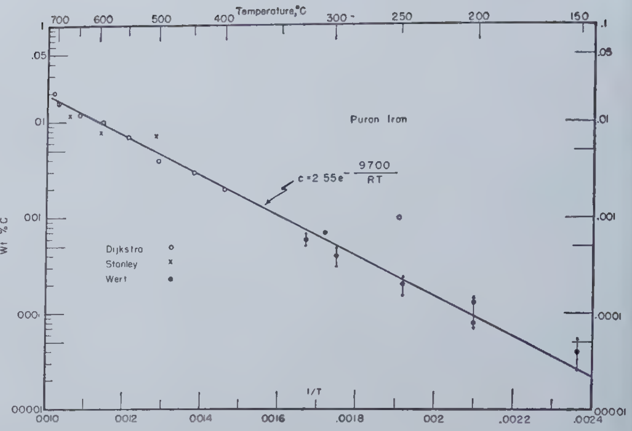

Fig. 1—Plot of solid solubility of carbon in α-iron vs. $1/T$.

Yield Strength

For the type of specimens used in this part of the work, a compromise was found necessary. For the determination of carbon concentrations by the

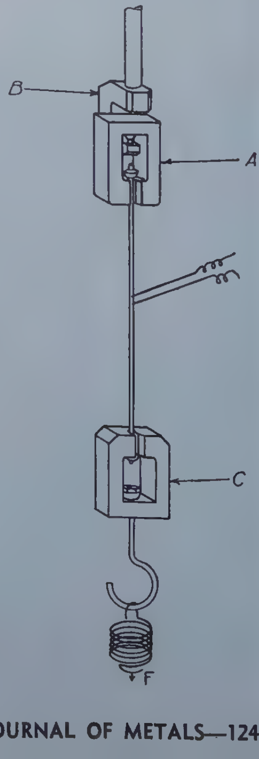

Fig. 2—Schematic drawing of apparatus used to determine yield points.

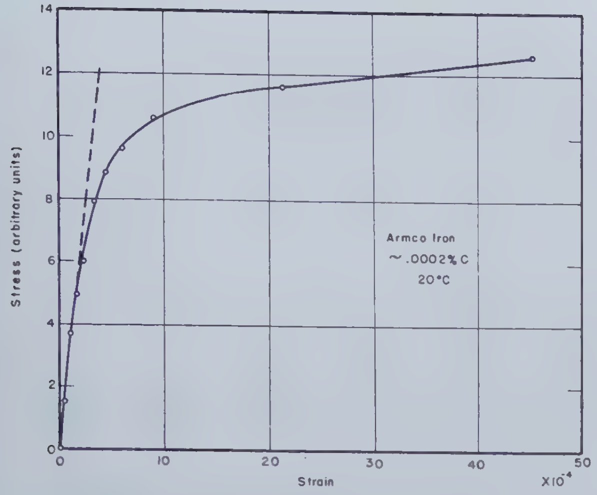

Fig. 3—A typical stress-strain curve.

method employed here, it is desirable that the specimens be thin wires. Unfortunately, good yield strength determinations are rather uncertain on such wires; during the preparation of the samples they are unavoidably bent somewhat; during tensile runs the straightening of the wire during the loading complicates matters to some extent. For these measurements, one would like specimens of somewhat larger dimensions than wires. In spite of these difficulties, by the method described here, it was found possible to obtain data consistent enough to show the desired effect.

The tensile specimens were Armco iron wires about 0.05 in. in diam and about 6 in. long. They had been swaged and drawn from a piece of ½ in. rod with appropriate intermediate vacuum anneals. The nitrogen and carbon were then removed by a wet H_2 treatment at 750°C for 4 hr. A measurement by means of internal friction showed no measureable amount of either nitrogen or carbon present (this means that nitrogen and carbon were surely present in the normal lattice in amounts less than 0.0001 wt pct). The samples were then carburized slightly and homogenized. After this treatment the carbon content was measured in the manner described in the previous section. The yield strength measurements were then made.

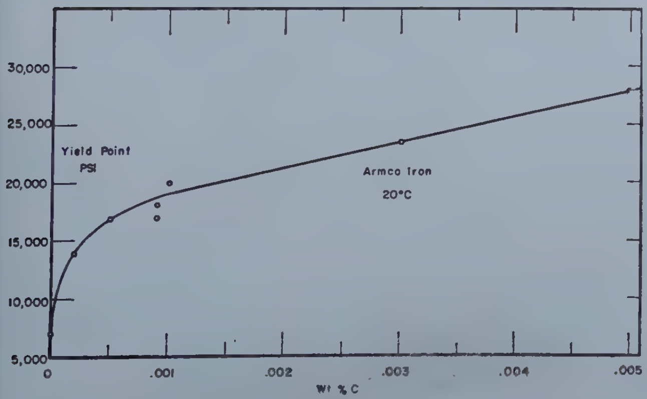

Fig. 4—Yield point vs. percent carbon (in all cases the C is in solid solution).

For these tests a soft tensile machine was used. The wires were suspended vertically as shown in fig. 2. On each end of the wire was soldered a spherical ball which rested in conical seats cut in the members *A* and *B*. Appropriate slots and holes were cut in these pieces to permit easy assembly. The top piece *A* was in turn supported on a 1/16 in. ball bearing fastened securely to *A* and resting in a slight depression in part *C*. The force was applied by means of a water load through a spring which was calibrated to read the load directly. All these parts were made in such a manner that the wire was under as nearly a purely tensile force as possible. The loading was done at about 500 psi per min.

The strain was measured using a strain gauge composed of a single 1 in. loop of 0.001 in. wire cemented to the central part of the specimen.

This strain gauge was one arm of a Wheatstone bridge whose state of unbalance was continuously recorded by a Brown potentiometer. A typical stress-strain curve is given in fig. 3. From such curves the yield strength was determined by noting the stress at which the strain had deviated 0.02 pct from a straight line extended from the elastic position of the curve. Because of the unbending of the wire it was not always possible to draw this line with great accuracy. Such difficulties give rise to an inaccuracy of only about 1000 psi in measured yield strength, however, so they are not considered too serious. This spread, too, is about the same as that found for different wires of the same composition.

The yield strengths determined as a function of carbon concentration are given in fig. 4. These data show that the most striking increase in yield strength occurs in the range zero to 0.0002 wt pct C. For high carbon concentrations, the magnitude is of the same order as those values obtained by Low and Gensamer.[3] The effect of impurities, again oxygen and other metals, can again not be ascertained in detail. The important fact is that for this iron the yield strength depends on carbon concentration in the way shown in fig. 4.

Summary

The two chief findings of this investigation are: (1) The solid solubility of cementite in α-iron in equilibrium with Fe_3C decreases to extremely low values with decreasing temperature. From these data the room temperature extrapolated value is much lower than had previously been supposed. (2) The amount of carbon necessary to affect the yield strength of ingot (Armco) iron is very small, about 0.0001 wt pct.

References

[1] L. J. Dijkstra: *Trans.* AIME, **185**, 252; *Journal of Metals* (March 1949) TP 2540E.

[2] J. K. Stanley: *Trans.* AIME, **185**, 752; *Journal of Metals* (Oct. 1949) TP 2679E.

[3] J. Low and M. Gensamer: *Trans.* AIME (1944) **158**, 207.

[4] D. J. Dijkstra: *Philips Research Report.* (1947) No. 2, 257.

Relative Energies of Grain Boundaries in Silicon Iron

by C. G. Dunn, F. W. Daniels, and M. J. Bolton

Relative grain boundary energies in silicon-iron crystals are determined for differences in crystal orientation (1) in the range 0 to 20° for a (110) series having grains with a <110> common axis and (2) in the range 0 to 45° for a (100) series having grains with a <100> common axis. Micrographic data to show movement and configurations of boundaries are given.

IN recent investigations[1, 2] data on relative grain boundary energies in silicon iron have been obtained. The present investigation is a continuation of this work along similar lines for the purpose of obtaining additional information on boundary energies. One aim has been to extend the data for a (110) series, which was formerly studied,[1] to small differences in orientation, since a recent theory[3, 4] based on a dislocation model of grain boundaries predicts a $E_o \Delta (A\text{-}\ln \Delta)$* form of energy curve for small differences in orientation. Another aim has been to provide data for a (100) series—all grains having (100) planes parallel with the surface of sheet specimens—and to compare the results with the predicted form of energy curve. Finally, information on the nature of approach to equilibrium conditions was to be obtained through observations on the movements of grain boundaries.

Recently published papers[2, 3, 5] have treated the mathematical problem of expressing equilibrium conditions for grain boundaries for the general case when boundary energy depends upon boundary orientation. The equilibrium equations, which relate equilibrium angles and grain boundary free energies, contain additional terms that express the variation of energy with boundary rotation. It has been necessary in the present investigation, however, to neglect these additional terms since no data for their evaluation were available. Dropping the additional terms leads to the following approximate equations which were used:

$$\frac{E_{12}}{\sin \theta_3} = \frac{E_{13}}{\sin \theta_2} = \frac{E_{23}}{\sin \theta_1} \tag*{[1]}$$

or those of the form:

$$E_{23} + E_{13} \cos \theta_3 + E_{12} \cos \theta_2 = 0 \tag*{[2]}$$

Experimental Procedure

Except for sample F1, all specimens were made from two lots of silicon iron called C and L respectively. The compositions of these are listed in table I.

In the preparation of 12 three-grain specimens for the present investigation, a controlled grain growth technique, which has been described previously,[1] was used. After preparation, the specimens were notched at the boundaries to shorten them as a means of providing more rapid approach to equilibrium in the anneals. Initial grain boundary angles were determined from micrographs taken at X500. Seven anneals, totaling about two days at 1300°C and two to four days at 1400°C, were run in an atmosphere of pure dry argon as described in a previous paper.[2] Boundary changes generally could be followed without metallographic surface preparation, because thermal etching occurred during the anneals. These observations indicated angle changes of as much as 35° in some instances, with the major changes occurring during the first anneal. Annealing was discontinued when the angles reached stationary values.

Fig. 1 gives a schematic diagram for purposes of defining crystallographic and boundary directions for three grains with common plane parallel with the sheet. Differences in orientations (expressed by Δ) are the angles between [001] directions. They can be calculated with the aid of the δ's. The grain boundary angles can be calculated from the ω's.

Results

Results are given in table II. Types of crystallographic planes refer to those parallel with the sheet. Orientations are given in terms of [001] directions as shown in fig. 1. Except for grain 3 of specimen H6, which was unintentionally tilted 7° out of a (100) plane, all grains generally were within 1° or 2° of the plane specified. The directions of boundaries were measured generally to within 1° on both upper and lower surfaces, and the average directions were determined for use in calculating the grain boundary angles. Variations in grain boundary directions refer to deviations from average directions. Boundaries near the junction point for all specimens generally were very close to perpendicu-

Table I. Percentage Composition of Common Elements in Two Lots of Silicon Iron*

Material	Si	C	P	S	Mn	Al	Ti	Cu
C (commercial)	3.38	0.005	0.013	0.010	0.04	0.01	0.0013	0.05
L (laboratory)	3.31	0.004	0.016	0.005	0.02	0.01	0.0009	0.01

* Further purification through the removal of carbon, phosphorus, and sulphur during annealing at high temperatures in pure dry hydrogen, which was carried out for some anneals, could be expected.

---

* E_o and A are constants and Δ is the difference in crystal orientation of the two grains forming a grain boundary, one crystallographic direction remaining constant with changing Δ.

C. G. DUNN, Member AIME, is Research Physicist, and F. W. DANIELS and M. J. BOLTON are Metallurgists, General Electric Co., Pittsfield, Mass.

AIME Chicago Meeting, October 1950.

TP 2930 E. Discussion (2 copies) may be sent to Transactions *AIME before Dec. 15, 1950. Manuscript received April 12, 1950; revision received July 11, 1950.*

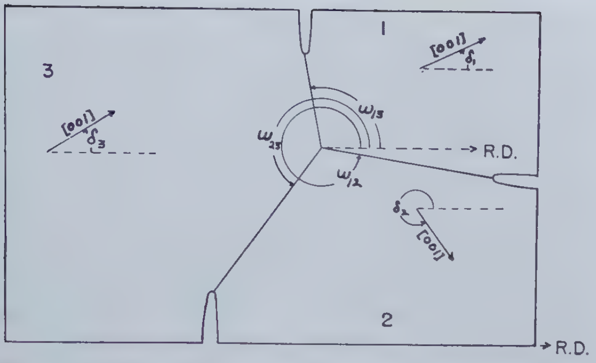

Fig. 1—Schematic diagram showing crystallographic and grain boundary directions in a three-grain specimen.

larity with the sheet. Consequently, the samples could be treated as two-dimensional in nature.

The general plan followed in calculating energies of boundaries in the low Δ range was to start with known energies in the high Δ range, which were available for the (110) series from published data.[1] The method employed for the (100) series will be described later.

The curve shown in fig. 2, giving the variation of *E* with difference in orientation, was constructed as the calculations proceeded. First, as much of the curve as possible was drawn using data from table I, ref. 1. The values shown with asterisk marks in table II (also shown as black dots in fig. 2) were then read from this curve. In the case of specimens F1 and S4, two high energy values were available to use in eq 2 to calculate the third *E* value. With specimens S3, S2, and S1, one *E* value was selected from the curve for use in eq 1 to calculate the other two energies; the selected *E* values for S2 and S1, enclosed in brackets, were determined by the final shape of the curve.

Before indicating how the calculations were made for the (100) series, specimen M1, which connects the (100) series with the (110) series, needs to be described. Referring to the stereographic projection in fig. 3, it will be seen that grains 1 and 3 belong to a (110) series and have a difference in orientation of 28.5° (chosen near 25°, where the energy curve becomes horizontal, for greater accuracy of the value of E_{13}). On the other hand, grains 1 and 2 have a [001] direction in common; so in three dimensions these two grains belong to a (100) type series with a difference in orientation of 44°. From the value 1.09 for E_{13} selected from the curve of fig. 2, one obtains, using eq 1, the value 1.14 for E_{12}. This provides a starting point for the (100) series, assuming, of course, that any differences due to altered crystallographic relationships of the boundary may be neglected providing that a 44° or 45° difference in crystal orientation is again obtained by rotation about a common <100> axis.

Referring to the orientations of grains 1 and 2 of specimens H4 and H5 listed in table II, it will be seen that these grains have the same orientation relationship as grains 1 and 2 of specimen M1. E_{12} for each, therefore, can be set equal to 1.14. Again using eq 1, one obtains values of *E* for Δ's of 21°, 24°, 17°, and 27°. From the *E* values of this partial (100) series, a tentative curve can be drawn for purposes of interpolation. (The final curve depends, of course, on other points—a process of adjusting has to be employed to allow for these changes.) In this way E_{12} for specimen H3 was selected at a value of 1.22. The remainder of the H series was similarly evaluated. In plotting the points for the curve in fig. 4 each interpolated point is indicated by a cross and each calculated point by an open circle.

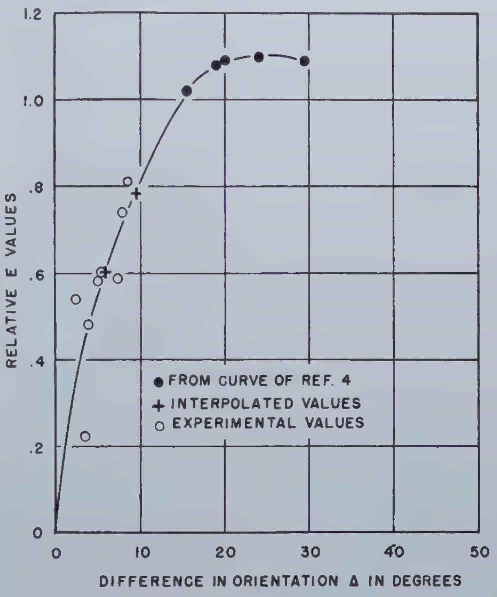

Fig. 2—Plot showing variation of relative energies with difference in orientation for grains with common (110) plane.

Microstructure

The appearance of the microstructure for laboratory and commercially prepared lots of silicon iron was much alike with only minor amounts of inclu-

Table II. Grain Orientations and Boundary Energies

Specimen	Material	Group	Orientation of Grains			Differences in Orientations			Orientations of Boundaries			Equilibrium Angles			Grain Boundary Energies			Equation No. Used
			δ_1	δ_2	δ_3	Δ_{12}	Δ_{13}	Δ_{23}	ϕ_{12}	ϕ_{13}	ϕ_{23}	θ_1	θ_2	θ_3	E_{12}	E_{13}	E_{23}	
F1	D	110	349.5	341	9.5	8.5	20	28.5	11.5±2	106 ±3	240 ±1	94.5	131.5	134	0.81	1.09*	1.09*	2
S4	L	110	15.5	10.5	351.5	5	24	19	342 ±1	104 ±4	252 ±½	122	90	148	0.58	1.10*	1.08*	2
S3	L	110	356	11.5	4	15.5	8	7.5	352.5	137.5±3	218.5	145	134	81	1.02*	0.74	0.59	1
S2	L	110	353	2.5	358.5	9.5	5.5	4	354 ±4	136 ±0	224.5±3	142	129.5	88.5	[0.78]	0.60	0.48	1
S1	L	110	357	3	0.5	6	3.5	2.5	30 ±2	146 ±3	231 ±1	116	159	85	[0.60]	0.22	0.54	1
M1	C	110 + 100		See fig. 3		44	28.5		12.5±2	123.5±½	246 ±0	111	126.5	122.5	1.14	1.09*	1.27	1
H4	C	100	20.5	65.5	41.5	45	21	24	14 ±1	125 ±1	249 ±0	111	125	124	(1.14)	1.13	1.28	1
H5	C	100	62	18	45	44	17	27	352 ±0	104 ±2	224 ±2	112	128	120	(1.14)	1.04	1.22	1
H3	C	100	107	70	86.5	37	20.5	16.5	321.5±0	93.5±0	207 ±0	132	114.5	113.5	[1.22]	1.21	0.99	1
H7	C	100	27	17	47	10	20	30	17 ±3½	127 ±1	262 ±0	110	115	135	0.92	[1.13]	[1.25]	2
H6	C	100	27	20	60	7	33	40	6	116	262	110	104	146	0.71	[1.24]	[1.19]	2
H1	C	100	50	39	44	11	6	5	2	135	223	133	139	88	[0.88]	0.58	0.64	1

* From curve of ref. 1.

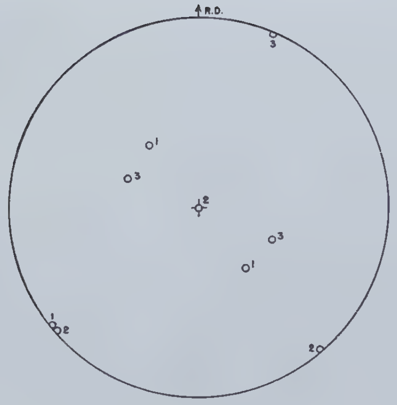

Fig. 3—Stereographic projection giving directions of cube poles of three grains in specimen M1.

sions visible. Further, the movements of boundaries produced by annealing were largely the same.

Boundaries: With good atmosphere control it was possible to maintain a relatively smooth and bright surface during annealing and at the same time develop visible boundaries through thermal etching. In some instances the surfaces became rough and repolishing was necessary. Such polishing, which was done on 3/0 emery paper, disclosed an orientation dependence of the thermally etched boundaries. These boundaries, which appeared as surface grooves, became progressively harder to erase with increasing difference in orientation in the low Δ range.

Another similar observation was that boundaries for small differences in orientation generally failed to straighten as rapidly or as far as those for large differences in orientation.

Illustrations of Boundary Changes: A series of photographs for specimen S3 are shown in fig. 5 giving the microstructure in the original condition,† as annealed 24 hr at 1200°C, and after 66 hr at 1400°C. These photographs illustrate a general observation in the present work (see experimental procedure) that initial grain boundary angles often are far from equilibrium values.

Another example of boundary migration is that observed for specimen M1. Initially, grain 2 was of peninsular shape near the junction point of the three grains, a shape conducive to the motion of the junction point toward grain 2. Actually the junction point did move during annealing for a total distance of 0.6 mm toward grain 2. Fig. 6 shows what happened during the first anneal when the junction point advanced 0.3 mm. Traces of the chemically etched boundaries indicate the initial configuration, and sharply defined thermally etched boundaries, the final position. The intermediate positions that appear to be boundaries were not visible at high magnification. Their visibility at X100 can be explained in terms of shallow grooves which formed in the surface when the boundaries stopped moving for a time or when they moved at a slow rate as compared with the average motion. The irregular shape of grain 2 would account for some of the uneven movement but possibly not all.

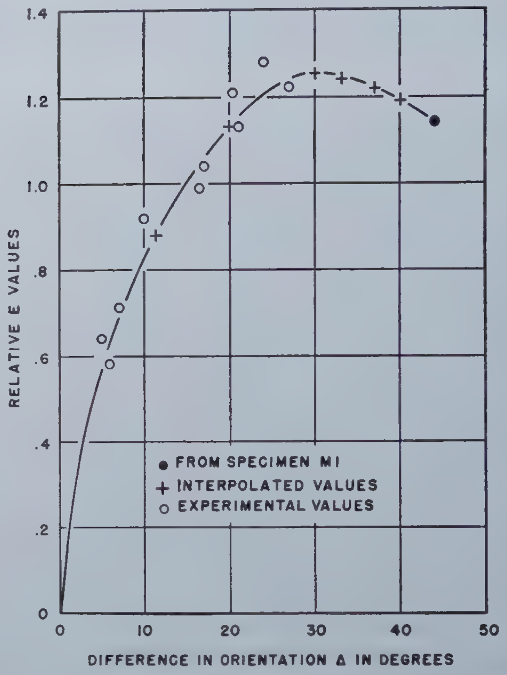

Fig. 4—Plot showing variation of relative energies with difference in orientation for grains with a common (100) plane.

Fig. 7 illustrates the final grain boundary configuration in specimen H6. The broad boundaries appearing in the microstructure are not due to wide grooves but to a slight offset of the grains. The extremities of these broad boundaries actually correspond to initial and final boundary positions for the last anneal.

Effect of Difference in Orientation

The curve obtained in fig. 2 is in good agreement with that obtained formerly by Dunn and Lionetti[1]

---

† During preparation all samples reached a temperature of about 1100°C for approximately 1 hr.

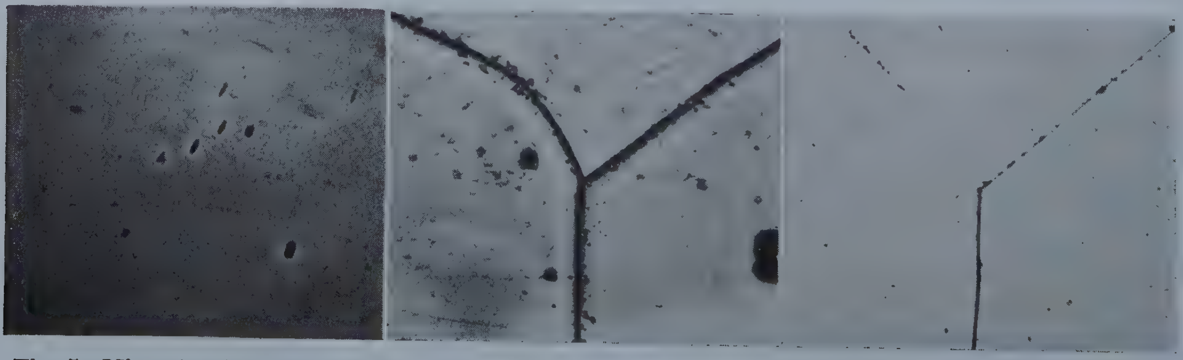

Fig. 5—Microstructure of specimen S3. ***a.*** **(left) Specimen as prepared. Polished and etched. X500.** ***b.*** **(center) After 24 hr at 1200°C. Thermally etched. X500.** ***c.*** **(right) After 66 hr at 1400°C. Polished and etched. X500.**

Area reduced approximately 20 pct for reproduction.

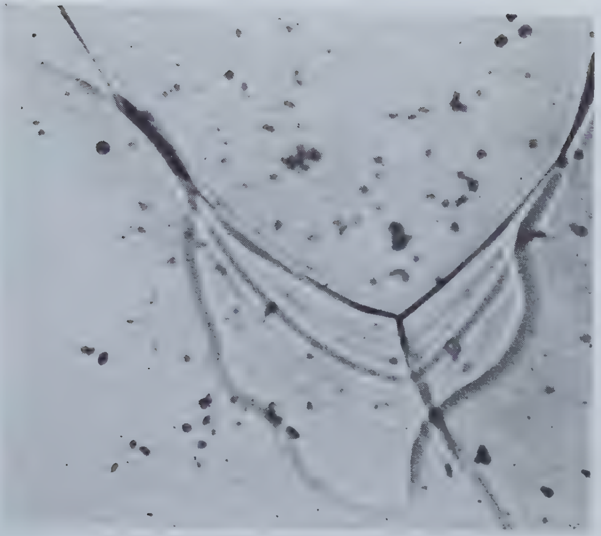

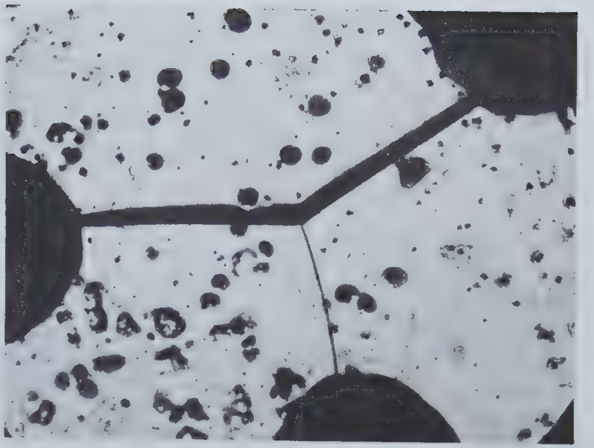

Fig. 6 (left)—Microstructure of specimen M1 in as-annealed condition after 24 hr at 1200°C. X100.

Fig. 7 (above)—Microstructure of specimen H6 after 48 hr at 1400°C. Thermal etch. X60.
Area reduced approximately 20 pct for reproduction.

in that it establishes a rapid drop in energy for Δ values below 15°. The present curve, however, is extended further into the low energy range, but the data are not sufficiently accurate to determine the exact shape of the curve in this region. The curve as drawn is in good agreement with a $E_o\Delta\ (A\text{-}\ln\Delta)$ variation of energy with difference in orientation, a theoretical form of energy curve that has been derived by Shockley and Read[3, 4] from dislocation models of grain boundaries.

Since the energy values obtained in the present investigation depend on the assumption that equilibrium angles are reached, the trends of angle changes are of importance in determining whether calculated energies are high or low. For example, the observation was made that θ_3 in specimen F1 increased during annealing. This means that E_{12} at a value of 0.81 was approached from above and that much longer annealing might have lowered this value somewhat. The final value of θ_3 in specimen S3, an acute angle, represents reduction from a larger angle (fig. 5), and this circumstance, of course, means that E_{13} and E_{23} must be substantially smaller than E_{12}. The final value of θ_3 is in substantial agreement with that formerly obtained[1] for a similar group. Furthermore, the directions of angle change observed for specimens S2 and S1 indicate lower energies for smaller differences in orientation. It is reasonable to conclude, therefore, that the form of energy curve obtained is not one of chance due to nonequilibrium conditions of the specimens but rather is a representation of a real effect of orientation difference on energy.‡

The curve obtained in fig. 4 for the (100) series has several surprising features. First there is a maximum boundary energy slightly above that for the (110) series. The relative values are based, of course, on one specimen M1; but it is believed that this sample can be considered as exceptionally reliable. At first a maximum energy for Δ less than 45° seemed surprising, but the dotted curve in fig. 3 of Shockley and Read's theoretical curve for a (100) series predicts a maximum point below 45°. A maximum point at 30° would require the value of A in $(A\text{-}\ln\Delta)$ to be 0.34, which apparently is quite reasonable.[3]

Although no conscious effort was made to have the initial part of the curve for the (100) series coincide with that of the (110) series, these parts of the curves are in good agreement. The curve for the (100) series satisfies a $E_o\Delta\ (A\text{-}\ln\Delta)$ relation remarkably well.

Summary and Conclusions

To determine relative grain boundary energies as a function of difference in crystal orientation, 12 three-grain specimens were investigated. The dependence of energy on orientation was studied through use of: (1) a (110) series wherein each grain had a (110) plane in the plane of the specimen, and (2) a (100) series wherein each grain had a (100) plane in the plane of the specimen. A microstructure investigation also was undertaken to establish conditions of equilibrium.

Results for the (110) series show a relatively rapid rise in grain boundary energy with difference in orientation, and this agrees well with a function of the form $E_o\Delta\ (A\text{-}\ln\Delta)$ where E_o and A are constants and Δ is the difference in orientation.

Results for the (100) series show a similar increase in grain boundary energy with difference in orientation with the curve reaching a maximum value at a difference in orientation of about 30°.

Acknowledgment

The authors are indebted to G. Sears for helpful discussion of the paper. W. T. Read and W. Shockley for clarification of theoretical aspects of the work, and Eugene F. Welter for aid in the preparation of the silicon-iron specimens.

References

[1] C. G. Dunn and F. Lionetti: The Effect of Orientation Difference on Grain Boundary Energies. *Trans.* AIME, **185**, 125; *Journal of Metals.* (Feb. 1949), TP 2517E.

[2] C. G. Dunn, F. W. Daniels, and M. J. Bolton: On the Measurement of Relative Interface Energies in Twin Related Crystals. *Trans.* AIME, **188**, 368; *Journal of Metals.* (Feb. 1950) TP 2804E.

[3] W. Shockley and W. T. Read: Dislocation Models of Crystal Grain Boundaries. *Physics Review.* (1950) **78**, 275.

[4] W. Shockley and W. T. Read: Quantitative Predictions from Dislocation Models of Crystal Grain Boundaries. *Physics Review.* (1949) **75**, 692.

[5] C. Herring: Surface Tension as a Motivation for Sintering. To be published.

[6] K. T. Aust and B. Chalmers: The Specific Energy of Crystal Boundaries in Tin. *Proc.* Royal Society, London. (1950) **201**, 210.

---

‡ The recently published work of K. T. Aust and B. Chalmers for grain boundary energies in tin gives excellent proof of this orientation dependence.[6]

Ordering Reaction in Cobalt-Platinum Alloys

by J. B. Newkirk, A. H. Geisler, D. L. Martin, and R. Smoluchowski

The order-disorder phenomenon in alloys near CoPt composition was studied during the progress of the ordering reaction. The changes in hardness, electrical resistance, X-ray diffraction, and microstructure which accompany the transformation at various temperatures were found to be similar to those characteristic of conventional heterogeneous precipitation reactions. The transformation is discussed in terms of four distinct processes which can appear in the reaction.

A FUNDAMENTAL investigation of the mechanism of the ordering reaction and of the accompanying changes in properties has been undertaken, since an extensive study of this process could well contribute to the knowledge of phase transitions in alloys. Cobalt-platinum alloys were chosen for the study since they exhibit interesting and unusual permanent magnet properties.[1, 2] In addition, the ordering reaction in cobalt-platinum alloys is a convenient one to study experimentally because of the high maximum ordering temperature, the large difference in the X-ray scattering power of cobalt and platinum atoms, and the relative ease with which the alloys can be plastically worked into wire and strip. In the early stages of this study, it became apparent that the published phase diagrams[2, 3] of the cobalt-platinum system contained questionable features, in the region of 40 to 60 atomic pct Co, which were considered in another publication by the authors.[4] That portion of the research reported elsewhere on the equilibrium states of cobalt-platinum alloys does not confirm the presence of a previously reported high temperature disordered tetragonal phase and a low temperature body-centered cubic phase. On the other hand, the structure of the ordered phase is face-centered tetragonal with an atomic distribution analogous to that of CuAu.[4] This lattice forms from the disordered face-centered cubic phase in such an orientation that the <100> directions are parallel to the <100> directions of the disordered phase. At compositions other than the ideal 50 atomic pct the ordered phase can exist in equilibrium at high temperatures with the disordered phase. A Widmanstätten pattern of plate-like particles of the ordered phase parallel to {110} planes of the disordered matrix is observed when an initially disordered alloy is held at these temperatures. The temperature range of the two-phase region has been determined for three alloys by X-ray diffraction analyses, microscopic examination, and electrical resistivity measurements, and these results are incorporated with some of those of Gebhardt and Köster in the revised phase diagram of fig. 1.

The purpose of the investigation reported here was to examine the mechanism of ordering in cobalt-platinum alloys by X-ray diffraction and metal-

---

J. B. NEWKIRK, Student Associate AIME, is a graduate student and Research Assistant, Department of Metallurgy, Carnegie Institute of Technology, Pittsburgh, Pa.; A. H. GEISLER and D. L. MARTIN, Members AIME, are Research Associates, Research Laboratory, General Electric Co., Schenectady, N. Y.; and R. SMOLUCHOWSKI, Member AIME, is Professor and Member of the Staff of the Metals Research Laboratory, Carnegie Institute of Technology.

AIME Chicago Meeting, October 1950.

TP 2947 E. Discussion (2 copies) may be sent to Transactions *AIME before Dec. 15, 1950. Manuscript received April 17, 1950; revision received July 28, 1950.*

This work is based on part of a Doctor of Science thesis submitted by the first-named author to Carnegie Institute of Technology. It was started while he was at the Research Laboratory of the General Electric Co. during the summer of 1948 and later was continued as a cooperative project with Carnegie Institute of Technology.

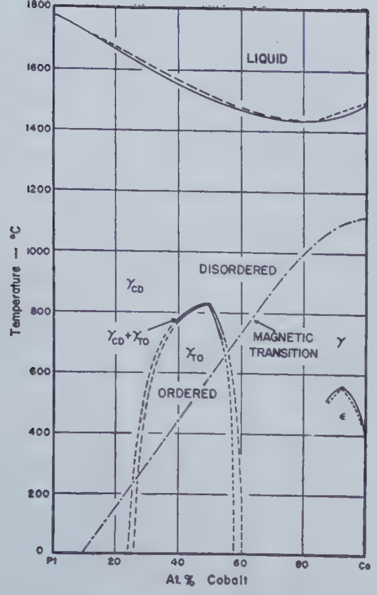

Fig. 1—Constitution diagram for the cobalt-platinum system according to the results of Gebhardt and Köster,[3] Newkirk, et al.[4]

The cubic disordered phase is designated γ_{CD} while the tetragonal phase is γ_{TO}.

lographic examination and to study the kinetics by observing the changes in various physical characteristics as initially disordered specimens were aged isothermally for various periods of time at temperatures between 400° and 800°C. The properties studied included electrical resistance, hardness, and magnetic hysteresis. The only prior study of this sort[2] was not very extensive and resulted in several erroneous conclusions. A strong similarity between this reaction and the process of precipitation from solid solution has become apparent on the basis of this investigation. Thus, a correlation with the sequence of stages that has been proposed as general for the precipitation alloys is used here as a guide in interpreting the observed effects.

Preparation of Specimens

Three 150-g alloys were made, containing about 42, 48, and 54 atomic pct Co, respectively. The exact analyses of the ingots after homogenization were 41.62, 47.64, and 53.80 atomic pct (17.71, 21.61, and 26.01 wt pct) Co. Platinum of higher than 99.5 pct purity was mixed with rondel cobalt, reported to be 99.9 pct pure, and melted by high frequency induction under an atmosphere of nitrogen in a crucible lined with magnesium oxide. The melt was allowed to freeze in the crucible. The resulting ingots were about 3 in. long by ⅝ in. in diam. After homogenizing in hydrogen for 100 hr at 1275°C, the alloys were hot swaged to ¼ in. in diam. Several magnetic specimens 1 cm long and about 20 thin discs for hardness tests and microscopic studies were cut from each rod. A 1-in. length of the 48 and 54 pct Co rod was then hot swaged and cold drawn to wire 0.020 in. in diam for use as X-ray and electrical resistance specimens. At first, the 42 pct Co alloy could not be drawn into wire but by careful handling one piece was hot rolled into a 0.015 in. thick strip. Slivers were sheared from this strip for Debye-Scherrer specimens and electrical resistance measurements.

All specimens were initially disordered by holding several hours at 900° to 1000°C while sealed in a quartz vial containing argon at low pressure. The disordered state was retained by quenching the vial into water and breaking it. Samples to be given an isothermal aging treatment were then individually sealed in small quartz or pyrex vials containing argon.

X-ray Studies: Debye-Scherrer Method

One of the most useful tools for studying the mechanism of ordering is X-ray diffraction analysis. A series of experiments was designed to show the manner in which Debye-Scherrer diffraction patterns change as the random face-centered cubic lattice transforms isothermally into the ordered face-centered tetragonal lattice. While the equilibrium degree of order is a function of temperature the *degree of transformation* is a function of both temperature and *time*. Two distinctly different sequences of diffraction patterns have been found. In the one sequence, which occurs most frequently at low aging temperatures, the tetragonality lines for the ordered phase appear in their final positions and become stronger at the expense of the original cubic lines. The change is "discontinuous," analogous to its counterpart in precipitation.[5] The other sequence, which occurs most frequently at high aging temperatures, is characterized by the gradual broadening of most of the cubic lines and the final resolu-

Fig. 2—Debye-Scherrer patterns illustrating discontinuous (*a* to *c*) and continuous (*d* to *f*) sequences. Filtered cobalt radiation.

a. Aged 7 hr at 500°C, unetched
b. Aged 13 hr at 500°C, unetched
c. Aged 25 hr at 500°C, unetched
} 48 atomic pct Co

d. Aged 3 min at 700°C, etched
e. Aged 24 min at 700°C, etched
f. Aged 1 hr at 700°C, etched
} 42 atomic pct Co

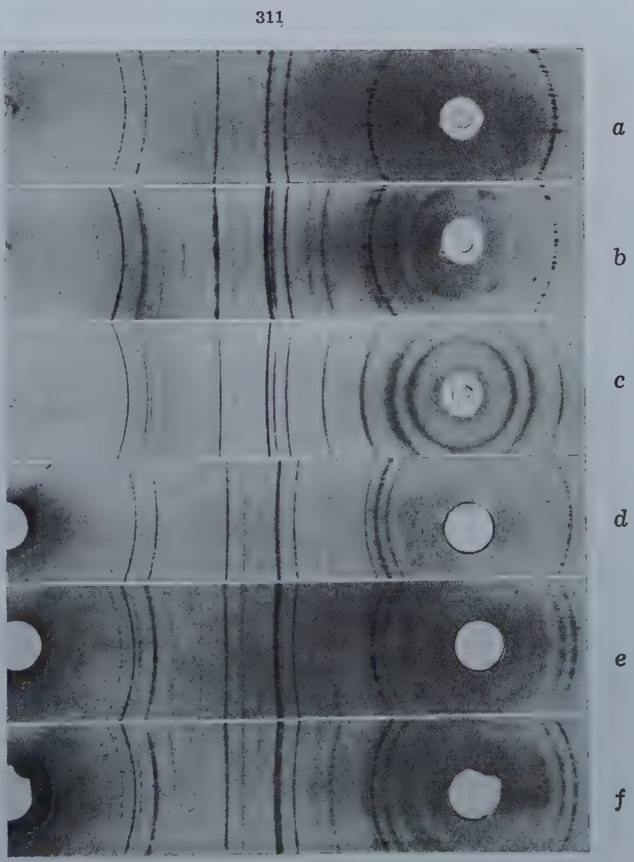

tion of the broadened bands into sharp tetragonality lines. The change in position of the lines is gradual and this will be referred to as the "continuous" type. Typical patterns illustrating the two sequences are shown in fig. 2. The distinguishing features of the two types of pattern sequences are best seen by following the changes of the {311} face-centered cubic line as aging proceeds. Other cubic lines, which double on ordering, show similar changes but not so clearly as does the {311} series. In the discontinuous sequence, fig. 2*a*, *b*, and *c*, the $\{311\}_{\text{cubic}}$ line decreases in intensity but remains relatively sharp, while the $(113)_{\text{tetragonal}}$ and $(311)_{\text{tetragonal}}$ lines increase in intensity beside it, remaining sharp themselves during this period. On the other hand, in the continuous sequence, fig. 2*d*, *e*, and *f*, the $\{311\}_{\text{cubic}}$ line at first becomes diffuse and then spreads into a band which ultimately resolves itself into the two $\{311\}_{\text{tetragonal}}$ lines. In both sequences the final structure is the same—fully transformed—although more than 1000 hr is required to attain this at 500°C in the 42 atomic pct Co alloy.

It was noticed that the interior of drawn wires, exposed by etching off the original surface, followed the continuous sequence at somewhat lower temperatures than did the original unetched surface. This effect is shown in fig. 3. It is presumed that this is another consequence of the surface condition which was discussed elsewhere.[4] As soon as the surface effect was discovered all succeeding specimens were etched after heat treatment.

Fig. 3—Debye-Scherrer patterns illustrating different sequences for surface and interior of drawn wire of 48 atomic pct Co alloy quenched from 1000°C. Filtered cobalt radiation.

a (upper). Discontinuous type. Aged 1 hr at 600°C, unetched
b (lower). Continuous type. Aged 4 hr at 600°C, etched.

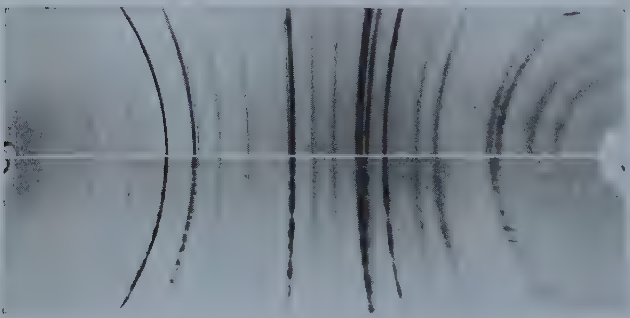

Table I. Summary of Debye-Scherrer Photographs Made In Study of Mechanism of Transformation*

Aging Temperature, °C	Aging Time, Hr										
42 Atomic Pct Cobalt Alloy (All Specimens Etched):											
500	½	2½	8	25	96	400	1,000				
	A	B′	B′	C′	C′	D′	D′				
600	¼	1	6	28	64	256	315				
	A	B	B	C	D	E	F				
650 for 54 hr, F											
700	0.05	0.1	0.2	0.4	1.0	2	36				
	B	B	C	C	D	E	F				
48 Atomic Pct Cobalt Alloy:											
400	120	408	936								
Unetched	B′	D′	D′								
Etched			B								
440	4	6	8	16	48	72	108	195	396	432	768
Unetched	A	A	A	B	B′	C′	D′	D′	D′	D′	D′
Etched					B		B		B		B
500	1	3	4	7	13	25	96	402			
Unetched	A	A	C′	C′	C′	D′	E				
Etched			B				D′	D′			
600	0.05	½	1	4	25	96	236	251	792	1,000	
Unetched			D′	D′		E	E		E		
Etched	B	B		C	D	E	E	E	F	F	
650 etched 54 hr, F											
700	0.1	¼	½	1	25	120	236				
Unetched		C	D	E		E	E				
Etched	C			E	E	F					
54 Atomic Pct Cobalt Alloy:											
500	1	4	18	48	100	240	527				
Unetched		B		D′	E						
Etched	B		B			B	B				
600	0.1	½	2	8	32	128					
Unetched	D										
Etched	B	B	C	D	E	E					
650 etched 54 hr, F.											
700	0.1	1	4	96	256						
Unetched	B	E		E							
Etched			B′	F	F						

*** The patterns are described by the following code:**

Discontinuous Sequence (Split Lines):

A —Single face-centered cubic pattern; sharp lines. Disordered.
B′ —Sharp face-centered cubic lines plus weak diffuse superlattice lines.
C′ —Sharp face-centered cubic lines plus weak face-centered tetragonal lines and diffuse superlattice lines.
D′ —Sharp face-centered cubic lines plus sharp face-centered tetragonal and superlattice lines.
E —Face-centered tetragonal and superlattice lines only; unresolved doublets. Strained ordered.
F —Face-centered tetragonal and superlattice lines only; resolved doublets. Strain-free ordered.

Continuous Sequence (Banded Lines):

A —Single face centered cubic pattern; sharp lines. Disordered.
B —Sharp face-centered cubic lines, some developing diffuse side-bands; weak diffuse superlattice lines.
C —Diffuse face-centered cubic lines, some spread into bands; diffuse superlattice lines.
D —Diffuse face-centered tetragonal and diffuse superlattice lines only.
E —Face-centered tetragonal and superlattice lines only; unresolved doublets. Strained ordered.
F —Face-centered tetragonal and superlattice lines only; resolved doublets. Strain-free ordered.

The descriptions of the X-ray patterns are summarized in table I. For convenience in tabulating and discussing the patterns a code was adopted. This is presented at the bottom of the table. The data clearly illustrate the two types of sequences; the discontinuous type being characteristic of specimens which were aged at the lower temperatures and of the fine-grained surface of the wire, and the continuous type being characteristic of higher temperatures and the coarse-grained metal below the surface. As with other phase transformations in metals, the rate rapidly increases with temperature so that a comparable degree of transformation is attained in much less time at the higher temperatures. In addition, the fine-grained surface of the specimens becomes ordered much faster than the interior, although resolution of the doublet lines is achieved sooner in the interior. The interpretation of the patterns will be discussed later. It will suffice to say here that they are consistent with the notion that ordering occurs by nucleation and growth of particles of the ordered phase at the expense of the disordered matrix.

Diffuse Diffraction Effects

Unusual diffraction effects were found when a partially ordered coarse-grained wire was exposed, without rotation, to characteristic cobalt radiation in the Debye-Scherrer camera. Such diffuse diffraction effects were not found for disordered or highly ordered specimens. A systematic study of this dif-

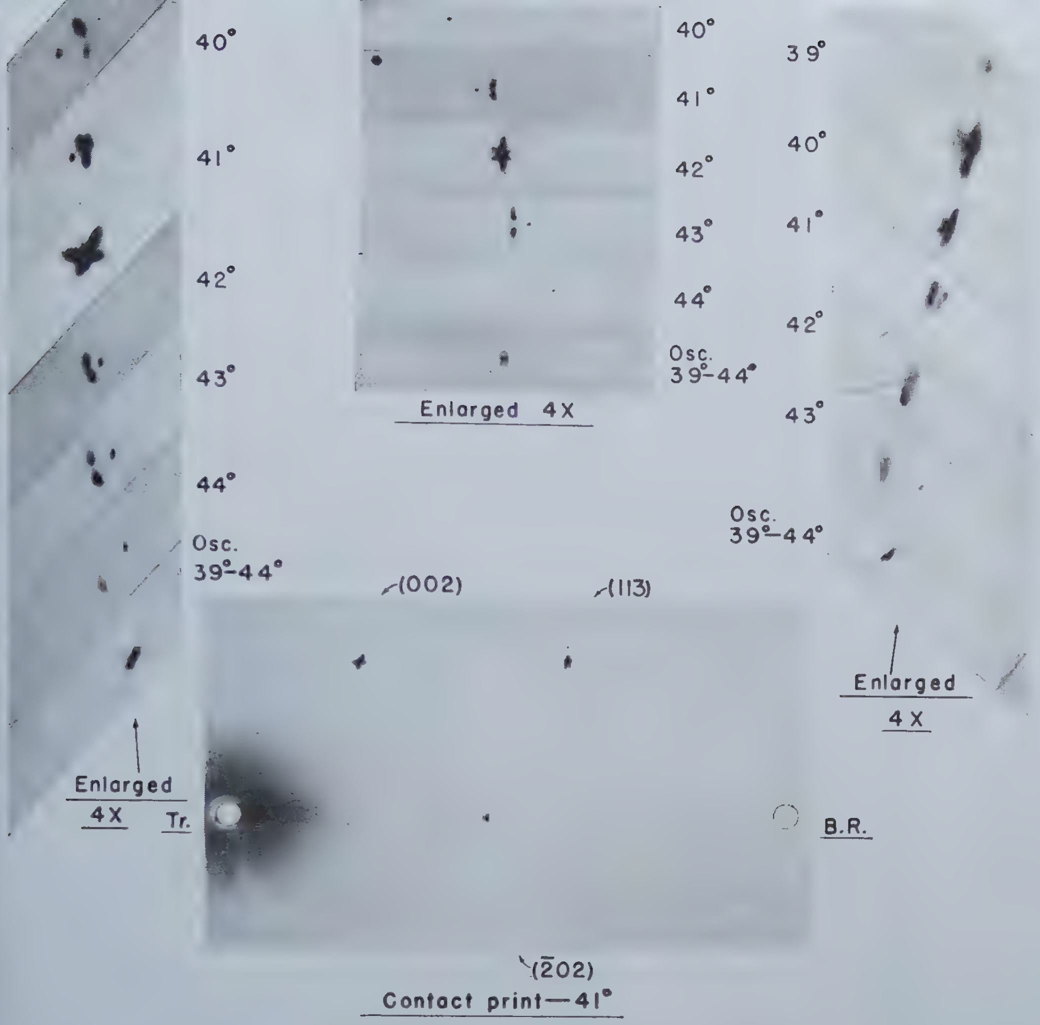

Fig 4—Diffuse diffraction effects in patterns of a small Co-Pt crystal aged 12 min at 600°C. Unfiltered cobalt radiation.

The [101] is vertical and [010] is 38° to 44° from parallel to the beam. Area reduced approximately 75 pct for reproduction.

fuse scattering was made using a single crystal of CoPt (49.6 atomic pct Co) which was isothermally aged to an early stage of the ordering reaction (12 min at 600°C) and then quenched. A detailed description of the technique used and the diffraction effects observed in this study are to be presented in another paper. Only the interpretation of the effects as they pertain to this investigation are given here. The method, which has been used as a tool in previous investigations of the mechanism of aging, involves the analysis of several series of Laue-type patterns, similar to those in fig. 4, from which the reciprocal lattice of the partially ordered crystal may be built up.[6] It was found that the reciprocal lattice exhibited a number of <110> rods extending through the normal reciprocal lattice points for a face-centered cubic crystal. A projection view of the (101) plane of the reciprocal lattice is given in fig. 5. At each reciprocal lattice point the number of <110> rods is less than the total number of possible directions in this family but is the same for equivalent points. Also the configuration of observed rods at equivalent points is symmetrical with respect to the origin. The lengths of the rods at different points are not the same, the longest ones being those which are farthest from the origin of the reciprocal lattice. Although special steps were taken to detect diffraction streaks extending into the direct beam spot, none were found. In one series of photographs, definite evidence of a different type of rod extending in the (100) direction was visible.

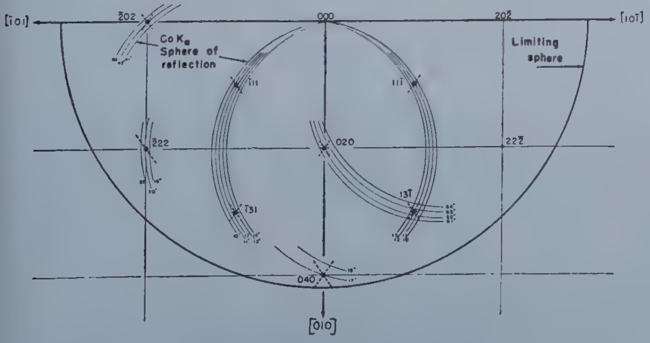

Fig. 5—Reciprocal lattice plot of data from several series of patterns of the type shown in fig. 4.

(101) is plane of Co Pt reciprocal lattice.
- - - - indicates observed rods at 30° to the plane.
0 indicates observed rods perpendicular to the plane.
For clarity rods are twice actual length.

The prominent effects can be explained by assuming that the crystal contained internal lattice strains in <110> directions caused by platelets of the tetragonal phase which are lying on, and are coherent with, {110} planes of the cubic matrix. This state of strain lowers the periodicity of the matrix lattice in the <110> directions and thereby results in a corresponding relaxation of the conditions for Bragg reflection. The above explanation is in accord with the previously drawn conclusion that coherency on {110} matrix planes is most probable on the basis of least strain.[4] It is also in agreement with the microscopic evidence of fig. 6c which shows a Widmanstätten pattern of plate-like particles parallel to {110} matrix planes analyzed previously.[4]

Since the presence of ordered platelets lowers the periodicity of the matrix not only in the <110> direction but also (to a lesser extent) in others, one may expect to find less intense rods in other directions. The intensity of the other rods will depend upon the atomic density of the reflecting planes and the angle which the platelets make with them. This would account for the evidence of a [100] rod through the (020) point, since in that direction the interplaner distance of the ordered lattice is much different from that of the disordered. In the <111> directions the change in interatomic distance is negligible and therefore no <111> rods would be expected.

Table II. Summary of Microstructure and X-ray Patterns of Specimens Used for Hardness Tests

Aging Temperature, °C	Time, Hr	Striations	Recrystallization	Crystal Structure
48 Atomic Pct Cobalt				
As quenched		none	none	
400	96	none	none	
500	4	none	none	
	18½	faint?	started	
	48	faint	started	
	240	faint	advanced	
	1,000	faint	advanced	O + slight D
600	0.4	none	none	
	48	faint	started	O
	96	faint	started?	
	308	prominent	advanced	O
	1,000	prominent	started	O
700	0.4	none	none	
	1	faint	started?	
	48	moderate	started	
	308	moderate	none	
	1,000	prominent	started	O
54 Atomic Pct Cobalt				
As quenched		none	none	
400	96	none	none	
500	4	none	none	
	18½	none	none	
	48	faint	started	
	240	faint	started	
	1,000	faint	started	D + O
600	0.4	faint	none	D + slight O
	48	moderate	started?	O
	96	faint	started?	
	308	moderate	started	
	1,000	prominent	started	O
700	1	faint	started?	
	48	moderate	none	
	308	moderate	started	
	1,000	prominent	started?	O

Microstructure

Several interesting features were observed in the microstructure as the alloys were ordered isothermally starting from the disordered state. These could be rationalized on the basis of the sequence that has been proposed as general for the precipitation alloys.[7] Specimens of the 48 and 54 atomic pct Co alloys, which had previously been used for the hardness surveys, were used. X-ray patterns were also made for a few of the specimens and the results of these are incorporated in table II. In the as-quenched disordered condition, the microstructure consisted only of equiaxed, twinned grains typical of many single-phase, face-centered cubic alloys. The changes in microstructure which accompany the isothermal ordering of these as-quenched alloys can be classified according to four prominent features. These are discussed in chronological order according to their appearance in the precipitation reaction.

Localized Ordering: Preferential formation of particles (presumably ordered) along grain boundaries and slip bands, as in fig. 6*a*, was observed in a few instances, particularly at very high aging temperatures where the ratio of rate of nucleation to rate of growth is low. The Debye-Scherrer photograph of this sample showed strong disorder lines plus weak order lines. This preferential nucleation effect was probably responsible for the greater number of particles along certain lines of the Widmanstätten pattern of fig. 6*c*. In that micrograph

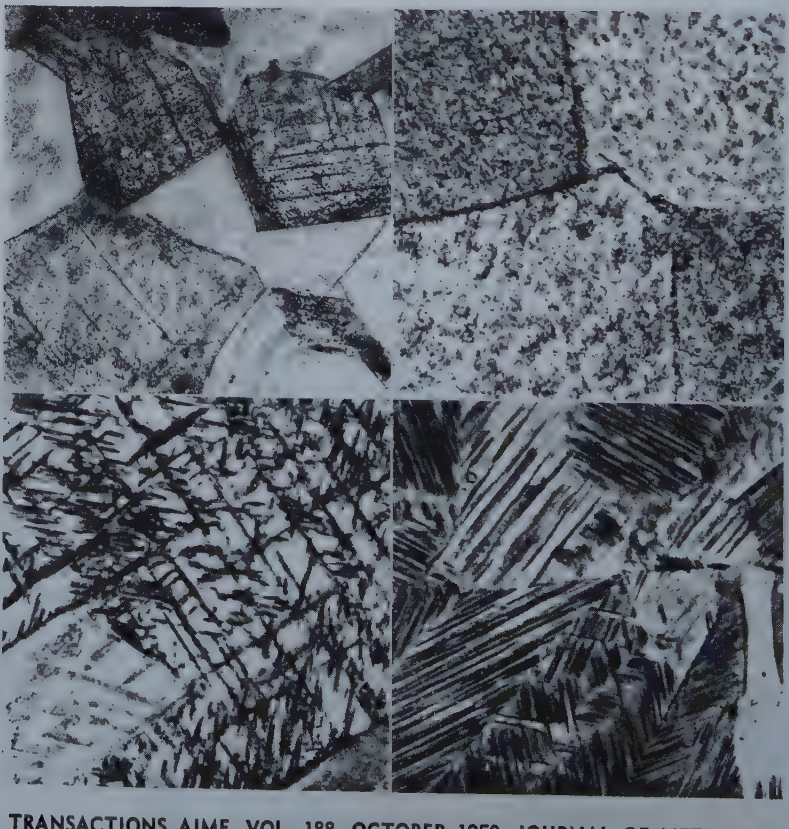

Fig. 6—Microstructures appearing during the ordering of the 54 atomic pct Co alloy quenched from 1000°C. Etch: aqua regia.

a (upper left). Aged 25 hr at 723°C. X250.
b (upper right). Aged 48 hr at 600°C. X1500.
c (lower left). Aged 50 hr at 728°C. X1500.
d (lower right). Aged 50 hr at 728°C. X1500.

Area reduced approximately 66 pct for reproduction.

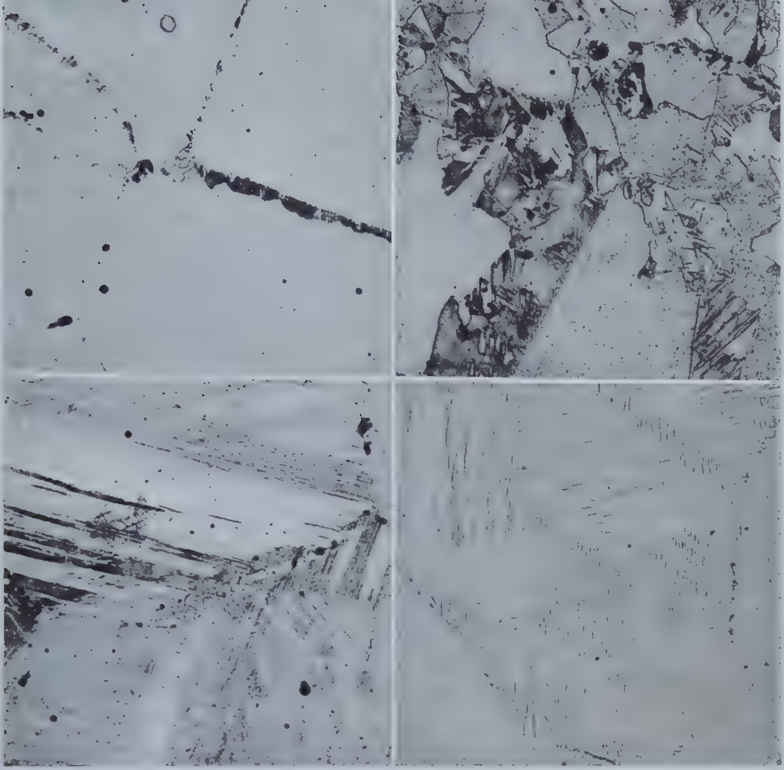

Fig. 7—Microstructures appearing during the ordering of the 48 atomic pct Co alloy quenched from 1000°C. Etch: aqua regia. X250.

a (upper left). Aged 48 hr at 500°C.
b (upper right). Aged 240 hr at 500°C.
c (lower left). Aged 1000 hr at 600°C.
d (lower right): Aged 48 hr at 700°C; etch: NaCN electrolytic.

Area reduced approximately 66 pct for reproduction.

the trace of one of the lines of preferred nucleation is parallel to a twin boundary, both in the parent grain and within the twin, indicating that the preferred sites are on the conventional (111) slip (and twinning) planes.

General Ordering: At low aging temperatures the general nucleation and growth of the ordered particles appears as an unresolved mottling (fig. 6*b*) or is obliterated by gross features of the microstructure as in fig. 7*c*. Debye-Scherrer photographs of these specimens (table II) show that at this stage of aging the structure is practically all ordered. At higher aging temperatures the gross features are suppressed and the Widmanstätten pattern becomes recognizable as in fig. 6*c*. Consideration of the number of traces and their directions relative to the twin boundary shows that this Widmanstätten figure is due to the presence of ordered plate-like particles lying on {110} matrix planes.[4]

Self Deformation: The twin markings, striations or "ripples" of fig. 6*d* were evident in the microstructure of specimens after many conditions of aging, particularly at the higher aging temperatures (table II). A similar structure is also found in ordered CuAu, in which case the striations are known to be less prominent in alloys further from the ideal composition. The most prominent example among precipitation alloys occurs in the Cu-Be system.[8] These striations are considered in our work to be manifestations of stresses which accompany the formation of the coherent ordered phase. Part of the strain energy is removed by this self-deformation process of twinning. A stereographic analysis of the directions of the strain markings shows that the traces are due to the intersection of {111} planes with the surface of polish. Debye-Scherrer examination shows that samples containing the striation type of microstructure may have ordered and disordered phases together or may have no detectable amount of disordered phase (table II). Microstructures showing striated structure as in fig. 6*d* have been reported for ordered CuAu,[9, 10] FePt,[11] CoPt,[2] and Ni_4W.[12]

Recrystallization: An alternate method for the removal of strains that occur during the ordering process consists of a secondary reaction in which new grains recrystallize from the parent grains. This occurs predominantly at grain boundaries, figs. 7*a* and 7*b*. The new grains have a different orientation from the old as revealed by a difference in appearance of etch pits and the presence of Debye-Scherrer arcs in Laue photographs of specimens which were known to be single crystals before aging. The new grains often grow with wavy irregular boundaries into one grain and occlude areas that are presumably twins of the new grain, i.e., thermal twins (fig. 7*b*). The recrystallized grains are de-

Fig. 8—Change in electrical resistance of 42 atomic pct Co alloy during ordering at 500°C.

a. Measurements made at 500°C.
b. Measurements made on quenched specimens at 0°C.

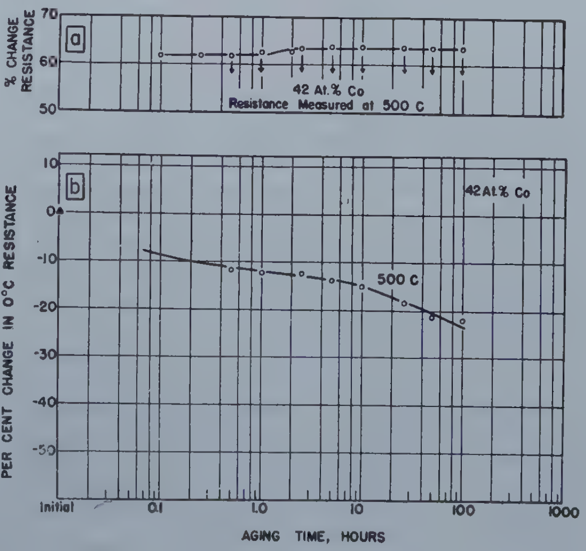

tectable rather early in the ordering process (48 hr, 500°C), when the deformation markings are only faintly visible. They continue to grow long after the structure has reached a high degree of order. Debye-Scherrer pictures show that the lattice can be either all ordered (fig. 7*c*) or mixed, ordered plus disordered (fig. 7*a*), after the recrystallization reaction has started. The recrystallization reaction is more prominent at the lower aging temperatures (fig. 7*b*); it is less pronounced at intermediate temperatures (fig. 7*c*) and is largely replaced by the self-deformation process (fig. 7*d*) as the mechanism of strain removal at higher temperatures. The recrystallization reaction is slower in the 54 atomic pct Co alloy than in the 48 atomic pct Co alloy.

Electrical Resistance Measurements

The changes in electrical resistance during the isothermal aging of initially disordered specimens were somewhat unexpected. Originally the measurements were made on the specimens held at the aging temperature; however, here the only change during ordering was a slight increase as shown by the upper curves in figs. 8*a* to 10*a*.* This, of course, is contrary to classical theory, although it is in agreement with the equilibrium studies which show that the ordered phase has a higher resistance than the disordered phase, when this property was measured at high temperatures.[4] When the specimens are cooled to 100°C or less for making the resistance measurements after the aging treatment, the data provide the conventional reaction curves shown in figs. 8*b* to 10*b*. While the data are not complete, they suggest that the 48 atomic pct Co alloy (the composition closest to the 50:50 ratio) orders the fastest of the three alloys. The curves in fig. 9*b* show that the rate of reaction increases with temperature in the usual manner for a diffusion-dependent transformation. In addition these curves show that the final equilibrium value of the resistance is lower at the lower aging temperatures and thus the degree of order is greater, which is in agreement with theory.

Fig. 9—Change in electrical resistance of 48 atomic pct Co alloy during ordering at 500°, 600°, 700°, 800°C.

a. **Measurements made at 605° and 805°C.**
b. **Measurements made on quenched specimens at 0°C.**

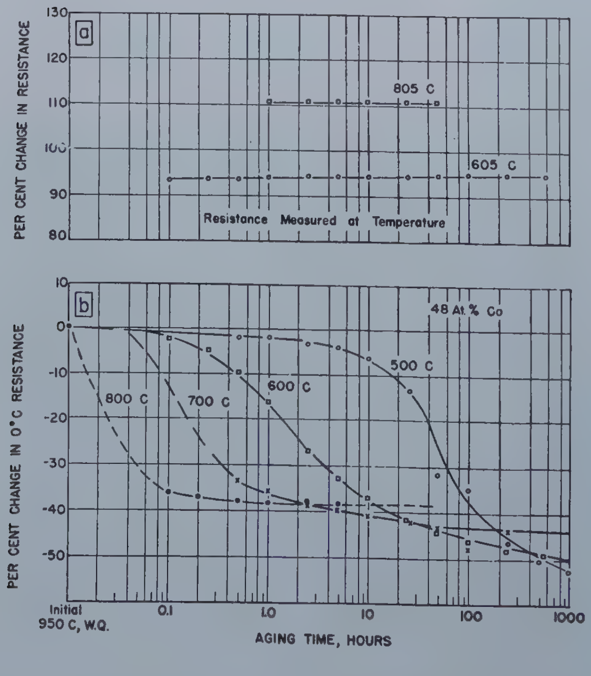

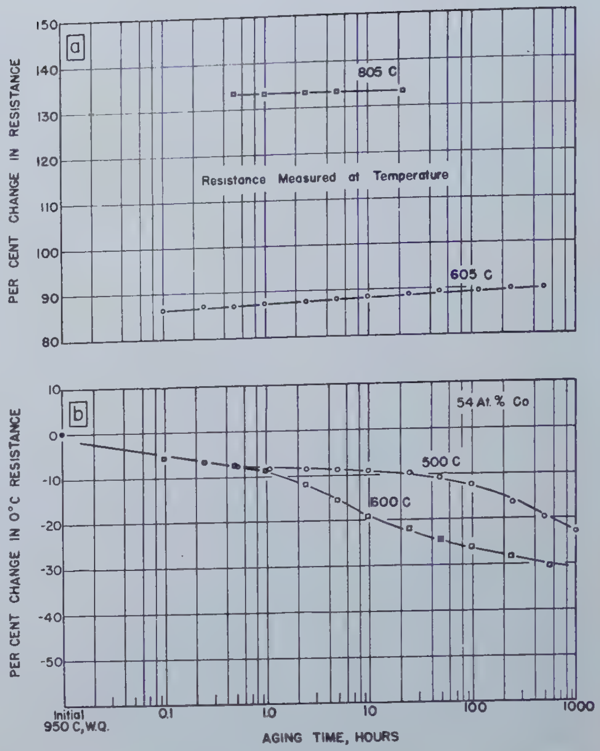

Fig. 10—Change in electrical resistance of 54 atomic pct Co alloy during ordering at 500° and 600°C.

a. **Measurements made at 605° and 805°C.**
b. **Measurements made on quenched samples at 0°C.**

The influence of measuring temperature on the electrical resistance of an alloy aging at 600°C is clearly shown in fig. 11. These data were obtained by aging the sample at 600°C, water quenching after various intervals (e.g. 30 min, 60 min, etc.) and measuring the resistance at 0°, 100°, 200°, 300°, and 400°C. After these series of measurements, the sample was given additional aging at 600°C and the sequence repeated. The curves for 600° and 400° exhibit little change as the specimen is ordered at 600°. A slight decrease occurs during ordering in the measurements at 300°C, while at lower temperatures the decrease becomes more pronounced. Obviously, the main effect of ordering at 600°C is on the thermal coefficient of resistivity.

Hardness Measurements

The changes in hardness that accompany ordering in the three alloys are illustrated by fig. 12. Each point is an average for at least three indentations, and two or three specimens were used for different aging times at each temperature. The occasional scatter in the data, i.e., that for the 700° aging in fig. 12*a*, is due to an unidentified difference in specimens. Regardless, the similarity to aging curves for precipitation is clear. In general, the rate of hardening increases with aging temperature, while the maximum attainable hardness decreases with increasing temperature. The alloys over-age, that is, the hardness decreases again after the maximum is reached. Greater maximum hardness is reached by alloys nearer to the ideal 50 atomic pct composition in agreement with less complete results of other investigators.[2]

---

* The aging curve for the 54 atomic pct Co alloy in fig. 10*a* can be considered as a control run since at 800°C this alloy does not order.

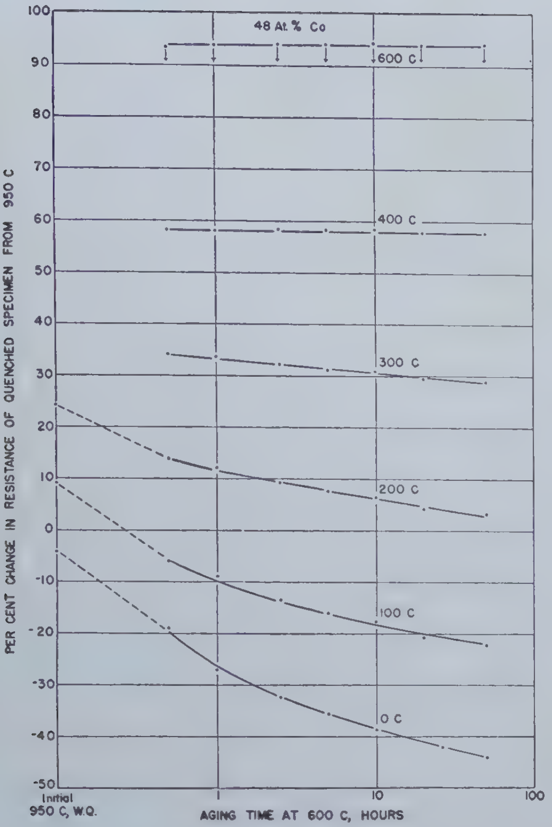

Fig. 11—Change in electrical resistance of 48 atomic pct Co alloy during ordering at 600°C.

The specimen was aged at 600°C, water quenched and resistance measured at 0°, 100°, 200°, 300°, and 400°C before additional aging at 600°C.

The curve for aging at 800°C in fig. 12*b* is unusual. This temperature is only 15° to 20° below the temperature at which the ordered phase is unstable, yet pronounced age-hardening occurs. Such would not occur for a precipitation alloy, since the amount of transformation product would be negligible at this low degree of undercooling. The inherent difference is probably that the potential amount of decomposition product in the ordering reaction is 100 pct of the initial phase.

Magnetic Properties

The magnetic tests were made with cylindrical specimens, ¼ in. in diam by 1 cm in length, which were tested in an Isthmus electromagnet at a maximum magnetizing field strength of 10,000 to 16,000 oersteds. The values of residual induction (B_r), coercive force (H_c), and maximum energy product (BH_{max}) for the three alloys investigated are plotted in figs. 13 to 15. During ordering the residual induction of the disordered alloy decreases at a rate that depends on aging temperature. This property changes in the same direction as the induction at saturation which has been found to be less for ordered Co-Pt alloys than that for the disordered alloys.[2] Ordering results in a decrease in the degree of ferromagnetism, and this is manifested in a regular decrease in residual induction analogous to electrical resistance. On the other hand, the coercive force and the related energy product increase to a maximum during ordering and then diminish. Coercive force is the resistance to demagnetization and can be considered as a magnetic hardness analogous to mechanical hardness which is the resistance to indentation. In regard to these alloys the coercive force decreases after the maximum more prominently than does mechanical hardness. The temperature dependence of the rate of change of the magnetic properties follows exactly that of the other properties described previously. The properties on aging at 600°C are generally higher than those for 700°C, the low magnitudes of the maxima for 500°C (fig. 14) were unexpected. The 48 atomic pct Co alloy exhibited the highest coercive force and energy product while the 54 atomic pct Co alloy had the highest residual induction in the disordered condition.

Discussion of Results

In view of the data presented above, a mechanism is proposed by which an initially disordered specimen of Co-Pt becomes ordered during isothermal aging. The question of whether or not the mechanism offered here is general for other ordering reactions probably should wait until many other systems have been closely studied. On the other hand, it has been possible to rationalize the data for many precipitation alloys on the basis of one carefully studied system, Al-Ag.[18] It is emphasized that secondary reactions, such as self-deformation and recrystallization which persist after full order is attained, may obscure effects of the primary ordering reaction and therefore lead to erroneous conclusions, if they are not properly interpreted. Some of these effects are now known to depend strongly upon the reaction temperature. The high temperatures at which Co-Pt alloys will order makes the system particularly suitable for studying the mechanism of the reaction at various temperatures. Since the effects found at low temperature aging closely parallel those already reported by many investigators for the classical Cu-Au alloys, it is thought that the ordering reaction in the Co-Pt system is basically the same as that occurring in the Cu-Au system, except that a higher maximum ordering temperature is possible. The Co-Pt system then offers more advantages than the Cu-Au system for fundamental studies of the primary ordering reaction, since secondary reactions may be suppressed by using a high reaction temperature.

The experimental effects described above for the isothermal ordering of Co-Pt alloys may be explained in terms of the four distinct processes suggested by microstructure studies, namely, (1) localized ordering, (2) general ordering, (3) self deformation, and (4) recrystallization.

Localized Ordering: If the ratio of the rate of nucleation to rate of growth is low, one would expect that the first nuclei of the ordered lattice will appear and grow at imperfections in the disordered parent lattice. Thus, if the rate of general nucleation of ordered particles throughout the matrix crystal is suppressed by allowing the reaction to proceed at a high temperature, one might expect to find preferential formation of particles along slip lines and grain boundaries as in fig. 6*a*. The phenomenon was clearly brought out by aging in the two-phase field (fig. 6*c*).

General Ordering: At lower aging temperatures one expects the nucleation rate of ordered particles throughout the grain to be much higher and to cause a large percentage of the alloy to assume the ordered structure, though dispersed in very small individual particles. This condition would generate large lattice strains due to the {110} coherency, which exists between the ordered regions and the matrix surrounding them, and would account for the increase in values of the strain-dependent physical properties. It would also account for the general dark and mottled etching effect so commonly found in these alloys after most aging treatments.

It is important to recognize a fundamental difference between this stage of the ordering process and its analog, general precipitation. In the case of precipitation the particles of the second phase which separate from the matrix will ultimately have a different composition, as required by the constitution diagram, from that of the parent alloy. With ordering alloys, however, all the matrix becomes ordered in time. The alloy passes through a two-phase stage, in which regions of the ordered phase nucleate and grow until they impinge, leaving finally a single phase again, which is composed of domains of long range order. Although in "off-composition" alloys there may be some tendency for coring as the ordered particles grow, one would expect it to be very slight since even at annealing temperatures within the two-phase region, where plenty of time was allowed for segregation, no significant change of composition of the two-phases was detectable. In the Ni-Pt system, however, marked segregation apparently does occur on annealing within the two-phase region.[14]

The continuous sequence of Debye-Scherrer patterns given in figs. 2*d* to *f* and 3*b* may be interpreted by assuming that the ordered lattice, forming in the disordered matrix, is restrained from assuming its normal tetragonal dimensions by virtue of its coherency with the cubic matrix. Thus the face-centered cubic diffraction lines spread into bands as the matrix lattice is strained, and then, as the tetragonal lattice grows into predominance, the bands resolve into recognizable pairs which ultimately sharpen into the final ordered pattern. At no time are any diffraction lines visible other than ones ranging from those of the initial face-centered cubic lines to those of the final tetragonality lines. Furthermore it is observed that at no time in the sequence do the diffuse bands extend beyond the final position of the tetragonality lines. These facts indicate that, while coherency is preserved, the c/a ratios of the lattice cells range from a value of one in the unstrained cubic matrix, to their final value less than one in the unstrained tetragonal structure. It is not possible to decide whether this range obtains within a single ordered particle or represents a distribution for various particles in a partially transformed matrix grain. Assuming the former, it might be argued that this transition lattice between ordered and disordered regions is not under strain because the degree of order within it may be such as to require the cell shape which already exists. Such rigorous correspondence of the degree of order with the tetragonality of the lattice joining ordered and disordered regions does not seem probable, however, since the strain-dependent properties reach a maximum at aging times which give a large amount of the transition lattice as judged by Debye-Scherrer effects.

Self Deformation: The transition from the cubic to the tetragonal pattern is very gradual, when the transformation occurs above 600°C. This indicates that the volume of strained metal having neither the initial cubic cell nor the final unstrained tetragonal cell remains relatively large during the transformation. The ordering strains then must be distributed over long distances. Apparently the self-deformation process consists of the relief of these long range strains by twinning and is accomplished by the movement of relatively large blocks of metal. Short-range coherency strains, giving rise to high coercive force, can still prevail within the blocks themselves.

The process of self-deformation limits the strain which the ordered and disordered lattices can suffer and therefore limits the hardness which can be developed by ordering. On the other hand, it also relieves stresses which would otherwise build up to a point where total recrystallization, with its attending large decrease in physical properties, would occur, as happens at lower aging temperatures. It may be that this self-deformation process is general for all ordering reactions of this type, since the striated microstructure is a frequent characteristic of so many ordering systems. Possibly the striated microstructures that have been found for other transformations such as the allotropic transformation in cobalt[15] and the eutectoid decomposition of Cu-Si alloys[16] are also of this nature rather than a true Widmanstätten pattern of one phase in a matrix of a second phase.

Recrystallization: The recrystallization process is also induced by the ordering stresses. It is most evi-

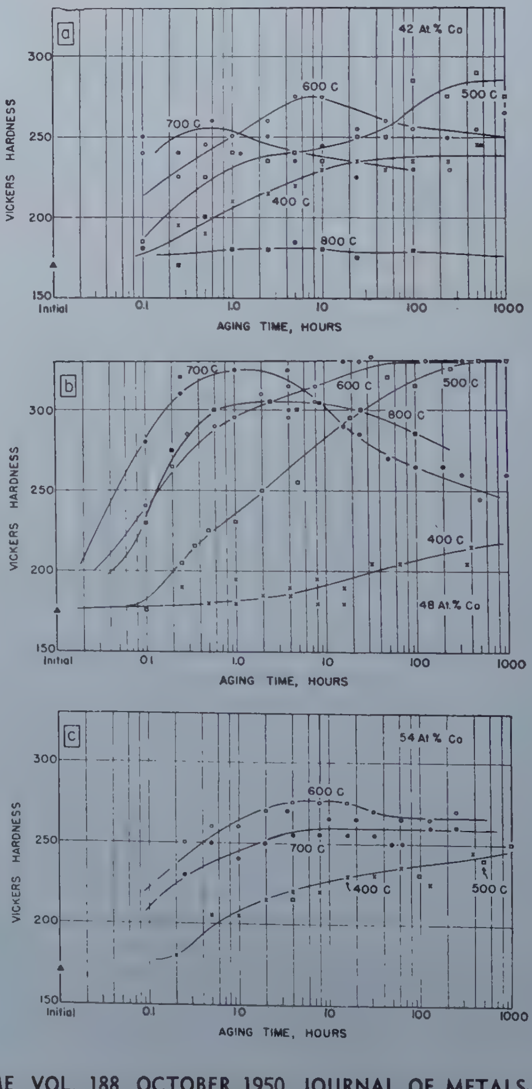

Fig. 12—Change in hardness of three alloys during ordering at various temperatures.

a. For the 42 atomic pct Co alloy.
b. For the 48 atomic pct Co alloy.
c. For the 54 atomic pct Co alloy.

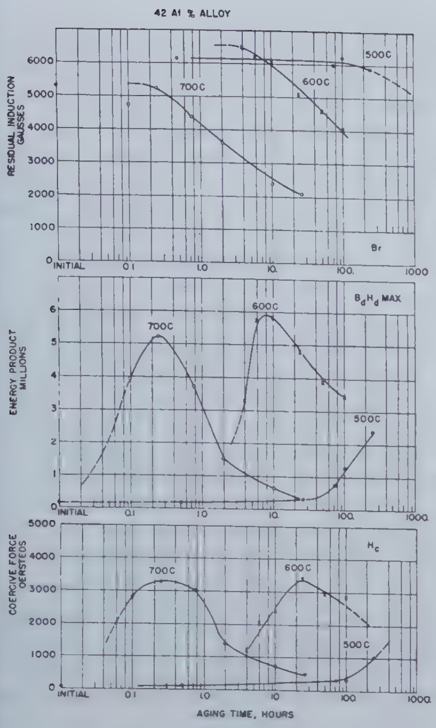

Fig. 13—Change in magnetic properties of 42 atomic pct Co alloy during ordering at various temperatures.

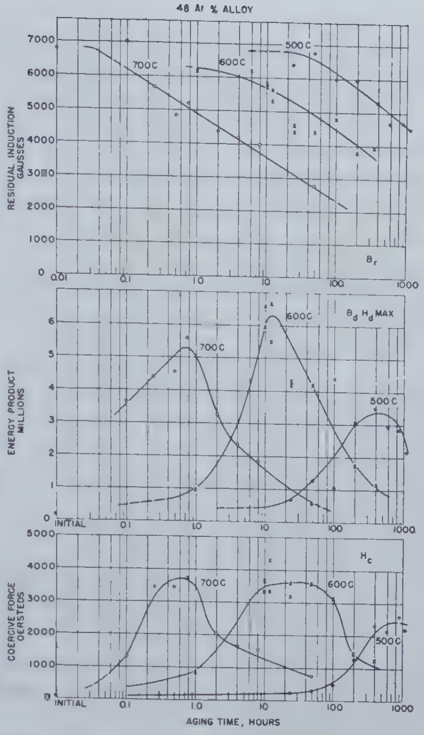

Fig. 14—Change in magnetic properties of 48 atomic pct Co alloy during ordering at various temperatures.

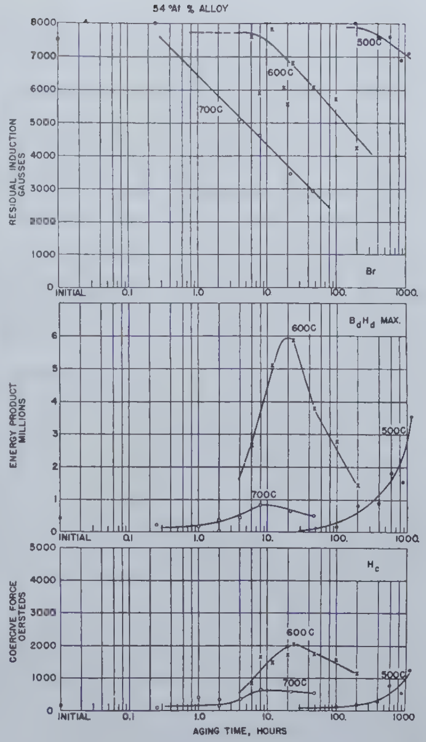

Fig. 15—Change in magnetic properties of 54 atomic pct Co alloy during ordering at various temperatures.

dent at lower aging temperatures, where thermal recovery is not effective and where stresses required for slip and twinning are high, but can also occur at moderately high temperatures in conjunction with the twinning process as indicated by fig. 7*c*. It was stated above that the recrystallized grains, whose orientations are different from the parent, are observed to start predominantly at grain boundaries and grow slowly into the body of the grain. Most likely the newly recrystallized material has the equilibrium structure for the aging temperature analogous to the equilibrium composition of the matrix in discontinuous precipitation. Evidence for this is given by the discontinuous sequence of Debye-Scherrer photographs (fig. 2*a* to *c*) in which the face-centered cubic pattern grows weaker and the ordered face-centered tetragonal pattern grows stronger with aging time. In this sequence the main lattice lines of both patterns remain fairly sharp at all times while the tetragonality lines gain in predominance. From this it must be concluded that the matrix lattice planes remain relatively unstrained throughout the process. To explain this, one may assume that at low aging temperatures the general ordering reaction does not proceed to any great extent before recrystallization starts. At crystal imperfections and grain boundaries however, where the movement of atoms requires less energy, ordering is able to progress faster, giving rise to high lattice strains and inducing local recrystallization which spreads through the body of the crystal. This might explain the low peak in the magnetic hardness curve for aging at 500°C (fig. 14).

The recrystallization reaction is not wholly confined to temperatures where the general ordering is sluggish. It was pointed out earlier that recrystallized grains were also found in highly ordered alloys which were aged at 600°C. In these specimens the microstructure contained not only the recrystallized grains but also the striations characteristic of higher aging temperatures, indicating that twinning had occurred. Here the recrystallization reaction must have cooperated with the other processes to relieve the ordering stresses. In this case one would expect the sharp but faint tetragonality diffraction lines of the recrystallized metal to be superimposed on the diffuse bands of the partially ordered metal and thereby escape detection.

Evidence for recrystallization as a result of ordering strains appears occasionally in the metallurgical literature although it is often not interpreted as such. For example, Samans[17] reports the formation of a "new phase" which appeared at grain boundaries during the aging of Cu-Ni-Mn alloys and which *disappeared* again on long annealing. He was not able to detect this "phase" by Debye-Scherrer methods nor to identify it by other means. A similar unidentified grain boundary constituent was observed by Averbach[18] in alloys of the same ternary system after they had been allowed to order. Dean[19] reports an unidentified grain boundary "precipitate" which he believes is responsible for the age hardening of Cu-Ni-Mn alloys. The "precipitate" appears on low temperature aging and gradually spreads throughout the grains as aging progresses. It was observed that the amount of grain boundary material formed at 450°C tends to *decrease* after aging for four weeks. The results of the present investigation and the clear descriptions given by the above named authors lead to the conclusion that the heretofore unidentified "grain boundary constituent" is the ordered phase which has recrystallized due to coherency stresses. The disappearance is a result of the slow absorption of small grains by the larger ones, after the reaction stresses have been thermally relieved.

It has been proposed that the beta phase of Ni_4W can form by two different mechanisms, viz. by a "phase change" at 950°C and, although in this peritectoid reaction the beta phase does not exist in the disordered condition, by an "ordering mechanism" at 925°C.[12] The different sequences of Debye-Scherrer patterns observed for the two aging temperatures were similar to those given in fig. 2 of this report. It may be that the recrystallization temperature for the Ni_4W alloy lies between 925° and 950°C, in which case the diffraction effects accompanying the formation of beta phase could be explained without assuming the different mechanisms of transformation.

Other features of the X-ray diffraction studies may be compared with previously reported results. Gebhardt and Köster,[2] also working with cobalt-platinum alloys, studied the changes of Debye-Scherrer patterns with aging temperature, but used one half-hour aging periods throughout the series. For that reason they missed the intermediate steps of the continuous sequence, in which single lines first broaden and then resolve into two. The transformation sequence that they observed was always discontinuous, consistent with their observation of a microstructure that has been identified here as characteristic of recrystallization. The one half-hour aging period was not long enough to complete the transformation, for Gebhardt and Köster reported that the pattern of the disordered phase accompanied that of the ordered after all treatments. The diffuse diffraction effects which were interpreted here as evidence for strained platelets of the ordered phase parallel to {110} planes of the disordered matrix have also been observed for Cu-Au alloys, but the geometry is different. Guinier and Griffoul[20] analyzed a partially ordered crystal of Cu_3Au on the basis of diffraction effects similar to those observed for Co-Pt. They interpreted their results in terms of coherent platelets of ordered regions about 150 Å thick on {100} planes of the disordered matrix. Undoubtedly, the habit plane depends upon crystallographic considerations of least strain as in precipitation alloys.

Having as a guide the four salient features of the ordering mechanism as proposed above, we may now briefly examine the physical properties of these Co-Pt alloys at various stages of aging as they relate to the suggested mechanism.

The coercive force and mechanical hardness reach maximum values at about the same time, after which the coercive force drops sharply and the mechanical hardness diminishes slightly. The increase in these and other properties may be due to the lattice straining which accompanies general ordering and has been found in many other systems which are highly strained by a solid phase transformation.[11, 21–23] The marked differences in the rate at which these two properties rise and fall indicate that the fundamental causes which produce them are not the same, as might well be expected, since the one property is the resistance to demagnetization and the other the resistance to deformation.† At present, the reasons suggested for this difference in behavior can be only speculative. Perhaps the coercive force is dependent upon small particles and short distance coherency strains between ordered and disordered regions, whereas the mechanical hardness is dependent upon the longer range disregistry strains between the already ordered domains. This supposition is supported by the observations that the coercive force reaches a maximum at a time when the amounts of ordered and disordered material are about equal, as indicated by the Debye-Scherrer surveys, and then declines steeply as the matrix is consumed by the particles of order. The behavior of the coercive force is very similar to the effect found by Jellinghaus[1] in the FePd alloy. In that case the coercive force rose from a value of 2 oersteds, for the disordered state, to 260 after aging for 15 hr at 500°C, and then fell again with further aging to 150 oersteds. The mechanical hardness, on the other hand, appears to rise steadily as the volume of ordered material increases and then fall off only slightly after the maximum is reached. The latter is characteristic of other order-hardening alloys such as AuCu,[24] CuPt,[24] CuPd,[25] Cu_3Au,[25] and Ni_4W.[12] It is believed that the loss of hardness is due directly to the recrystallization reaction and to thermal recovery from strain.

The fact that higher peaks in magnetic and mechanical hardness are reached at 600°C than at 700°C may be a consequence of the greater stress required for self-deformation at the lower temperature or, as in precipitation, it may be related to the larger number of smaller particles at the lower temperature, consistent with nucleation theory. It is possible that if specimens had been aged at temperatures below 600°C for long enough times to reach the maxima for these properties, even higher values would be attained. However, the stress-relieving recrystallization reaction is probably most rapid between 500° and 600°C, where atomic mobility is appreciable and reaction strains are not released to a great extent by the self-deformation process. The possibility exists, therefore, that softening due to recrystallization will overtake the hardening due to the general ordering process between 500° and 600°C, so that at these ordering temperatures the maximum hardness will not reach that attained at higher temperatures. This is confirmed by the curves for coercive force and energy product of the 48 atomic pct Co alloy aged at 500°C.

The decline of the residual magnetization of Co-Pt alloys as a function of time is a consequence of the loss of ferromagnetism which they are known to suffer on ordering[3] and is directly associated with the effect of interatomic distance upon the exchange forces. It is less dependent on strain than is coercive force.[7]

The dependence of the change in electrical resistivity on measuring temperature apparently is one of the little-known phenomena of the ordering reaction. The slight increase in resistance when measured at the ordering temperature was at first thought to be due to strains, since the magnitude is about the same as that which is associated with coherency hardening;[7] however, the ordered phase at high temperatures is characterized by a higher resistance than the disordered phase.[4] Thus, the gradual increase is consistent with the theory that ordering occurs by the gradual nucleation and growth of ordered particles at the expense of the disordered matrix. Measurements made at low temperatures show the normal decrease in resistance as ordering proceeds. The fact that finite time is required for ordering even at the highest temperatures and that the disordered phase can be retained on quenching from about 850°C exclude the possibility that either the degree of order or the degree of transformation is changed on quenching the specimens to lower temperatures for making the measurements. The atomic distribution is the same regardless of measuring temperature.‡ The only conceivable difference is in the thermal vibrations of the atoms. While the mechanism is not yet clear, the resistivity apparently is independent of the kind of atoms on adjacent lattice sites when the atoms are all in a state of high thermal vibration, but when the motion is diminished the resistivity is controlled to a greater extent by the ordering of the lattice. The older theory would explain these observations entirely on the basis of the temperature dependence of the degree of order, but the present X-ray diffraction work has shown that a fairly high degree of order can be retained at high temperatures up into the two-phase region of the phase diagram. The aging curves in fig. 9 certainly show that long times are required to establish order at the lower temperatures. This reflects much doubt on the significance of low temperature portions of heating and cooling curves when finite rates are used, a subject to be covered in more detail in a future publication by one of the authors.

---

† The difference in behavior of influencing factors on these properties is well demonstrated by solid solution hardening. It is well known that the addition of an element in solid solution markedly increases the mechanical hardness, but it has no influence on coercive force.[7]

Summary and Conclusions

The mechanism and kinetics of ordering have been studied by means of X-ray diffraction, microscopic examination, and measurements of hardness, electrical resistance and magnetic properties of three alloys which were aged isothermally at temperatures between 400° and 800°C.

At all reaction temperatures, ordering is a heterogeneous reaction in which particles of the ordered phase nucleate and grow at the expense of the disordered matrix. The particles are too small to resolve microscopically when formed at the lower aging temperatures, but by using single-crystal X-ray techniques they are shown to be strained coherent platelets which are oriented parallel to {110} planes of the parent matrix. Localized ordering at grain boundaries and slip lines was identified microscopically. Two secondary phenomena, self-deformation and recrystallization, accompany the general ordering reaction. These are alternate methods for removal of ordering strains, the former operating predominantly at high aging temperatures and the latter at lower temperatures. Their recognition solves some of the alleged anomalies in previously studied ordering alloys. They may also be identified in other reactions in metals and alloys. The self-deformation process in Co-Pt alloys is manifested by the appearance of striations that are parallel to {111} matrix planes analogous to twinning. The type of sequence in the change of the Debye-Scherrer X-ray pattern is related to the prominence of these reactions as a function of temperature.

The changes in properties have been correlated with the structure. The initial increases in hardness and coercive force are attributed to the formation of a fine dispersion of strained particles of the coherent ordered phase. Subsequent softening is attributed to removal of the strains either by thermal recovery, self-deformation, or recrystallization. The change in electrical resistivity depends not only on the degree of transformation and degree of long range order as governed by aging time and temperature but also on the temperature at which the measurements are made. Features of the mechanism and kinetics of ordering in Co-Pt are analogous to many of those of the precipitation process and it is proposed that the ordering reaction in other alloy systems be considered in terms of the same characteristic features found here.

Acknowledgments

The first author wishes to express his gratitude to the General Electric Co. for a fellowship that helped make this research possible. The work was also supported in part by an A.E.C. contract at Carnegie Institute of Technology. Valuable discussions with F. N. Rhines of the Metals Research Laboratory are greatly appreciated. Our thanks are extended also to R. F. Mehl and W. E. Ruder for their continued interest in this investigation. Persons of the General Electric Co. who contributed to the data reported here include J. K. Hill and C. Tucker who made some of the X-ray patterns, E. Kontoleon, M. Mayotte and I. Paniccia who conducted some of the microscopic examinations, H. Round and J. Wright who made the magnetic tests, and E. A. Smith, G. Burger and J. Ross who conducted some of the heat treatments, hardness tests, and electrical resistivity measurements.

References

[1] W. Jellinghaus: *Ztsch. f. tech. Phys.* (1936) **17**, 33.

[2] E. Gebhardt and V. W. Köster: *Ztsch. f. Metallk.* (1940) **32**, 253-262.

[3] R. F. Vines and E. M. Wise: Platinum Metals and Their Alloys. (1941) International Nickel Co. Publication.

[4] J. B. Newkirk, A. H. Geisler, D. L. Martin and R. Smoluchowski: Submitted to *Journal of Applied Physics.* (1950).

[5] R. F. Mehl and L. K. Jetter: A.S.M. Symposium on Age-hardening of Metals.

[6] A. H. Geisler and J. K. Hill: *Acta Crystallographica.* (1948) **1**, 338.

[7] A. H. Geisler: *Trans.* AIME (1949) **180**, 230-254; *Metals Technology* (Aug. 1948) TP 2436E.

[8] D. Harker and M. J. Murphy: *Trans.* AIME (1945) **161**, 75-89.

[9] D. Harker: *Trans.* A.S.M. (1943) 210.

[10] J. L. Haughton and R. J. M. Payne: *Journal Institute of Metals.* (1931) **46**, 457.

[11] H. Lipson, D. Shoenberg and G. V. Stupart: *Journal Institute of Metals.* (1941) **67**, 333.

[12] E. Epremian and D. Harker: *Trans.* AIME, **185**, 267-273; *Journal of Metals* (April 1949) TP 2551E.

[13] A. H. Geisler, C. S. Barrett and R. F. Mehl: *Trans.* AIME (1943) **152**, 182-200.

[14] U. Esch and A. Schneider: *Ztsch. f. Electrochemie.* (1944) **50**, 268.

[15] W. P. Sykes: *Trans.* American Society of Steel Treating. (1933) **21**, 385.

[16] C. S. Barrett: *Trans.* AIME, **188**, 123-135; *Journal of Metals* (Jan. 1950) TP 2754E.

[17] C. H. Samans, et al.: *Trans.* A.S.M. (1949) **41**, 961.

[18] B. L. Averbach: *Metals and Alloys.* (1941) **13**, 730.

[19] R. S. Dean, et al.: *Trans.* A.S.M. (1945) **34**, 481.

[20] A. Guinier and R. Griffoul: *Compt. Rend.* (1947) **224**, 1168.

[21] A. Komar and N. Volkenstein: *Inst. Chim Gen.* (USSR) (1943) **16**, 105.

[22] A. H. Geisler and J. B. Newkirk: *Trans.* AIME (1949) **180**, 101; *Metals Technology* (Aug. 1948) TP 2444E.

[23] A. J. Bradley: *Proceedings Physical Society* (1940) **52**, 80.

[24] L. Nowak: *Ztsch. f. Metallk.* (1930) **22**, 94.

[25] G. Sachs: *Praktische Metallkunde III.* (1935) 68-81.

---

‡ Long holding times at high measuring temperatures obviously must be avoided since they would permit the transformation to progress.

Alloys of Titanium with Carbon, Oxygen, and Nitrogen

by R. I. Jaffee, H. R. Ogden, and D. J. Maykuth

IN THE past year, Jaffee and Campbell[1] and Finlay and Snyder[2] reported on the mechanical properties of titanium-base alloys, some of which were in the same ranges of composition as are covered in this paper. In this paper, evidence confirming that given by Finlay and Snyder on the effects of carbon, oxygen, and nitrogen on titanium will be presented; and, in addition, new data will be given on the effects of these elements on the flow properties and phase transformation of titanium.

Materials and Preparation of Alloys

The preparation and general properties of iodide titanium have been adequately described elsewhere.[3, 4] As-deposited iodide titanium rod, prepared at Battelle, of Vickers hardness less than 90 was employed as the base metal in the present work. This was the same material as that used by Finlay and Snyder.[2] The probable analysis reported by them for standard quality metal holds here also: N 0.005 pct, O 0.01 pct, C 0.03 pct, Fe <0.04 pct, Al <0.05 pct, Si <0.03 pct, and Ti 99.85 pct. Carbon was added in the form of flake graphite supplied by the Joseph Dixon Crucible Co. Oxygen was added in the form of c.p. grade TiO_2 powder, produced by J. T. Baker Chemical Co. Nitrogen was added in Ti_3N_4 powder, supplied by the Remington Arms Co. Individual ingots weighed 7 or 8 g. Carbon, oxygen, or nitrogen was added by placing the corresponding powder in a capsule made from as-deposited iodide titanium rods and melting the capsule with the balance of the charge. The charge was arc-melted with a tungsten electrode on a water-cooled copper hearth under a partial vacuum of very pure argon (99.92 pct minimum).

Melting was practically contamination free. Vickers hardness increases of less than 10 points were normal for unalloyed iodide titanium control melts. Nitrogen analyses of arc-melted iodide titanium showed a nitrogen content of 0.005 pct, about the same as is present in the as-deposited rod. No tungsten pickup was found in a melt of iodide titanium analyzed for tungsten. Weight losses in melting nitrogen-free alloys were very small and varied consistently from nil to 0.015 g (0 to 0.2 pct). This permitted the use of nominal composition for these alloys. Chemical analyses made for carbon, which can be analyzed conveniently by combustion methods, justified this procedure. Where nitrogen was added, considerable splattering took place. Here it was necessary to analyze for nitrogen by the Kjeldahl method.

The ingots were hot rolled at 850°C to about 0.045 in. thick. After hot rolling, the strips were descaled by mechanical grinding, and then given a cold reduction of 5 to 10 pct to insure a uniform thickness throughout the length of the specimen. The edge strips and the tensile strips were annealed in a vacuum of 1×10^{-4} mm Hg pressure for 3½ hr at 850°C and furnace cooled.

Methods of Investigation

Hardness Measurements: At least five Vickers hardness measurements were taken using a 10-kg load on each sample in the following conditions: (1) top and bottom of each ingot, (2) top and bottom surface of as-rolled and annealed sheet, and (3) on cross-section of annealed sheet and all quenched specimens.

Tensile Tests: Tensile tests were conducted on Baldwin-Southwark testing machines having load ranges of 600 or 2000 lb. Tests were made on 1-in. gauge-length specimens, 3¼-in. overall length, ½ in. wide, 0.040 in. thick, with a reduced section 1¼ in. long and 0.250 in. wide. Two SR-4, A-7 strain gauges, one mounted on each side of the specimen, were used to measure the strain over a limited range to determine the modulus of elasticity. After the modulus of elasticity readings had been taken, load vs. strain readings were taken, using only one strain gauge, at increments of 0.0001 in. until the yield points were passed and then at 0.001-in. increments to the limit of the strain-gauge indicator (0.02 in.). Strain readings above 0.02 in. per in. were taken every 0.01 in., using dividers to measure the strain between the 1-in. gauge marks until the maximum load had been reached. Crosshead speed, when using the SR-4 gauges, was 0.005 in. per min, and, when using dividers, 0.01 in. per min.

Flow Curves: Flow curves were determined using the true stress-true strain data obtained during the tension test. The usefulness of this type of information has been dealt with very adequately elsewhere by L. R. Jackson,[5] J. H. Hollomon,[6] and many others. Flow curves of true stress vs. true strain could be converted to the more conventional cold-work curve of 0.2 pct offset yield strength vs. percentage of cold reduction by means of the transformation, $\frac{1}{1_o} = \frac{1}{1-R}$, where R is the fraction reduction in cold working. Thus, the true strains corresponding to percentage reduction can be calculated, and the 0.2 pct offset yield strengths scaled off the σ—δ curve by taking the true stresses corresponding to the values of $\delta + 0.002$ strain.

Heat Treatment: For the transformation studies, the alloys were heat treated in a horizontal-tube furnace using a dried 99.92 pct argon atmosphere, and quenched into water. Essentially no contamination was found after several hours of heat treatment at temperatures up to 1050°C.

Metallography: Specimens were prepared in the

R. I. JAFFEE, Member AIME, H. R. OGDEN and D. J. MAYKUTH, Junior Members AIME, are Assistant Supervisor and Research Engineers, respectively, in the Nonferrous Metallurgy Division, Battelle Memorial Institute, Columbus, Ohio.

AIME Chicago Meeting, October 1950.

TP 2955 E. Discussion (2 copies) may be sent to Transactions *AIME before Dec. 15, 1950. Manuscript received April 15, 1950; revision received Aug. 2, 1950.*

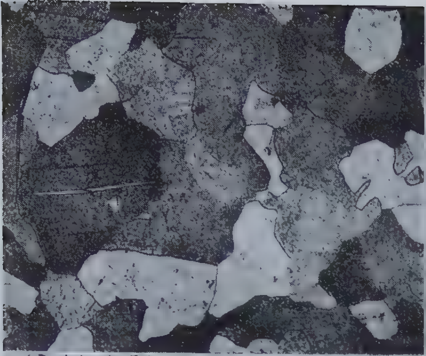

Fig. 1 (upper left)—Iodide titanium, hot rolled and annealed in alpha field at 850°C. Equiaxed alpha grains (0.11-mm diam). X100.

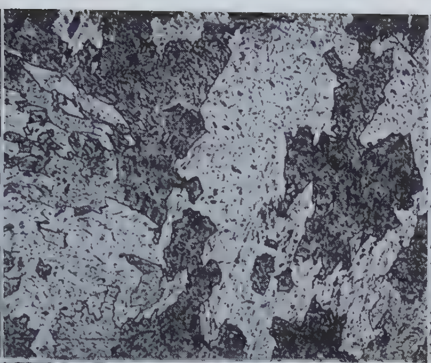

Fig. 2 (upper center)—Iodide titanium, as annealed ½ hr in beta field at 890°C and water quenched. Serrated transformed-beta structure. X100.

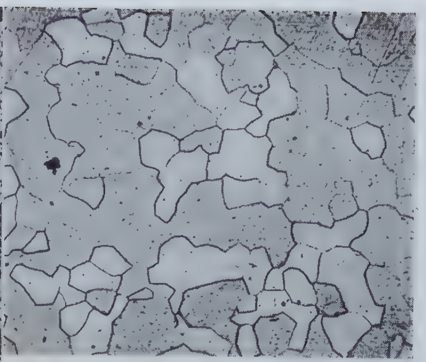

Fig. 3 (upper right)—Titanium-0.25 pct carbon alloy, annealed 3½ hr in the alpha field at 850°C. Equiaxed alpha grains. X100.

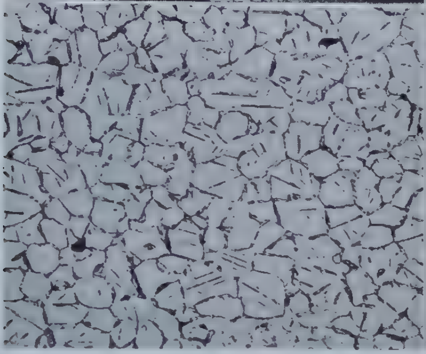

Fig. 4 (lower left)—Titanium-0.25 pct carbon alloy, held 30 min in the alpha-beta field at 900°C and water quenched. Transformed beta surrounding equiaxed alpha. X100.

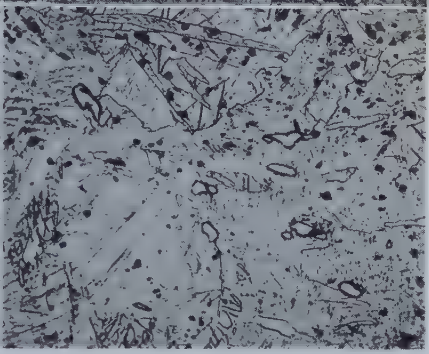

Fig. 5 (lower center)—Titanium-0.25 pct carbon alloy, held 30 min in the beta-titanium carbide field at 920°C and water quenched. Transformed beta with rounded islands of titanium carbide. X500.

Fig. 1-6—Area reduced approximately 40 pct for reproduction.

usual way on metallographic papers through 600X and lapped with diamond dust on a wool lap. Etching was done with 3 pct HNO_3 plus 1½ pct HF in water.

Structure and Transformation Range

Titanium: Iodide titanium fabricated by standard hot-rolling procedures and finished with the standard 3½ hr vacuum anneal at 850°C shows the equiaxed alpha grain structure illustrated in fig. 1.

Water quenching of unalloyed titanium from temperatures above the transformation point results in a transformation structure of the type shown in fig. 2. This structure is characterized by large serrated Widmanstätten plates formed during cooling through the transformation.

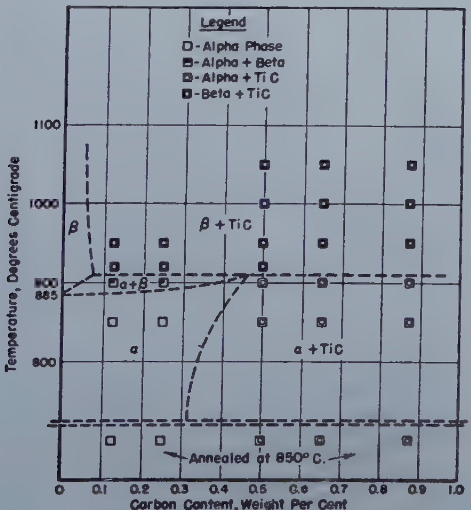

Fig. 6—Transformation range of titanium carbon alloys.

Experiments done early in this work using the inverse-rate method of thermal analysis have shown the alpha-to-beta transformation temperature for iodide titanium to be 888°C, average for three determinations. This temperature is in good agreement with the value of 882°C reported by other investigators.[7, 8]

Quenching experiments performed on iodide titanium having an equiaxed alpha structure showed this structure to persist unchanged on quenching from temperatures up through 850°C. Heating to 890°C resulted in the transformation of the alpha modification to the beta form.

Ti-C Alloys: Five binary titanium-carbon alloys containing 0.125, 0.25, 0.50, 0.65, and 0.87 pct C, by chemical analysis, were studied. Examination of these alloys as annealed at 850°C showed carbon to be soluble in alpha titanium to at least 0.25 pct. Fig. 3 illustrates the equiaxed, single-phase alpha structure observed in these low-carbon-content alloys. The addition of 0.5 pct C to titanium results in the formation of a second phase, titanium carbide. This second phase appears oriented in the rolling direction and occurs in greater amounts in the alloys with increasing carbon content.

Examination of quenched alloys showed that carbon raises the alpha-to-beta transformation temperature of titanium. A peritectoid reaction at temperatures between 900° and 920°C results in a lower

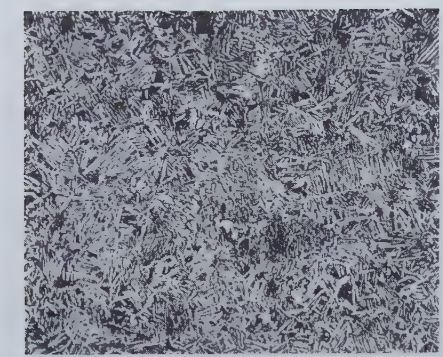

Fig. 7—Titanium-0.25 pct oxygen alloy, held ½ hr at 950°C and water quenched. Transformed-beta structure. X100.

Area reduced approximately 40 pct for reproduction.

solubility of carbon in beta titanium. A transformation diagram for titanium-carbon alloys is presented in fig. 6. Figs. 4 and 5 for a 0.25 pct carbon alloy quenched from the alpha-beta and the beta-carbide fields, respectively, illustrate the progress of the peritectoid reaction.

Alpha plus transformed beta structures were observed only in the 0.125 pct C and 0.25 pct carbon alloys as quenched from 900°C. All the alloys quenched from temperatures of 920°C, and above, showed rounded particles of titanium carbide distributed uniformly in a matrix of the basket-weave type of transformation structure. The data indicate a very low-carbon solubility in beta titanium, estimated to be less than 0.1 pct C. The quantity of titanium carbide phase present in those alloys quenched from 920°C, and above, increases with increasing carbon content. Raising the quenching temperature above 920°C does not appear to affect the quantity of the carbide phase, indicating that the solubility of carbon in beta titanium does not change appreciably.

The presence of more of the carbide phase in the annealed alpha-carbide alloys, as compared with these same alloys quenched from 900°C, indicates that the solubility of carbon in alpha titanium increases with increasing temperatures and reaches a maximum at the peritectoid temperature.

Ti-O Alloys: Five binary titanium-oxygen alloys containing nominally 0.125, 0.25, 0.50, 0.75, and 1.00 wt pct O were studied. Examination of these alloys as annealed at 850°C showed oxygen to be soluble in alpha titanium at these compositions.

Examination of the microstructures of quenched alloys showed that oxygen additions result in extending upward both the alpha and the beta solvus lines. The transformation phase diagram for titanium-oxygen is shown in fig. 8. Fig. 7 shows representative structure for titanium-oxygen alloys as quenched from the beta region. The beta transformation structure for binary titanium-oxygen alloys is seen to be basket-weave rather than the serrated-plate Widmanstätten structure characteristic of beta-quenched iodide titanium.

Ti-N Alloys: Five titanium-nitrogen alloys containing 0.09, 0.16, 0.21, 0.48, and 0.72 wt pct N were studied. Examination of these alloys as annealed at 850°C showed nitrogen to be completely soluble in the alpha-titanium phase.

Microscopic examination of quenched titanium-nitrogen alloys showed that nitrogen additions to titanium extend upward both the alpha and beta solvus lines. This is shown in the transformation diagram in fig. 9. Nitrogen appears more effective than oxygen in raising the beta solvus line. The beta transformation structures are of the acicular basket-weave type, as in the titanium-oxygen alloys.

Mechanical Properties

Unalloyed Titanium: Average mechanical properties of nine separate specimens of annealed unalloyed titanium are shown in table I, together with the average properties found by Finlay and Snyder[2] for similar material with a fine-grained alpha structure. Agreement between the two averages is fair, the principal difference appearing in the values for 0.2 pct offset yield. Of the nine specimens tested, four had equiaxed alpha grains of 0.1-mm avg. diam; one had a finer grained alpha structure; and four had a plate-like Widmanstätten alpha structure. There were no significant differences in the mechani-

Table I. Average Mechanical Properties of Nine Annealed Unalloyed Titanium Specimens

Properties	Present Work	Finlay and Snyder[2]
Proportional limit, psi	11,000	
0.1 pct offset yield, psi	23,200	
0.2 pct offset yield, psi	27,000	21,400
Ultimate strength, psi	43,200	46,000
Elongation, pct	40 (1 in.)	50 (½ in.)
Reduction in area, pct	61	
Vickers hardness	105 (10 kg)	103 (5 kg)

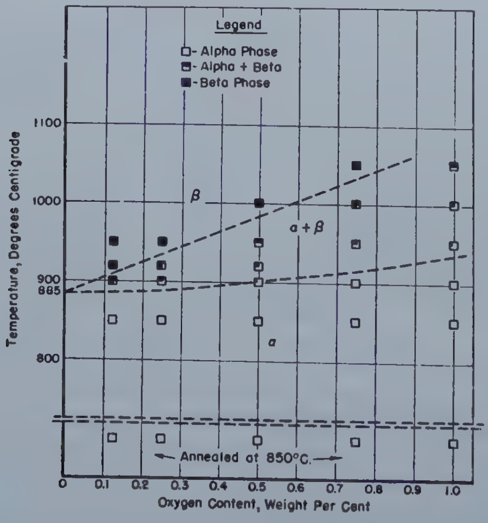

Fig. 8—Transformation range of titanium-oxygen alloys.

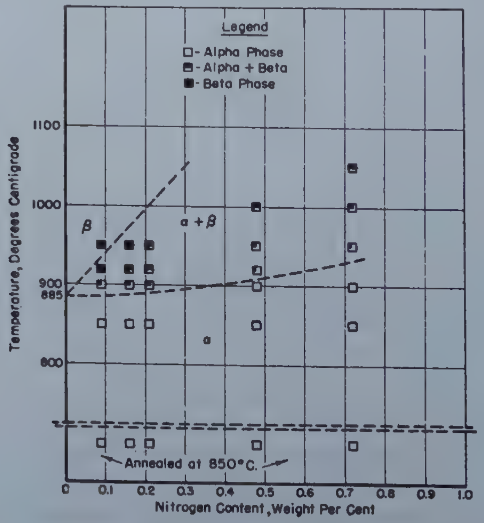

Fig. 9—Transformation range of titanium-nitrogen alloys.

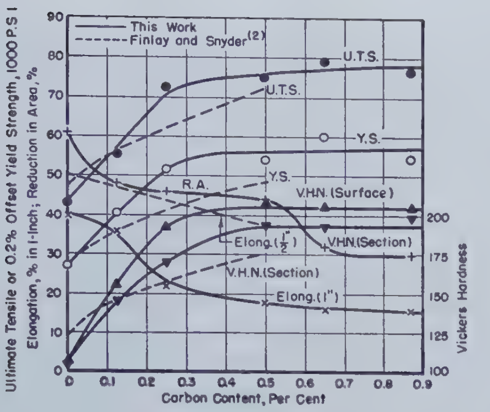

Fig. 10—Mechanical properties of titanium-carbon alloys, annealed at 850°C. Also shown are data of Finlay and Snyder.[2]

cal properties of these specimens. Also, there were no differences between surface and cross-sectional hardness of sheet titanium in any condition. These facts, coupled with the fact that titanium does not change in hardness on quenching through its transformation, indicate that the mechanical properties of high-purity unalloyed titanium are relatively insensitive to structure.

Binary Alloys: The mechanical properties of titanium-carbon alloys up to about 0.9 pct C are shown in fig. 10. Strength increases almost linearly up to 0.25 pct C, about the limit of solid solubility, and then levels off in the range where carbides are present. Ductility decreases as strength increases. The major drop in elongation occurs at 0.25 pct C, while the reduction in area drops most rapidly at 0.65 pct C. The level of ductility remains relatively high throughout. Surface hardness of alpha-titanium alloys is generally higher than cross-section hardness because of the preferred orientation of the hexagonal basal planes parallel to the surface. The difference between surface and cross-section hardness increases from 0 to 20 Vickers points as the carbon content increases to above 0.2 pct.

The mechanical properties of the binary titanium-oxygen alloys are given in fig. 11. The strength and hardness of titanium are increased with oxygen content up to 0.75 pct. The ductile range of binary titanium-oxygen alloys may be placed at up to 0.75 pct O, with the range of good ductility, above 20 pct elongation, located at up to 0.5 pct O. The difference between surface and cross-section hardness of rolled and annealed binary titanium-oxygen alloys is much more pronounced than that exhibited in binary titanium-carbon alloys. The hardness differential increases with increasing oxygen content up to a maximum of 50 Vickers points at about 0.75 pct O. Above 0.75 pct O, the hardness differential remains constant.

The mechanical properties of titanium-nitrogen alloys are given in fig. 12. Nitrogen has a more potent effect on the strength and hardness of titanium than oxygen. The ductile range is much more restricted, however, and is estimated from these data to be between 0.2 and 0.5 pct N. Nitrogen causes a sharp decrease in ductility values. The decrease of strength with increase in hardness of alloys with nitrogen contents of 0.5 pct, and above, is indicative of the brittleness induced by excessive nitrogen. The difference between surface and cross-section hardness reaches a maximum of about 50 Vickers points at 0.4 pct N and remains constant at higher nitrogen contents.

Ternary Alloys: To permit evaluation of ternary effects, several ternary alloys with oxygen, nitrogen, and carbon were made. Vickers hardnesses of these alloys in the 850°C annealed condition are shown in fig. 13. For ternary alloys containing carbon, the conclusion appears justified that their hardness is additive from the binary hardening effects of the constituents. This follows from the parallel nature of the hardness curves for ternary alloys containing carbon. The data for ternary alloys containing oxygen and nitrogen do not appear to follow any rule. Hence, no conclusion may be made as to whether ternary effects in Ti-O-N alloys are additive or not.

Correlations: Comparison of the effects of the

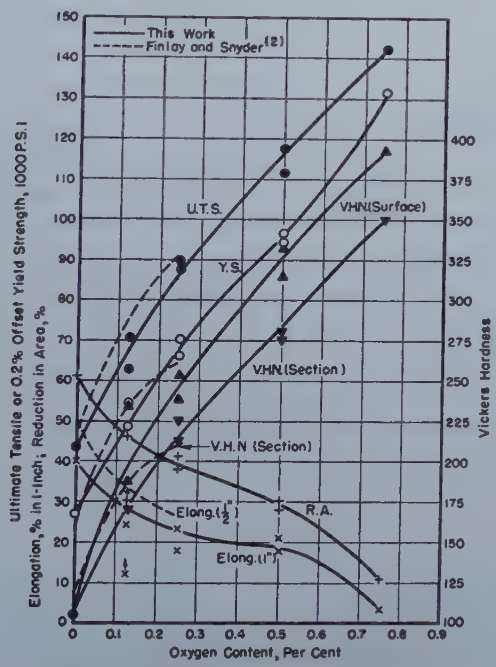

Fig. 11—Mechanical properties of titanium-oxygen alloys, annealed at 850°C. Also shown are data of Finlay and Snyder.[2]

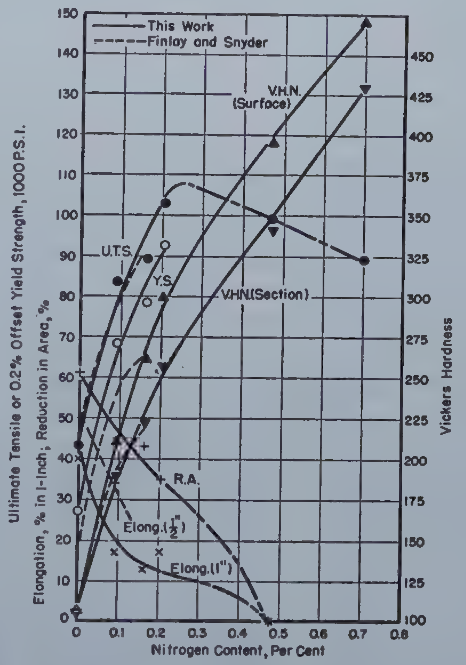

Fig. 12—Mechanical properties of titanium-nitrogen alloys, annealed at 850°C. Also shown are data of Finlay and Snyder.[2]

Table II. Modulus of Elasticity Values for Titanium Alloys

Composition, Pct (Balance Ti)	Modulus of Elasticity, 10^6 psi		
	Tuckerman Extensometer Method	SR - 4 Strain Gauge Method	Average
100 Ti	15.8	15.9	15.8^5
0.2 O	15.2	15.5	15.3^3
0.1 N	15.6	16.0	15.8
0.2 N	15.5	16.2	15.8^5
0.125 C	15.8	16.0	15.9
0.25 C	16.5	16.1	16.3

three alloying additions on the mechanical properties of titanium indicates that nitrogen has the greatest strengthening and hardening effect, oxygen next, and carbon least. The reverse generally holds true for ductility, although, at about 0.5 pct alloy content, the elongation of Ti-C and Ti-O alloys is about the same. Up to about 1 pct alloy content, carbon-containing alloys show no signs of becoming brittle. At about 0.75 pct O, the Ti-O alloys became brittle. For Ti-N alloys, brittleness sets in somewhere between 0.2 pct and 0.5 pct, with the actual value probably lying closer to 0.5 pct N.

Hardness vs. ultimate strength correlation data, shown in fig. 14, fit a straight line. The equation of the line, ultimate tensile strength equals 400 Vickers hardness number, is useful in estimating strengths of annealed alloys from hardness data. This factor is much less than the 500 Vickers hardness number conversion used for steels in estimating ultimate strength from hardness.

Comparison of this work with that of Finlay and Snyder[2] is given in figs. 10, 11, and 12. The results for titanium-oxygen alloys are in remarkably good agreement. Strengths and hardness curves for titanium-nitrogen alloys also are in very good agreement, but the elongation values found in the present work are lower than those of Finlay and Snyder by an amount greater than might be expected for the difference in gauge length in the specimens used in the two investigations. A real divergence in results is found for titanium-carbon alloys. The present work shows the initial rate of strengthening and hardening by carbon is much greater than that found by Finlay and Snyder. This initial greater rate then levels off, so that the two sets of curves would be expected to coincide or merge at about 0.75 pct C. It is suggested that the reason for the divergence lies in the relative amounts of carbon in solution in the alpha titanium phase. In the present work, the alloys were annealed 3½ hr at 850°C, and microscopic evidence showed that at least 0.25 pct C was in solution. Finlay and Snyder, after cold rolling their alloys, annealed them for 1 hr at 700°C. It is known from private communication with these investigators that their alloys, for a given carbon content, contained more carbide than did the alloys in the present investigation. This follows from the diminishing solubility of carbon with decreasing temperature. Solid-solution strengthening would be expected to be less for the 700°C annealed alloys than for the 850°C annealed alloys. Similarly, the alloys reported by Finlay and Snyder would not be expected to level off in properties so sharply as the present alloys but would tend to increase in strength and hardness at a moderate rate as more carbide appeared in the structure.

Table III. Flow-equation Constants, A and n, for for Titanium Alloys

Alloy No.	Composition	Strain Coefficient, A, psi	Strain Exponent, n	Strain at Maximum Load, δ_m, In. per In.
B66	100 Ti	84,000	0.25	0.30
B43	0.125 C	85,000	0.15	0.21
B44	0.25 C	112,000	0.15	0.16
B45	0.5 C	112,000	0.13	0.11
B46	0.65 C	122,000	0.15	0.12
B47	0.87 C	116,000	0.14	0.13
B67	0.125 O	104,000	0.12	0.12
B68	0.25 O	131,000	0.13	0.12
B69	0.5 O	170,000	0.14	0.13
B38	0.092 N	119,000	0.11	0.11
B39	0.163 N	116,000	0.08	0.07
B40	0.206 N	143,000	0.10	0.11

Modulus of Elasticity: A difference of over 1,000,000 psi in modulus of elasticity has been reported[4] between high-purity iodide titanium (14—15.5x10^6 psi) and magnesium-reduced titanium (16—16.5x10^6 psi), which has been attributed to the effect of the contaminants, oxygen, nitrogen, and carbon. In this investigation, it has been found that high-purity titanium has a modulus of almost 16x10^6 psi, and individually none of these three elements causes a marked increase in modulus of elasticity. Both the Tuckerman extensometer and electrical strain gauge methods were used for these determinations, which are given in table II. Of the three additives, carbon causes a slight increase and oxygen a slight decrease in the modulus value.

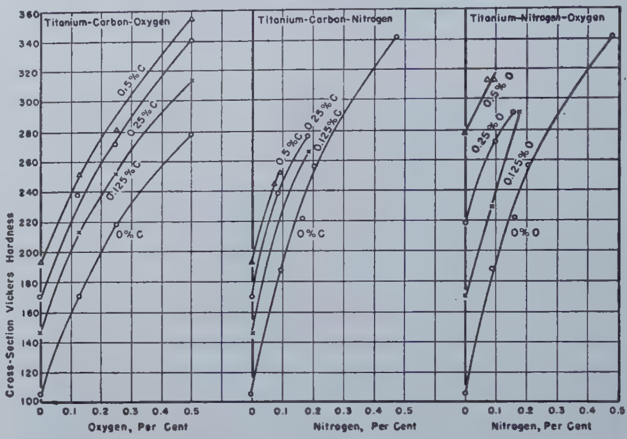

Fig. 13—Effect of ternary combinations of carbon, oxygen, and nitrogen on the hardness of titanium.

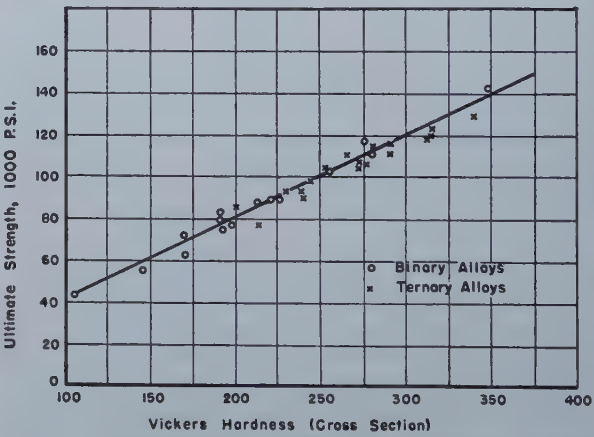

Fig. 14—Correlation of Vickers hardness and ultimate strength of annealed alloys.

Flow Properties

Flow curves of true stress vs. true strain, plotted on a log-log scale, for Ti-C, Ti-O, and Ti-N alloys are composed of two straight lines, the intersection of which occurs at strains in the range of 0.01 to 0.1 in. per in. The initial slope of the flow curve for titanium is 0.12; at a strain of 0.11 in. per in., the slope changes to 0.25. For Ti-C alloys, the initial slope is about 0.09, and for Ti-O and Ti-N alloys the initial slope is about 0.06. Changes in slope for the alloys, in general, occurred at about 0.02 in. per in. strain. Table III lists the flow-curve constants found for the titanium alloys in this work. Also included in table III are values of the true strain at maximum load, δ_m. This maximum uniform strain, δ_m, should equal the value of the strain exponent, n, in cases where the flow equation applies.[6] The experimental agreement between the two is seen to be fairly good. The n values decrease as alloy content increases. The relative order of decrease is in line with the decrease of other ductility parameters: carbon least, oxygen next, and nitrogen greatest. The A values, which give an estimate of strengthening, increase with alloy content, and are in the opposite order: nitrogen greatest increase and carbon least.

Hollomon[6] has correlated strain exponent, n, with yield strength at a strain of 0.01 for steels and found that steels with the same carbon content fit the equation, $n = \dfrac{K}{(\sigma)\ 0.94}$. The constant, K, varied with carbon content. Fig. 15 shows the n vs. $\delta_{0.01}$ correlation for titanium alloys. The points are very scattered, but, in general, show a downward trend. The n-$\delta_{0.01}$ correlation found for low-carbon steel by Hollomon[6] is also shown in fig. 15 for comparison. The titanium alloys appear to be pretty well scattered around the line for low-carbon steel. This would indicate that the flow properties of the titanium alloys are of the same order of magnitude as those of low-carbon steel.

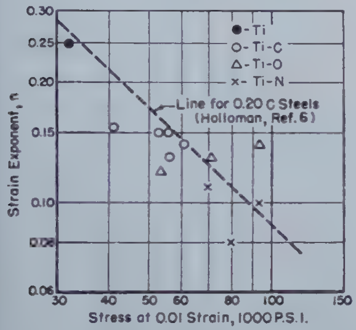

Fig. 15—Correlation of yield strength ($\sigma_{0.01}$) and strain component, n.

One of the useful things that can be done with flow curves is to convert them to curves of yield strength vs. cold reduction. Fig. 16 shows these curves for the Ti-C, Ti-O, and Ti-N alloys. The discontinuity shown in the curve for unalloyed titanium arises from the marked change in slope found in the true stress-strain curve. For each of the alloys, the change in slope of the true stress-strain curve is not very pronounced and occurs at low values of strain. Consequently, the discontinuities are not as apparent in the yield strength-cold work curves for the Ti-C, Ti-O, and Ti-N alloys.

Summary

1. The solubility of carbon in alpha titanium is limited. In its range of solubility, it extends the alpha and beta solvus lines upward from 885°C up to 910°C, where a peritectic reaction takes place between alpha of about 0.4 to 0.5 pct C and beta of less than 0.1 pct C, forming titanium carbide. The solubility of carbon in alpha phase appears to be a maximum at the peritectic temperature and to decrease at lower temperatures. Both oxygen and nitrogen extend upward the alpha and beta solvus lines. The solubility of nitrogen in beta at any given temperature appears to be considerably less than that of oxygen.

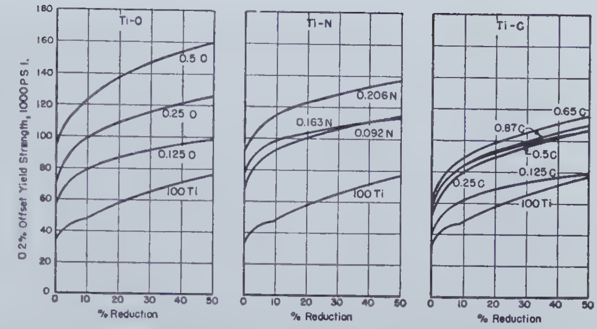

Fig. 16—Yield strength-cold work curves for titanium alloys calculated from flow curves.

2. Mechanical properties determined on binary Ti-C, Ti-O, and Ti-N alloys, in their ductile ranges, indicate that the strengthening effect of nitrogen is greatest and that of carbon is least. Ductility indexes generally were in reverse order. Carbon alloys, in the alpha-carbide region, showed a leveling off in strength properties. Ternary alloys in the Ti-C-O and Ti-C-N systems appeared to have hardnesses additive from the hardening effects of the respective binary alloys. Data for ternary Ti-O-N alloys were not self consistent.

3. Flow curves were determined for three sets of binary alloys. Plotted in a log-log scale, they were composed of two straight lines, intersecting at strains in the range of 0.01 to 0.1 in. per in. The latter part of each flow curve was fitted to the flow equation, $\sigma = A\delta^n$. As alloy content increased, n decreased, nitrogen causing the greatest decrease, and carbon the least decrease. In general, the A values increased with alloy content, nitrogen causing the greatest increase and carbon the least. Cold work-yield strength curves were calculated from the flow curves.

Acknowledgment

The authors are grateful to the Remington Arms Co., Inc., for permission to publish this work, which was done at Battelle Memorial Institute under their sponsorship. They also wish to thank W. L. Finlay of Remington for valuable suggestions and discussion, and Bruce W. Gonser of Battelle for his unfailing encouragement.

References

[1] R. I. Jaffee and I. E. Campbell: The Effect of Oxygen, Nitrogen, and Hydrogen on Iodide-Refined Titanium. *Trans.* AIME, **185**, 646-654; *Journal of Metals* (Sept. 1949) TP 2681E.

[2] W. L. Finlay and J. A. Snyder: Effects of Three Interstitial Solutes (Nitrogen, Oxygen, and Carbon) on the Mechanical Properties of High Purity Alpha Titanium. *Trans.* AIME, **188**, 277-286; *Journal of Metals* (Feb. 1950) TP 2759E.

[3] I. E. Campbell, R. I. Jaffee, J. M. Blocher, J. Gurland, and B. W. Gonser: Preparation and Properties of Pure Titanium. *Trans.* Electrochem. Soc. (1948) **93**, 6.

[4] B. W. Gonser and F. B. Lytton: Composition, Structure, and Properties of Iodide Titanium. *Metal Progress* (1949) **55**, 346.

[5] L. R. Jackson: Work-Hardening and Rupture in Metals. *Trans.* AIME (1947) **171**, 622-637; *Metals Technology* (Oct. 1946) TP 2072.

[6] J. H. Hollomon: Tensile Deformation. *Trans.* AIME (1945) **162**, 268.

[7] J. H. de Boer, W. G. Burgers, and J. D. Fast: *Proceedings* Academy of Science, Amsterdam. (1936) **39**, 515.

[8] A. D. McQuillan: *Nature* (1949) **164**, 537.

Dendritic Crystallization of Alloys

by B. H. Alexander and F. N. Rhines

MUCH attention has been directed to the effects of grain size upon the properties of alloys, but there has been scant study either of the conditions that determine the pattern and dimensions of dendrites in metal systems, or of the influence of their shape and size upon the overall properties of castings. The aim of the research that is about to be described has been to investigate the effect of various factors upon the mode of formation of dendrites in alloys by measurements of the distance between adjacent dendrite arms (dendrite spacing).

Early investigators, including Grignon[1] and Tschernoff,[2] showed that a metal dendrite is composed of a tree-like system of stalks and branches arranged in a simple geometrical pattern. Northcott and Thomas[5] demonstrated that, in the face-centered cubic solid solutions of copper-base, these stalks and side arms all lie in (100) directions in the crystal. Several investigators, including Sauveur and Chou,[6] Sauveur and Reed,[7] and Martin and Martin[8] have reported that the addition to steel of alloying elements, such as nickel, chromium, and molybdenum, not only makes the dendrites easier to reveal by etching, but makes them coarser. The latter authors[8] proposed that the coarsening of the dendrites is roughly proportional to the increase in the temperature range of freezing, caused by adding the alloying elements. Sauveur and Chou[6] showed, in addition, that the dendrites are coarsened by a decreased rate of cooling of the casting.

Measurement of Dendrite Arm Spacing

Among the physical conditions that could be expected to have an influence upon the dendrite arm spacing, that appears in a cast metal, are: composition, rate of freezing, crystal structure, and type of constitution. The relationships obtaining between these variables and the dendrite dimensions have been examined, in the present research, by measuring the arm spacing in a wide variety of alloys, listed in tables II through VI. Alloy compositions are recorded in the tables by showing the symbol of the major metal followed by the percentage and symbol of the alloying agent; thus, "Al-10Ag" is an aluminum-base alloy containing 10 pct of silver. Although none of the alloys were analyzed, an impression of their degree of purity may be obtained from that of their component metals given in table I.

Table I. Degree of Purity of Metals

Metal	Grade	Major Metal, Pct
Al	7A	99.98
Ag	Electrolytic	99.9
Cu	O.F.H.C.	99.93
Zn	Electrolytic	99.99
Mg	Distilled	99.99
Si	Technical	97
Sb	Star band	99.6
As	Lump	99.5
Pb	Electrolytic	99.99
Bi	Refined	99.9
Sn	Chempur	99.98
Cd	Electrolytic	99.9
Ni	Electrolytic	99.9
Tl	High purity	99.9
Te	Lump	99.7

Five hundred grams of each alloy was made by melting in small clay-graphite crucibles in an electric muffle furnace. After alloying the temperature was adjusted to 50° to 75°C above the liquidus and the melts were poured into cast iron molds, at room temperature, the molds having a wall thickness of 1 in. and a cavity 1½ in. sq in cross-section. Each ingot, thus cast, was sectioned at mid-height and the sectioned surface was polished and etched for metallographic examination. Dendrite spacing measurements were made at three positions, namely, adjacent to the mold wall, midway between the wall and the center of the ingot, and at the center (designated *e*, *m*, and *c* respectively, in the tables). A typical series of microstructures is presented in fig. 1. For each measurement, the average was taken of the dendrite spacing of several grains covering a zone about 2 mm wide. Only those grains which had a major dendrite axis nearly in the plane of polish were selected in order to eliminate corrections for orientation differences from grain to grain.

Although the dendrite spacings were measured to the nearest thousandth of a millimeter, the values listed in the tables are thought to be significant only to the nearest hundredth of a millimeter. The largest difference in readings found, when various observers rated the same specimens, was 0.012 mm; the largest difference between corresponding measurements upon duplicate specimens was 0.027 mm.

B. H. ALEXANDER, Junior Member AIME, is now Section Head, Metallurgical Laboratory, Sylvania Electric Products Inc., Bayside, N. Y. and formerly was Assistant Professor of Metallurgical Engineering, Carnegie Institute of Technology, Pittsburgh, Pa. F. N. RHINES, Member AIME, is Professor of Metallurgical Engineering and Member of the Staff of the Metals Research Laboratory, Carnegie Institute of Technology.

AIME Chicago Meeting, October 1950.

TP 2956 E. Discussion (2 copies) may be sent to Transactions *AIME before Dec. 15, 1950. Manuscript received Feb. 12, 1950; revision received Aug. 2, 1950.*

This paper represents part of a thesis submitted by B. H. Alexander to the Graduate Committee of the Carnegie Institute of Technology, Pittsburgh, Pa., in partial fulfillment of the requirements for the degree of Doctor of Science, June, 1948.

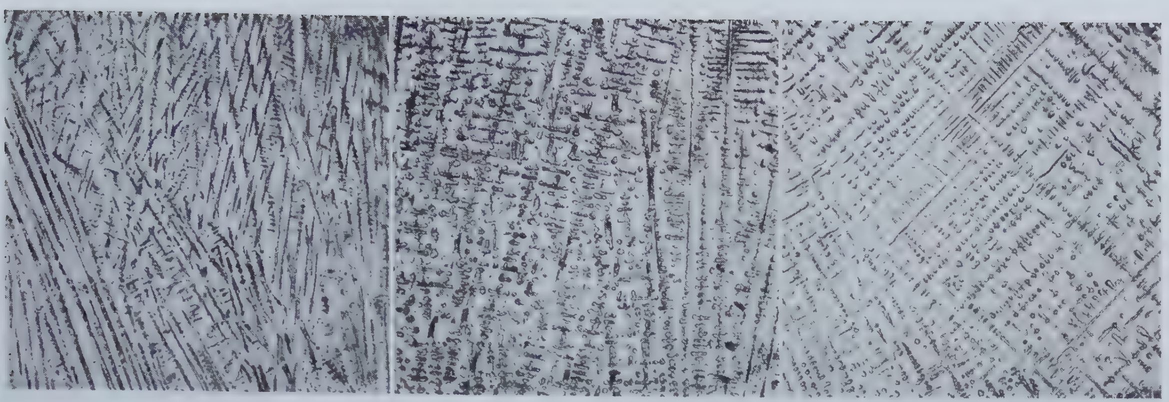

Fig. 1—Typical dendritic structure at three positions in an ingot of Cu-6Si; position (*e*) next to mold wall; position (*m*) midway between wall and center; position (*c*) at center of ingot.

Among the factors that limit the precision of the measurement are the following:

1. There is an element of judgment, and consequently a source of experimental error, in the selection of grains that are suitably oriented for dendrite spacing measurements.
2. It is often observed that there are, along the main stalk of a dendrite, many stunted side arms; the fully developed arms usually occur at fairly regular intervals, with from 2 to 10 underdeveloped arms between. In order to make the measurements consistent, only the fully developed arms, which establish the "rhythm" of the spacing, were considered. There were some border-line cases where it again became a matter of judgment whether to include or exclude certain partially developed arms.
3. Where the grain size was not large, in comparison with the dendrite spacing, it became impossible to obtain significant measurements. In all cases where this relationship was very unfavorable, the readings have been omitted from the tables. There remain some border-line cases, however, where the precision of the measurement may have been impaired by this factor.
4. Occasionally, near the centers of some ingots it was found that two prominent spacings occurred in the same grain. In such cases the larger spacing has been reported.

Influence of Composition, Crystal Structure and Constitution Upon the Dendrite Spacing

The dendrite spacing measurements at position (*m*), as reported in tables II to VI, are summarized with respect to composition in figs. 2 to 6, inclusive. Although the results appear somewhat erratic, there are important trends that are shown clearly:

1. *The dendrite arm spacing always increases with increasing concentration of the solute element.* In most cases the spacing was found to increase

Table II. Dendrite Arm Spacing in Aluminum Alloys

Nominal Composition	Pouring Temp, °C	Grain Size (mm)		Dendrite Spacing in mmx10^3		
		Columnar	Equiaxed	*e*	*m*	*c*
Al — 10 Ag	700	0.7	0	131	166	185
Al — 20 Ag	680	1.0	0	139	185	208
Al — 30 Ag	670	1.1	0	152	200	218
Al — 40 Ag	660	1.1	0	139	166	185
Al — 5 Cu	700			125	133	139
Al — 10 Cu	690			165	170	180
Al — 20 Cu	650			225	300	350
Al — 10 Mg	650	0.4	0.9	125	133	147
Al — 15 Mg	625	0.4	0.9	139	154	167
Al — 1.0 Si	700	1.3	2.0	139	166	161
Al — 1.5 Si	700	0.8	2.0	156	200	250
Al — 5.0 Si	670	1.3	3.0	166	250	333
Al — 5.0 Si	670	1.3	3.0	166	250	333
Al — 20 Zn	670	0.6	0.9	222	333	370
Al — 40 Zn	630	0.8	1.3	238	357	400
Al — 60 Zn	600	0.9	1.4	166	278	333

Table III. Dendrite Arm Spacing in Copper Alloys

Nominal Composition	Pouring Temp, °C	Grain Size (mm)		Dendrite Spacing in mmx10^3		
		Columnar	Equi axed	*e*	*m*	*c*
Cu — 10 Ni	1,200	0.5	0.5	124	139	159
Cu — 20 Ni	1,240	0.4	1.0	126	145	166
Cu — 30 Ni	1,280	0.3	0.7	133	151	175
Cu — 40 Ni	1,330	0.3	0.4	145	166	185
Cu — 50 Ni	1,360	0.3	0.4	166	208	250
Cu — 60 Ni	1,390	0.4	0.5	154	200	222
Cu — 70 Ni	1,420	0.3	0.5	166	238	275
Cu — 10 Pb	1,100	0.3	0.3	94	111	139
Cu — 20 Pb	1,060	0.3	0.3	111	133	151
Cu — 2 Sb	1,120	0	0.2	104	126	139
Cu — 5 Sb	1,110	0	0.2	119	139	151
Cu — 10 Sb	1,060	0	0.2	125	147	159
Cu — 20 Sb	750	0	0.2	128	159	167
Cu — 2 Si	1,100	0.7	2.0	138	160	175
Cu — 4 Si	1,050	0.5	1.7	185	208	222
Cu — 6 Si	990	0.4	1.4	145	208	278
Cu — 1 Sn	1,130	0.4	0.8	100	102	111
Cu — 5 Sn	1,100	0.3	0.4	105	116	125
Cu — 10 Sn	1,050	0.3	0.3	111	125	139
Cu — 15 Sn	1,000	0.3	0.3	115	139	165
Cu — 20 Sn	950	0.3	0.3	128	166	250
Cu — 10 Zn	1,100	0.3	1.1	108	124	133
Cu — 20 Zn	1,050	0.3	1.1	133	151	185
Cu — 30 Zn	1,000	0.2	1.1	208	222	256
Cu — 2 Be	1,060	0	2.5			238

Table IV. Dendrite Arm Spacing in Magnesium Alloys

Nominal Composition	Pouring Temp, °C	Dendrite Spacing in mmx10^3		
		e	*m*	*c*
Mg — 1 Sn	700	100	105	111
Mg — 5 Sn	690	185	222	256
Mg — 10 Sn	680	238	256	303
Mg — 15 Sn	670	178	278	333
Mg — 20 Sn	660	145	175	208
Mg — 30 Sn	630	105	139	119
Mg — 10 Tl	690	196	222	250
Mg — 25 Tl	675	333	475	500
Mg — 2 Zn	700	151	175	222
Mg — 5 Zn	690	166	185	238
Mg — 10 Zn	670	185	208	250
Mg — 20 Zn	630	172	200	222
Mg — 30 Zn	580	166	182	208

Note: No grain size measurements were made.

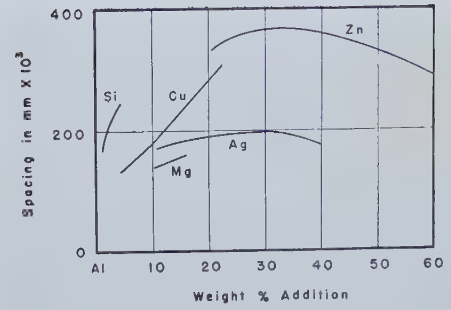

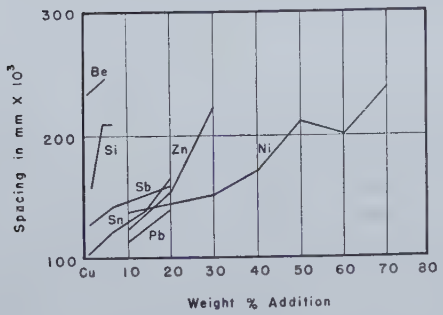

Table V. Dendrite Arm Spacing in Antimony Alloys

Nominal Composition	Pouring Temp, °C	Grain Size (mm) Col-umnar	Grain Size (mm) Equi-axed	Dendrite Spacing in mmx10^3		
				e	*m*	c
Sb — 5 As	675	0.5	1.1	158	208	278
Sb — 10 As	665	0.4	0.9	166	303	370
Sb — 10 Bi	660	0.4	0.3	72	139	238
Sb — 20 Bi	645	0.4	0.3	83	167	278
Sb — 30 Bi	620	0.3	0.4	166	358	400
Sb — 40 Bi	600	0.4	0.5	139	333	358
Sb — 50 Bi	575	0.4	0.7	208	384	435
Sb — 60 Bi	540	0.5	1.2	278	416	476
Sb — 70 Bi	500	0.4	2.5	140	250	350
Sb — 80 Bi	460	0.5		139	238	378
Sb — 90 Bi	400	0.5		86	167	278
Sb — 5 Sn	670	0.6		208	303	333
Sb — 10 Sn	660	0.7	1.4	303	333	370
Sb — 15 Sn	630	0.5	2.5	238	280	356
Sb — 20 Sn	600	0.4	1.7	303	417	565
Sb — 2 Te	675	0.5	1.4	185	256	278
Sb — 5 Te	670	0.6	1.7	196	333	370
Sb — 10 Te	650	0.6	2.0	208	370	417
Sb — 5 Zn	650	0.6	1.1	238	333	370
Sb — 10 Zn	620	0.8	2.0	278	333	417
Sb — 15 Zn	580	1.0	1.7	303	370	475

Table VI. Dendrite Arm Spacing in Some Miscellaneous Alloys

Nominal Composition	Pouring Temp, °C	Grain Size (mm) Col-umnar	Grain Size (mm) Equi-axed	Dendrite Spacing in mmx10^3		
				e	*m*	c
Ag — 5 Cu	960	*	*			67
Ag — 10 Cu	940	*	*			80
Ag — 20 Cu	890	*	*			50
Zn — 2 Ag	470	*	*	128	159	175
Zn — 3 Ag	480	*	*	180	200	238
Zn — 5 Ag	550	*	*	151	185	208
Cd — 3 Zn	355	0	0.2	151	167	185
Cd — 5 Zn	350	0	0.2	159	222	303
Cd — 10 Zn	330	0	0.2	139	169	222
Pb — 20 Sn	330	*	*	55	63	91
Pb — 30 Sn	310	*	*	55	67	100
Pb — 40 Sn	290	*	*	63	71	111
Sn — 2 Zn	275	*	*	125	200	222
Sn — 5 Zn	270	*	*	133	250	286
Sn — 8 Zn	250	*	*	84	111	125

* Note: Grain size not measured.

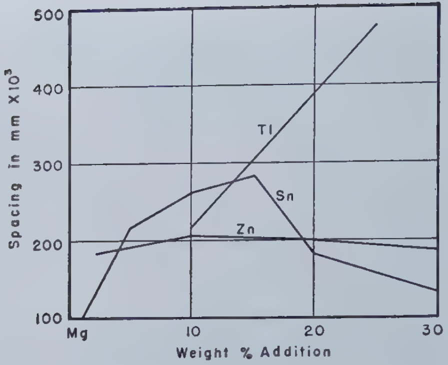

Fig. 2 (upper left)—Dendrite spacing vs. alloy concentration in Al-base alloys.

Fig. 3 (lower left)—Dendrite spacing vs. alloy concentration in Cu-base alloys.

Fig. 4 (upper right)—Dendrite spacing vs. alloy concentration in Mg-base alloys.

throughout the range of composition that was studied, but in isomorphous series, such as that of the Sb-Bi system, fig. 5, a maximum spacing was found near the mid composition. A similar maximum appears in the Al-Zn system, fig. 2, which has a very broad range of solid solution alloys.

2. *There is a tendency for the dendrites to be coarser when the crystal structure of the dominant metal is of a more complex (less densely packed) type.* Thus, the curves in figs. 2, 3, and 4 (cubic and hexagonal metals), if extrapolated to the composition of the pure base metal, would cluster about a dendrite spacing of about 100x10^{-3} mm, or a little smaller, while the curves for rhombohedral Sb and tetragonal Sn, figs. 5 and 6, would extrapolate to somewhat larger dendrite spacings at the pure metal composition.

Beyond this, there appear to be no clear associations between the dendrite spacing and the crystal structure and constitution. The possibility of a connection between the temperature range of freezing and the dendrite spacing, such as was proposed by Martin and Martin,[8] has been explored carefully; while there is a somewhat indirect association of these two factors that will be discussed presently, in connection with deviations from regular behavior, it can be said, quite definitely, that there is no direct relationship between freezing range and dendrite spacing. Also, the intrusion of a second solid phase, such as is encountered in the richer alloys of eutectic and peritectic types, seems to be without influence upon the dendrite dimensions. This may be presumed to be because the establishment of the dendrite pattern precedes the crystallization of the low melting phases.

Influence of Rate of Growth Upon the Dendrite Spacing

In order to explore the possible effect of rate of growth upon the dendrite spacing, measurements were made at three depths below the ingot surface in each of the samples examined, it being known that the velocity of freezing would diminish with distance from the mold wall. Results from two typical alloy series are shown in figs. 7 and 8. From these it is apparent that the *spacing increases with depth below the ingot surface, i.e. with the deceleration of growth.*

It will be noted that a linear relationship between dendrite spacing and depth beneath the ingot surface is indicated in figs. 7 and 8. To be sure, there are both positive and negative deviations from linear behavior among the curves presented, and this condition is borne out by the balance of the readings listed in tables II to VI; but the frequency of the occurrence of a linear relationship is suggestive of the existence of a principle. It suggests that the spacing may be inversely proportional to the rate of freezing, because the inverse of the freezing velocity is also a linear function of the depth frozen. The latter relationship can be derived from the experimental fact[9] that the depth frozen (D) is proportional to the square root of time (t); that is:

$$D \sim t$$

and since the velocity of freezing (V) is:

$$V = \frac{dD}{dt}$$

the reciprocal of the velocity will be proportional to the depth frozen:

$$\frac{1}{V} \sim D.$$

Reasons for the observed departures from the linear relationship will be considered presently.

To obtain more accurate freezing rate measurements, an additional study was undertaken, using the well-established method of casting a series of ingots and upsetting the molds to ascertain the thickness of the shell of solidified metal after various intervals of time. An aluminum alloy (17S) and a 6x6 in. sq mold, 12 in. deep, were used. If the thickness of the solidified shell is plotted as a function of the times of freezing and a smooth curve is drawn through the points, fig. 9, the instantaneous rate of freezing can be determined, for any position in the ingot, from the slope of the curve at the same distance from the mold wall. The results of such a determination are presented in table VII (col. 3), where the inverse rate is expressed in terms of the number of seconds per inch of growth.

Observed measurements of the dendrite spacings in several positions in the large ingots are shown in table VII (col. 4). These readings are to be compared with those in col. 5, which were computed by making the ratio between the first dendrite spacing in each group and each succeeding reading the same as the ratio between the first rate-of-growth measurement in each group (col. 3) and each succeeding reading. The correspondence between the observed and "calculated" dendrite spacings is taken as confirmation of the principle that *the dendrite spacing is inversely proportional to the rate of crystal growth.* It may be noted that a given freezing velocity corresponds to somewhat different spacing values, where the degree of superheating, prior to pouring, is different, table VII; here it is to be expected that the correspondence between the measured freezing rate and the true rate will vary with the degree of superheating, because of the difference in the temperature gradient that would be established thereby.

Deviation from linearity in plots such as those in figs. 7 and 8 can now be explained. The finding, at the center of the ingot, of a dendrite spacing that is smaller than expected is clearly to be associated with a final acceleration of the freezing rate, owing to the rapid decrease in the ratio of the freezing area to the area of the external surface of the ingot through which heat is flowing. This effect is apparent in the curves of fig. 9 which turn sharply upward at the end, corresponding to the center of the ingot. Such behavior is most pronounced in systems having a relatively short freezing range (fig. 8). Where the freezing range is relatively long, the depth in the ingot over which crystallization is occurring simultaneously becomes significant. The liberation of heat of crystallization in a zone behind the front of growth of the dendrite tips would be expected to have a retarding influence upon the rate of advance of this front; and this would lead to a coarsening of the dendrite spacing, above that anticipated, which becomes progressively greater as the center of the ingot is approached. An example of this kind of behavior is presented in fig. 7, where

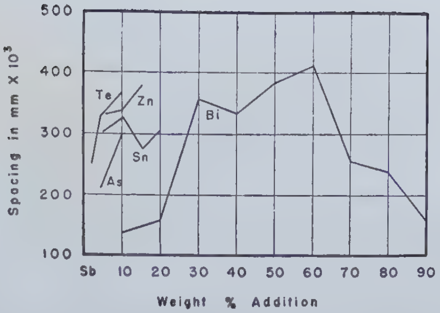

Fig. 5—Dendrite spacing vs. alloy concentration in Sb-base alloys.

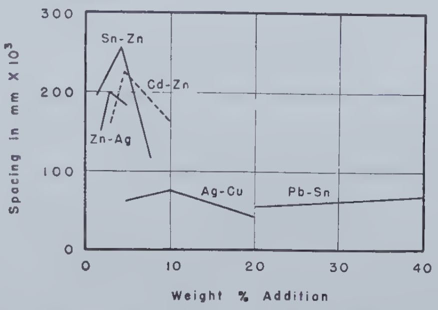

Fig. 6—Dendrite spacing vs. alloy concentration in some miscellaneous alloy series.

Table VII. Rate of Freezing vs. Dendrite Spacing in Large Ingots of 17S Aluminum Alloy

Pouring Temp, °C	Inches from Surface	Rate of Growth in Sec per In.	Dendrite Spacing in mmx10³ Observed	Dendrite Spacing in mmx10³ Calculated	Length of Columnar Zone in In.
800	0.25	44	418	418*	
800	0.75	48	455	456	
800	1.25	54	529	513	0.85
900	0.25	38	333	333*	
900	0.75	44	378	385	
900	1.00	46	407	403	
900	1.75	58	500	508	1.45
1,000	0.25	41†	294	294*	
1,000	0.75	52†	363	373	
1,000	1.75	56†	400	401	
1,000	2.00	64†	475	459	1.75

*Note: This value arbitrarily taken the same as that in col. 4 in solving for the others of the same group.

† Note: Insufficient data for an accurate reading; may be in error as much as 10 sec per in.

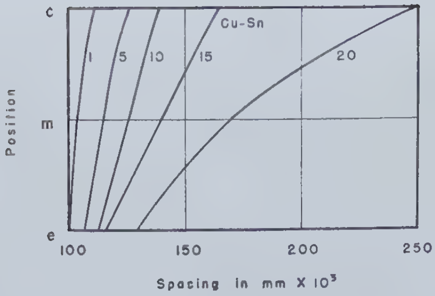

Fig. 7—Dendrite spacing vs. position in the ingot (*e* = edge, *m* = mid-distance, *c* = center) for Cu-Sn alloys. Curves identified by the percentage of Sn.

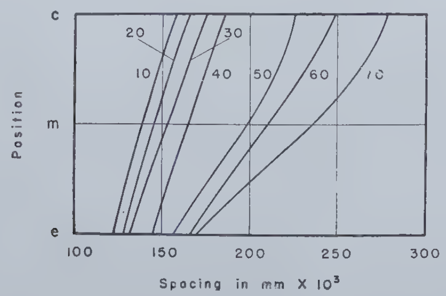

Fig. 8—Dendrite spacing vs. position in the ingot (see fig. 7) for Cu-Ni alloys. Curves identified by the percentage of Ni.

Cu-Sn alloys, having a long freezing range, are seen to exhibit deviations toward larger dendrite spacing. The behavior, in this respect, of each of the alloys studied, can be seen by comparing the spacings in columns *e*, *m*, and *c* of tables II to VI.

Grain Size and Dendrite Spacing

There is no apparent relationship between the grain size and the dendrite spacing in a casting. This can be seen by comparing the grain size measurements with the dendrite spacings recorded in tables II to VI. Where "columnar grain size" is reported, the figure refers to the width, not the length, of the grain. Perhaps a more striking demonstration is to be had by comparing cols. 4 and 6 of table VII. It can be seen here that individual columnar grains in the aluminum ingots generally extend across several zones in which dendrite spacings were read and different readings were obtained in each position. In other words, the dendrite spacing can, and does, vary significantly within a single grain. Moreover, the increase in the columnar grain length, as the casting temperature is raised, is not associated with a corresponding increase in dendrite spacing.

Since the dendrite dimensions of a given alloy are determined by the rate of freezing alone, and since it is known that the cast grain size is determined cooperatively by the rate of crystal growth and by the rate of nucleation of crystals, it is apparent that the grain size and dendrite spacing of a casting can, within limits, be controlled independently.

Mechanism of Dendrite Growth

The most stable form of a crystal, in equilibrium with its melt, is thought to be idiomorphic, i.e., bounded by plane facets. When crystals grow very slowly from a melt, or in a saturated liquid solution, they are characteristically idiomorphic. It is only when crystallization proceeds rapidly that dendritic growth is encountered. Vogel,[4] among others, has demonstrated this relationship between crystal form and rate of growth, in this instance for the freezing of $FeSb_2$. Thus, it is clear that the occurrence of dendrites is to be associated with a significant disturbance of equilibrium conditions during crystallization.

It was pointed out by Lehmann[10] that a crystal growing in a water solution impoverishes the solution with respect to the crystallizing elements in its immediate neighborhood. Since the corners of the crystal have a relatively larger volume of solution to draw upon, than do the facets, the impoverishment is less pronounced next to the corners, as has been demonstrated by Berg,[11] and this condition favors more rapid deposition of matter upon the sharp angles of the crystal. This has been called the "point effect of diffusion." If growth is rapid, so that there is insufficient time for the crystal to maintain its equilibrium shape through the transfer of matter from the corners to positions along the facets,[12] then protruberances will appear at the corners. These constitute the beginning of dendritic growth.

While the crystal is yet small, the growth advantage of the corners is slight, because the distances concerned are so small that diffusion in the liquid phase can maintain a nearly uniform concentration all around the crystal and the idiomorphic shape is maintained. With increasing size, however, the advantage of the corners increases, until, at some critical size, the crystal corners begin to grow preferentially. The faster the rate of growth the greater will be this advantage and the smaller will be the critical size at which dendrite arms begin to form.

In applying this argument to the freezing of metals, it is evident that there will be a marked disturbance of the thermal equilibrium, because the release of the latent heat of crystallization is known to be sufficient to arrest natural cooling until the entire mass of metal is solid. Thermal gradients will be superimposed upon concentration gradients during the freezing of alloys. With pure metals, where concentration gradients are impossible, there can still be thermal gradients present during freezing. The occurrence of dendritic crystallization in pure metals, then, gives rise to the proposal[4] that the

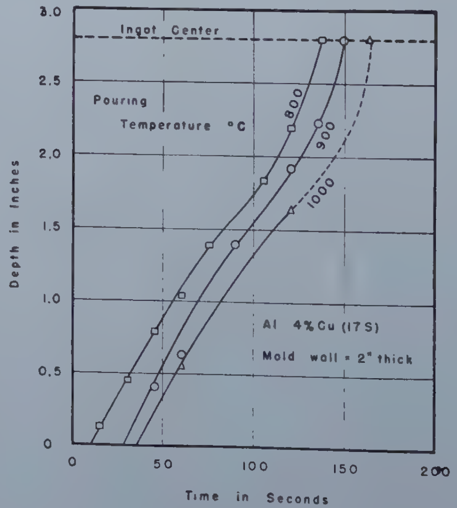

Fig. 9—Rate of freezing of 17S aluminum 6x6 in. ingots cast at three temperatures.

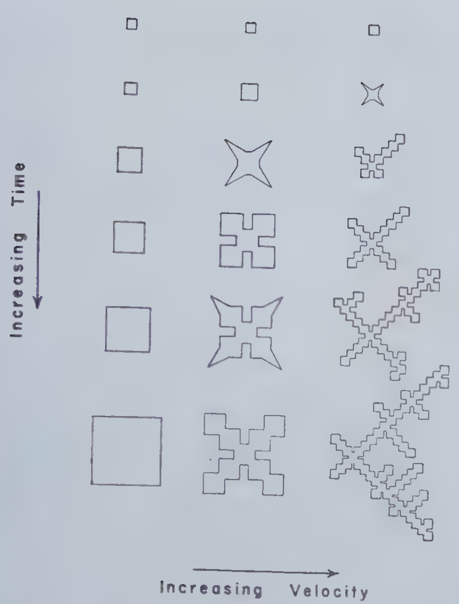

Fig. 10—Schematic representation of the modes of crystal growth at three rates increasing from left to right with growth proceeding from top to bottom.

dendritic modification of crystal growth can be induced as well by thermal as by concentration fluctuation. Because the diffusion of heat and the diffusion of matter obey similar rate laws, it follows that these two factors should support each other in their influence upon the crystallization of alloys.

The extensive studies of Papapetrou[13] upon the crystallization of nonmetallic substances led him to the conclusion that, at moderate rates of growth, the corners which begin to develop preferentially do not continue to grow as rods but grow into other crystals of the same size and shape and physically continuous with the one from which they originated. This process is continued and results in a series of idiomorphic crystals connected at their corners, thus producing the primary stalk of a dendrite system.

It is evident, then, that the number and direction of the stalks of the dendrite system must depend upon the number and location of the corners on the idiomorph, which in turn are determined by the intersections of its facets. If the equilibrium form of the crystal is known, the symmetry of the dendrite becomes apparent. According to the law of Bravais, the planes of closest atom packing in a crystal should appear as principal facets upon the idiomorph. A face-centered cubic metal, upon this basis, should crystallize in the form of octahedra with six corners coinciding with the cube directions in the crystals. Accordingly, a face-centered cubic dendrite should have six main stalks lying in three mutually perpendicular directions. This corresponds with Northcott and Thomas'[5] observations on dendrites in copper-base alloys. The analysis becomes complicated in its application to some types of crystals and there are cases where alternate arrangements are encountered.

The mechanism described so far does not account for the regular development of secondary arms upon the primary stalks of the dendrite, nor for the development, upon these, of tertiary arms. Lehmann and Vogel, as well as Papapetrou, assume that concentration or temperature fluctuations are present in the liquid into which the primary arm is growing, or that these fluctuations occur as a consequence of the discontinuity of growth, and that these fluctuations, or "waves," lead to the formation of side arms. This view stems from the theory of Liesegang rings, which are thought to occur as a result of concentration fluctuations established by a spasmodic precipitation from a solvent.

Although this proposal may be fundamentally sound, it is somewhat vague, and it appears more satisfying to consider the process in greater detail. Beginning with the crystal chain of connected idiomorphs, observed by Papapetrou, it is evident that each idiomorph presents several corners that provide potential sites for secondary arm growth. Each of these corners might grow into a side arm, but observation indicates that only some (from 1/3 to 1/20) of the potential arms actually grow. A possible reason for this behavior emerges if one considers the first and second idiomorphs of the primary chains, adjacent to the parent idiomorph. The corners of the first idiomorph should be less favored for growth than those of the second because of shielding by the adjacent primary arms that are extending at right angles from the corners of the original idiomorph (shielding, that is, in the sense that temperature and concentration gradients emanating from these arms would encroach upon the growth domain of the first idiomorph and rob it of some of its growth potential). By the same reasoning, the corners of the third idiomorph are still more favored for preferential growth, and so on. At some point along the chain, side growth will actually proceed and the resulting arm will establish a new shield for the next few potential sites of side arm growth. The frequency of secondary (and tertiary) arm growth is expected to be limited, on the one hand, by the size of the original idiomorph, which limits the frequency of opportunities and, on the other hand, by the pattern of material and heat gradients; all of which depend, in the last analysis, upon the fundamental rates of material and heat diffusion.

A graphical outline of the process thus far described is presented in fig. 10. In successive vertical columns are pictured three sequences of crystal growth at slow, intermediate, and fast rates, respectively. The process starts at the top of the chart with a small square representing the initial idiomorph and growth proceeds, according to its velocity, to produce a large idiomorph, an elementary dendrite of primary arms only, or a complex dendrite. To make this picture fully realistic, for the case of metals, the undeveloped corner sites should perhaps be shown rounded instead of sharp, because this is usually observed. It may be supposed that the rounding results from a transfer of matter away from the corners under the driving force of surface tension, decreasing the total surface area of the dendrite.

While this picture of dendrite growth does not readily lend itself to the derivation of a formalized expression of the relationship between dendrite spacing and the factors affecting rate of growth, it does make it seem more reasonable that there should be an inverse relationship between the spacing and the growth rate, for both are seen to depend upon the same factors, but in opposite ways.

Alloying has been found to increase the dendrite spacing in all cases. That this effect comes from the influence of alloying upon the rate of material diffusion seems improbable, because the diffusion coefficient may either increase or decrease with alloying. The heat conductivity, however, is always lowered by alloying. This is the right kind of change to account for the effects observed, and it is concluded from this that the rate of heat transfer is probably of greater importance than is the rate of material transfer in establishing the dendrite spacing in metal systems. It will be noted, further, that the frequent observation of coarse dendritic growth in metals of complex crystal structure is consistent with this conclusion, because the metals of complex crystal structure are usually poor conductors of heat.

While the depression of the thermal diffusivity by alloying provides qualitative correspondence with the increased dendrite spacings, the actual values of heat conductivity do not set the alloys in the same order as that established by the spacings. This may be the result of differences from alloy to alloy in the quantity of latent heat that must diffuse away, inasmuch as there is a fairly good correlation, within any one alloy series, between the dendrite spacing and the ratio of the heat of fusion to the thermal diffusivity (table VIII).

Table VIII. Correlation between Dendrite Spacing and Ratio of Heat of Fusion to the Thermal Diffusivity

Nominal Composition	Dendrite Spacing at Position *m* (in mmx10^3)	Ratio of Heat of Fusion over Thermal Diffusivity (in cal cm^{-5} sec)
Al — 1 Si	166	296
Al — 1.5 Si	200	311
Al — 5 Si	250	400
Al — 20 Zn	333	414
Al — 40 Zn	357	430
Al — 60 Zn	278	272
Cu — 10 Zn	125	650
Cu — 20 Zn	151	793
Cu — 30 Zn	222	835
Cu — 1 Sn	102	715
Cu — 5 Sn	116	1,860
Cu — 10 Sn	125	2,730
Cu — 15 Sn	139	2,550
Cu — 20 Sn	166	3,020
Cu — 10 Pb	111	1,440
Cu — 20 Pb	133	1,700
Cu — 2 Si	160	2,560
Cu — 4 Si	208	4,070
Cu — 6 Si	208	5,450
Pb — 20 Sn	63	294
Pb — 30 Sn	67	310
Pb — 40 Sn	71	315
Ag — 5 Cu	67	370
Ag — 10 Cu	80	409
Ag — 20 Cu	50	421
pure Ni		5,010
Ni — 20 Cu		4,200
Ni — 30 Cu	238	7,510
Ni — 40 Cu	200	9,180
Ni — 50 Cu	208	8,820
Ni — 60 Cu	166	9,160
Ni — 70 Cu	151	7,670
Ni — 80 Cu	145	5,340
Ni — 90 Cu	139	4,410
pure Cu		582

A full understanding of the factors influencing dendrite spacing will be of practical usefulness, for it may be expected to lead to the development of methods for dendrite spacing control. The spacing is important in such ways as its influence upon the time required for homogenization by heat treatment and its influence upon the distribution of microconstituents in castings.

Summary

The spacing of the dendrite arms has been measured in a large group of nonferrous alloys cast under comparable conditions, from which it has been learned that:

1. The dendrite arm spacing and the grain size are independent.
2. The dendrite spacing is inversely proportional to the rate of freezing.
3. Alloying coarsens the dendrite.
4. The dendrite spacing in any one alloy system varies in the same manner as the ratio of the heat of fusion to the thermal diffusivity.

References

[1] Grignon: Memories de Physique, sur l'Art de Fabriquer le Fer, etc. (1775) Paris.

[2] D. Tschernoff: *Revue Universalle des Mines* (1880) **7**, 129.

[3] W. Campbell: Uber das Gefuge des Metalle, deren Veranderunger durch Bearbeitung und Warmbehandlung. *Metallurgie* (1907) **4**, 801-809, 825-834.

[4] R. Vogel: Dendritische Crystallization und Ihre Beeinflussung bei der Festigkeit metallische Legierungen. *Zeit. anorg. Chemie* (1921) **116**, 21-41.

[5] L. Northcott and D. E. Thomas: Dendritic Structures, Part I—The Influence of Crystal Orientation. *Journal*, Institute of Metals. (1939) **65**, 205-216.

[6] A. Sauveur and C. H. Chou: Influence of Rate of Cooling on Dendritic Structure and Microstructure of Some Hypoeutectoid Steels. *Trans.* AIME (1930) **90**, 100-113.

[7] A. Sauveur and E. L. Reed: Dendrites in Nickel Steel. American Society for Steel Treatment (1931) **19**, 89-96.

[8] D. J. Martin and J. L. Martin: The Dendritic Structure of Some Alloy Steels. *Trans.* AIME (1939) **135**, 245-252.

[9] J. Chipman and C. R. Fondersmith: Rate of Solidification of Rimming Ingots. *Trans.* AIME (1937) **125**, 370-377.

[10] O. Lehmann: Molekularphysik. (1888) Leipzig.

[11] W. F. Berg: Crystal Growth from Solutions. *Proceedings* Royal Society (London). (1938) **A164**, 79-95.

[12] M. Volmer: Kinetik des Phasenbildung. (1939) Dresden.

[13] A. Papapetrou: Untersuchung uber dendritisches Wachstum von Kristallen. *Zeit. Kristallographie* (1935) **92**, 89-130.

[14] L. Northcott: Dendritic Structures of Columnar Crystals. *Journal*, Institute of Metals. (1946) **72**, 283-291.

CORRECTION

In the August 1950 issue: *Discussion—Institute of Metals Division: The Transverse Bending of Single Crystals of Aluminum* by M. K. Yen and W. R. Hibbard, Jr. P. 1040: 2nd column, 26th line should read, in part, "bands form on the (110) plane," instead of "(111) plane;" and the 29th line should read, in part, "Crystals having their axes near [111]," instead of "[110]."

Thermal Expansion Characteristics of Beryllium

by R. M. Treco

A study has been made of the thermal expansion characteristics of vacuum-cast beryllium. Linear expansion coefficients for annealed and extruded beryllium are given for temperatures up to 1000°C. Results of expansion measurements on a single crystal of beryllium are discussed in relation to preferred orientation. The volume coefficient of expansion has been calculated.

THE thermal expansion of pure beryllium was first investigated by Hidnert and Sweeney[1] in 1925 on a single cast specimen stated to be of 98.9 pct purity. A study of the coefficients of expansion by X-ray methods has recently been made by P. Gordon[2] on powder obtained from the Brush Beryllium Co. assaying 97 wt pct beryllium with about 2 wt pct oxygen as an impurity.

The present work pertains to about the highest purity metal obtainable from the Brush Beryllium Co. This metal was in the form of lumps which were remelted and cast in a high-vacuum induction furnace. Expansion data in this paper deal with beryllium extruded into bars of rectangular cross-section 4x½ in. and the anisotropic expansivity of a large cast single crystal.

Analysis of the cast metal after extrusion indicated a beryllium assay of 99.28 pct. Impurities were 0.170 pct Fe, 0.140 pct Al, 0.014 pct Mg, 0.086 pct Si, 0.020 pct Cu, 0.020 pct Mn, 0.007 pct Ni, 0.007 pct Ca, 0.080 pct C, 0.179 pct O_2 (as BeO).

Part I—Extruded Metal

Thermal expansion measurements were obtained with a fused quartz-tube differential type dilatometer[3] on specimens cut from the extruded sections in longitudinal and transverse directions. Specimens were machined to a diameter of 0.250 in. and a length of 3.000 in. One sample from each direction was vacuum annealed for 1 hr at 800°C.

The dilatometer tube was placed in a vertical tube furnace having a uniform temperature zone which was twice the length of the sample. Average time for a complete thermal cycle to 500°C was 18 hr. Temperatures were observed with two chromel-alumel thermocouples attached to the sample about 1½ in. apart. The accuracy of temperature measurement was ± 0.25°C. An argon gas atmosphere surrounded the specimen to prevent oxidation of the beryllium.

Table I. Identification of Samples

Sample No.	Location in Bar	Treatment
4	Longitudinal	Annealed after extrusion
5	Longitudinal	As extruded
6	Transverse	Annealed after extrusion
7	Transverse	As extruded

Samples were identified as shown in table I.

Results

The original plan included measuring expansion up to 1000°C, but the first two runs on sample No. 5 showed that a permanent contraction occurred from

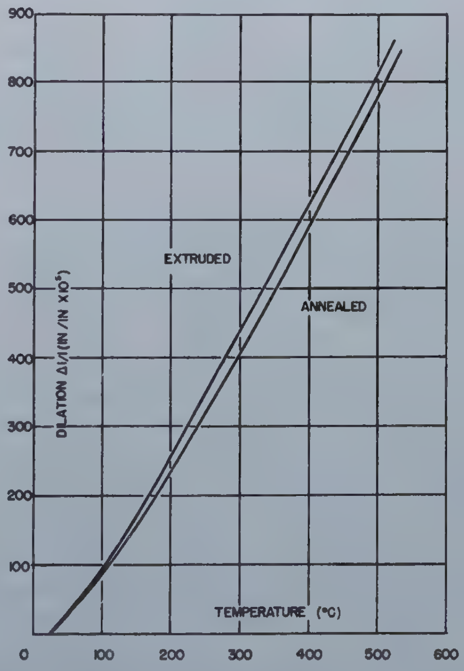

Fig. 1—Expansion of longitudinal specimens Nos. 4 and 5.

R. M. TRECO, Junior Member AIME, is associated with the Division of Industrial Cooperation, Massachusetts Institute of Technology, Cambridge, Mass.

AIME Chicago Meeting, October 1950.

TP 2954 E. Discussion (2 copies) may be sent to Transactions AIME before Dec. 15, 1950. Manuscript received April 3, 1950; revision received Aug. 7, 1950.

This work was carried out at the Massachusetts Institute of Technology Metallurgical Project under Contract No. W-7405-eng-175 with the U. S. Atomic Energy Commission. This paper has been condensed from the report MIT-1043 (Same title) obtainable from: Technical Information Division, USAEC, Oak Ridge, Tenn.

Table II. Linear Coefficients of Expansion (In. per In. per °C x 10^6)

Temp Range (°C)	Hidnert and Sweeney	Gordon (X-ray*)	Transverse Annealed, No. 6	Longitudinal Annealed, No. 4	Transverse Extruded, No. 7—Run No. 1	Transverse Extruded, No. 7—Run No. 2	Longitudinal Extruded, No. 5—Run No. 1	Longitudinal Extruded, No. 5—Run No. 2	Longitudinal Extruded, No. 5—Run No. 3	Mean Co-efficient
25-100	12.3	11.6	14.3	10.3	9.6	10.1	12.6	11.4	12.5	11.54
25-200	13.3	13.5	14.5	13.2	11.8	12.1	14.5	13.4	14.7	13.46
25-300	14.0	14.5	14.8	14.5	12.7	13.1	15.2	15.1	15.7	14.44
25-400	14.8	15.3	15.3	15.6	13.6	14.0	15.9	15.7	16.6	15.24
25-500	15.5	15.9	15.8	16.6	14.5	14.7	16.6	16.3	17.2	15.95
25-600	16.1	16.5					17.2	17.0		
25-700	16.8	17.0	(16.5)	(18.3)	(16.1)	(16.1)	17.6	17.5	(18.5)	17.23
25-800		17.4					18.1	17.9		
25-900		17.9					18.6	18.6		
25-1000		18.4	(17.5)	(20.4)	(18.0)	(17.6)	18.9	19.0	(20.0)	18.77

* Calculated from $(2\alpha_{\perp} + \alpha_{\parallel})/3$ for random orientation.

the weight of the measuring equipment. The maximum temperature possible without creep effects was 525°C. The contraction data for the first two runs indicated that the slope of the expansion curve would not change between 525° and 1000°C if loading effects could be eliminated.

Typical expansion curves for the longitudinal samples are shown in fig. 1 in which expansion per unit length (corrected for quartz) is plotted directly against temperature. Fig. 2 shows the same data for the transverse samples. It is apparent from these curves that the expansion of beryllium is not a linear function of temperature, and it proved to be impossible to represent the curves with any degree of accuracy by the usual form of the expansion equation:

$$L_T = L_0 \ (1 + \alpha T + \beta T^2 + \gamma T^3 \ldots)$$

where L_T = length at temperature T°C

L_0 = length at 0°C

α, β, γ, etc. are empirical coefficients.

It was a necessary objective of this work to determine the linear expansion coefficient as accurately as possible over the entire temperature range of the tests. The method of drawing tangents to the curves was discarded for two reasons: (1) The curves exhibit unusual changes in slope in the initial portions, and (2) the graphical error in plotting these curves was greater than desired.

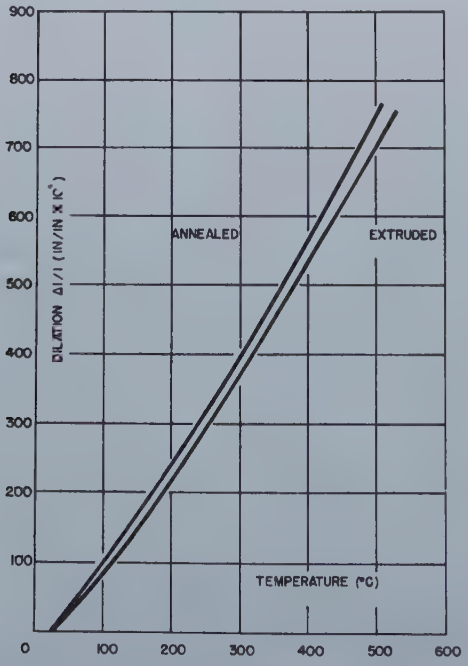

Fig. 2—Expansion of transverse specimens Nos. 6 and 7.

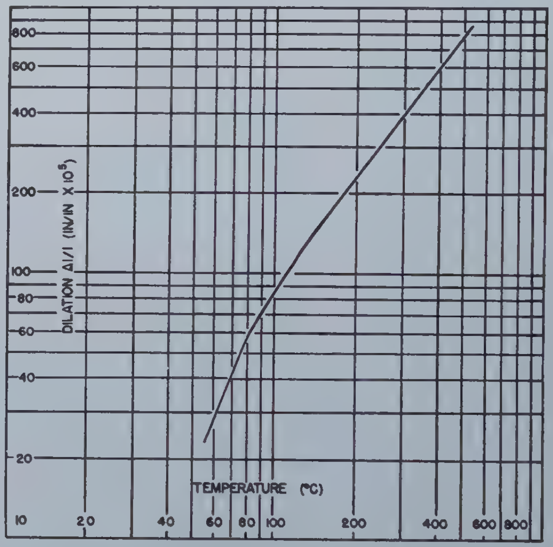

Fig. 3—Contraction curve for extruded and annealed longitudinal sample No. 4.

A more accurate method of obtaining the coefficients resulted when the expansion data were plotted on log-log paper. Linear curves resulted which could be analyzed by the method of averages. Such a plot is shown in fig. 3. An equation of the form $L_T = L_1 \ (1 + aT^b \times 10^{-6})$, where a and b are empirical constants, was derived for each heating and cooling cycle. The linear coefficient was obtained from the relation:

$$\alpha = \left(\frac{L_T - L_{25}}{L_{25}} \right) \left(\frac{1}{T - 25} \right)$$

where L_{25} = length at 25°C and T = °C.

Table II lists the expansion coefficients obtained along with those of Hidnert and Sweeney[1] and of Gordon.[2] For comparison purposes, the values of the expansion coefficient parallel and perpendicular to the principal hexagonal axis given by Gordon have been combined to give a mean linear coefficient for randomly oriented polycrystalline metal; i.e.,

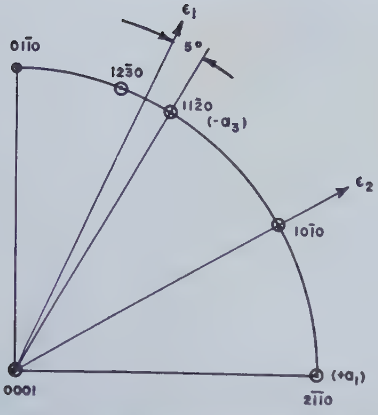

Fig. 4—Pole figure showing direction for measurement of expansion ε_1 and ε_2 perpendicular to hexagonal axis.

$\alpha = (2\alpha_\perp + \alpha_\parallel)/3$. The agreement of the observed data with the X-ray measurements was fair but not entirely consistent for the individual runs, although the calculated mean coefficient for all runs given in the last column agrees well with the X-ray data. The values of Hidnert and Sweeney are somewhat lower than the mean values with one exception. Values of α in parentheses have been extrapolated from the lower temperature data.

Part II—Expansion of a Beryllium Single Crystal

A large single crystal from a high-purity, vacuum-refined casting was carefully ground on one side parallel to the cleavage (0001) planes and then cut at right angles to the basal plane. Baldwin-Southwark SR-4 type A-8 bonded resistance strain gauges were cemented to the exposed surfaces of the crystal and also to a Vycor flat 2x1x¼ in. ($\alpha = 0.8 \times 10^{-6}$ in. per in. per °C).

Crystal and Vycor flats with cemented gauges were placed in a thermo-regulated constant temperature bath having a range of 0 to 50°C ± 0.03°C. Expansion data obtained in this manner lay on a straight line conforming to the usual relation: $L_T = L_1(1 + \alpha T)$. Values of α were calculated for the direction parallel to the principal axis, designated $\alpha_\parallel$, and perpendicular to this axis, $\alpha_\perp$. A small correction for the Vycor[4] has been added to give the coefficients listed in table III.

X-ray analysis showed that the strain coefficient designated $\alpha_\parallel$, was measured within ¼° of parallel to the c axis, and the strain coefficient perpendicular to the same axis made an angle of 5° with one of the a axes (ϵ_1, fig. 4). In order to check the method and at the same time determine any directional variation in the basal plane, the last two measurements were obtained with a new strain gauge mounted 35° from the first direction (ϵ_2, fig. 4). No significant deviation from the previous values was found in this direction.

Table III. Linear Coefficients of Expansion (α) for Beryllium (0 to 50°C)

No. Cycle	$\alpha_\parallel \times 10^6$	$\alpha_\perp \times 10^6$	Direction Measured for $\alpha_\perp$ (See fig. 4)
1	10.21	11.46	ϵ_1
2	10.27	11.69	ϵ_1
3	10.06	11.85	ϵ_1
4	10.07	11.67	ϵ_1
5	10.00	11.33	ϵ_2
6	10.03	11.57	ϵ_2

The best weighted mean values together with their probable errors are as follows:

$$\alpha_\perp = (11.580 \pm 0.050) \times 10^{-6} \text{ in. per in. per °C } (0 \text{ to } 50°\text{C})$$

$$\alpha_\parallel = (10.076 \pm 0.026) \times 10^{-6} \text{ in. per in. per °C } (0 \text{ to } 50°\text{C})$$

Beryllium is quite anisotropic in nature, having a 15 pct difference in the expansion coefficients of the major crystallographic directions.

From the mean values, the average linear coefficient of expansion for polycrystalline metal of random orientation was calculated to be $(11.079 \pm 0.042) \times 10^{-6}$ in. per in. per °C using the relation $1/3(2\alpha_\perp + \alpha_\parallel)$. This value is significantly greater (about 10 pct) than measured values on polycrystalline metal and probably reflects the absence of grain boundary restraint. The volume coefficient of expansion, β, equals $(33.24 \pm 0.08) \times 10^{-6}$ (0 to 50°C).

Discussion of Results

Gordon[5] has shown that the basal (0001) planes become parallel to the longitudinal axis of extruded rods with random orientation around the rod axis. Similarly with an extruded flat, metal parallel to the longitudinal direction should expand proportional to $\alpha_\perp$. This is borne out by the coefficients in table II for samples 4 and 5 which agree well with Gordon's values for $\alpha_\perp$.[5] The effect of thermal cycling is slight, but annealing decreases the expansion coefficient below 400°C. With increasing temperature, the coefficients for the transverse extruded metal did not agree well with previous data providing only an approximate confirmation of the preferred orientation determined from X-ray work.

Beryllium shows no apparent hysteresis in thermal cycling.

The marked decrease in oxygen content of the metal used in the present work had no significant effect on the expansion properties.

Summary

Linear thermal expansion coefficients for extruded and annealed polycrystalline beryllium have been listed in table III. The linear expansion coefficient has been shown to be greater in the direction perpendicular to the hexagonal axis and independent of rotation about this axis.

Acknowledgment

The author is indebted to A. R. Kaufmann for his helpful suggestions during the progress of the work and to E. B. Read for the difficult chemical analyses.

References

[1] P. Hidnert and W. T. Sweeney: U. S. Bureau of Standards. *Scientific Papers* (1927 to 1928) 22, No. 565.

[2] P. Gordon: A High Temperature Precision X-Ray Camera. Some Measurements of the Thermal Coefficients of Expansion of Beryllium. Declassified Document No. AECD-2426. Technical Information Division, USAEC, Oak Ridge, Tenn. (1948).

[3] P. Hidnert: U. S. Bureau of Standards. *Scientific Papers* (1926 to 1927) 21, No. 524.

[4] E. Wichers, A. N. Finn and W. S. Clabaugh: U. S. Bureau of Standards. *Journal of Research.* (1941) 26, No. RP 1394, 537.

[5] P. Gordon: Preliminary Studies on the Physical Metallurgy of Beryllium. Declassified Doc. No. MDDC-1370, Technical Information Division, USAEC, Oak Ridge, Tenn. (1945).

Aging Characteristics of Magnesium-Lithium Base Alloys

by P. D. Frost, J. G. Kura, and L. W. Eastwood

Although magnesium-lithium base alloys have several desirable properties, they also possess certain undesirable characteristics, one of which is the tendency to overage at 150° to 200°F. This problem is discussed in the paper. Recently developed alloys, described in the paper, have stability of properties at 200°F nearly equal to that of commercial magnesium alloys.

THE preparation and general properties of magnesium-lithium base alloys have been described in earlier papers.[1, 2] Lithium forms solid solutions with pure magnesium, lowers its density, and improves its formability. The improved isotropy and better formability of these alloys are attributed to the ability of lithium to convert the magnesium lattice from hexagonal (alpha phase) to body-centered-cubic (beta phase) structure. This change in structure is, however, accompanied by some limitations which make it difficult, if not impossible, to combine all the desirable properties in one composition. The most important of these limitations is the tendency of the high-strength alloys to overage and lose strength at temperatures of the order of 150° to 200°F.

A study was made of the effects of composition and heat treatment on the age-hardening characteristics of the alloys. Stability of properties was determined by hardness and tensile testing of the alloys at room temperature after various periods of exposure to elevated temperatures.

P. D. FROST, Member AIME, is Research Engineer, J. G. KURA is Assistant Supervisor, and L. W. EASTWOOD, Member AIME, is Supervisor, Battelle Memorial Institute, Columbus, Ohio.

AIME Chicago Meeting, October 1950.

TP 2961 E. Discussion (2 copies) may be sent to Transactions *AIME before Dec. 15, 1950. Manuscript received April 17, 1950; revision received Aug. 7, 1950.*

The work described in this paper was sponsored by the Navy Department, Bureau of Aeronautics under Contracts Nos. NOa(s) 9526 and NOa(s) 10026. The period this work covered was Jan. 1, 1949, to April 1, 1950.

Precipitation-hardening curves are shown for a number of magnesium-lithium-zinc alloys in fig. 1. All the alloys were solution treated at 700°F and aged at 200°F. The reason for using the drastic quench, toluene at —105°F, was to reduce the rapid precipitation of the hardening phase which takes place at room temperature.

Previous experience has shown that a hardness of about 90 to 95 Rockwell E is indicative of yield strengths in the range of 35,000 to 40,000 psi. This is a desirable strength level for magnesium-lithium base alloys with specific gravities of the order of 1.65 or less.

Although the hardness level is raised by large zinc contents, a corresponding decrease in the cold formability of these alloys occurs with increasing zinc content. Thus, alloys containing up to about 10 pct Zn and having hardnesses of the order of 70 to 75 Rockwell E may be bent over a very small radius; however, the 16 pct Zn alloy requires a bend radius of more than 8T.

The hardness relationships illustrated in fig. 1 can be explained by the partial phase diagram shown in fig. 2. The zinc-free magnesium-lithium alloys are entirely body-centered cubic (100 pct beta phase) when the lithium content of the binary is 10.3 pct or higher. When zinc is added, the boundary between the beta and alpha-plus-beta fields at 700°F is shifted to lower lithium contents. In addition, the solubility of zinc at 700°F decreases with decreasing lithium content. It is shown by a study of microstructures that the limit of solid solubility of zinc in the 6Mg/Li* matrix at 700°F is about 19 pct. It is believed from a study of the aging curves that this limit is about 2 to 3 pct at 200°F.

Zinc additions up to about 2 pct increase the hardness and strength of the magnesium-lithium base solid solution. Larger additions of zinc effect further hardness increases, but precipitate during prolonged aging at 200°F. Alloys having 14 to 20 pct Zn precipitation harden extremely rapidly during quenching, even when quenched in toluene at —105°F. The high-zinc alloys overage at 200°F but are capable of maintaining reasonably high hardnesses for periods up to 1000 hr.

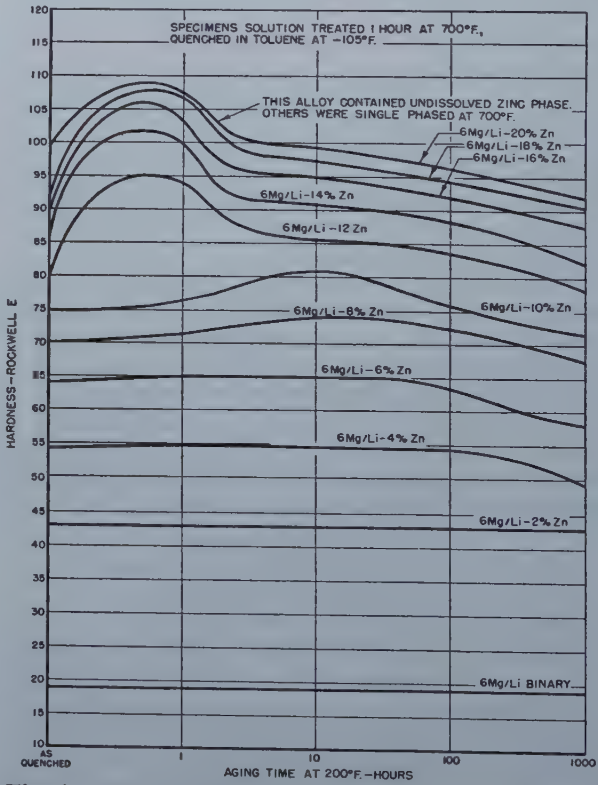

Fig. 1—Effect of zinc content and prolonged aging at 200°F on the hardness level of several 6Mg/Li-Zn ternary alloys.

---

* In composing new complex alloys, it was often desirable to maintain a constant ratio of magnesium to lithium. Thus, a 6Mg/Li binary contains 14.3 pct Li and a 6Mg/Li-19 pct Zn alloy contains 11.6 pct Li. However, in both cases the ratio of magnesium to lithium is the same.

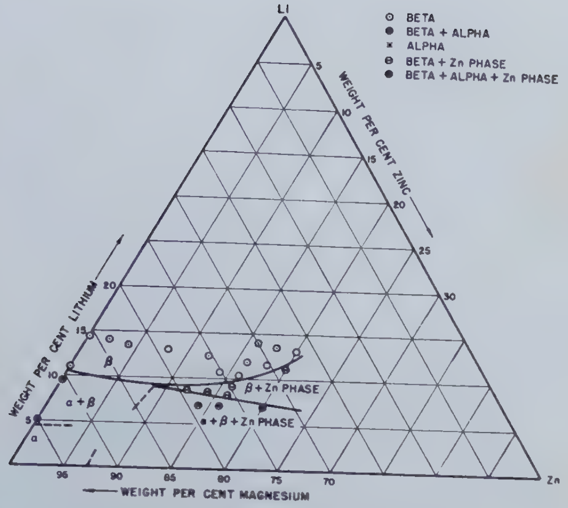

Fig. 2—Approximate phase relationship for one part of the Mg-Li-Zn ternary system at 700°F, as estimated from the microstructures of several alloys. Specimens were extruded, rolled, and solution treated for 1 hr at 700°F.

The aging curves of fig. 1 are similar, in general, to those of Mg-Li-Zn alloys having different ratios of magnesium to lithium.

Although the high-zinc ternary alloys maintain fairly high hardness and strength levels following exposure to temperatures up to 200°F, they have, in general, poorer corrosion resistance and higher densities than the magnesium-lithium-aluminum base alloys described in the following sections.

Age-Hardening Characteristics of Mg-Li-Al Alloys

Aging curves for a few magnesium-lithium-aluminum ternary alloys, solution heat treated at 700°F, are shown in fig. 3. Again, the hardness relationships shown here can in part be accounted for by the partial phase diagram shown in fig. 4.

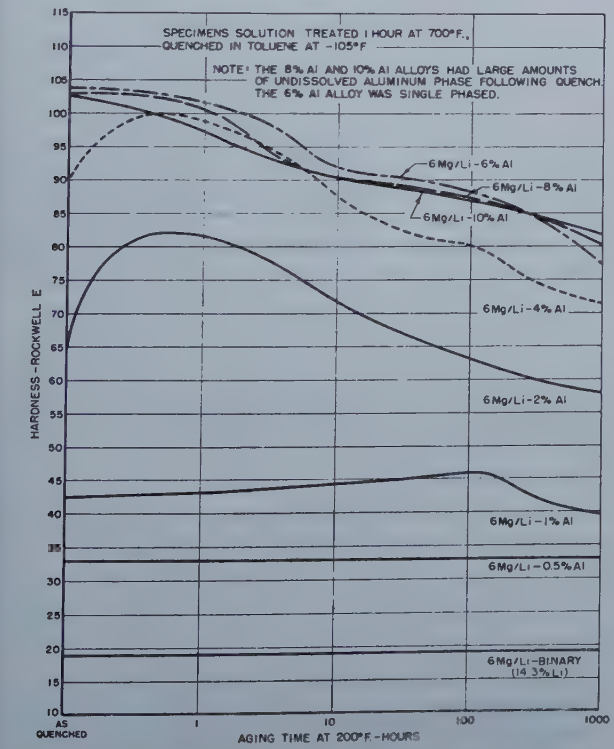

Fig. 3—Effect of aluminum content and prolonged aging at 200°F on the hardness level of several 6Mg/Li-Al ternary alloys.

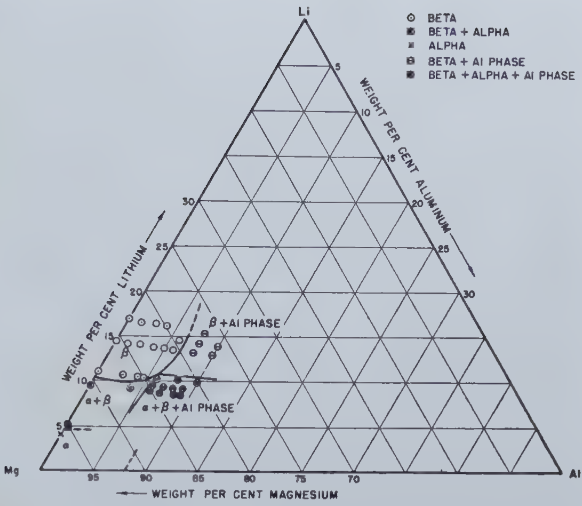

Fig. 4—Approximate phase relationship for one part of the Mg-Li-Al ternary system at 700°F, as estimated from the microstructures of several alloys. Specimens were extruded, rolled and solution treated for 1 hr at 700°F.

The solid solubility of aluminum in the magnesium-lithium matrix at 700°F is less than that of zinc, and unlike zinc, the addition of aluminum shifts the boundary between the beta and alpha-beta fields toward higher lithium contents. The occurrence of aging at 200°F indicates the limit of solid solubility of the aluminum phase at 200°F to be less than 1 or 1.5 pct in 5Mg/Li, 6Mg/Li, and 8.1Mg/Li base alloys. Aluminum is a more potent hardener than zinc on a weight percent basis but of the same degree on an atomic percent basis. Like zinc, aluminum in sufficient quantities produces alloys which age rapidly and have high as-quenched hardnesses. The maximum hardness of the alloys occurs in the as-quenched condition when the aluminum content is slightly above 8 pct in the 5Mg/Li base, less than 6 pct in the 6Mg/Li base, and less than 4 pct in the 8.1Mg/Li base. Because of the rapid precipitation of the hardening constituent, these high as-quenched hardnesses cannot be suppressed even when the alloys are quenched from 700°F into toluene at —105°F. The low-lithium, high-aluminum alloys have higher hardnesses after aging 1000 hr at 200°F than do the higher lithium alloys. There is little benefit gained by increasing the aluminum content above 6 pct. Apparently, the reason for this is that 6 pct Al is close to the limit of solid solubility at 700°F, as illustrated by fig. 4.

Cubic alloys, such as those whose aging curves are shown in fig. 3, are not so stable at 200°F as alloys having a predominately hexagonal structure. In fig. 5, the 5Mg/Li-8 pct Al alloy, which contains body-centered-cubic beta phase plus undissolved aluminum-rich phase at 700°F, changes greatly in hardness over the 1000-hr aging period at 200°F. The 6Mg/Li-8 pct Al alloy, which also contains body-centered-cubic beta plus undissolved aluminum-rich phase at 700°F, has a somewhat flatter curve. However, the 9.5Mg/Li-8 pct Al alloy, which contains beta phase, a large amount of hexagonal alpha phase, and a small amount of undissolved aluminum-rich phase, shows little variation in hardness during the aging period.

The effect of quenching medium on the age-hardening characteristics of the alloys was studied. A low-temperature quench bath, such as toluene at —105°F, retards precipitation hardening in alloys of intermediate hardness, but has no effect on the as-quenched hardnesses of the very soft and the very hard alloys. Precipitation, if any, occurs so slowly in the soft alloys that the drastic quench is not necessary. On the other hand, precipitation is so rapid in alloys containing comparatively large quantities of aluminum or zinc that the low temperature of the toluene-quench bath does not arrest it. This was also found to be true even when specimens were quenched first in toluene at −105°F, immediately transferred to a liquid nitrogen bath, and held in this bath until a hardness measurement could be obtained.

Some additional phase relationships in the magnesium-lithium-aluminum system are shown in fig. 6. This figure was photographed from a publication by Shamrai.[3] In an earlier paper,[1] the hardening agent in magnesium-lithium base alloys was tentatively established as $MgLi_2X$, where X may be zinc, aluminum, or certain other elements. The only three-component phase reported by Shamrai is Phase X, which he identified as Al_2MgLi. He stated that his diagrams were not to be considered final, and indicated that additional three-component phases may be present in the vicinity of the Al_2MgLi region. A few attempts to produce Al_2MgLi have been made in order to check Shamrai's observations. X-ray diffraction studies of one alloy containing 47 atomic pct Al, 24.5 atomic pct Mg, and 28.5 atomic pct Li revealed the presence of a large amount of an unknown phase and a small amount of $MgLi_2Al$. It is quite possible that the unknown phase corresponds to the compound Al_2MgLi mentioned by Shamrai.

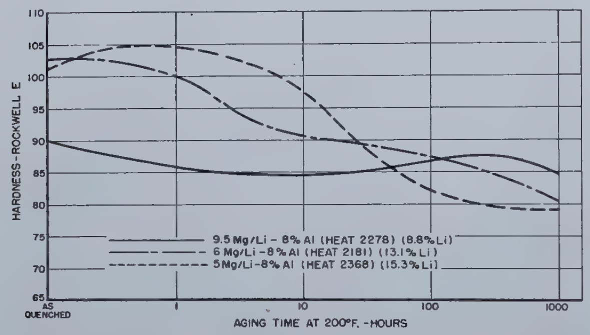

Fig. 5—Effect of lithium content on the hardness levels of several Mg-Li-8 pct Al alloys.

Aging Characteristics of Complex Mg-Li-Al Base Alloys

The magnesium-lithium-aluminum base alloys which contain sufficient lithium to render them body-centered cubic are of interest because of their extremely low density and good tensile properties. For example, in one condition of heat treatment, the 6Mg/Li-6 pct Al alloy has tensile properties as shown in table I. These properties were obtained on forged and rolled ⅜-in. plate, solution treated at 500°F, and aged ¾ hr at 200°F.

This alloy has a specific gravity of 1.44.

A concerted effort was made to improve the stability of properties of these all-beta magnesium-lithium-aluminum base alloys, but this effort was not successful. The effect of minor additions of slightly soluble elements was studied quite thoroughly. Fig. 7 is indicative of the results obtained in this study. In the particular experiment depicted by fig. 7, complex alloys containing 0.05 or 0.10 pct of each of the alloying elements listed in the caption were studied. The compositional design embraced 27 alloys. The heavy dark line in fig. 7 is the aging curve of the 6Mg/Li-6 pct Al base alloy at 200°F. The shaded area covers the range in which the hardnesses of the remaining alloys fell.

Table I. Tensile Properties of the 6Mg/Li-6 Pct Al Alloy

Direction of Tests	Tensile Yield Strength, psi	Tensile Ultimate Strength, psi	Elongation in 1 In., Pct
Longitudinal	37,000	40,800	10
Transverse	38,400	42,300	2

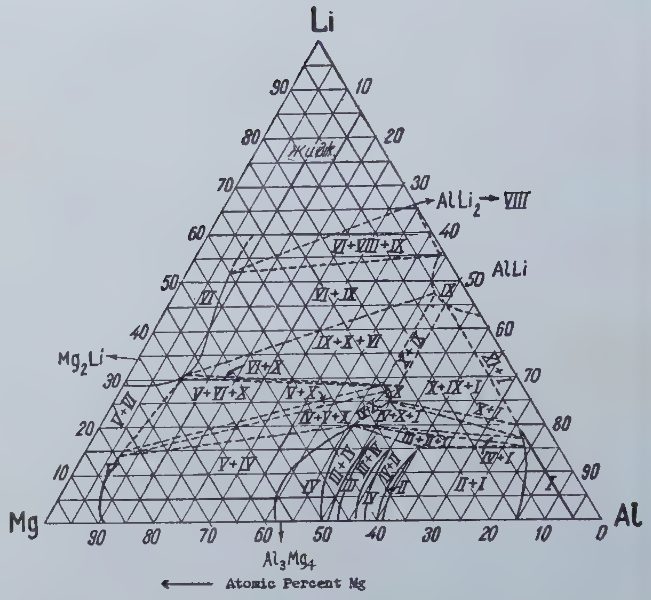

Fig. 6—Isothermal section at 400°C (752°F) through the constitution diagram of the system Al-Mg-Li.

The Li corner of the diagram is liquid. The phases shown are as follows: I—Solid solution of Li and Mg in Al. II—Al_3Mg_2. III—AlMg. IV—Al_3Mg_4. V—Hexagonal solid solution of Al and Li in Mg. VI—Mg_2Li. VIII—$AlLi_2$. IX—AlLi. X—Al_2MgLi. Figure reproduced from ref. 3.

A similar effect was observed for all other slightly soluble elements investigated. These included Fe, Co, Ni, Mn, Cr, Ti, Zr, Sb, Bi, Ce, V, and Be.

The only elements which improve the hardness stability of the 6Mg/Li-6 pct Al base alloy are those which, like aluminum and zinc, are relatively soluble at elevated temperatures in the magnesium-lithium base. Such elements include silver, cadmium, and mercury. Comparatively large quantities of these elements are required to raise the hardness

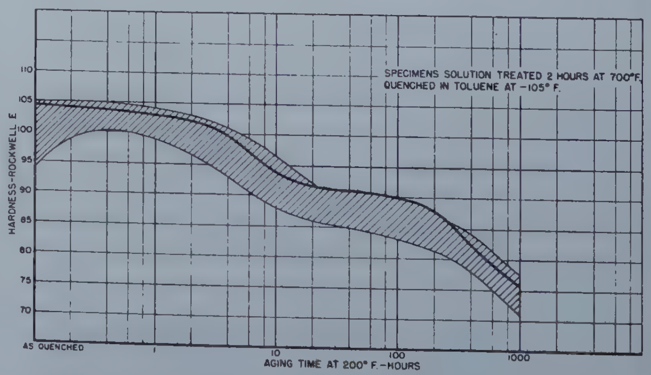

Fig. 7—Aging characteristics at 200°F of a series of 6Mg/Li-6 pct Al-Cu-Ca-Sr-Ba-Si-Sn-Pb alloys. Shaded area represents hardness range covered by individual aging curves for 27 alloys. Heavy curve is for the 6Mg/Li-6 pct Al base alloy.

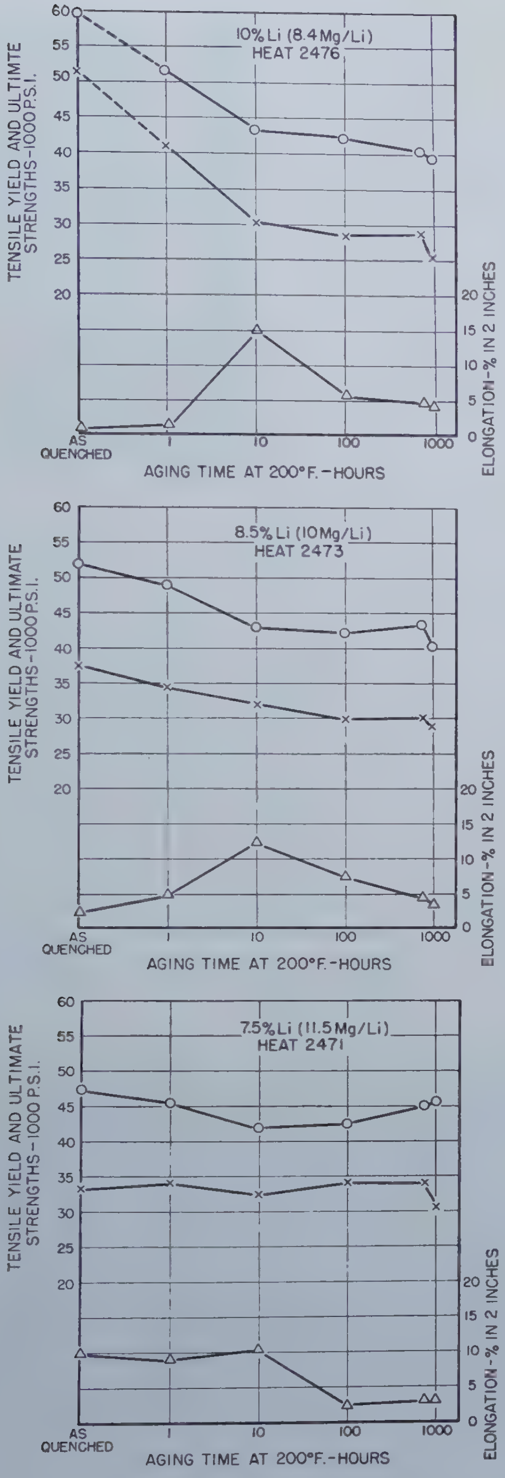

Fig. 8—Effect of lithium content on the tensile properties and stability of Mg alloys containing 6.5 pct Al. Specimens were water quenched from 800°F.

level of the base alloy at the end of 1000 hr at 200°F. For example, an alloy containing 6Mg/Li-6 pct Al-5 pct Ag has a hardness of 86 Rockwell E at the end of 1000 hr, as compared with 74 to 76 for the 6Mg/Li-6 pct Al alloy. It might be added that indium and thallium, like silver and cadmium, are also beneficial and have high solid solubility in the magnesium-lithium base. Because such large quantities of these expensive, heavy elements are necessary to produce the desired effects, they do not form alloys of much practical interest.

Because the previously described methods of producing a satisfactory all-beta magnesium-lithium-aluminum base alloy were unsuccessful, attention was turned to alloys containing both hexagonal and body-centered-cubic phases. The fair stability of these alloys was illustrated by the aging curve for the 9.5Mg/Li-8 pct Al alloy, shown in fig. 5.

Some mechanical properties and other data on the more stable magnesium-lithium-aluminum base alloys will be described in the following pages. Fig. 8 shows the effect of lithium content on the tensile properties of a magnesium-lithium-aluminum ternary alloy containing 6.5 pct Al. It also shows the effect produced on the properties by aging at 200°F. All the alloys shown in this figure contain some alpha phase. Heat 2476, containing 10 pct Li, is on the boundary between the beta and the alpha-beta region. The other alloys contain increasingly greater quantities of hexagonal metal because of their lower lithium contents. It will be noticed that the highest yield and tensile strengths were obtained in the alloys containing the largest amounts of lithium. Some liberty was taken in extrapolating the strength values of Heat 2476 in the quenched condition. This alloy was too brittle in this condition to obtain yield and tensile data. Values as high as those shown are not, however, uncommon in the magnesium-lithium alloy system.

Additions of tin to a magnesium-lithium-aluminum base containing 9.5Mg/Li-7 pct Al were found to increase the strength, and improve the stability at 200°F, and the resistance to stress-corrosion cracking. The tensile properties and stability of the 9.5Mg/Li-7 pct Al-1 pct Sn alloy are shown in fig. 9.

The microstructure of the 9.5Mg/Li-7 pct Al-1 pct Sn alloy is compared with that of the same base alloy without tin in fig. 10. These alloys are characterized by a two-phase matrix consisting of body-centered cubic beta and hexagonal-alpha structures. The tin-bearing alloys usually contain a small amount of the undissolved tin-rich phase, which, in the micrograph, fig. 10, appears as small black particles. Upon aging at 200°F, a very fine, lamellar precipitate, shown in fig. 11, appears in the white alpha regions of these alloys. The presence of tin causes the formation of larger quantities of this precipitate than normally occur in the magnesium-lithium-aluminum ternary alloy.

In alloys having tin contents of about 0.5 pct or under, additions of manganese markedly improve the tensile ductility, as shown in table II. The specimens referred to in this table were produced from 0.064-in. extruded and rolled strip. They were

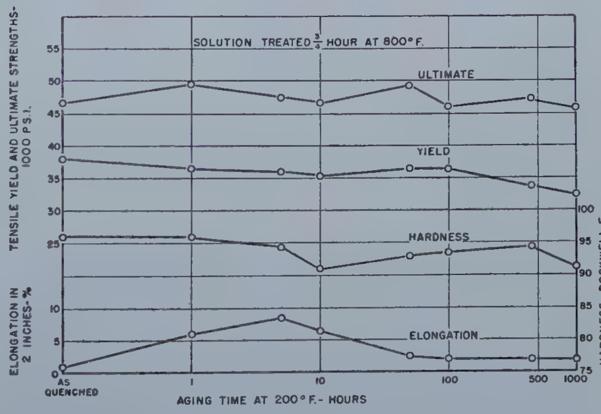

Fig. 9—Effect of aging at 200°F on properties of forged and rolled 0.065-in. sheet of the 9.5Mg/Li-7 pct Al-1 pct Sn alloy following 800°F solution treatment (Heat 2467).

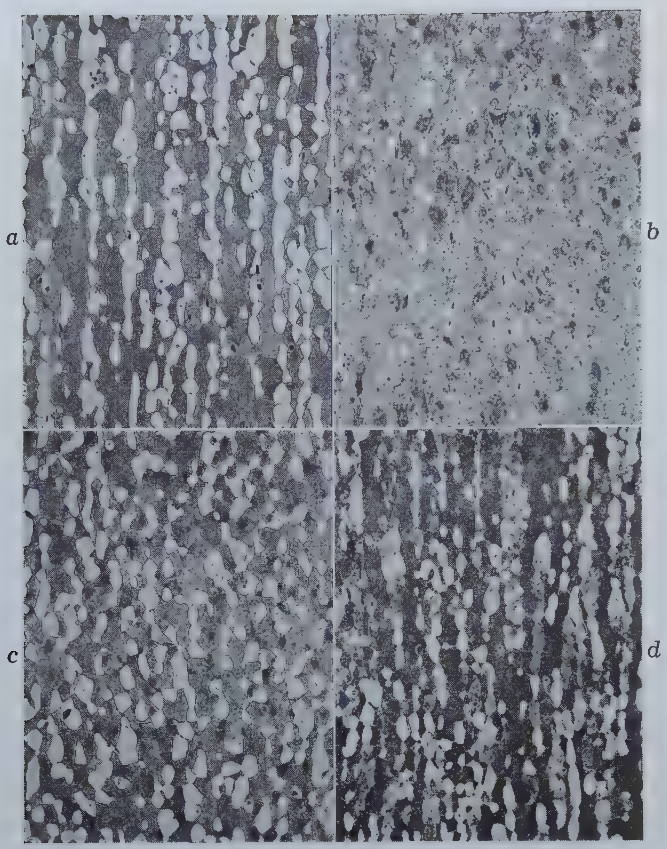

Fig. 10—Microstructure of alloys.

a. The 9.5Mg/Li-7 pct Al-1 pct Sn alloy, as quenched from 800°F. Gray background is b.c.c. beta solid solution. White phase is hexagonal alpha solid solution. Black particles are undissolved tin-rich phase. *b.* Same alloy, aged 1000 hr at 200°F. Alpha phase is largely obscured by a fine lamellar precipitate believed harmful to ductility. *c.* The 9.5Mg/Li-7 pct Al ternary alloy, as quenched from 800°F. *d.* Same alloy, aged 1000 hr at 200°F. Note that a smaller quantity of lamellar precipitate is present in *d* than *b.* (All specimens etched in 2 pct HF.) X100.

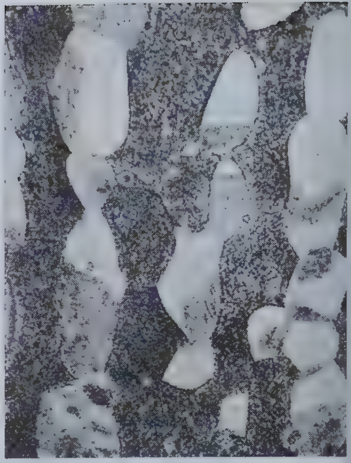

Fig. 11—Same structure as shown in fig. 10*d*. Shows more clearly the lamellar nature of the precipitate in the alpha phase. Note also the fine unresolved precipitate in beta phase. X500.

solution treated ¾ hr at 800°F, water quenched, and aged 20 hr at 200°F.

The same improvement is not effected in the higher-tin alloys, and in the latter case manganese additions have an adverse influence upon the stability of the properties of the alloy.

Zinc, added to the alpha-beta magnesium-lithium-aluminum base alloys, with or without manganese, produces interesting tensile properties. Some of the best combinations of tensile properties and stability are found in alloys having a ratio of Mg/Li = 9. A few examples are given in table III. These properties were obtained on rolled 0.064-in. sheet, quenched from 800°F and aged at 200°F.

In order to maintain a yield strength above 30,000 psi for 1000 hr at 200°F, substantial quantities of zinc are required, and this is a disadvantage from the standpoint of weight. Thus, the specific gravity of the 9Mg/Li-5 pct Al-8 pct Zn alloy is 1.65, while that of the 9.5Mg/Li-7 pct Al-1 pct Sn alloy is only 1.56.†

Resistance to Stress-Corrosion Cracking: Some of the alloys described above were subjected to a stress-corrosion test in an industrial atmosphere. The type of fixture used is shown in fig. 12. Sheet specimens 0.065 in. thick were subjected to a bending load which imposed a tensile stress in the outer fiber equal to 30 or 75 pct of the yield strength of the material. Control specimens of AZ31X-h sheet (Mg-3 pct Al, 1 pct Zn, 0.3 pct Mn alloy, hard rolled) were used. The results are shown in table IV.

Although the results given in table IV do not represent many tests, there is an indication that these particular magnesium-lithium base alloys may have resistance to stress-corrosion cracking nearly equal to that of the commercial alloy, AZ31X-h.

Formability: Although many high-strength body-centered-cubic magnesium-lithium base alloys have good formability, the heat-treated alpha-beta alloys described above require large radii for forming at room temperature. However, in the hot-rolled condition the bend test results shown in table V were obtained on sheet specimens ½ in. wide x 0.064 in. thick.

Annealing the alloys does not improve their formability. However, they are amenable to warm forming, as may be seen from table VI.

Both alloys suffer a loss in tensile strength during the warm-forming heat treatments. Results of a few tests are shown in table VII.

The alpha-beta type alloys are easily hammer-and-press forged directly from the cast condition at 600° to 700°F. Their optimum hot-rolling temperature is about 700°F and their optimum extruding temperature is 600° to 650°F.

Conclusions

As shown in the preceding pages, two of the most promising types of high-strength magnesium-

Table II. Effect of Manganese on Tensile Ductility of a Mg-Li-Al-Sn Alloy

Intended Composition	Tensile Yield Strength, psi	Tensile Ultimate Strength, psi	Elongation in 2 In., Pct
9.5Mg/Li-7 pct Al-0.05 pct Sn	31,900	43,500	4
9.5Mg/Li-7 pct Al-0.05 pct Sn-1 pct Mn	32,800	43,300	9.5

Table III. Tensile Properties of Several Mg-Li-Al-Zn Alloys

Intended Composition	Aging Time, Hr	Yield Strength, psi	Ultimate Strength, psi	Elongation in 2 In., Pct
9Mg/Li-7 pct Al-8 pct Zn-1 pct Mn	20	36,900	52,900	4
9Mg/Li-7 pct Al-8 pct Zn-1 pct Mn	1,000	34,400	49,500	1.5
9Mg/Li-5 pct Al-8 pct Zn	20	36,700	54,100	6.5
9Mg/Li-5 pct Al-8 pct Zn	1,000	31,500	48,500	2.5
9Mg/Li-5 pct Al-8 pct Zn-1 pct Mn	20	35,200	52,800	9
9Mg/Li-5 pct Al-8 pct Zn-1 pct Mn	1,000	30,400	45,500	2.5
9Mg/Li-6 pct Al-6 pct Zn-1 pct Mn	20	35,100	51,900	7
9Mg/Li-6 pct Al-6 pct Zn-1 pct Mn	1,000	29,700	46,100	3

---

† The specific gravity of commercial AZ31X is 1.77.

Table IV. Resistance of Several Alloys to Stress Corrosion Cracking in an Industrial Atmosphere*

Material	No. of Specimens	Applied Stress		Avg. No. of Days Before Failure	Starting Date
		Pct Yield	psi		
9.5Mg/Li-7 pct Al-3 pct Sn	3	75	28,400	46	(Started 10-26-49)
9.5Mg/Li-7 pct Al-3 pct Sn	3	30	11,300	No failures	(Started 10-26-49)
AZ31X-h	2	75	24,900	55	(Started 10-26-49)
AZ31X-h	2	30	9,960	No failures	(Started 10-26-49)
9.5Mg/Li-7 pct Al-1 pct Sn	6	75	26,300	27	(Started 3-16-50)
9.5Mg/Li-7 pct Al	6	75	25,900	13	(Started 3-16-50)
AZ31X-h	6	75	24,900	52	(Started 3-16-50)
9Mg/Li-5 pct Al-8 pct Zn	6	75	27,500	54	(Started 5-27-50)
AZ31X-h	6	75	24,900	63	(Started 5-27-50)

* The magnesium-lithium base alloys were quenched from 800°F and aged 20 hr at 200°F.
The AZ31X-h was exposed in the as-received (hard rolled) condition.

Table V. Minimum Bend Radii Required for Hot-Rolled Alloys

Alloy	Minimum Bend Radius	Hardness, Rockwell E
9.5Mg/Li-7 pct Al-1 pct Sn	5-7T	80-82.5
9Mg/Li-5 pct Al-8 pct Zn	10T	88

lithium base alloys at the present time are as follows:

1. 9.5Mg/Li-7 pct Al-Sn
2. 9Mg/Li-Al-Zn

These alloys are fairly satisfactory from the standpoints of material cost and stability at 200°F. Preliminary data indicate that they also possess fair resistance to corrosion. Alloys of this type are somewhat more notch sensitive than existing magnesium-base alloys and may require improvement in this respect. They might also be improved with respect to room-temperature formability. However, they are amenable to warm forming.

Ingots of these alloys are easily hammer-and-press forged at 600° to 700°F. They can also be rolled and extruded at these temperatures.

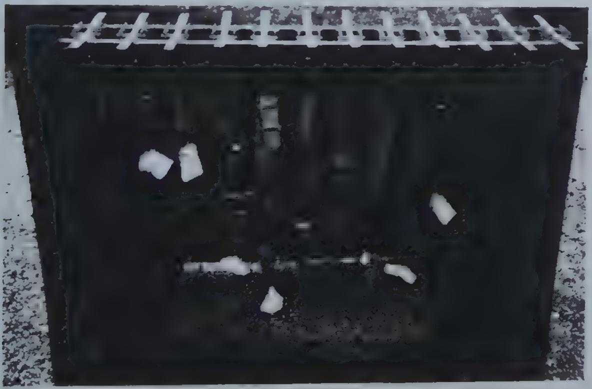

Fig. 12—Stress-corrosion fixture used in testing the 9.5Mg/Li-7 pct Al-3 pct Sn alloy.

Specimens 0.065 in. thick were subjected to a bending load equal to 75 pct of their yield strength. Exposure medium: industrial atmosphere. The weights are normally covered by a panel.

Table VI. Minimum Bend Radii Required for Warm Forming of Alloys

Alloy	Forming Temp, °F	Minimum Bend Radius
9.5Mg/Li-7 pct Al-1 pct Sn	450	1-2T
	500	1T
9Mg/Li-5 pct Al-8 pct Zn	300	2-3T
	350	1-2T
	450	1T

Table VII. Effect of Warm-Forming Temperatures on Tensile Properties of Alloys

Alloy	Condition	Yield Strength, psi	Ultimate Strength, psi	Elongation in 2 In., Pct
9.5Mg/Li-7 pct Al-1 pct Sn	As aged 10 hr at 200°F	35,500	47,000	7
9.5Mg/Li-7 pct Al-1 pct Sn	Formed at 450°F	28,400	42,700	5
9Mg/Li-5 pct Al-8 pct Zn	As aged 20 hr at 200°F	36,700	54,100	6.5
9Mg/Li-5 pct Al-8 pct Zn	Formed at 350°F	34,200	45,000	1

Acknowledgment

The authors are indebted to the Navy Department, Bureau of Aeronautics, for permission to publish this paper, and to N. E. Promisel and H. J. Boertzel of that bureau for their supervision of the project. They are also grateful to C. H. Lorig and other members of the Battelle staff who assisted in the planning and conducting of the work.

References

[1] J. H. Jackson, P. D. Frost, A. C. Loonam, L. W. Eastwood, and C. H. Lorig: Magnesium-Lithium Base Alloys—Preparation, Fabrication, and General Characteristics. *Trans.* AIME **185**, 149-168; *Journal of Metals* (Feb. 1949) TP 2534E.

[2] P. D. Frost, J. H. Jackson, A. C. Loonam, and C. H. Lorig: The Effect of Sodium Contamination on Magnesium-Lithium Base Alloys. *Trans.* AIME **188**, 1171-1172; *Journal of Metals* (Sept. 1950) TP 2923E.

[3] F. L. Shamrai: The Ternary System Aluminum-Magnesium-Lithium. *Bulletin* of the Academy of Sciences of the U.S.S.R., Section of Chemical Sciences, Part I, No. 6 (1947), 605-616; Part II, No. 1 (1948), 83-94; Part III, No. 3 (1948), 290-301.

Technical Notes

Activity of Liquid Silver-Silicon Alloys

by H. M. Schadel, Jr., G. Derge, and C. E. Birchenall

EXISTING distribution data[1] for silicon between liquid iron and silver at steelmaking temperatures, 1500° to 1600°C, has made activity relationships in liquid silver-silicon alloys desirable as a method of determining the silicon activity in molten iron.

To this end, through the use of radioactive Ag^{110} and the molecular beam technique described in a previous paper,[2] the vapor pressure of silver as a function of temperature has been measured over three silver-silicon alloys containing 3.9, 9.3, and 15.4 atomic pct (eutectic composition) silicon. The technique was that described for pure silver with the exception that a porcelain liner was used inside the tantalum oven. A preliminary rerun of pure silver in the porcelain gave excellent agreement with the vapor pressure curve established by the earlier work.

A sample curve of the data obtained for the vapor pressure of silver in the 15.4 atomic pct silicon alloy is given in fig. 1*a*. The pressure for silver in an ideal solution of this same composition is also shown. Similar curves were obtained for the 3.9 and 9.3 atomic pct alloys. Fig. 1*b* shows smoothed curves of the activity coefficients referred to pure liquid silver for three arbitrary temperatures within the range of this investigation. For the compositions used, as dictated by the equilibrium diagram,[3] the experimental error is appreciable compared with the deviations from ideality. This is especially so for the more dilute alloys at the higher temperatures. It is to be noted that the positive deviations indicate an appreciable solid solubility of silicon in silver contrary to the silver-silicon phase diagram reported by Hansen.

H. M. SCHADEL, JR., G. DERGE, Member AIME, and C. E. BIRCHENALL, Junior Member AIME, are associated with the Metals Research Laboratory, Carnegie Institute of Technology, Pittsburgh, Pa.

TN 45 E. Manuscript received Aug. 29, 1950.

This work was done by the Metals Research Laboratory, Carnegie Institute of Technology, under the sponsorship of the Office of Naval Research.

From the data presented, it is evident that the deviations from ideality will be negligibly small for the distribution studies made at 1500° to 1600°C with the silicon concentration in silver always less than 5 atomic pct.

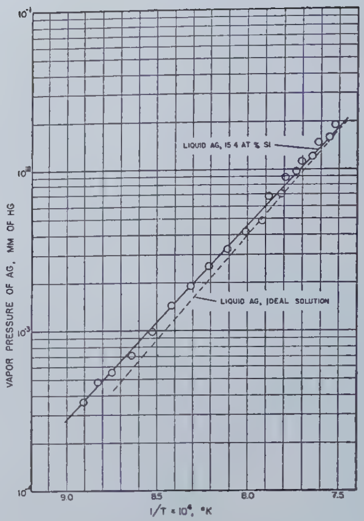

Fig. 1*a*—Curve for vapor pressure of silver in 15.4 atomic pct silicon alloy.

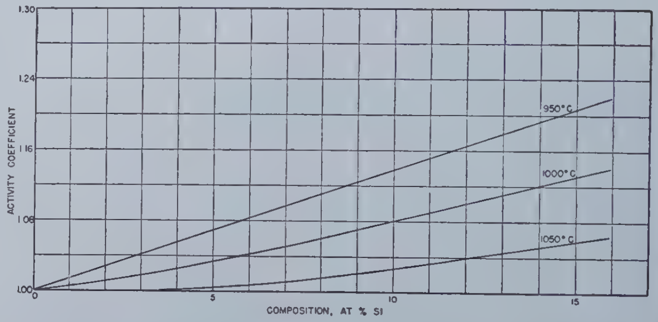

Fig. 1*b*—Smoothed curves for activity coefficients of silver.

References

[1] Y. H. Chou: Distribution of Certain Alloying Elements between Liquid Iron and Silver. Doctorate Thesis, Department of Metallurgy, Carnegie Institute of Technology, 1947.

[2] H. M. Schadel, Jr., and C. E. Birchenall: The Vapor Pressure of Silver. *Trans.* AIME, **188**, 1134; *Journal of Metals* (Sept. 1950) TP 2911E.

[3] M. Hansen: Der Aufbau der Zweistofflegierungen. 1936. Berlin. J. Springer.

Crystallography of the Sigma Phase

by Paul Pietrokowsky and Pol Duwez

RECENTLY a comprehensive investigation of the various sigma binary alloys was published by Duwez and Baen.[1] It was shown that the following conditions are necessary for the formation of the sigma phase: (1) the difference in atomic diameters of the two alloying metals must not be more than about 8 pct; (2) of the two elements which form sigma, one must exhibit a body-centered cubic structure while the second metal must be face-centered cubic, at least in one of its allotropic forms. In addition, a tetragonal unit cell was proposed and powder patterns of six sigma phases were indexed for *d* spacings greater than 1.640 *kx*. Since the indexing, based on tetragonal symmetry, led to only fair agreement, the possibility of sigma being orthorhombic was investigated. Various methods for indexing orthorhombic powder patterns are described in the literature.[2] The method used in this investigation was a graphical examination of the differences in values of $\sin^2 \theta$ for the adjacent lines of the powder diffraction pattern. This method led to a complete indexing of the Cr-Co (60-40) pattern. Because of the strong similarity between the various sigma alloys, it was then possible to assign indexes to the patterns of Fe-Cr (50-50), Fe-Cr-Mo (30-30-40), Fe-V (50-50), Co-V (50-50), and Ni-V (50-50).

PAUL PIETROKOWSKY, Junior Member AIME, is Research Engineer, California Institute of Technology, and POL DUWEZ, Member AIME, is Associate Professor of Mechanical Engineering, California Institute of Technology, Pasadena, Calif.

TN 43 E. Manuscript received July 31, 1950.

The values of $\sin^2 \theta$ and indexes of the six sigma alloys, together with visually estimated intensities, are presented in table I. In general, the similitude between the six patterns is quite good. For spacings greater than 1.75 *kx* a few differences are noticeable. In the Ni-V pattern, no (320) exists and the two strong lines (030) and (031) are separated by only two lines of lower intensity, unlike any of the other sigma patterns. However, very little is known about the Ni-V phase diagram and it is possible that the equal atomic percentage composition in this system lies in a two-phase region. At lower spacings there is a close analogy between the patterns. The planes

Table I. Orthorhombic Indexing of Various Sigma Alloys

hkl	Cr-Co		Fe-Cr-Mo		Fe-Cr		Fe-V		Co-V		Ni-V	
	$\sin^2 \theta$, Observed	$\sin^2 \theta$, Calculated	$\sin^2 \theta$, Observed	$\sin^2 \theta$, Calculated	$\sin^2 \theta$, Observed	$\sin^2 \theta$, Calculated	$\sin^2 \theta$, Observed	$\sin^2 \theta$, Calculated	$\sin^2 \theta$, Observed	$\sin^2 \theta$, Calculated	$\sin^2 \theta$, Observed	$\sin^2 \theta$, Calculated
011	0.0814 vw	0.0842					0.0812 vw	0.0793	0.0788 w	0.0802	0.0777 vw	0.0786
111	0.1001 vw	0.1014					0.0943 vvw	0.0962	0.0964 vw	0.0956	0.0949 vvw	0.0960
210									0.1060 vvw	0.1024		
310	0.1916 vw	0.1885	0.1751 vw	0.1751								
201									0.1274 vw	0.1162	0.1199 w	0.1150
002			0.1845 vw	0.1844							0.1790 vw	0.1816
102					0.2088 vw	0.2118						
012	0.2343 w	0.2357	0.2156 m	0.2155	0.2344 vw	0.2282			0.2364 vvw	0.2212		
020							0.1259 vvw	0.1304	0.1358 vvw	0.1328	0.1341 w	0.1328
211									0.1441 vvw	0.1494	0.1480 vw	0.1482
120							0.1480 vvw	0.1473			0.1541 w	0.1502
300									0.1563 vvw	0.1557	0.1563 vw	0.1566
221	0.2556 w	0.2541	0.2324 m	0.2345	0.2533 m	0.2534	0.2446 w	0.2446	0.2489 m	0.2490	0.2446 m	0.2478
202	0.2697 vw	0.2708	0.2425 w	0.2485	0.2649 vw	0.2640						
400	0.2824 vw	0.2752	0.2556 w	0.2560	0.2798 vw	0.2784					0.2797 m	0.2784
320	0.2893 s	0.2896	0.2661 s	0.2684	0.2891 s	0.2918	0.2811 s	0.2825	0.2850 s	0.2885		
030	0.3070 m	0.3089	0.2811 m	0.2799	0.3061 m	0.3042	0.2932 m	0.2934	0.3017 m	0.2988	0.2989 s	0.2988
130	0.3231 m	0.3205	0.2954 m	0.2959	0.3202 m	0.3216	0.3106 m	0.3103	0.3167 m	0.3161	0.3106 vw	0.3162
321	0.3405 m	0.3401	0.3112 m	0.3145	0.3374 m	0.3404	0.3270 m	0.3292	0.3336 m	0.3305	0.3264 m	0.3348
031	0.3534 s	0.3538	0.3237 s	0.3260	0.3523 s	0.3528	0.3394 s	0.3401	0.3468 s	0.3458	0.3401 s	0.3442
131	0.3701 m	0.3710	0.3398 m	0.3420	0.3697 m	0.3702	0.3563 m	0.3570	0.3635 m	0.3631	0.3533 vw	0.3516
312	0.3911 w	0.3905	0.3567 m	0.3595	0.3885 w	0.3848	0.3756 w	0.3715	0.3830 w	0.3769	0.3777 vw	0.3714
231	0.4253 w	0.4226	0.3889 w	0.3900	0.4228 w	0.4224	0.4083 w	0.4077	0.4171 w	0.4150	0.4097 vw	0.4138
402	0.4766 vw	0.4752			0.4720 vw	0.4728	0.4597 vw	0.4572			0.4586 vvw	0.4600
113	0.5055 vw	0.5054									0.4586 vvw	0.4542
420									0.4647 vw	0.4648		
601			0.6260 m	0.6221								
322	0.4895 vw	0.4916			0.4871 vw	0.4862	0.4709 vw	0.4693	0.4794 vw	0.4765	0.4725 vvw	0.4694
203					0.5048 vw	0.5070	0.4876 vw	0.4879	0.4967 vw	0.4922	0.4725 vvw	0.4702
213	0.5584 w	0.5564										
140	0.5584 w	0.5564										
041	0.5895 w	0.5897										
431					0.6356 vw	0.6312						
332					0.6501 vw	0.6552						
340	0.6955 vw	0.6940	0.6383 m	0.6416	0.6914 vw	0.6974						
611	0.7131 w	0.7034	0.6584 w	0.6532								
521	0.7173 vw	0.7153							0.6191 vw	0.6123		
341	0.7458 w	0.7445	0.6805 m	0.6877	0.7424 vw	0.7460	0.7205 w	0.7204	0.7314 vw	0.7339		
323	0.7458 w	0.7441	0.6805 m	0.6833	0.7194 w	0.7292						
133	0.7736 vw	0.7750	0.7173 vw	0.7108								
531	0.7881 vw	0.7838										
004					0.7760 m	0.7776						
233	0.8306 m	0.8266	0.7623 m	0.7588								
621	0.7992 vw	0.8045			0.7980 vw	0.8102			0.7992 vw	0.8026	0.8055 w	0.8046
602	0.8306 m	0.8266			0.8264 vw	0.8208	0.8019 m	0.7952	0.8158 vw	0.8108	0.8055 w	0.8080
050	0.8481 w	0.8425	0.7770 w	0.7775	0.8455 m	0.8450	0.8183 w	0.8150			0.8301 w	0.8300
700	0.8481 w	0.8428			0.8529 vw	0.8526						
204							0.8183 w	0.8148			0.7930 m	0.7960
423					0.8529 vw	0.8510					0.8196 m	0.8148
150	0.8601 m	0.8597	0.7876 m	0.7935	0.8628 m	0.8624	0.8314 w	0.8319	0.8435 vw	0.8473	0.8475 w	0.8474
710	0.8601 m	0.8600					0.8669 w	0.8607	0.8828 vw	0.8809	0.8842 w	0.8858
214							0.8462 w	0.8474				
441	0.8646 w	0.8649	0.8052 w	0.7997	0.8699 w	0.8678			0.8586 vw	0.8550		
423	0.8646 w	0.8645										
204	0.8770 m	0.8768										
342	0.8988 m	0.8960	0.8269 m	0.8260			0.8669 w	0.8605				
333	0.9118 m	0.9126	0.8372 w	0.8388	0.8960 m	0.8982	0.8669 w	0.8658				
024			0.8372 w	0.8388	0.9077 m	0.9128	0.8798 vw	0.8776	0.8828 vw	0.8848		
630			0.8522 vw	0.8559	0.9275 m	0.9306						
205									0.8974 vw	0.8993		
250											0.9019 vvw	0.8990
532	0.9326 m	0.9353	0.8682 vw	0.8643			0.9004 vw	0.9027	0.9157 vw	0.9193		
603											0.9233 w	0.9252
711			0.8682 vw	0.8612	0.9485 w	0.9350	0.9157 vw	0.9074	0.9328 vw	0.9279	0.9328 w	0.9312
622	0.9495 m	0.9460	0.8850 w	0.8848	0.9580 w	0.9560	0.9279 vw	0.9293	0.9438 vw	0.9436		
304	0.9624 m	0.9628	0.8850 w	0.8816			0.9004 vw	0.8993				
251	0.9624 m	0.9618					0.9279 vw	0.9293	0.9438 vw	0.9462		

s = strong, m = medium, w = weak, vw = very weak, vvw = very, very weak.

(341), (050), (150), (441), (711), and (622) appear to be common to most of the alloys. It is also apparent from the data given in table I that the patterns of the three vanadium alloys, which are very similar to each other, have rather definite deviations from the patterns of the three other compounds. Further work on the structure of the sigma phase may uncover the reasons for the observed discrepancies.

On the basis of the information in table I, the dimensions of the unit cell of sigma in the Fe-Cr (50-50) alloy are: $a = 8.66$ *kx*, $b = 6.21$ *kx*, and $c = 5.18$ *kx* units. From this data, in which no correction for absorption has been made and taking the density $\rho = 7.600 \pm 0.005$ (ref. 1), the calculated number of atoms per unit cell is 23.82.

References

[1] Pol Duwez and S. R. Baen: X-ray Study of the Sigma Phase in Various Alloy Systems. ASTM Preprint No. 47, Fifty-third Annual Meeting, Atlantic City, June 26-30, 1950.

[2] C. S. Barrett: Structure of Metals. p. 125. 1943. New York. McGraw-Hill Book Co.

aime NEWS

Woman's Auxiliary Dinner in New York

All members of the AIME are cordially invited to attend a dinner of the New York Section of the Woman's Auxiliary, American Institute of Mining and Metallurgical Engineers, to be held on Wednesday, Oct. 25, 1950, at the Engineering Woman's Club, 2 Fifth Ave., New York City. Speaking on the subject, "Untapped Manpower: The Handicapped in Mobilization", Dr. Howard A. Rusk, Associate Editor of the New York *Times;* Professor and Chairman of the Department of Physical Medicine and Rehabilitation, New York University-Bellevue Medical Center; and Consultant in Rehabilitation to the United Nations, will discuss the rehabilitation program at the Medical Center with which he is associated. He was Director of the Army Air Force war-time rehabilitation program and received the Distinguished Service Medal for his outstanding achievements.

More than usual interest is expected in Dr. Rusk's address, since the Woman's Auxiliary has had a large share in this work since its organization at Bellevue. Dinner reservations, at $3.25 per person, will be handled by Mrs. Clifford Bowden, Jr., 2104 Albemarle Terrace, Brooklyn 26, N. Y.

Errata

Earle E. Schumacher, chief metallurgist of Bell Telephone Laboratories, Inc., will deliver the Fall Lecture of the Institute of Metals (London) during the week of Sept. 15, 1950, instead of before the British Iron and Steel Institute, as indicated on p. 1075 of the September issue of JOURNAL OF METALS.

Annual Meeting Paper Deadline

Oct. 15, 1950 is the deadline for all Institute of Metals, Extractive Metallurgy, and Iron and Steel Division papers to be preprinted for the Annual Meeting to be held in St. Louis, Feb. 19 to 22, 1951.

The size of the AIME Annual Meeting necessitates two hotels in St. Louis. Metals Branch activities will be at the Hotel Statler. Mining Branch headquarters and the banquet will be at the Hotel Jefferson.

James Draper Francis—Rand Medalist

Announcement was made at the Aug. 15 joint meeting of the Executive and Finance Committees that Howard N. Eavenson, Chairman of the Rand Foundation Award Committee, had recommended to the AIME Board of Directors that the Rand Medal for Mining Administration for 1950 be awarded to James Draper Francis of Huntington, West Virginia, Chairman of the Board of Directors of Island Creek Coal Company and Pond Creek Coal Company and various affiliates, with the following citation:

"For successfully administering coal properties for more than thirty-five years until these two companies have become one of the largest and most successful units in the coal industry; for opening and managing new properties, for improvements in marketing and business methods, for his general interest in all industrial matters, his continued interest in research and his excellent citizenship in promoting not only his own, but all other interests in his general community."

The report was accepted, and the recommendation of the Committee was approved.

Proposed for Membership—Metals Branch AIME

Total AIME membership on July 31, 1950, *was* 16,466; *in addition* 4261 *Student Associates were enrolled.*

ADMISSIONS COMMITTEE

E. C. Meagher, Chairman; Albert J. Phillips, Vice-Chairman; George B. Corless, H. P. Croft, Lloyd C. Gibson, Ivan A. Given, F. W. Hanson, T. D. Jones, P. Malozemoff, Richard D. Mollison, and John Sherman.

Institute members are urged to review this list as soon as the issue is received and immediately to wire the Secretary's office, night message collect, if objection is offered to the admission of any applicant. Details of the objection should follow by mail. The Institute desires to extend its privileges to every person to whom it can be of service but does not desire to admit persons unless they are qualified.

In the following list C/S means change of status; R, reinstatement; M, Member; J, Junior Member; AM, Associate Member; S, Student Associate.

Alabama
Sheffield—Sherwin, Ralph S., Jr. (M).

Connecticut
Derby—Stokesbury, Jr., Charles Henry (J) (C/S—S-J).
E. Hartford—Falcone, Alfred S. (J) (C/S—S-J).
New Haven—Kaveney, Thomas F. (J) (C/S—S-J).
Suffield—O'Malley, F. W. (C/S—S-J).

District of Columbia
Washington—Brotzen, Franz R. (C/S-S-J).

Florida
Gulfport—Brown, John Archibald (J) (C/S—S-J).

Illinois
Chicago—Craig, Walter F., Jr. (M). McCune, John P. (A).

Louisiana
Lafayette—Law, James W. (C/S—S-J).
New Iberia—Buckner, Gene E. (M).

Maryland
Dundalk—Jonas, Ernest A. (J) (C/S—S-J).

Massachusetts
Marblehead—Kelley, George Henderson (J) (C/S—S-J).

Michigan
Flint—Walker, Walter W. (J) (C/S—S-J).
Pontiac—Paul, Robert N. (J) (C/S—S-J).

Missouri
Kansas City—Litman, Arnold P. (J) (C/S—S-J).

New Jersey
Collingswood—Hurlebaus, Richard P. (J) (C/S—S-J).
South River—Edmunds, Edward K. (M).

New Mexico
Hurley—Gage, Walter L. (J) (C/S—S-J).

New York
Brooklyn—Corigliano, Horace J. (J) (C/S—S-J).
Hastings-on-Hudson—Brown, Darwyn I. (M).
New York—Dastur, Minu N. (M) (C/S—S-M).

Ohio
Cleveland—Cox, Cecil T. (M) (C/S—A-M).
Dayton—Stoll, Richard E. (J) (C/S—S-J).
Steubenville—Coulson, Albert C. (J) (C/S—S-J).

Oregon
Troutdale—White, Gordon E. (J).

Pennsylvania
Monaca—Doelling, Robert F. (J).
Palmerton—Hurst, Thomas L. (M).
Pittsburgh—Tisdale, Norman F., Jr. (J) (C/S—S-J).
York—Bernhardt, Hans H. (C/S—S-J).

Tennessee
Maryville—Yerger, John D., Jr. (J) (C/S—S-J).

Texas
El Paso—Cronin, John Ahearn (J) (C/S—S-J).
Houston—Shapiro, Robert Marvin (J) (C/S—S-J).

Alaska
Anchorage—Cutting, Audrey I. (A).

Brazil
Rio de Janeiro—Araujo, Luiz A. (J).

Canada
Montreal—Walsh, John Heritage (J) (C/S—S-J).
Ontario—Cupp, Calvin Robert (J) (C/S—S-J). Hay, Robert H. (M). Jarrell, John Frederick (J) (C/S—S-J). Newton, George F. (J) (C/S—S-J).

Mexico, D. F.
Bis.—Hurley, Harold Francis (M) (R,C/S—A-M).

Netherlands
Eindhoven—Rathenau, Gerhart (M).

Supplementary Reading For Metallurgists and Smelter Operators

In the publication of *Mining Engineering*, the journal serving the Mining Branch of AIME, there have appeared during 1950 several articles that may have a borderline interest to subscribers of the JOURNAL OF METALS. These articles deal mainly with the processing of metallic ores at the mine, prior to smelting and refining. However, as these processes quite often determine the required subsequent processes, metallurgists and smelting plant men are vitally concerned. The titles of such articles, the authors, the month of their appearance in *Mining Engineering*, and a brief summary of their contents are published as a guide in checking back on this information.

Measurement of Equilibrium Forces between an Air Bubble and an Attached Solid in Water, T. M. Morris

The forces acting between a small rod, one end of which was made water repellent, adhering to a much larger air bubble in water were measured. An equation is deduced, which correlates these forces and the influence of each force is discussed. The importance of the size of bubbles in a flotation cell is emphasized. January, 1950.

Developments in the Application of Activated Carbon to Cyanidation, E. H. Crabtree, Jr., V. W. Winters, and T. G. Chapman

This paper traces the experimental and pilot plant work completed by the authors since 1939 including the various methods which have been developed in applying coarse activated carbon to cyanidation. The methods and results developed by the authors in desorbing gold and silver from carbons are given and the possibilities for the re-use of the desorbed carbons are discussed. February, 1950.

Organizing and Financing Cooperative Research, Elmer R. Kaiser

Cooperative research is an established and important activity of modern business by which whole industries can advance on a broad front. The economy of jointly sponsored research as well as the limited research talent available direct attention to the advisability of projects in which a number of companies participate.

After outlining the growth of industrial research, the paper discusses one successful method for organizing and financing group research programs. A systematic procedure is advocated by which engineers and scientists can bring to management practical plans for cooperative research and development programs. March, 1950.

Development in the Use of Steel for Underground Support, F. J. Haller

The need for permanent, fireproof support indicated structural steel sets. Experience over the past six years, involving more than five miles of permanent underground openings, has proved that steel is permanent, safer and, in the long run, cheaper than either treated or untreated wood supports. Excavation is reduced, as are installation, transportation, and handling costs. A number of hazards are reduced or eliminated by the use of steel. April, 1950.

Corrosion Resistant Materials and Coatings in Trail Chemical Operations, E. A. Colls

Discusses corrosion in Trail chemical plants producing ammonia, sulphuric, nitric, and phosphoric acids, ammonium phosphates, sulphate and nitrate, together with miscellaneous allied material problems and their solution using erosion or corrosion proof materials. Conclusion, that for work of this nature, most costly material may well be cheapest in the long run. April, 1950.

Use of an Induced Nuclear Reaction for the Concentration of Beryl, A. M. Gaudin, John Dasher, James H. Pannell, and Wilfred L. Freyberger

A new sorting process for beryllium minerals is described. This depends upon emission of neutrons by gamma rays, a nuclear reaction which is specific for beryllium at the appropriate energy level. Signals given by neutrons when ore passes on a belt are changed to mechanical commands through amplifiers and other electrical equipment. April, 1950.

The Burt Filter, W. G. Woolf and A. Y. Bethune

Filtration of hot (60°C) supersaturated zinc sulphate solution (sp gr 1.540) from slimy leach residues at the electrolytic zinc plant of Sullivan Mining Co., Kellogg, Idaho, is described. Separation of liquids and solids in the finished leach is by Burt filters modified to meet conditions of high-acid, high-density process for electrolytic zinc. Operating characteristics of the Burt filter on this pulp are presented. May, 1950.

Kaolin Production and Treatment in the South, Paul M. Tyler

A general view of the kaolin industry of the country is given with special emphasis upon wet methods of beneficiation. Whereas dry milling procedures have become well-standardized, wet treatment technique differs widely and each company has its own flow-sheet. Owing to the policy of secrecy in this highly competitive industry plant descriptions are ruled out but methods and equipment employed by major producers are discussed for the principal treatment steps, crushing, blunging, grit removal, fractionating the clay, bleaching, filtering, and drying. May, 1950.